

A COLLECTION OF PAPERS

9th International Seminar
Mathematical Modeling of Furnace Design and Operation

1st Glass Forming Simulation Workshop

June 27 – 29, 2007
Velké Karlovice, Czech Republic

PROGRAMME COMMITTEE

Mr. Josef Chmelař, GLASS SERVICE, INC.
Mr. Erik Muijsenberg, GLASS SERVICE B.V.
Mr. Lubomír Němec, Institute of Inorganic Chemistry AS CR

ORGANIZING COMMITTEE

GLASS SERVICE, INC.
Rokytnice 60
755 01 Vsetín
Czech Republic
www.gsl.cz

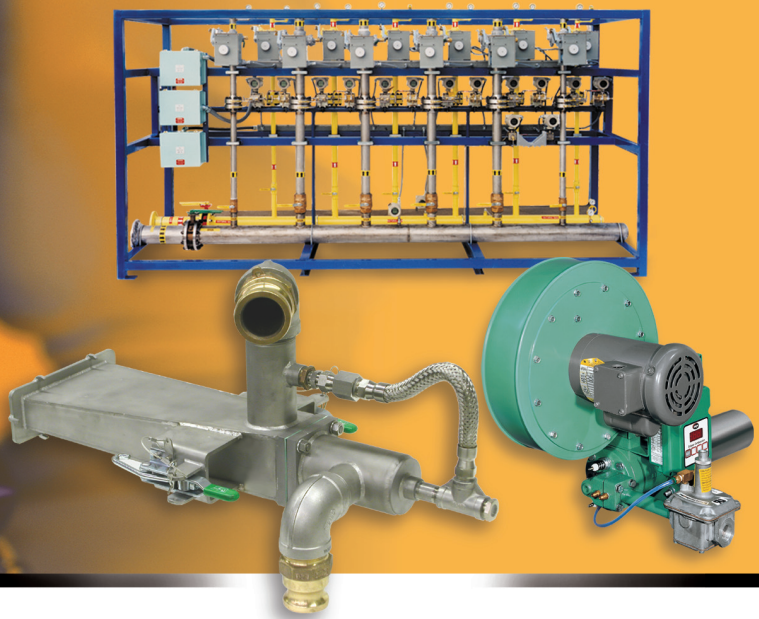
Companies consenting to sponsor this event:



*In a world of new strategies for
thermal process efficiency...*

Stand tall with the proven leader.

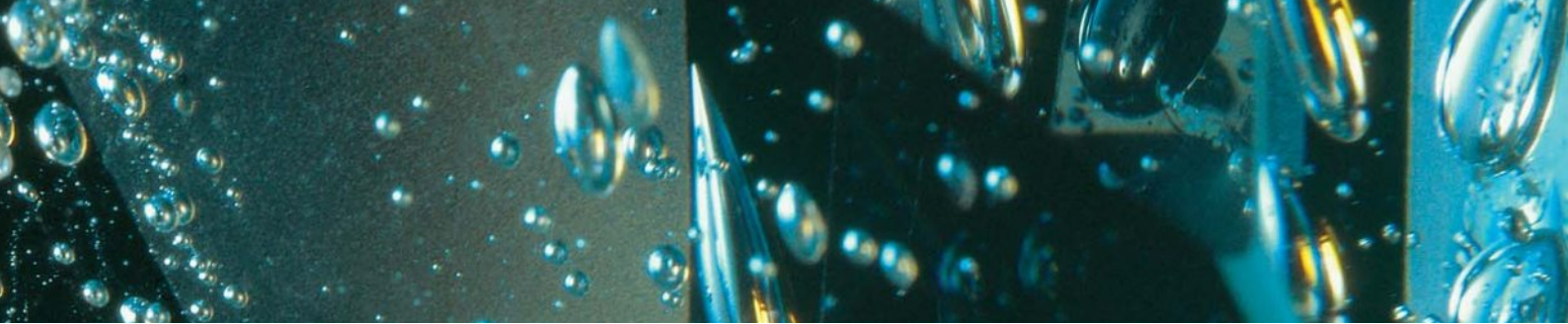
Total Combustion Solutions



The world's leading supplier of combustion systems for the glass industry, Eclipse offers unmatched technical support and service, along with the greatest depth of experience with plant-wide combustion solutions. Call on Eclipse for design assistance to enhance the efficiency of your melt process, annealing system, lehrs and other operations. We stand ready to help with combustion experts in more than 80 locations worldwide.

ECLIPSE[®]
Innovative Thermal Solutions
www.eclipsenet.com

1665 Elmwood Road
Rockford, Illinois 61103 U.S.A.
Phone 815.877.3031



GIA 522

Gas inclusion analyser

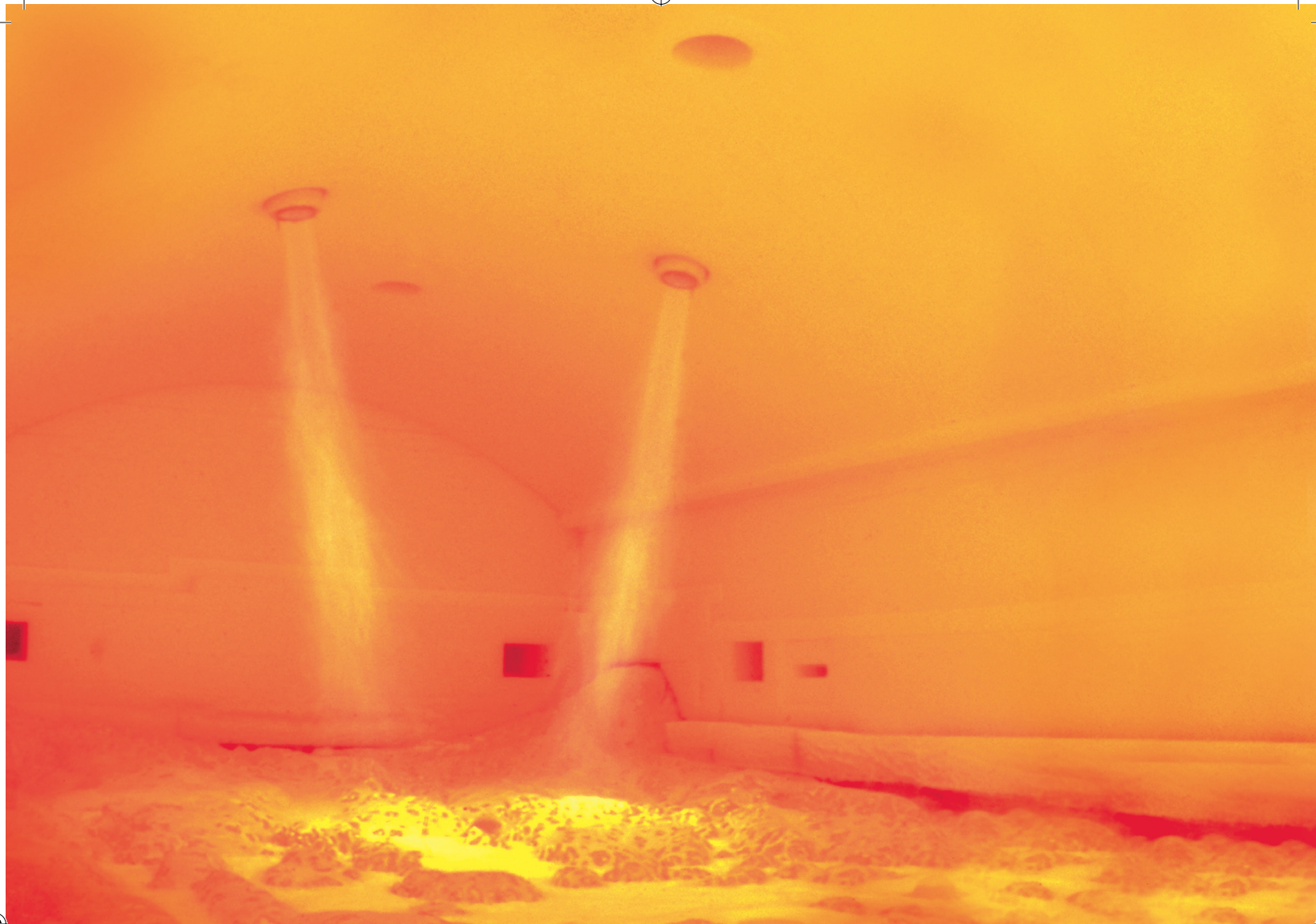
Blister analysis with
unmatched performance

- Bubble size: 5.0 to 0.05 mm
- Detection limit < 1 picolitre
- High dynamic measurement range (6-7 decades)
- Fully automated data analysis
- Internal database for more than 10000 analyses



InProcess Instruments
Otto-Lilienthal-Str. 19
28199 Bremen
Germany
Tel. +49 (0) 421. 52593-0
Fax. +49 (0) 421. 52593-10
mail@in-process.com
www.in-process.com

 InProcess
Instruments



For maximum productivity. CGM™ advanced glass melting.

CGM™ is a unique oxyfuel boosting technology, which transfers more energy to the glass by positioning the burner vertically instead of horizontally to the batch surface.

Benefits

- Increased melting capacity
- Improved glass quality
- Extended furnace life
- Adaptable to either air-fuel or oxyfuel furnaces
- Installation with furnace in operation, no production loss
- 20 % increase in pull rate over conventional air-fuel furnaces and 10 % increase over conventional oxyfuel furnaces
- Freedom to select desired number of burners
- Proven by large-scale laboratory test furnaces and application in more than 30 operating glass furnaces

Linde Gas – ideas become solutions.

Linde AG

Linde Gas Division, Linde Gas Headquarters, Seitnerstrasse 70, 82049 Pullach, Germany
Phone +49.89.74 46-0, Fax +49.89.74 46-12 30, www.linde-gas.com

Linde Gas

CGM™ is a trademark of The BOC Group, Inc.



... your Profit

Greater productivity –
with more flexibility at lower cost

Maximize ...

totally integrated

automation



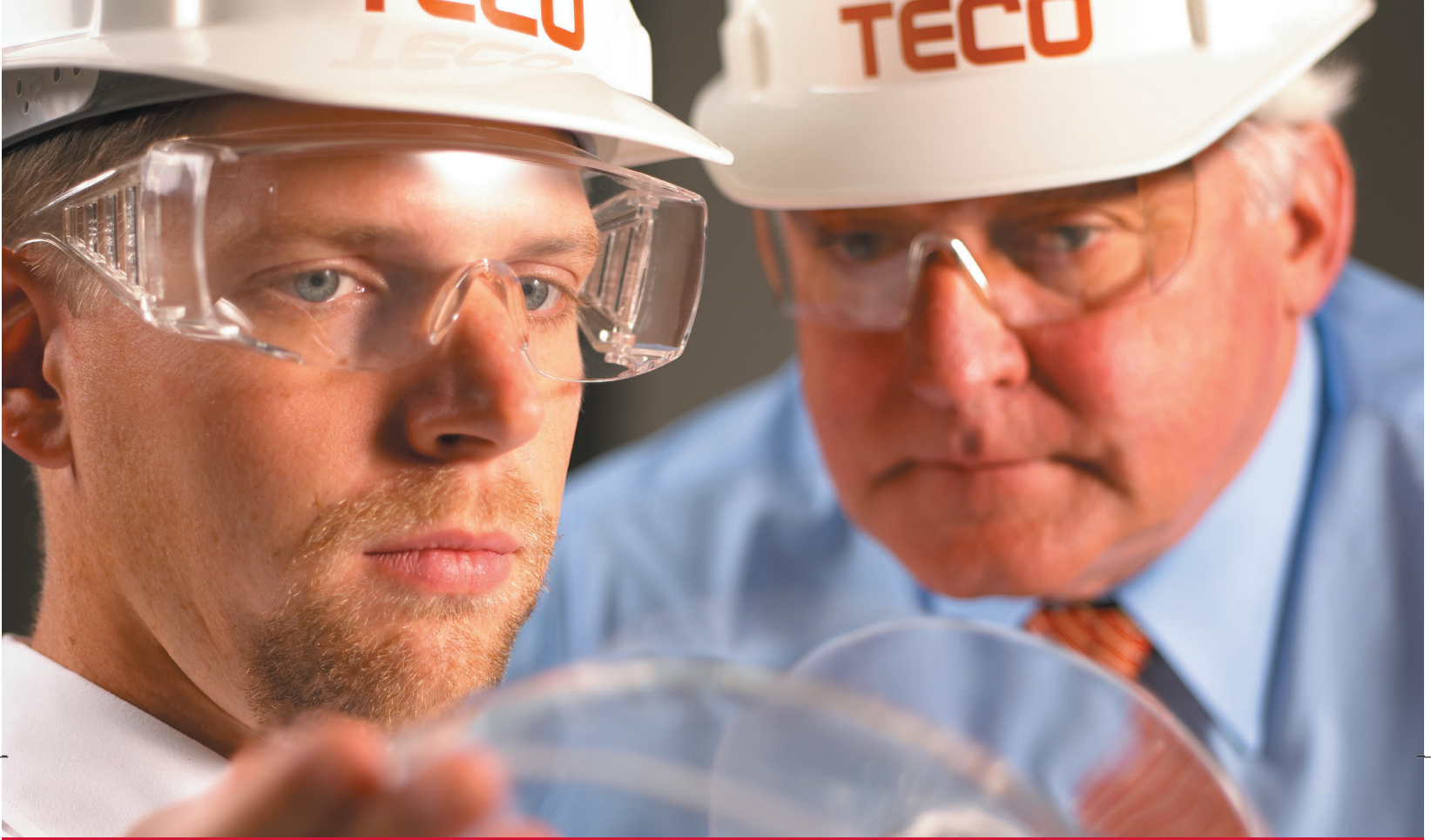
Our top priority? Keeping productivity curves on the upswing for the glass industry. The Siemens Glass team, backed by innovative technologies and years of experience in the glass industry, is expert in creating profitable solutions that remain viable into the future. Our approach integrates all levels of your enterprise from the field to management, and all processes from raw materials to finished glass products. Whether you're installing a new facility or upgrading an existing one, we'll integrate your field instrumentation, IT and automation and energy technologies to create a complete, comprehensive solution. For you, **Totally Integrated Automation** means increasing flexibility, higher quality, minimized costs – and a clear competitive advantage for your company. You can contact us directly at glass.industry.automation@siemens.com

SIEMENS

www.siemens.com/glass

A World of Glass Plant Solutions

GREATER GLASS QUALITY, INCREASED EFFICIENCY AND IMPROVED OPERATING FLEXIBILITY



GLASS FURNACES

BATCH PLANTS

EMISSION CONTROL

REBUILDS

PROJECT MANAGEMENT

INSTALLATION

With more than 75 years of global experience, TECO is a world leader in glass plant design, engineering, construction and rebuilding. We offer solutions that not only help control costs today, but also improve quality, efficiency, productivity and environmental compliance for the long run. So, when you need to take on your next glass plant project, turn to the experts at TECO.



ENGINEERING THAT FITS YOUR EQUATION.

3400 Executive Parkway
P.O. Box 2927
Toledo, Ohio 43606
Ph: 419-537-9711
Fax: 419-537-1369
www.teco.com

Understanding glass, engineering progress

Materials and solutions resulting
from engineering
for modern glass industries



Overview of Platinum Engineered Materials

Engineering

- › Materials technology
- › Strength of materials
- › Lightweight construction
- › Thermodynamics
- › Electrical engineering
- › Fluid dynamics

Materials

- › Cast Pt alloys (Rh Ir Au)
- › Dispersion-strengthened materials
- › FKS Pt
- › FKS Pt Rh 10

Products

- › Stirrers
- › Plungers
- › Stirring cells
- › Refiners
- › Tube mandrels
- › Orifice rings
- › Gob and stream feeders
- › Danner pipes
- › Crucibles
- › Electrodes
- › Patented Solutions

Umicore AG & Co. KG
Technical Materials

Platinum Engineered Materials
Rodenbacher Chaussee 4
63457 Hanau-Wolfgang
Germany

www.platinum-engineered-materials.com

CONTENTS

LECTURES - MATHEMATICAL MODELING OF FURNACE DESIGN AND OPERATION

Quality Forecasts With Numerical Glass Tank Models Prospects – Challenges – Limits	1
W. Muschick	
Bubble Concentration Model	17
William W. Johnson	
Combustion Product Flow Patterns And Discrete Particles Trajectories In A Submerged Melter	23
Grigory Aronchik, Bruno A. Purnode, David Rue	
The Influence Of Glass Flow Character On Bubble Removal In Horizontal Channels	33
Petra Cincibusová, Lubomír Němec, Marcela Jebavá	
The Bubble Removal From Glass Melts In A Rotating Cylinder	43
Vladislava Tonarová, Lubomír Němec, Marcela Jebavá	
The Search For Glass Quality	53
YiFang Cai, Aaron Huber	
Reduction Of Color Change Time On Float Furnaces By The Help Of 3D Numerical Simulations	60
Fabrice Fasilow	
Experiences With Float Furnace Modeling	71
Petr Schill, Jiří Brada, Miroslav Trochta	
Fast Approach To Regenerator Modelling – A Validation Study	76
Menno Eisenga, Erik Muijsenberg, Marketa Muijsenberg, Miroslav Trochta, Josef Chmelař	
Advanced Particle Tracing In Glass Bath And Combustion Space	77
D. Hegen, C. Müller and colleagues, A. M. Lankhorst	
Perspectives On CFD Applications In Materials Processing	78
Manoj Choudhary, Jaydeep Kulkarni	
The Fossil Fuel Fired Glass Furnace – A Thermochemical Reactor Attached To An Imperfect Heat Exchanger	90
Reinhard Conradt	

Glass Homogeneity And Physical Modelling	100
Jan Kučera, Tomáš Krobot	
Laser Evaluation Method Of Physical Model Homogenization	109
Jan Kučera, Tomáš Krobot, Miroslav Skřivan, Róbert Bódi	
Expert System III On Glaverbel Float Lines – From Theory To Practice	114
Laurent Bakalarz, Olivier Mal, Michael Demeyere, Antonella Contino	
10 Years' Experiences With Advanced Furnace Control (Expert Systems ES II™ and ES III™)	121
Josef Müller, Josef Chmelař, Róbert Bódi, František Matuščík	
Advanced Modelling Of Foam And Volatilization For Evaluation Of Different Combustion Systems	134
L. Thielen, A. F. J. A. Habraken, A. M. Lankhorst, P. J. P. M. Simons, O. S. Verheijen	
Significance Of Rayleigh Number For All–Electric Melting	145
Josef Smrček	
Glass Tank Reinforcements	155
Wolfgang Simader	
<u>LECTURES – GLASS FORMING SIMULATION WORKSHOP</u>	
Approach To The Modelling And Optimization Of Glass Forming Cycle	168
Ivo Matoušek	
Advanced Simulation Of 3D Glass Bottle Forming	181
Gerard de Leede, Rik Koch, Vincent Bouwman, Gertjan Kloosterman	
Modeling Of Some Quality Aspects In Tableware Forming Processes	182
P. Vrábel, N. Krečmer, V. Cúth, L. Zhang, G. de Leede, R. Koch	
Improving The Bottle Production By Modelling	183
Rik Koch	
Simplified Bundle Model For Fibers Forming	184
M. Moravský, J. Boroš	
Forming Modelling Of Float Glass: Tin Bath, Bending And Tempering Modelling	185
Gerard de Leede, Petr Schill, Erik Muijsenberg	

LECTURES

9th International Seminar Mathematical Modeling of Furnace Design and Operation

June 28 – 29, 2007

Hotel Horal
Velké Karlovice, Czech Republic

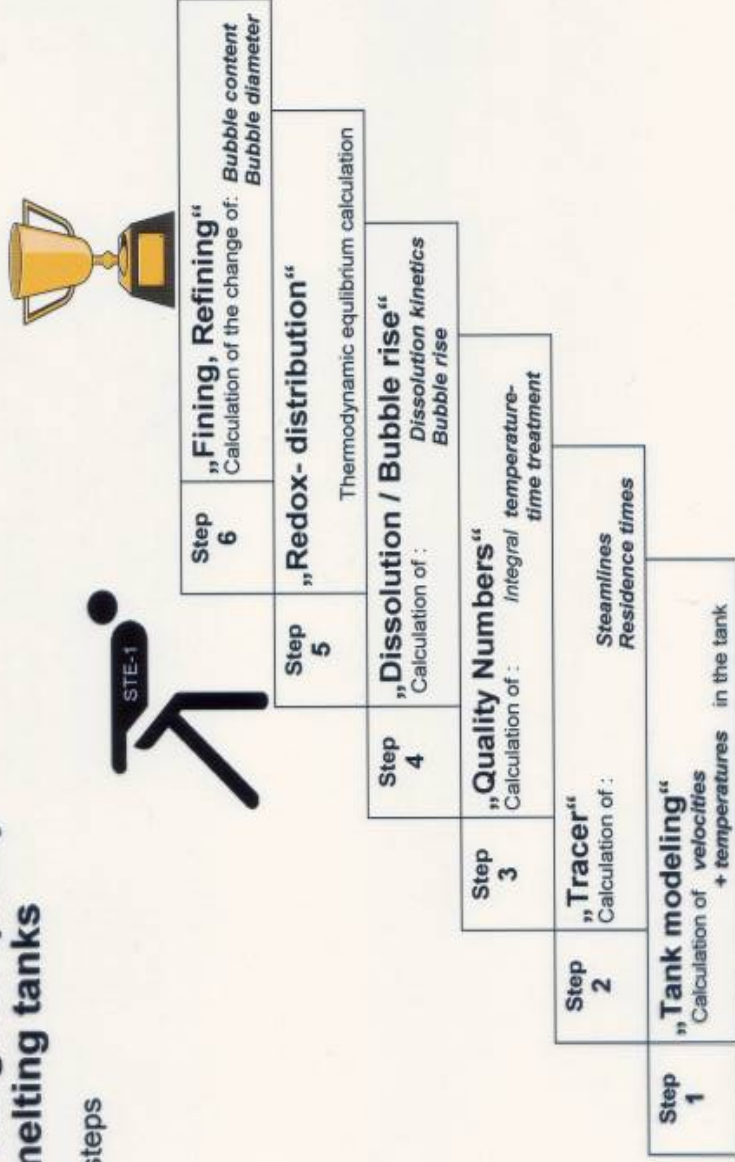
Quality forecasts with numerical glass tank models

Prospects – challenges - limits

W. Muschick

Modeling the glass quality of glass melting tanks

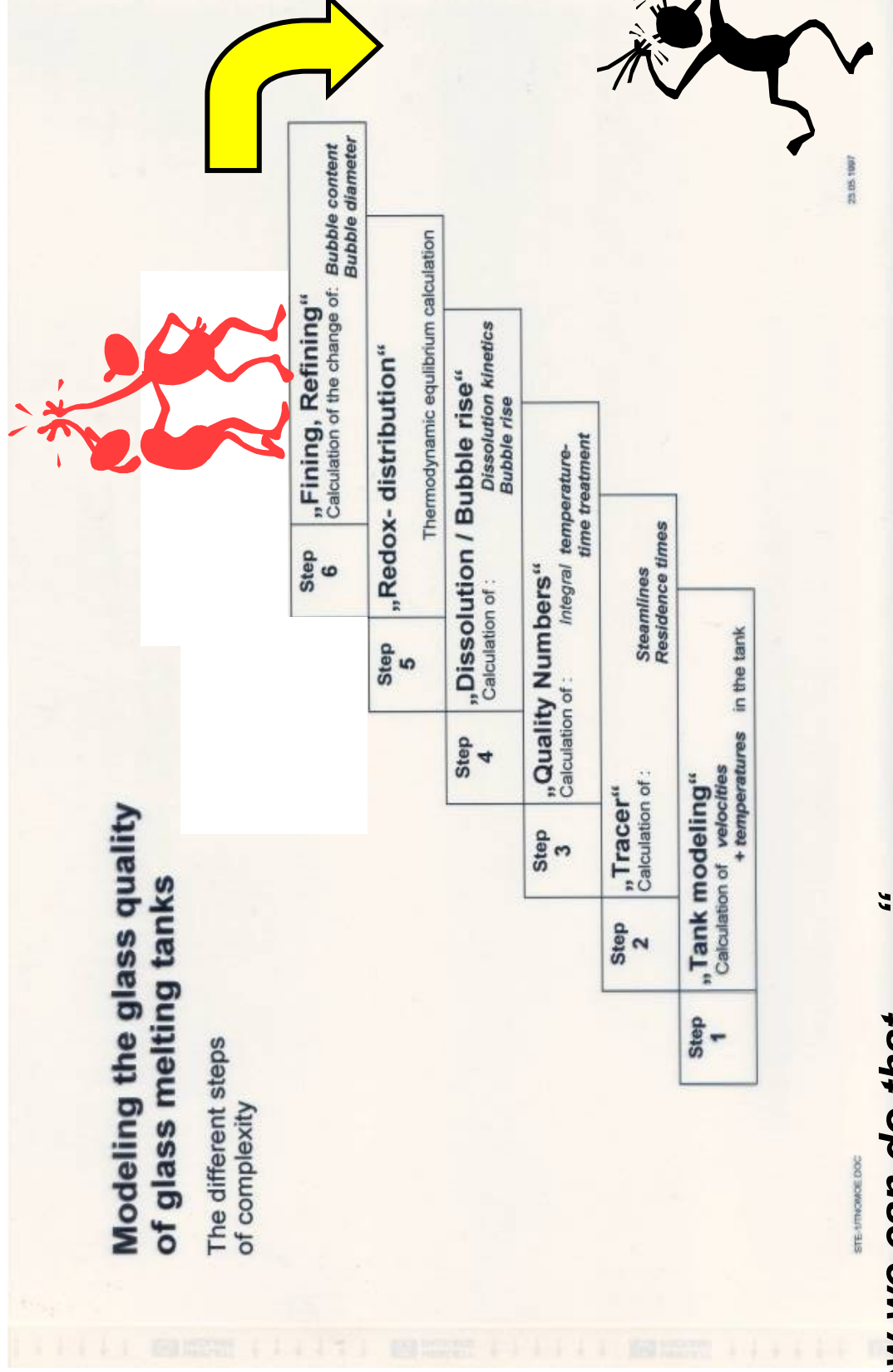
The different steps of complexity



STE-1/KNOWDE.DOC

23.05.1997

„Picture from my first presentation at this seminar“



„Now we can do that“

„BUT in some cases *the results are wrong*“

Why ?

Reasons for wrong model results

HUMAN Errors

Wrong input

Wrong understanding of the problem

Not knowing or including all boundary conditions > *Generation of other faults*

SOFTWARE errors

Improper simplifications of the code and the sub models

Insufficient post processing

INPUT DATA errors

Wrong measurements

No measured data > *improper approximations*

“HUMAN“ errors

Wrong input

Numbers: (GTM: more then 100 input data)

Geometry:

Grid:

remedy

- > manageable input file
- > good graphical illustration
- > basic knowledge about current

Wrong understanding of the problem

an example is given orally

Not knowing or including all relevant boundary conditions

- > **Generation of other faults**

an example is given orally

- > perfect communication with the plant

- > perfect communication with the plant

SOFTWARE „errors“

All current numerical models are far from being perfect

All codes have quite a lot approximations and simplified submodels

Here I will discuss only some few (in my view) prominent examples

Calculation of velocity and temperature distribution

- 1) Boussinesq approximation
- 2) Rosseland approximation
- 3) „Pure melt“ approximation

Submodels

- I. Batch
- II. Foam
- III. Fining / postprocessing

SOFTWARE „errors“

Calculation of current and temperature distribution

1) Boussinesq approximation

Tests with FLUENT gave no significant differences

2) Rosseland approximation

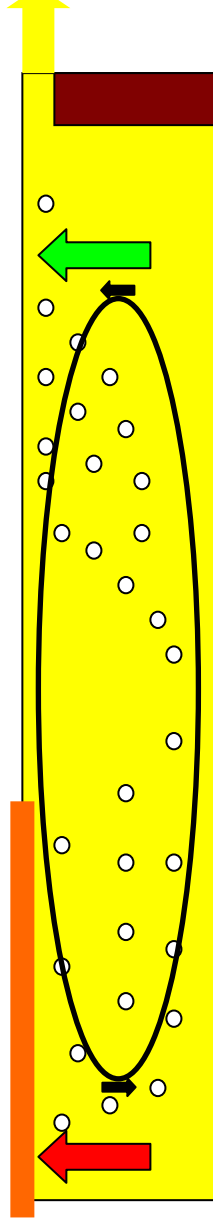
Simulations of very clear glass in very small furnaces gave reasonable results

3) „Pure melt“ approximation

In a few cases we got only reasonable result, if we assumed an influence of seeds on the current
(examples next page)

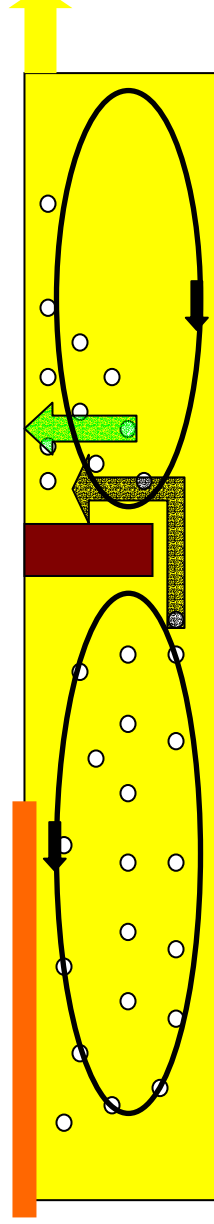
SOFTWARE „errors“
„Pure melt“ approximation (examples)

1) „Normal“ case: *melting and fining in on volume*



The influence of seeds on the current is mostly balanced

2) Critical case: *melting and fining separated*



Second loop faster by extra upward velocity after throat !!

SOFTWARE „errors“ ***Submodells (Overview)***

I. Batch

Though current batch models often give reasonable results, further developments are still necessary. A major, still open topic, is a good description of the rheology, which affects the distribution of the melting batch.

II. Foam

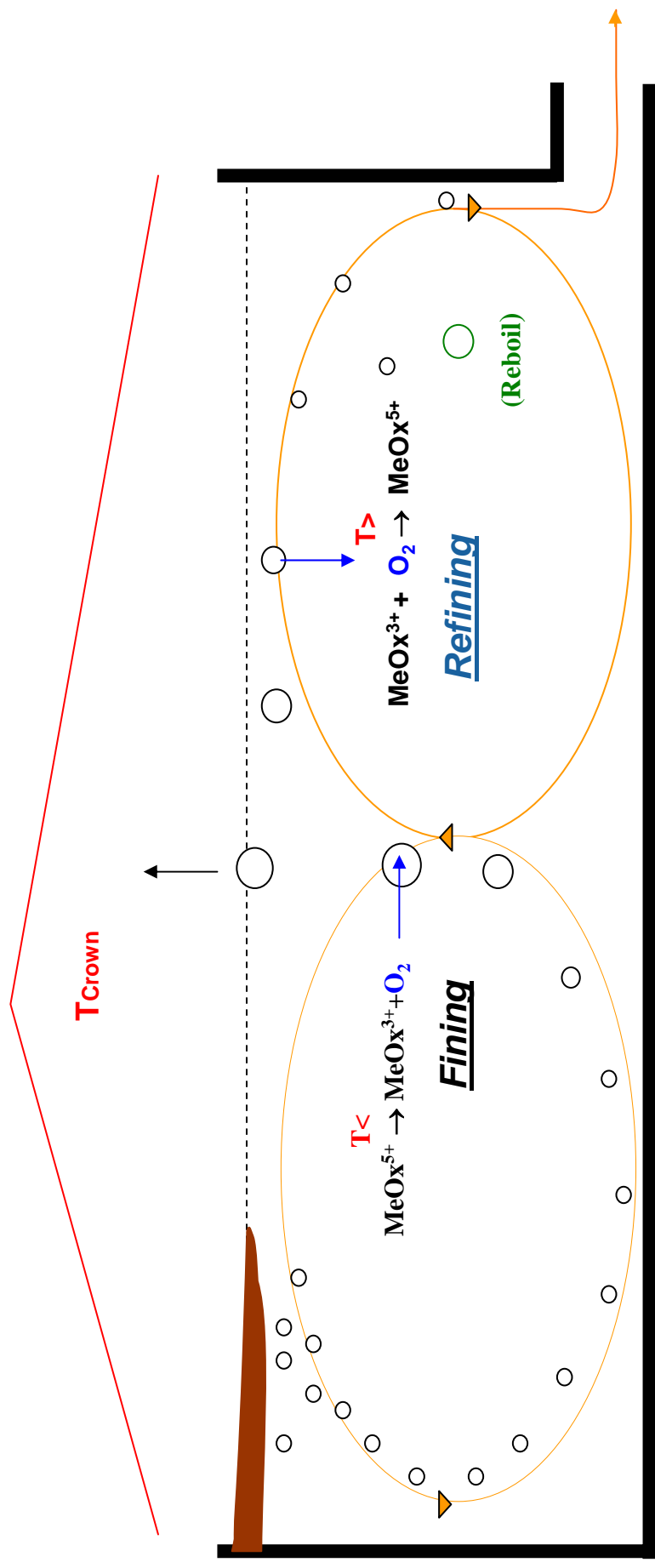
The distribution and thickness of the foam determines the heat transfer from crown to melt. Up to now foam is mostly set as a fixed boundary condition. Dynamic foam models are rare, imperfect and time-consuming and need therefore further enhancements **urgently**.

III. Fining/post processing

In most cases quality forecast means seed count forecast. Sometimes you can do this by some quality numbers derived from the time-temperature history. But in many cases this is not possible. Here you have to simulate the fining process. The sub models for fining are far from being perfect, but much better than the required material values.

SOFTWARE „errors“

Submodell III: fining /postprocessing



„Good“	<u>Fining</u>	<u>Refining</u>	<u>Reboil</u>
Temperature >	+	-	+
Time >	+	+	-
History			

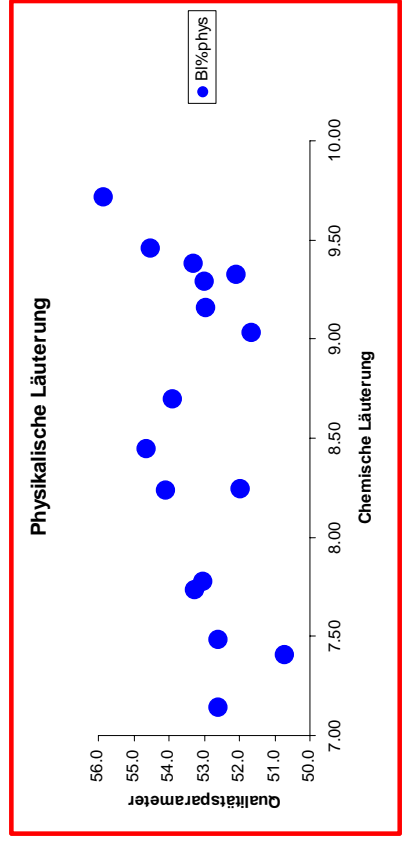
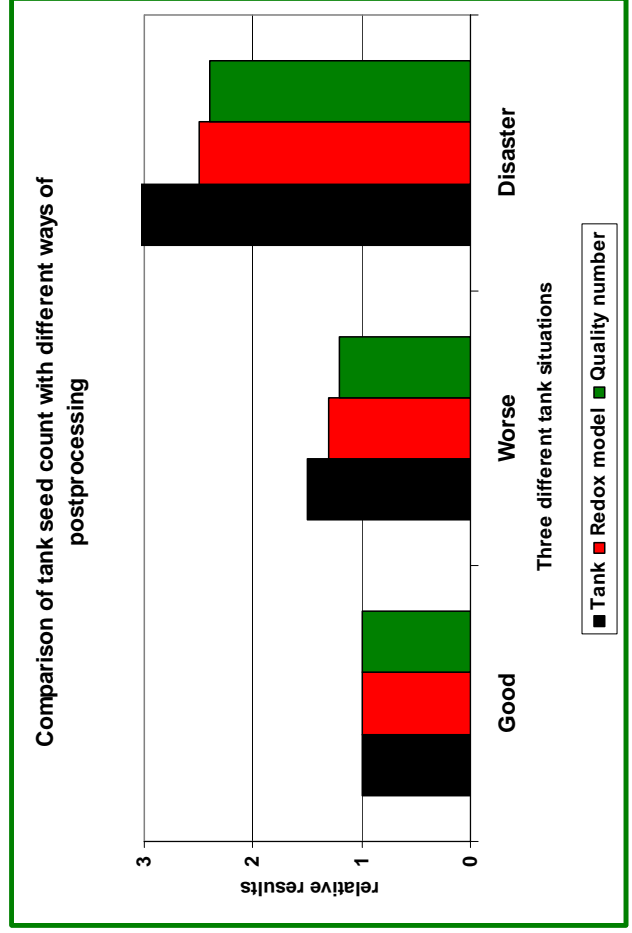
SOFTWARE „errors“

Submodells III: fining /postprocessing

„Good“			
Temperature >>			
Time >>			
History			
	<u>Fining</u>	<u>Refining</u>	<u>Reboil</u>
	+	-	+
	+	+	-

Quality numbers are sufficient

Simulation of fining process necessary



INPUT DATA errors *(mostly material data)*

Laboratory measurements different from tank values

Viscosity

Thermal conductivities of refractory material

Difficult measurements with large error

Thermal expansion factor of melt

Overall thermal conductivity of melt

All data concerning fining

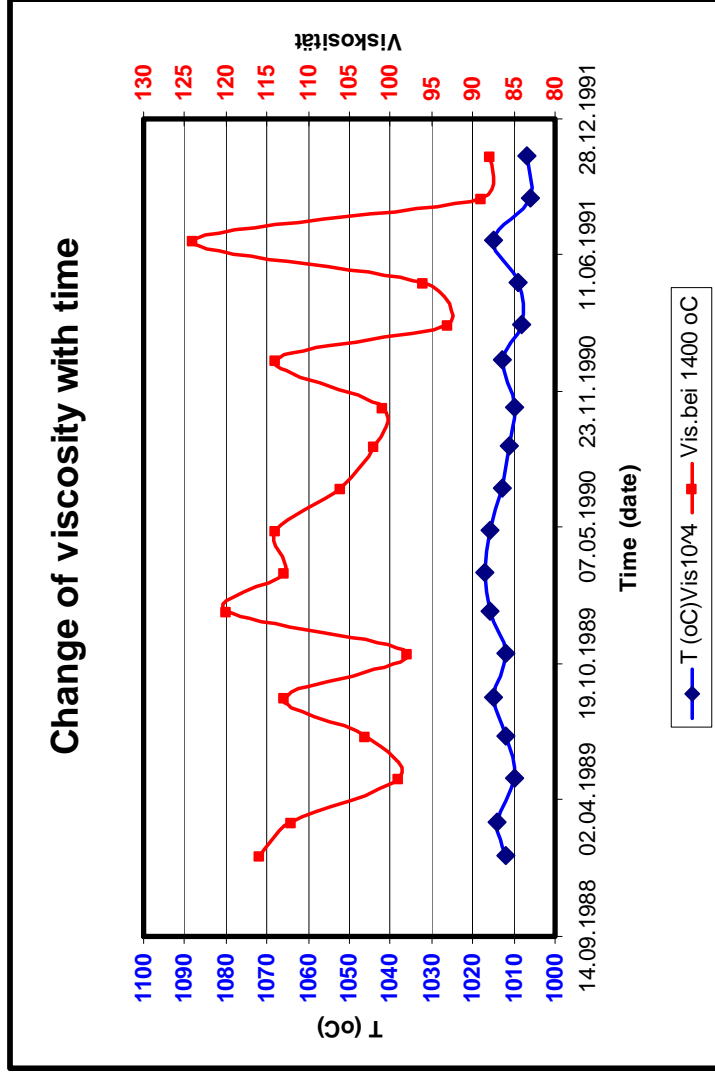
No measured data but theoretical approximations or data from simular glasses

In many cases nearly **ALL** (except viscosity and electric conductivity)

INPUT DATA errors

Laboratory measurements different from tank values

Viscosity



The viscosity at the tank is changing notable

Possible reasons: different humidity, mixing, changing quality of raw material ?

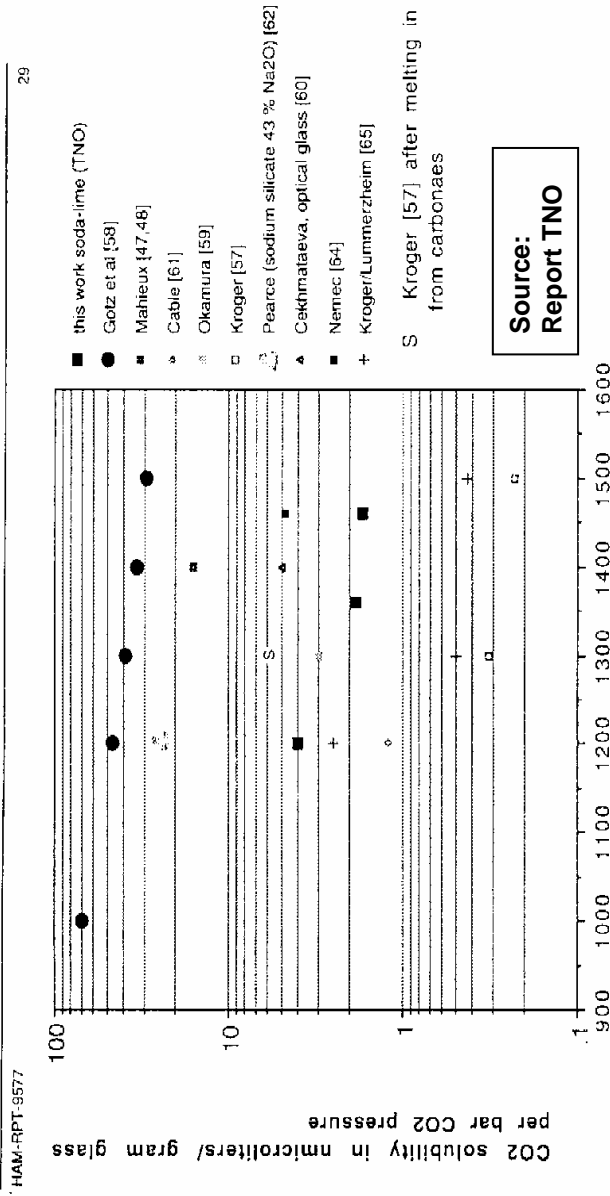
Messungen Betriebslabor Glas FFS		
Datum	T (oC)Vis10^4	Vis.bei 1400 oC
05.11.1991	1007	88
03.09.1991	1006	89
02.07.1991	1015	124
03.05.1991	1009	96
01.03.1991	1008	93
08.01.1991	1013	114
01.11.1990	1010	101
04.09.1990	1011	102
03.07.1990	1013	106
03.05.1990	1016	114
01.03.1990	1017	113
05.01.1990	1016	120
03.11.1989	1012	98
01.09.1989	1015	113
04.07.1989	1012	103
03.05.1989	1010	99
01.03.1989	1014	112
10.01.1989	1012	116
MW	1012	106
STDABW	3	11
MAX	1017	124
MIN	1006	88
MAX-MIN	11	36
MAX-MIN %	1.1	34.1

INPUT DATA errors

Difficult measurements with large errors

All data concerning fining:

Example: literature values for the solubility of CO2 of soda lime glase



The values differs up to the factor 100

H.2 CO2 solubility data from literature and TNO study for mainly soda-lime-silica melts (container glass or floatglass) and TV-screen glass compositions

Summary

MY priority list for optimising the numerical glass tank models

- 1) Input data
- 2) Input data
- 3) Input data
-
- 4) Dynamic foam model
- 5) Enhanced batch model especially regarding rheology
- 6) Better fining model > Simulation of the seed density > influence on melt

***If you has only poor fuel.....
the design of a sophisticated engine makes no sense***

Thank you very much

BUBBLE CONCENTRATION MODEL

William W. Johnson
 Corning Incorporated
 Corning, NY, USA

Abstract

Present-day glass-melting furnace models typically assume glass is a homogeneous fluid, with density being only a function of temperature. Thermally induced density gradients drive molten-glass convection.

However, in the actual process, gas release and segregation during melting, volatilization, and refractory dissolution work against the ideal view of the melting furnace. Bubbles and chemical inhomogeneities affect density and can overwhelm the thermal effect.

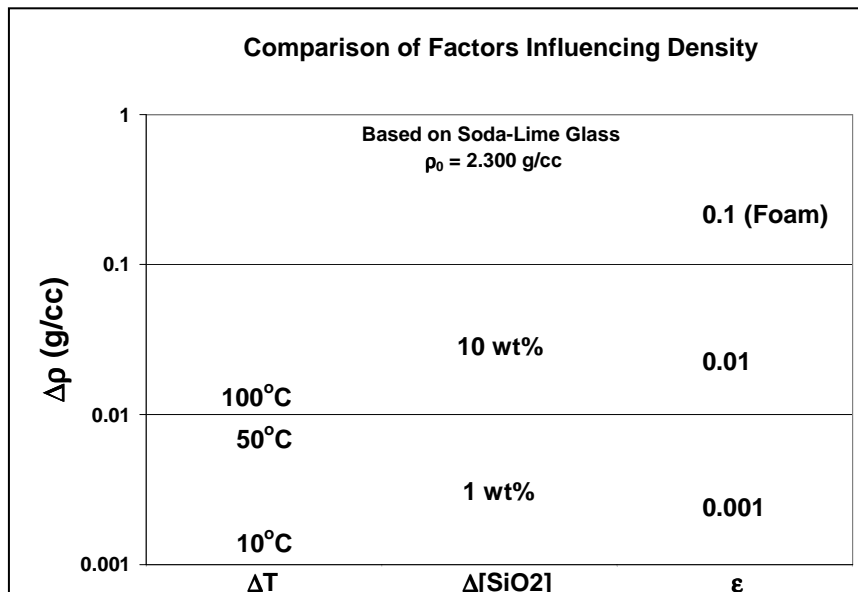
An improved model will be described that adds the effect of bubble concentration to the buoyancy source term. The utility of the model will be illustrated by examples.

BACKGROUND

Present-day glass-melting furnace models typically assume glass is a homogeneous fluid, with density being only a function of temperature. Thermally induced density gradients drive molten-glass convection.

However, in the actual process, gas release and segregation during melting, volatilization, and refractory dissolution work against the ideal view of the melting furnace. Bubbles and chemical inhomogeneities affect density and can overwhelm the thermal effect. Figure 1 compares the magnitude of thermal and chemical gradients, and void fraction on density change.

Figure 1: Comparison of Factors Influencing Density



A few percent chemistry change, or a 1% void fraction can totally overwhelm the thermal effect on density. This presentation considers by modeling, the change in bulk density related to bubbles in the glass melt.

Two examples will be shown using a modified 2-dimensional version of the TC21 round-robin furnace (9 m Length x 1 m Depth). Simple boundary conditions are imposed for the batch melting region and crown-to-glass radiative heat-transfer. Glass properties and model setup are listed below.

Table 1: Properties and Setup Used in Model Examples

Density	= 2333. kg/m ³
Expansion	= 6.e-5 /degC
Viscosity	= 10.**(-1.58+4332./(TdegC-248.))
Thermal Conductivity	= 100 W/m-C
Heat Capacity	= 1300. J/kg-C
Length	= 9m
Depth	= 1m
Pull	= 0.167 kg/s-m

EXAMPLE 1: BUBBLE INDUCED CONVECTION

The model in Figure 1 shows glass flow calculated by thermal-convection only. A high concentration of bubbles is imposed as a boundary condition in the batch region. The bubbles are advected and diffused within the glass flow, with a vertical drift related to bubble rise. In this case, there is no influence of bubbles on the glass flow, only the glass flow moving bubbles.

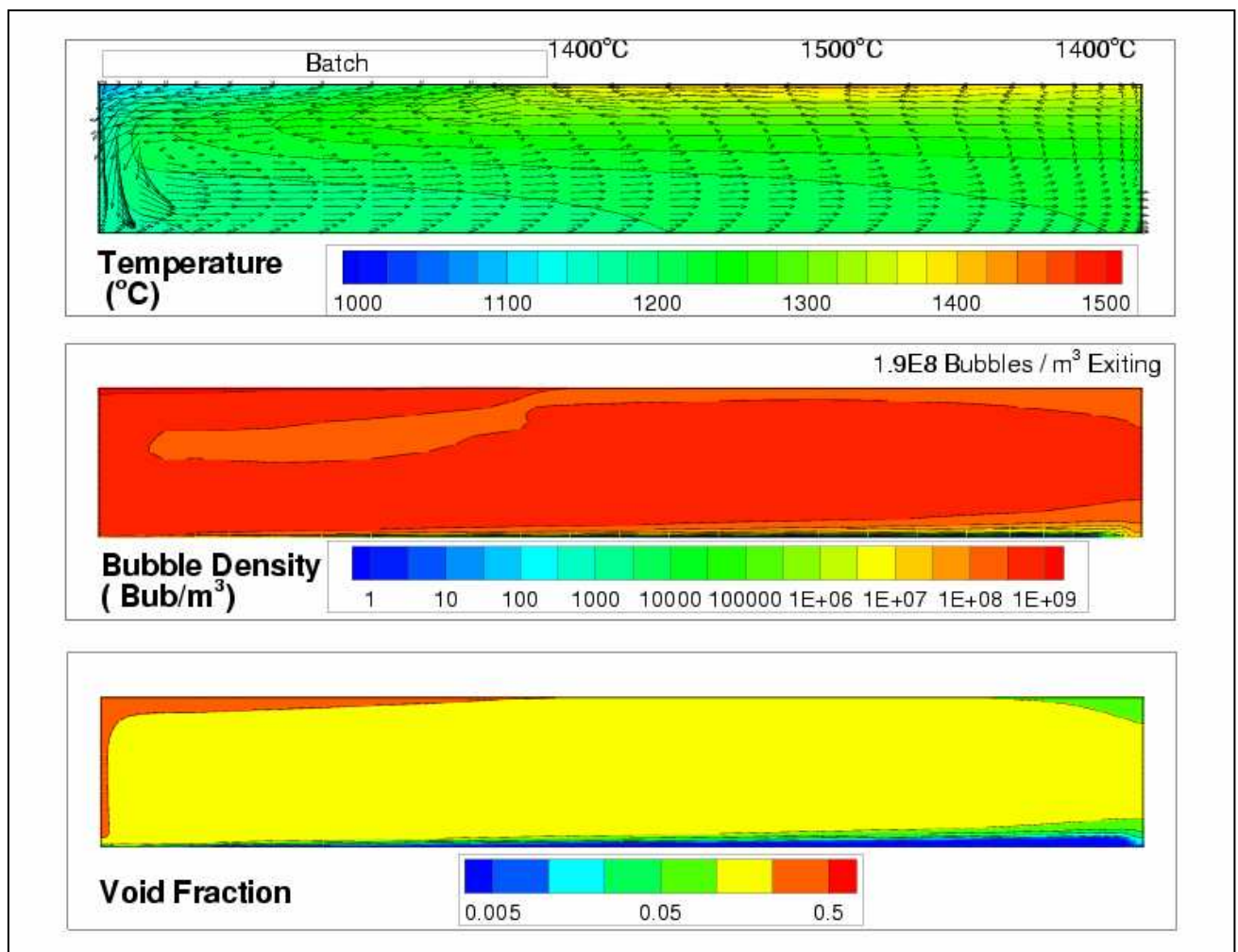
Figure 2 shows a similar model, except the influence of bubbles on glass density, and buoyancy is considered.

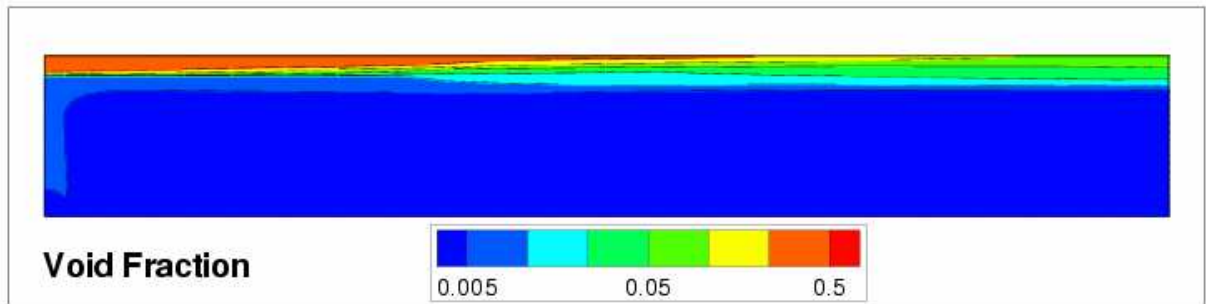
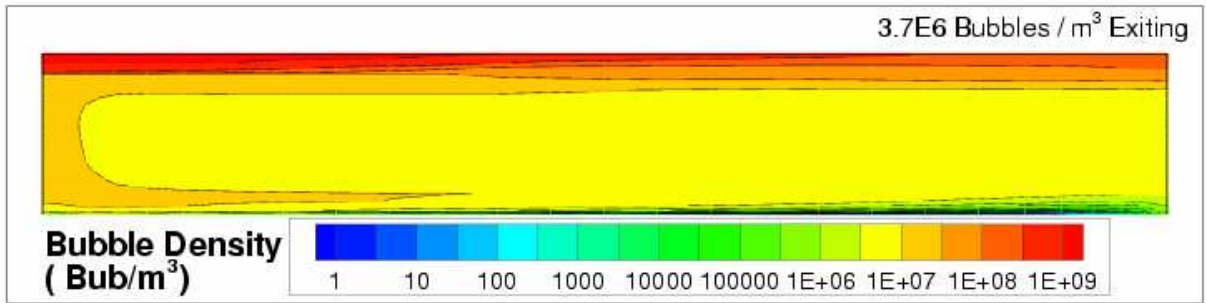
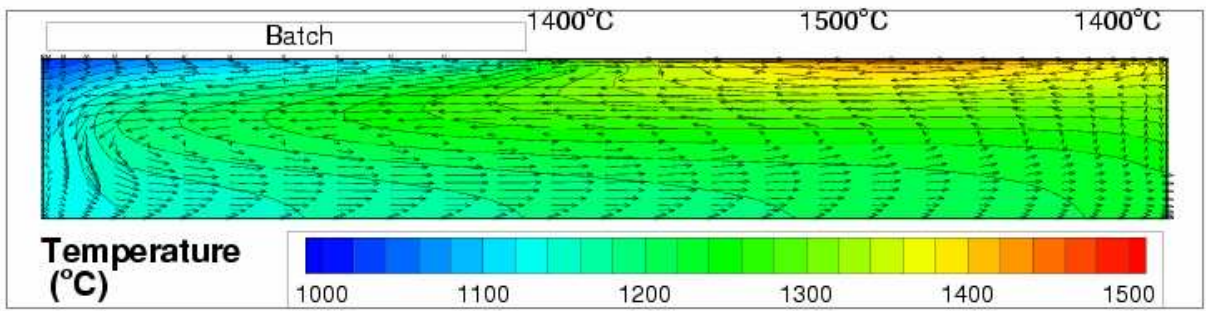
The motion of the glass and bubbles is very different than the base simulation. The bubbly glass stratifies horizontally by density, rather than merely following glass movement into the depths of the furnace.

The difference in void fraction between under the batch pile, and the forward surface, drives a density-driven flow forward across the surface. This type of motion is very different than a conventional model that considers only thermal convection.

The bubbles concentrating on the free surface is much like a foam. This provides a natural way to simulate the foam layer that typically develops upon melting. Foam in this model approach will respond to pull, temperature, and fining agent when in its complete form (not shown here). This approach advances the conventional approach of assuming a foam layer position. This type of foam simulation does not consider detailed physics occurring at the bubble lamella or chemistry level so calibrations from experiment or furnace observations are required.

Figure 1: Base Simulation: Thermal Convection Only
Figure 2: Thermal + Bubble Driven Convection





EXAMPLE 2: BUBBLERS

Bubblers are often used in glass melting to enhance convection. The conventional simulation approach is to assume a vertical zone of influence, located from the bubbler to the glass surface. Based on the bubbling rate and bubble size, and effective source-term for the y-momentum equations is implemented into the assumed zone of influence.

Simulating bubblers with a bubble concentration model is a more natural approach. The bubbling rate and bubble size are an input to the bubble concentration model, and the mutual interaction between the bubbles and glass is calculated.

Including the mutual interaction of glass and bubbles, is closer to reality than the assumed one-way effect of the conventional approach. Additionally the bubble concentration formulation allows computation of gas-exchange between the bubbles and glass.

Figure 3: Simulation of a Bubbler

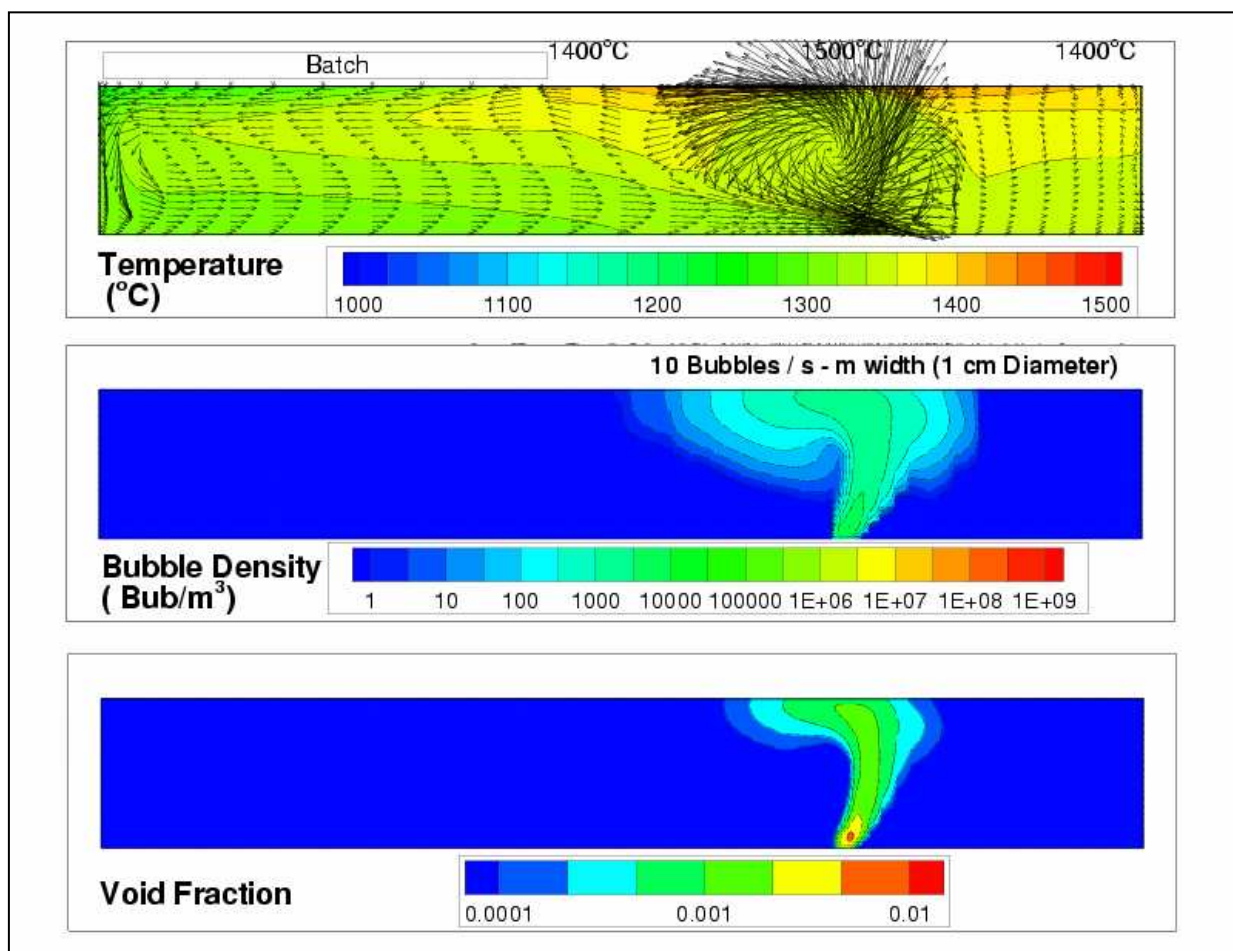
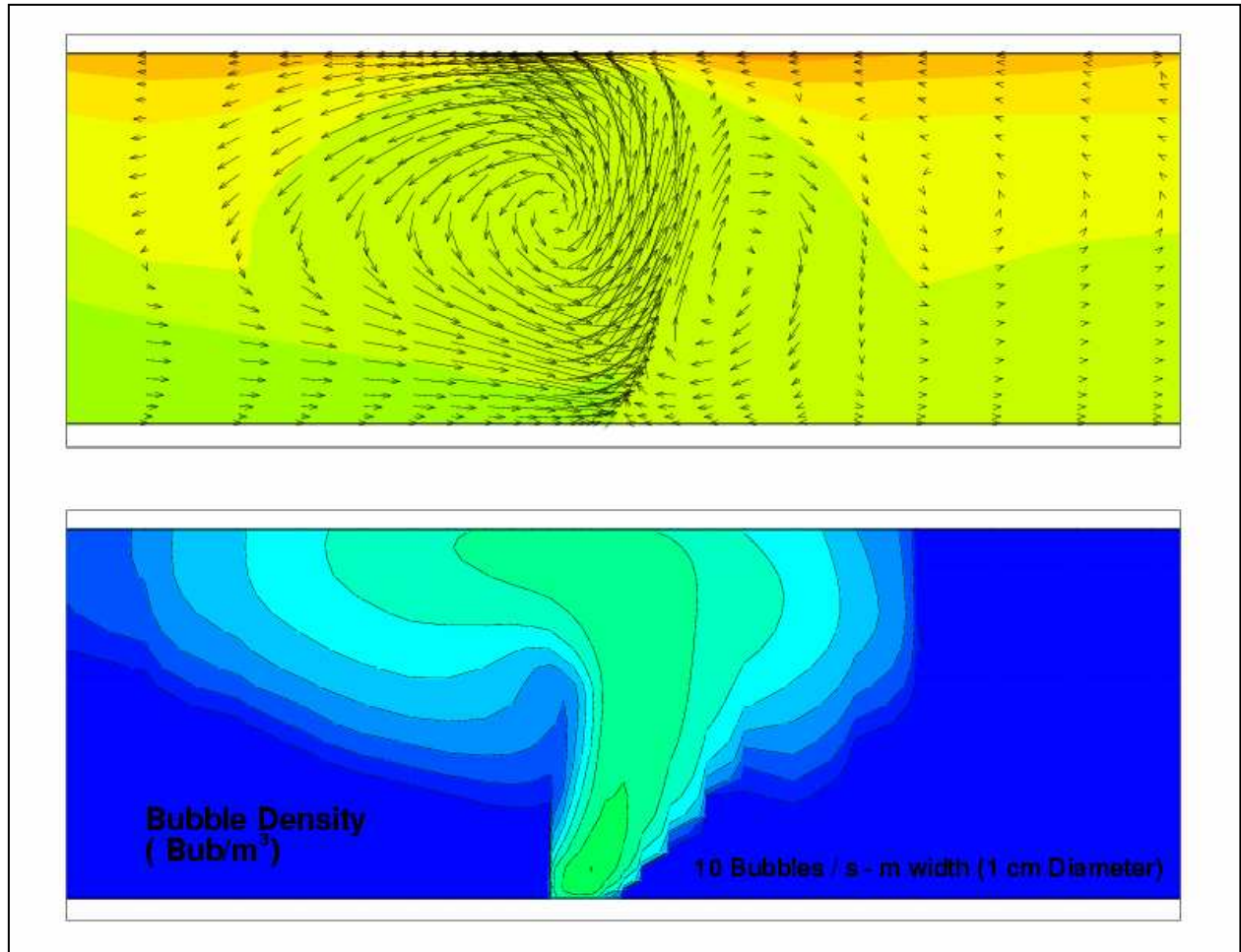


Figure 4: Close-up View of Bubbler



CONCLUSIONS

1. The long held assumption of treating molten glass as a homogenous liquid is challenged.
2. Bubbles can be an important factor in density-driven convection.
3. A bubble concentration model is described which is useful in simulating many aspects of glass melting.

REFERENCE

Johnson, WW, "Bubble Concentration – Redox Model", Proceedings of the 5th International Seminar on Mathematical Simulation in Glass Melting", 1999

COMBUSTION PRODUCT FLOW PATTERNS AND DISCRETE PARTICLES TRAJECTORIES IN A SUBMERGED MELTER

Grigory Aronchik

Gas Technology Institute, 1700 S. Mt Prospect Road, Des Plaines, IL 60018, U.S.A

Bruno A. Purnode

Owens Corning, Science & Technology Center, 2790 Columbus Road, Granville, OH 43023,
U.S.A.

David Rue

Gas Technology Institute, 1700 S. Mt Prospect Road, Des Plaines, IL 60018, U.S.A

Abstract

There is a strong trend in the glass industry to find ways to lower capital and energy costs. The submerged melting technology offers the potential to meet this goal. Submerged melting is a process for producing melts in which fuel and oxidant are fired directly into the bath of material being melted. The combustion gases bubble through the bath, creating an intense heat transfer exchange. The forced convection-driven shear stresses provide rapid particle dissolution and enhance temperature uniformity in the bath.

At this stage, very little is known about the details of the process and very little data exists. Therefore, in order to support submerged melter designs and to better understand the complicated melting phenomena, an important modeling effort has been initiated.

In this paper, we investigate how exhaust gas flows may entrain batch particles. Two feeding system designs are investigated. We do show that top feeding exhibits a risk of carrying away the smallest batch particles. Modeling can therefore be used as a design tool for submerged melters

1. INTRODUCTION

The glass industry is considered amongst the top highly energy-intensive industries in the US according to studies conducted in the late 90's by the Office of Industrial Technologies of the United States Department of Energy. The glass industry produces 21 million tons of consumer goods annually valued at \$28 billion consuming 400 trillion BTUs, which accounts for approximately 15 percent of production costs. Theoretically, glass making requires about 2.2 MBtu of energy per ton of glass, but usually more than twice that amount is actually used due to various losses.

The Glass Melting Technology Technical and Economic Assessment published by the Glass Manufacturing Industry Council (2006) calls for technological improvements in several areas. The most important is clearly that the glass industry needs a less capital intensive, lower energy cost, and cleaner way to melt glass. It seems like incremental changes in current melters is insufficient for future survival of the industry. Only a Next Generation Melting System (NGMS) using a 'segmented' approach is capable of meeting the high priority research needs. The submerged combustion melting (SCM) technology is the ideal melting and homogenization stage of NGMS. This is a melting approach that provides large capital and energy savings to the glass industry. Submerged combustion melting is a process for

producing mineral melts in which fuel and oxidant are fired directly into the bath of material being melted. The combustion gases bubble through the bath, creating a high heat transfer rate to the bath material and turbulent mixing. Batch handling systems can be simple and inexpensive because the melter is tolerant of a wide range in batch and cullet size, can accept multiple feeds, and does not require perfect feed blending.

The need for a new glass melting technology has led to the formation of an unprecedented consortium of five glass companies that are working with the Gas Technology Institute (GTI) to design, demonstrate, and validate the melting stage of a Next Generation Melting System (NGMS). The project is funded by the U.S DOE.

SCM was developed by the Gas Institute (GI) of the National Academy of Sciences of Ukraine and was commercialized a decade ago for mineral wool production in Ukraine and Belarus. Five 75 ton/day melters are in operation (Pioro et al. (2006)).

Despite those various industrial applications, very little is currently known about the complex physics present in the process and very little process data exist. In order to support the design of submerged melter and to better understand the complicated melting phenomena, an important modeling effort has been initiated. Therefore a major part of the SCM project is dedicated to this task.

The ultimate goal of mathematical and CFD modeling of fluid flow and heat transfer in submerged melters is to obtain recommendations on their designs and operating parameters. Unfortunately, the presence of extremely complex physics and the very disparate times scales make solving of the full problem impractical. Therefore a specific, stepwise modeling approach has been established in order to find a compromise between faithfully describing the physics of the process while still relying on reasonable computational cost. This methodology is described in Purnode et al. (2007) along with results thereof. In this paper, we concentrate on simulating gas flows above the melt and their influence on the batch particles. In particular, we evaluate the difference between side feeder design and a top feeder.

2. SUBMERGED COMBUSTION

Submerged combustion melter is a bubbling bath furnace where fuel and oxidant are fired directly into the bath of material being melted. The high temperature bubbling combustion inside the melt creates a complex gas-liquid structure and a large heat transfer surface. This

increases the exchange of heat between the products of combustion and the processed materials (see Figure 1).

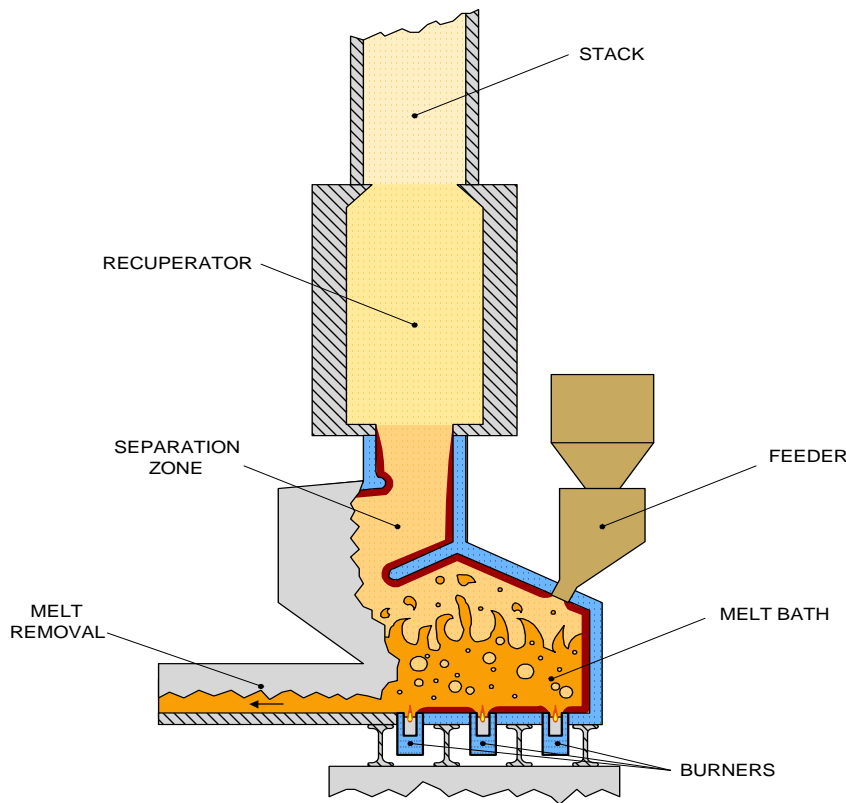


Figure 1: Submerged Combustion (from Olabin et al. (1996))

The modeling of such a process with several burners is challenging for three reasons. First, the complex character of the three dimensional physics and chemistry involved in the process. Second, the very disparate time scales present in the system. Fast moving turbulent combustion gases are coexisting with slow moving laminar glass and raw materials. Third, it is a rather new process with very little guidance from previous data available from the facilities that run such a process.

A staged analysis strategy is the most promising for balancing accuracy, fidelity to the physics and the associated computational cost. The method is presented in Purnode et al (2007).

In this paper, we analyze the effect of the gases as they travel above the melt surface and specifically their influence on the batch particles that they might carry-over. Computational Fluid Dynamics (CFD) simulation of combustion products flow patterns and discrete particles

trajectories are used to estimate a difference between Top-Feeder and Side-Feeder in terms of the risk of carryover of raw material particles. We do show that modeling can therefore be used as a design tool for submerged melters. In section 3 we only consider the gas flows, then in section 4 batch particle tracking is investigated.

3. GAS FLOW PATTERNS

We only do consider the gas space above the melt and there is no interaction between glass melt and the combustion products above it. The k- ϵ model is being used for modeling turbulence. Besides, other assumptions of the model are:

- The temperature of combustion products is 1673K. All walls are assumed adiabatic.
- The burners heat loads are 1.5 Mbtu/hour. Excess oxygen is 5%.
- The combustion products density is described by ideal law model with standard density of 1.32 kg/m³.
- There is no interaction between gas flows and discrete particles simulating raw material (batch) flow.
- Side-Feeder and Top-Feeder are considered as two square holes at the sidewall and at the roof of the melter.

The geometry of gas space to be modeled is shown in

Figure 2. The schematic contains two possible locations of the feeder as mentioned above.

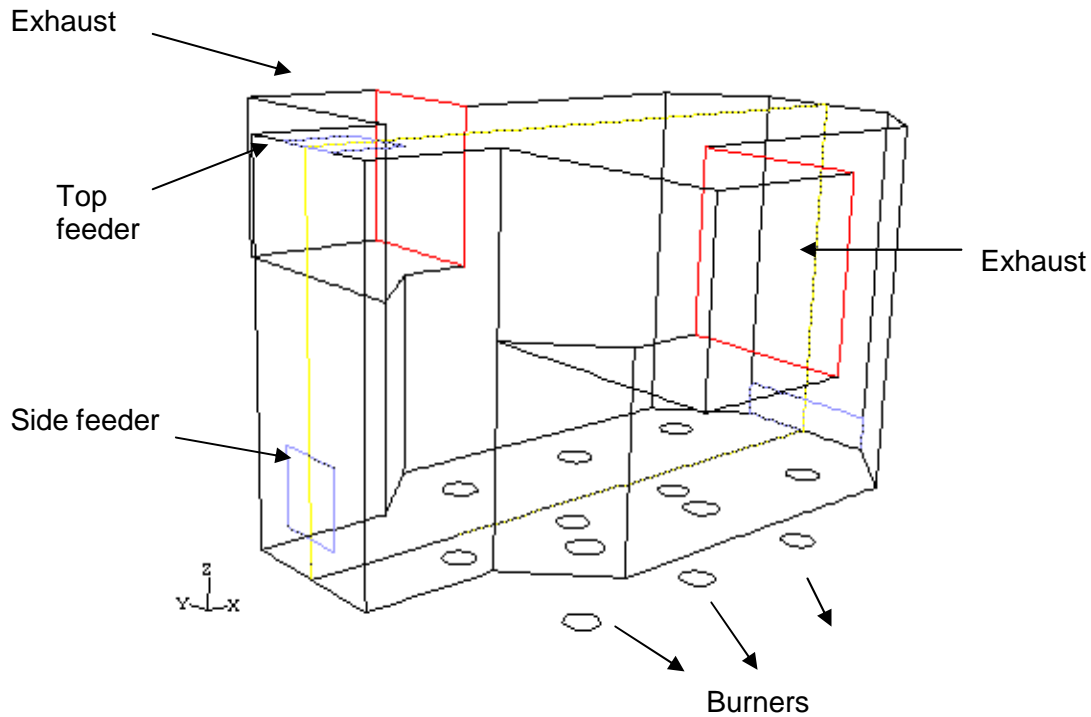


Figure 2 Melter geometry: gas space

The gas velocity field in the plane of the burners is shown in Figure 3. The planes at $z=0$ and $z=1\text{m}$ correspond to glass melt level and to the roof of the melter respectively. The vector velocity field in the horizontal planes at $z=0.2\text{m}$ is shown in

Figure 4a. The horizontal component of velocity along the furnace at $z=0.2$ in the area of Side Feeder falls within the range of $v_x \approx (1.4, 2.4 \text{ m/s})$ approximately. The component $v_y \approx 0$, i.e. the gas flow in the area of Side Feeder is directed along the lengthwise axis of the melter.

The vector velocity field in the horizontal planes at $z=0.9\text{m}$ is shown in Figure 4b. The horizontal component of velocity carrying particles out of the symmetry plane at $z=0.9$ in the area of Top Feeder falls within the range of $v_y \approx (1.5, 3.5 \text{ m/s})$ approximately.

The vector velocity field in plane of symmetry is shown in Figure 5. It clearly demonstrates downward flow in the central part of the feed pocket.

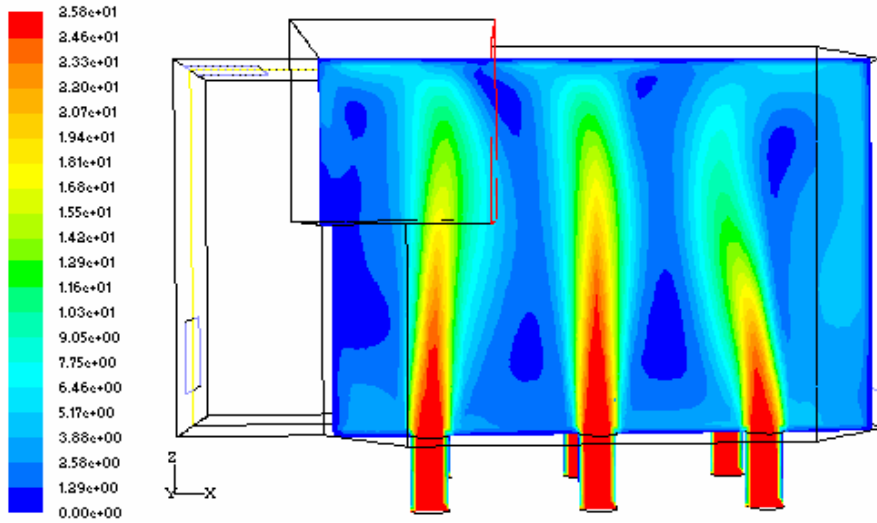


Figure 3 Velocity magnitude in the plane of the burners

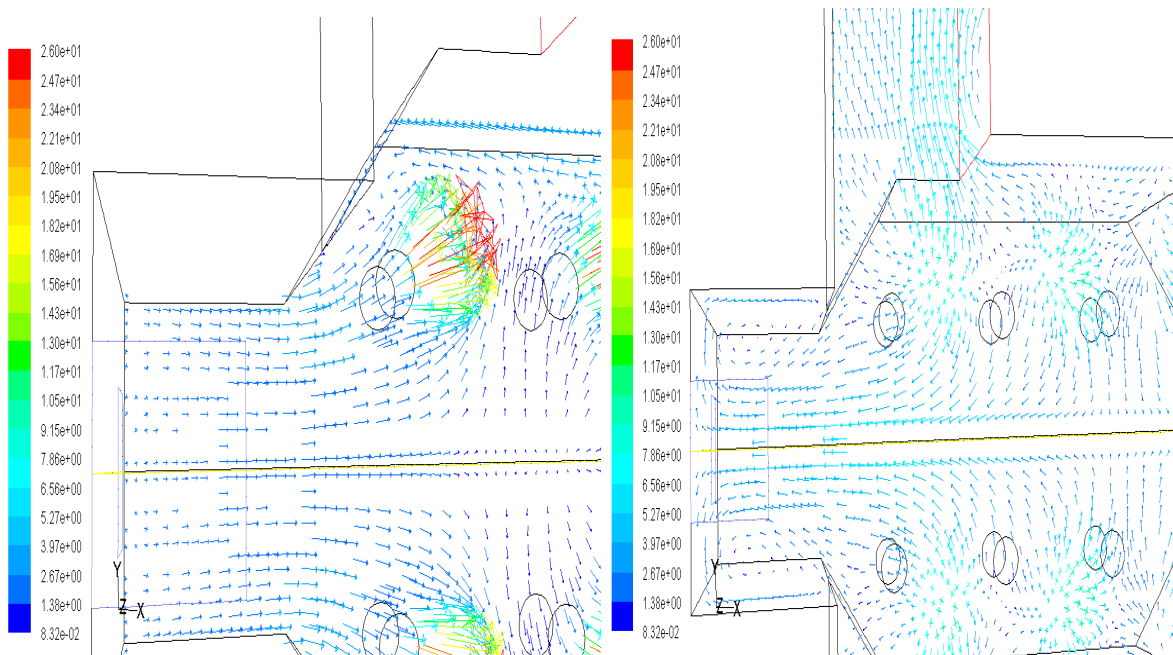


Figure 4 Velocity vectors at a) $z=0.2$ m (left) and b) $z=0.9$ m (right)

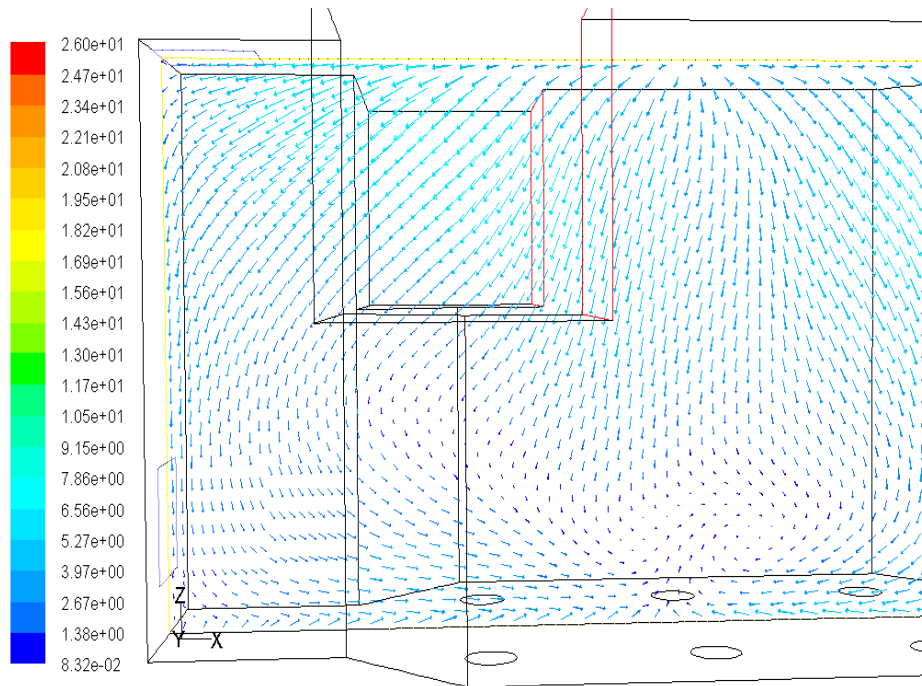


Figure 5 Velocity vectors in the plane of the burners

4. DISCRETE PARTICLES FLOW - BATCH FLOW SIMULATION

Batch flow has been simulated by a set of discrete particles with density of 2400 kg/m^3 . The incoming particles velocity for Top-Feeder has been chosen to be 6 m/s (corresponds to velocity of particle falling down from the height of 2 m). The incoming particles velocity for Side-Feeder has been chosen to be 0.1 m/s . The glass particles sizes are:

- 1) Silica: $0.074 \sim 0.25 \text{ mm}$
- 2) Limestone: $0.074 \sim 0.25 \text{ mm}$
- 3) Clay: $0.044 \sim 0.25 \text{ mm}$
- 4) Soda Ash: $0.149 \sim 0.595 \text{ mm}$

According to ranges above, the particles diameters of 0.05 , 0.1 , 0.2 , 0.3 , 0.4 , and 0.5 mm have been chosen for particles trajectories simulation.

The comparison of particles trajectories for Top-Feeder and Side-Feeder at the same diameter of particles is demonstrated below in Figure 6 to Figure 9.

According to those, all incoming particles reach the glass melt level for both Top-Feeder and Side-Feeder until their diameters are greater than 0.1 mm .

Particles of 0.1 mm diameter incoming through the Top-Feeder are split into two flows directed to sidewalls of the feed pocket, but finally they also reach the glass melt level (Figure 8a). For the side feeder, particles do reach the glass surface right away (Figure 8b).

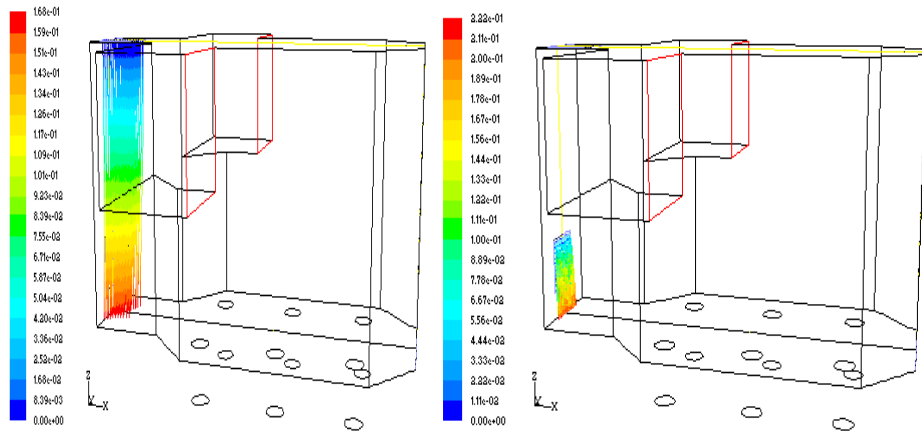


Figure 6 Trajectories and Residence times for 0.5 mm particle size a) top feeder (left) b) side feeder (right)

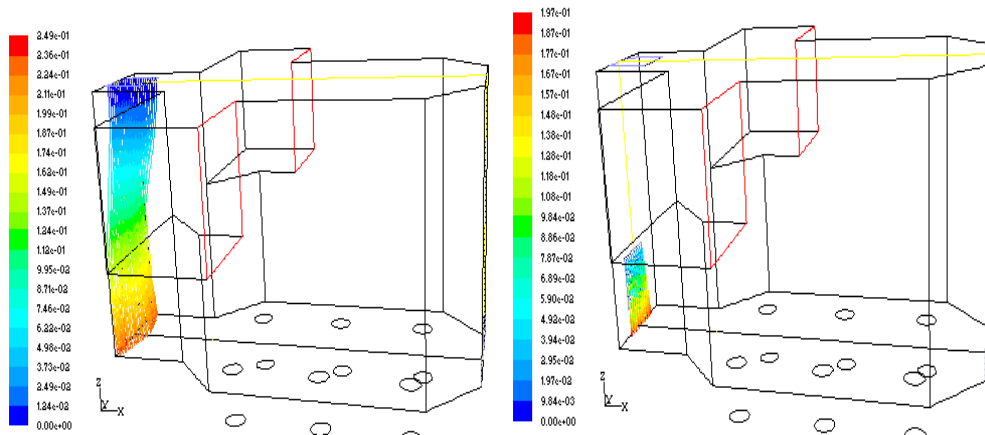


Figure 7 Trajectories and Residence times for 0.2 mm particle size a) top feeder (left) b) side feeder (right)

However, particles of 0.05 mm diameter incoming through the Top-Feeder is split into two flows directed to sidewalls of the feed pocket and to the exhaust (Figure 9a). This indicates that those small particles will be carried away.

According to the results obtained, there is a probability of carrying out smallest particles of silica, limestone, and clay in case of feeder located at the top of the melter. No problem is anticipated for the large particles (soda ash particles). Side feeder however does not exhibit such problems whatever the particles size.

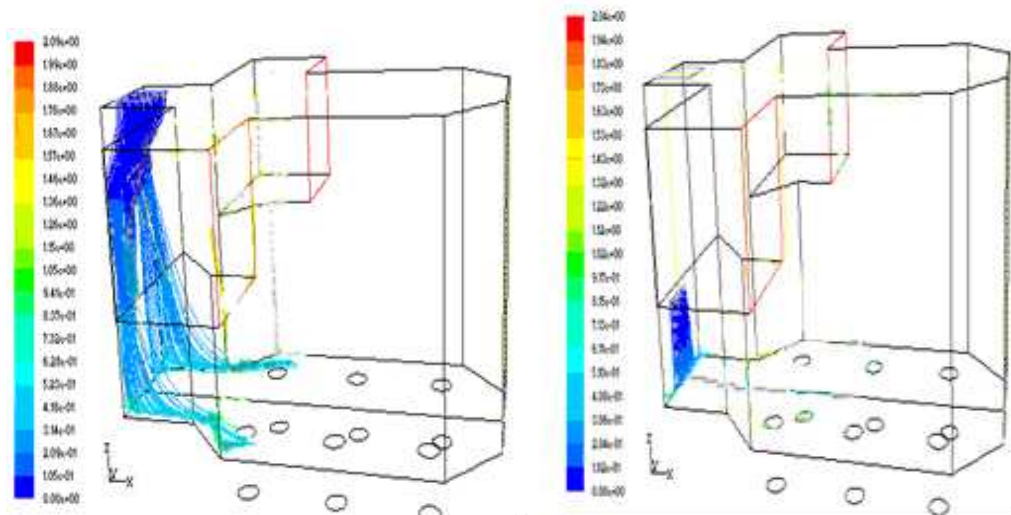


Figure 8 Trajectories and Residence times for 0.1 mm particle size a) top feeder (left) b) side feeder (right)

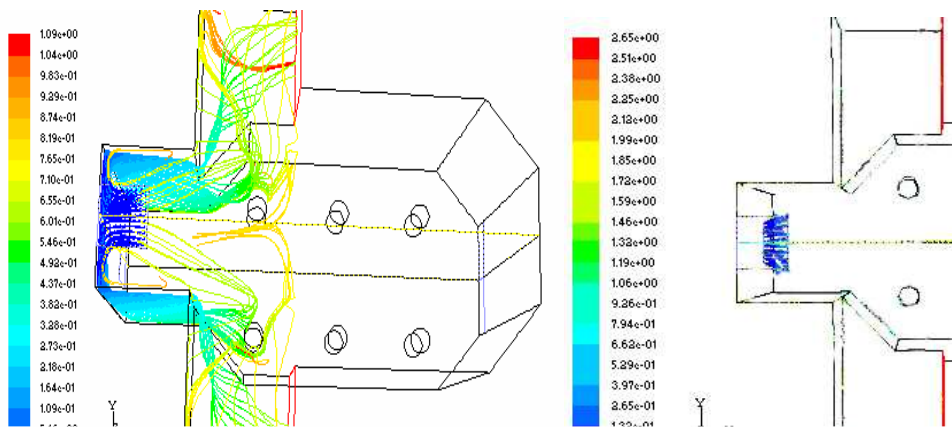


Figure 9 Trajectories and Residence times for 0.05 mm particle size top view a) top feeder (left) b) side feeder (right)

5. CONCLUSIONS

In this paper, we have analyzed the effect of the gases as they travel above the melt surface and specifically their influence on the batch particles that they might carry-over. While some carry-over is anticipated for the smallest particles in the case of a top feeder, no such problem is anticipated for a side feeder. This feature is helping in the design and operation of the submerged melter.

The very first trials the pilot melter at the Gas Technology Institute (GTI) seem to support the modeling approach exposed here and seem to validate its results. However, upcoming trials over the next few months will allow us to fully assess the model.

ACKNOWLEDGMENTS

The authors wishes to acknowledge the help of other consortium members: Aaron Huber (Johns Manville), Nic Leblond (Corning) and Carsten Weinhold (Schott), Lewis Collins, Raj Venuturumilli, Jaydepp Kulkarni (Ansys/Fluent) and the financial support of the US Departement of Energy.

REFERENCES

- Ansys/Fluent 3.0 Documentation & User's manual, Lebanon, NH(2006)
- Glass Melting Technology, A Technical and Economic Assessment, A project of the Glass Manufacturing Industry Council (GMIC), U.S Dept of energy ITP (2004)
- Olabin, V.M., Piro, L.S. Maximuk, A.B., Kinkhis, M. , Abbasi, H.A. *Submerged Combustion furnace for glass melts*. Ceram Eng. Sci. Proc., Vol .17, No 2, pp 84-92 (1996)
- Piro, L.S. Piro, I.L., Kostyuk, T.O., Soroka, B.S., Industrial Application of Submerged Combustion Melters, Kyiv Fact Publishers, (2006)
- Purnode, B.A., Venuturumilli, R, Kulkarni, J., Collins, R.L., Aronchik, G. *A Modeling study of the submerged combustion melting process*, Submitted to Proc. XXI International Congress on Glass, Strasbourg, France(2007)

THE INFLUENCE OF GLASS FLOW CHARACTER ON BUBBLE REMOVAL IN HORIZONTAL CHANNELS

Petra Cincibusová, Lubomír Němec, Marcela Jebavá
Laboratory of Inorganic Materials, Joint Workplace of the Institute of Chemical
Technology Prague, Technická 5, Prague 6 and the Institute of Inorganic Chemistry AS CR,
Řež, Czech Republic

E-mail: Lubomir.Nemec@vscht.cz, Petra.Cincibusova@vscht.cz, Marcela.Jebava@vscht.cz

Keywords: Glass melt, Fining channel, Fining efficiency, Growing bubbles, Plug flow,
Temperature gradients, Circulation flow

Abstract

This paper deals with removal of single bubbles in horizontal channels with different character of glass flow. The fining performance of the channel producing no bubble defects is the followed technological quantity. The glass for production of TV bulbs has been used as the model glass. The experimentally measured bubble growth rates were used to evaluate the fining process. To appreciate the impact of glass flow character in a given channel on the fining efficiency, the relations valid for the process in channels with plug flow [1] were used and the numerical model was applied. The results have shown existence of relation between the fining performance and the fraction of dead space in channels with longitudinal circulative flow and between the fining performance and the average angular velocity of rotating melt in channels with transversal circulative flow.

INTRODUCTION

The entire glass melting process may be classified into several partial processes: batch heating and chemical reactions in the batch, dissolution of batch particles, as well as chemical inhomogeneities, and bubble removal. The last two processes are usually evaluated from the point of view of the energy consumption and the melting or fining performance. Unfortunately, determined optimal conditions for these processes are not always identical. For that reason the separation of both processes is an acceptable way to progressive melting facility design. This paper deals only with the bubble removal process, which is influenced by these factors:

- temperature ensuring activity of the refining agent
- glass composition (refining agent concentration, redox state of glass)
- reduced pressure
- glass flow character
- additional forces (ultrasonic, centrifugal, microwave)

The aim of this work is to find out the influence of glass flow character on bubble removal from glass melts in a horizontal channel. Followed quantity was the fining performance of the space (glass melt flow rate at which none of bubbles leave the channel). The given glass melt flow characters were obtained by application of different temperature distributions in

channels. In this work, there was investigated the influence of following types of linear temperature gradients put on the glass level:

1. zero temperature gradient (isothermal channel)
2. vertical temperature gradient (higher temperature on the glass level)
3. horizontal longitudinal temperature gradient (higher temp. at the input to the channel)
4. reversed horizontal longitudinal temperature gradient (lower temp. at the input to the channel)
5. transversal temperature gradient
6. mixed horizontal temperature gradients (both longitudinal and transversal temp. grad.)

CALCULATIONS

Calculations were carried out in the simple model space with length $l = 1 \text{ m}$, depth $h = 0.5 \text{ m}$ and width $w = 0.5 \text{ m}$.

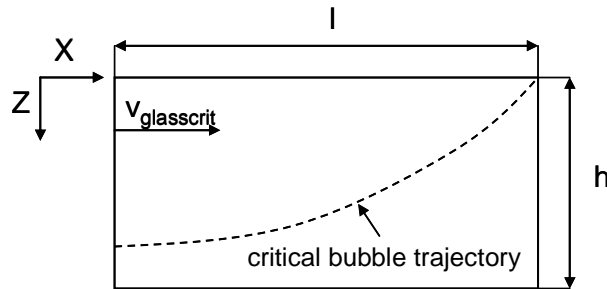


Fig. 1: The motion of the critical bubble in the horizontal channel.

Glass for production of TV bulbs was used as a model glass. This glass is characterized by following properties:

$$\rho = 2790 - 0.2378T \text{ (teplota v K)}; [kg / m^3]$$

$$\eta = \rho \exp[-11.501 + 6144.6 / (T - 710.64)]; [Pa \cdot s]$$

The experimentally measured dependence of the bubble growth rate on temperature in K, approximated by the following polynomial equation, was used for computation [3]:

$$\dot{a} = 5.758E - 14T^3 - 2.654E - 10T^2 + 4.076E - 7T - 2.086E - 4; [m / s]$$

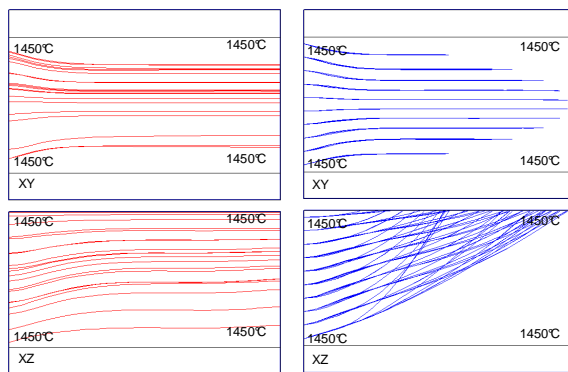
The initial bubble radius was $a_0 = 5E - 5 \text{ m}$, which corresponds to the anticipated radius of the smallest (critical) bubbles in a complex. The average glass melt temperature was kept at approximately 1450°C . The numerical model *Glass Model* was used for computation of the glass melt temperature and velocity distributions and also for the illustration of bubble and massless particle paths in the channel [2].

The computation procedure

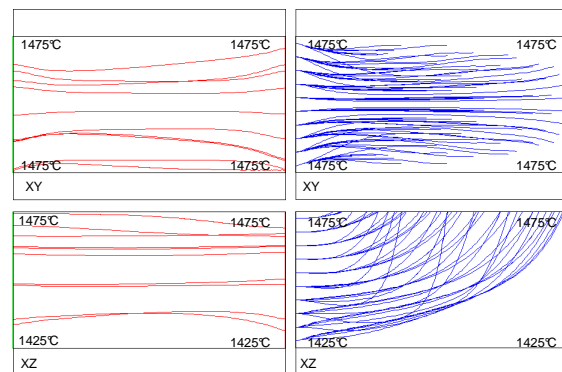
The glass melt flow structure was created by application of appropriate boundary conditions (temperature gradients). After the calculation of temperature and velocity distributions in the glass melt, one thousand bubbles were input across the entry profile to the channel. These bubbles were then tracked through the channel. The pull out of the channel was subsequently varied till the bubble on the critical trajectory left the melt just before leaving the channel (Fig. 1). The average glass melt residence time and fraction of the dead space or the average angular velocity of rotating melt were then calculated.

RESULTS AND DISCUSSION

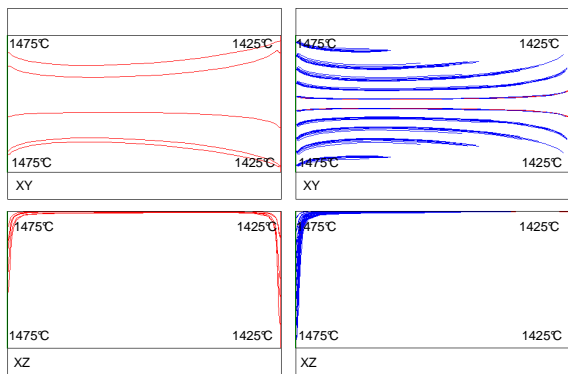
Selected trajectories of massless particles and bubbles in projections XY and XZ in horizontal channels with different temperature gradients are presented in Figures 2 - 7.



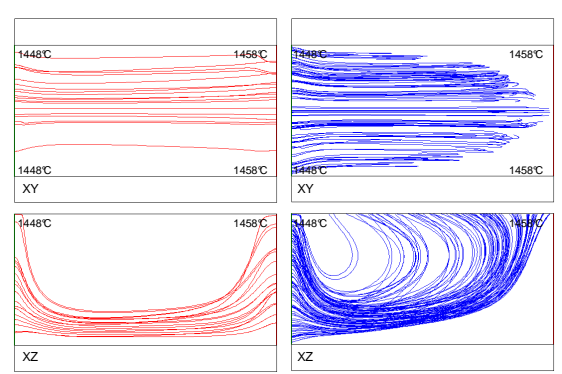
a) **Fig. 2:** Horizontal isothermal channel
a) massless particles trajectories
b) bubbles trajectories



a) **Fig. 3:** Horizontal channel with vertical temp. grad. 100°C/m: a) massless particles trajectories
b) bubbles trajectories



a) **Fig. 4:** Horizontal channel with longitudinal temp. grad. 50°C/m: a) massless particles trajectories
b) bubbles trajectories



a) **Fig. 5:** Horizont. channel with reversed long.temp.grad. 10°C/m: a) massless particles trajectories
b) bubbles trajectories

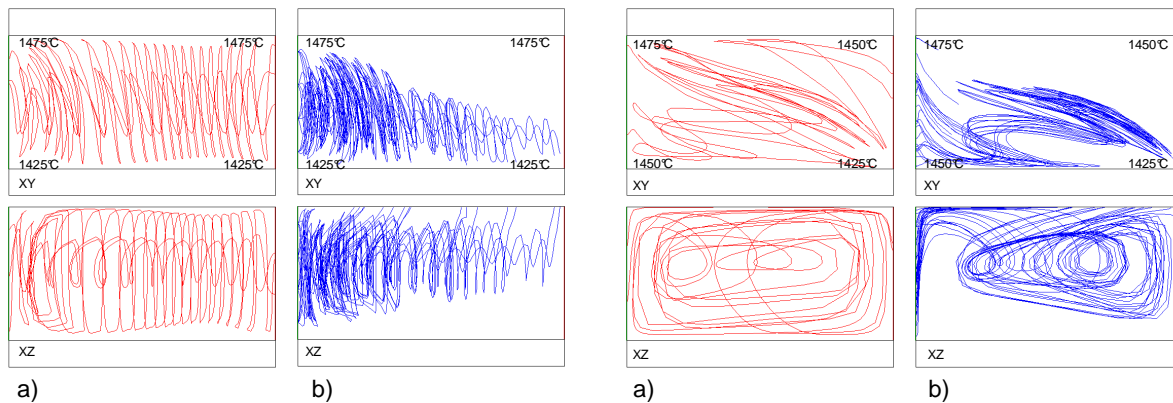


Fig. 6: Horizontal channel with transversal temp. grad. 100°C/m: a) massless particles trajectories
b) bubbles trajectories

Fig. 7: Horizontal channel with mixed temp. grad. 25°C/m (longitudinal) and 50°C/m (transversal):
a) massless particles trajectories
b) bubbles trajectories

1. The horizontal isothermal channel

The fining performance of the horizontal isothermal channel can be calculated according to the analytical equation [4, equation (5)] or numerically. The critical starting point of entering bubbles is approximately in the third of channel depth (Fig. 2). The isothermal channel has the highest fining performance in comparison with non-isothermal channels but achievement of the strictly homogenous temperature distribution is technically difficult.

2. The influence of vertical temperature gradient

The typical massless particle and bubble trajectories are presented in Figure 3. In Figure 8 there is plotted the dependence of the critical fining performance and the vertical temperature gradient. The values were calculated according to the equation given in the reference [4, equation (15)]. The fining performance decreases with increasing vertical temperature gradient, although - at the same average temperature - temperature on the glass surface increases. The low temperature gradients are acceptable because the decrease of fining performance is not too steep in this region. The critical bubbles come from the bottom of the channel, where is located the area of lowest temperatures.

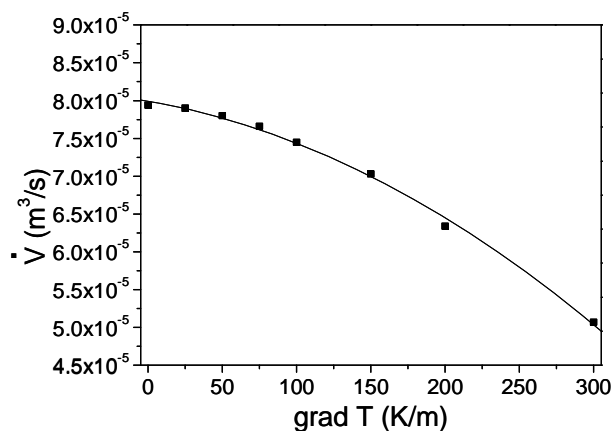


Fig. 8: The dependence of the channel fining performance and the vertical temperature gradient.

3. The influence of the horizontal longitudinal temperature gradient

The massless particle and bubble trajectories are presented in Figure 4. The utilization of the channel space for glass flow influences significantly the bubble removal from the channel. The decrease in the active space leads to shorter average residence times of the melt in the channel and decreases the channel fining performance. Consequently, the longitudinal temperature gradient applied in Fig. 4 is unsuitable for the bubble removal process. The fining performance of the channel with longitudinal temperature gradient is dependent on the dead space fraction according to the derived equation [4]:

$$\dot{V}_m = \dot{V}_{plug} \cdot K(1-m)^{2/3}; \quad (1)$$

$K = 1$one circle

$K = 0.5$two circles

m – fraction of the dead space

\dot{V}_{plug} - fining performance of the channel with plug flow

In Figure 9, there is plotted dependence of fining performance on the fraction of dead space in channels with different longitudinal temperature gradients. The dependence was calculated according to the equation (1). The points in this graph were obtained from the numerical model. It is obvious that equation (1) is in a good agreement with results obtained from the numerical model.

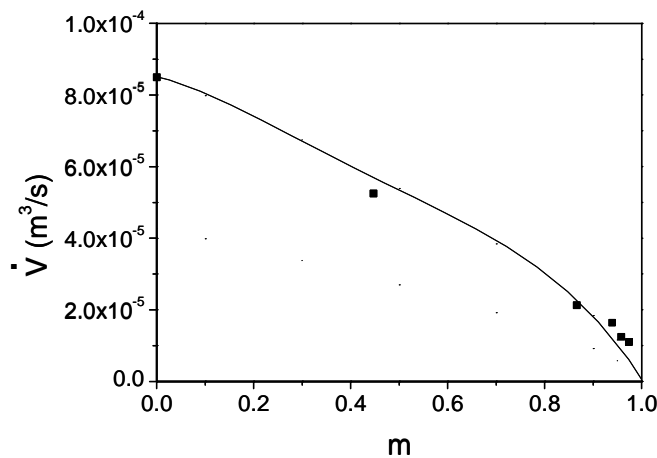


Fig. 9: The dependence of the channel fining performance on the longitudinal temperature gradient.

4. The influence of the reversed longitudinal temperature gradient

The longitudinal temperature gradients with higher temperature at the exit from the channel evoke as well longitudinal glass circulation but the direction of the close to level flow is opposite to the main glass flow. The typical massless particle and bubble trajectories are presented in Figure 5. The dependence between the fining efficiency of the channel and the reversed longitudinal temperature gradient is plotted in Figure 10. The role of the fraction of dead space is not so ultimate in comparison with the previous case.

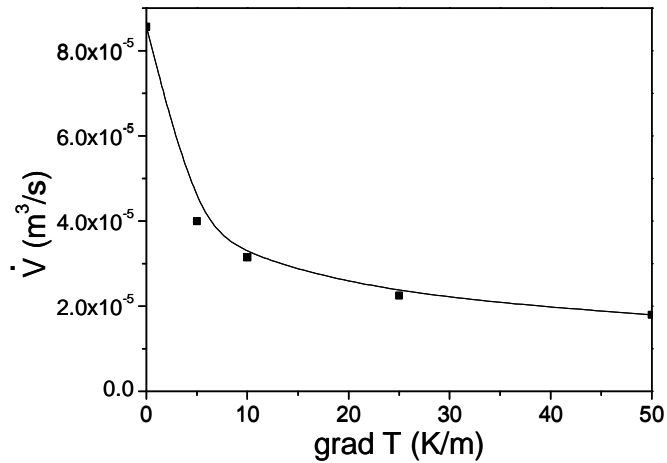


Fig. 10: The dependence of the fining performance and the reversed longitudinal temperature gradient.

5. The influence of the horizontal transversal temperature gradient

The spaces with the transversal temperature gradient exhibit low fraction of dead space. That is why another quantity characterizing glass flow should determine the fining performance. The glass melt flow has a spiral character in the case of transversal temperature gradient (Fig. 6) and with increasing transversal temperature gradient increases the intensity of glass melt flow and decreases fining performance of the channel (see Fig. 11).

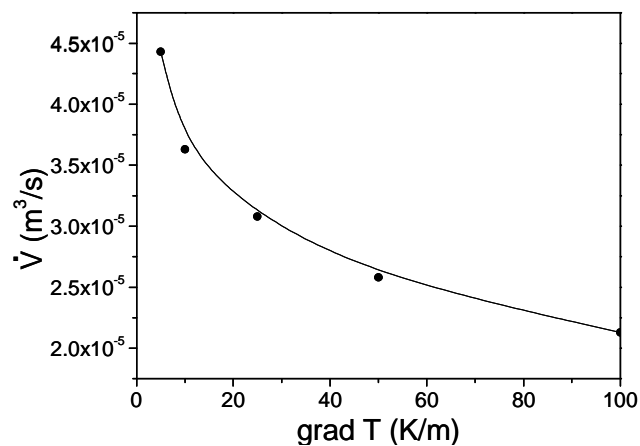


Fig. 11: The dependence of the channel fining performance and the transversal temperature gradient.

Critical bubbles circumscribe spiral trajectories with different rotation centre than has the glass melt (Fig. 12). The bubble movement is caused by the combination of the buoyancy force and the spiral flow of glass melt. The critical bubble is moving in the downward melt flow. In the left part of its spiral trajectory, the bubble upward velocity is higher than the downward velocity of glass melt and in the right part is the bubble upward velocity lower than the melt downward velocity. This fact brings about bubble circulation. If the bubble radius grows, the radius of the circle trajectory grows too and trajectories are shifted to the right. Finally bubble leaves its trajectory due to the buoyancy force and reaches glass surface.

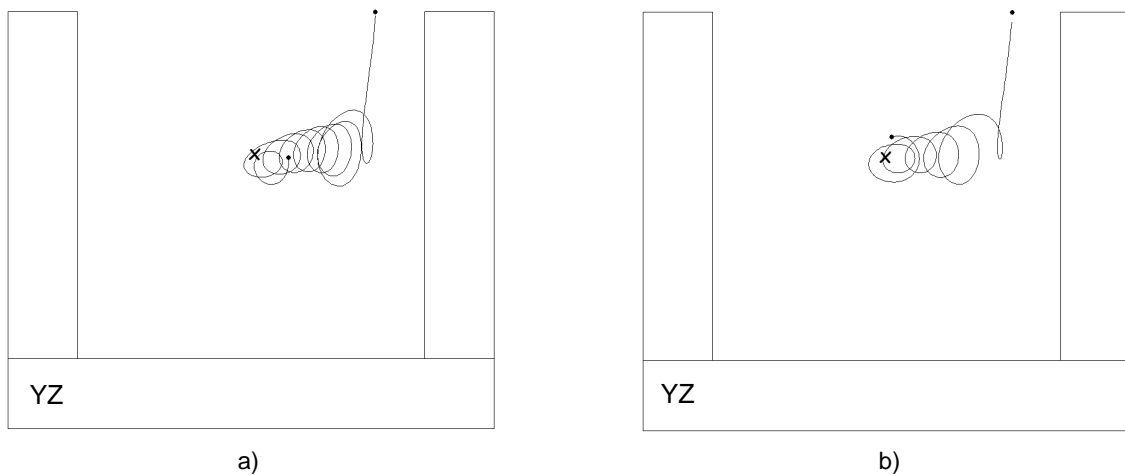


Fig. 12: The XZ projections of the critical bubble trajectories in the channel with the transversal temperature gradients a) grad $t = 50^\circ\text{C}/\text{m}$, b) grad $t = 25^\circ\text{C}/\text{m}$

The efficiency of the bubble removal process in the mentioned case is determined by the average angular velocity of rotating glass melt. In Figure 13, there is plotted the dependence between the fining performance and average angular velocity of rotating melt fitting the semiempirical equation:

$$\dot{V}_{\bar{\omega}} = 6E - 5 \exp(-100\bar{\omega}); \quad (2)$$

Where $6E-5$ is the fining performance of the isothermal channel.

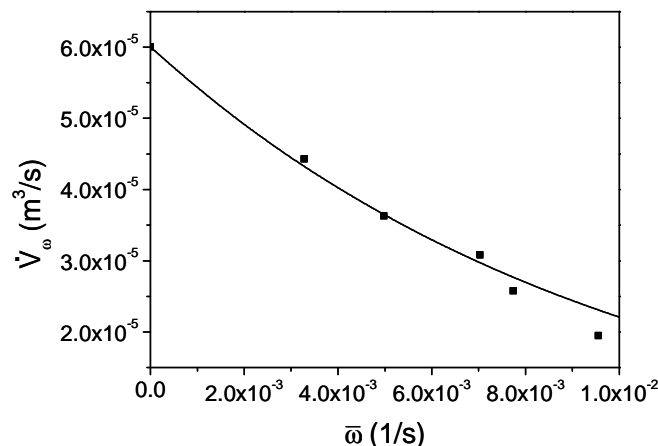


Fig. 13: The dependence of the channel fining performance on the average angular velocity of rotating melt.

The points in the graph of Figure 13 were obtained by the numerical model. It is obvious that the equation (2) is in good agreement with results obtained from the numerical model.

6. The influence of the mixed horizontal gradients

The mixed temperature gradients (both longitudinal and transversal) evoke complicated spiral glass melt flow and bubble trajectories are dependent on the ratio between the value of transversal and longitudinal temperature gradient. The typical massless particle and bubble paths are presented in Figure 7.

The dependence of the fining performance on the different types of temperature gradients is shown in Figure 14. The longitudinal temperature gradients are there plotted on the axis x and transversal temperature gradients are plotted on the axis y. When $y = 0$, only longitudinal gradients and when $x = 0$ only transversal gradients are present.

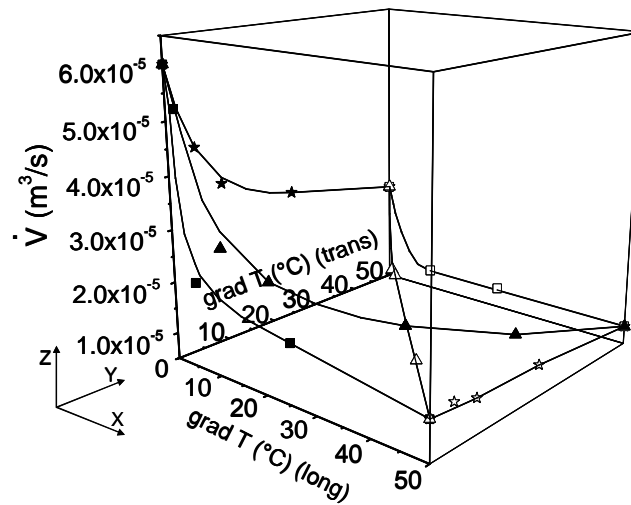


Fig. 14: The overall dependence of the channel fining performance on the different types of temperature gradients.

The longitudinal temperature gradient markedly decreases the fining performance of the channel. The unfavorable influence of the transversal temperature gradient is less significant. The resulting fining performance depends on both the fraction of dead space and the angular velocity of transversal flow.

If the mixed temperature gradients with the horizontal gradient, characterized by higher temperature at the channel exit are applied, the refining performance is by about 50 % higher than presents Figure 14. The most probable reason of the beneficial behavior is better utilization of the channel volume for the bubble removal. Figure 15 presents the dependence between the channel fining performances and both types of mixed temperature gradients. The applied combinations of gradients involve always equal values of longitudinal and transversal temperature gradients.

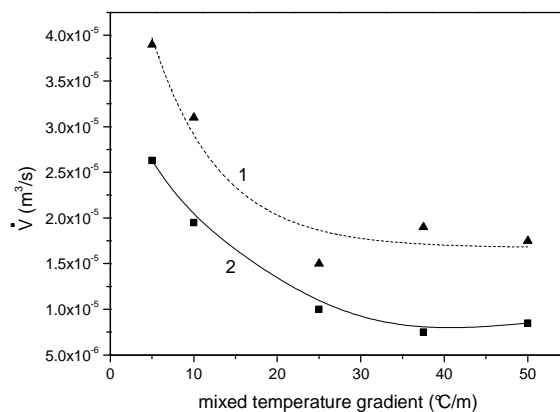


Figure 15: The dependence between the fining performance of the horizontal channel and the value of the mixed temperature gradient (the longitudinal and transversal temperature gradient in given case are equal).

- 1- the longitudinal temperature gradient with higher temperature at the channel input
- 2- the longitudinal temperature gradient with higher temperature at the channel output

The obtained relations ask for a theoretical explanation in terms of glass flow character and the fraction of space utilized for the process.

CONCLUSION

The influence of glass melt flow character on bubble removal was investigated. The fining performance of the channel producing no bubble defects is the followed technological quantity. The computation was realized in the simple model space. The glass for production of TV bulbs has been used as the model glass. The glass melt flow structure was created by application of linear different temperature gradients. The numerical model *Glass Model* was used for computation of the melt temperature and velocity distributions and also for the illustration of bubble and massless particle paths in the channel. The results have shown that the isothermal channel has the highest fining performance in comparison with non-isothermal cases. Low vertical temperature gradients are acceptable for efficient bubble removal process if the average melt temperature is kept on the same value. The longitudinal temperature gradient with higher temperature at the channel input is unsuitable for bubble removal process because of low fraction of the space utilized for the fining process. The role of the fraction of dead space in channel with reversed longitudinal temperature gradient is less unfavorable in comparison with the previous mentioned case. The characteristic quantity of the transversal flow is the average angular velocity of glass, determining the behavior of critical bubbles. The resulting fining performance of the channel with mixed horizontal temperature gradients is probably dependent on both the fraction of the dead space and the angular velocity of rotating melt. The presented results are useful for setting up the optimum temperature conditions in model fining spaces working under action of gravitational force. The establishment of simple relations between the fining performance and the character of the glass melt flow is a useful tool when the new fining spaces are to be designed.

ACKNOWLEDGEMENT

This work was a part the project No 2A-1TP1/063, "New glass and ceramic materials and advanced concepts of their preparation and manufacturing", realized under financial support of the Ministry of Industry and Trade.

REFERENCES

1. Němec, L., Jebavá, M., Tonarová, V.: Glass melting analysis and new melting arrangements. Proceedings of the VIII International Seminar on Mathematical Modeling and Advanced Numerical Methods in Furnace Design and Operation, May 19-20, 2005, Velké Karlovice, CR, p. 24-47.
2. Schill, P: Models of glass melting furnaces. Proceedings of the II. International Seminar on Mathematical Simulation in the Glass Melting, (1993), pp. 102-116.
3. Unpublished results.
4. Němec, L., Jebavá, M., Cincibusová, P.: The Removal of Bubbles from Glass Melts in Horizontal or Vertical Channels with Different Glass Flow Patterns, *Ceramics-Silikáty* 50 (2006), no. 3, p. 140-152

THE BUBBLE REMOVAL FROM GLASS MELTS IN A ROTATING CYLINDER

Vladislava Tonarová, Lubomír Němec, Marcela Jebavá
Laboratory of Inorganic Materials, Joint Workplace of the
Institute of Chemical Technology Prague,
Technická 5, 166 28 Prague 6, and the Institute of Inorganic Chemistry AS CR, 250 68
Řež, Czech Republic

E-mail: Vladislava.Tonarova@vscht.cz, Lubomir.Nemec@vscht.cz,
Marcela.Jebava@vscht.cz

Keywords: Glass melt, fining cylinder, fining time, centrifugal force

Abstract

The goal of this work is to present results of the mathematical modeling of bubble behaviour in the centrifugal field. The multicomponent bubbles were examined under different conditions. The effect of the cylinder rotation velocity, the degree of its filling by the melt, the cylinder radius, temperature, the bubble size and the bubble initial position in the cylinder on the bubble removal time were studied. The results show, that the bubble removal under effect of centrifugal force is a complicated process affected by several mutually contradicting factors. The most problematical is the removal of the small bubbles having size under 0.2mm. The very small bubbles are completely dissolved in the melt, but the complete dissolution is a slow process. The searching for optimum conditions of the centrifugal fining needs to get rid of small bubbles by melt pretreating or to inhibit the bubble partial dissolution at higher rotation velocities.

INTRODUCTION

Bubbles are removed from glass melts mostly by a separation process based on the different density of glass and bubbles. Alternative mechanism - removing multicomponent bubbles by dissolution - requires extremely low concentrations of gases in the melt, their high solubility in melt or high pressures. Glass melts are however saturated by gases coming from the decomposition of raw materials and consequently, bubble growth during the melting process is preferred before their dissolution. That is why refining agents are added into glass batch or lowered pressure is applied to promote bubble growth. The external force separating bubbles from melt is naturally the buoyancy force of the gravitational field which may be supported by bubble growth due to refining agents, by glass saturation by rapidly diffusing gases /1/ or by reduced pressure /2-4/. However, also supersonic waves /5/, surface forces and centrifugal force may be used to evoke or accelerate the bubble separation rate. The potentially feasible arrangement of the refining in the centrifugal field assumes treating the glass melt in a rotating cylinder under proper temperature and melt flow regime. The effect of both gravitational and centrifugal forces influences however the pressure inside of the melt and consequently, the bubble growth or dissolution in the melt is affected. The goal of this paper is to present fundamental equations and calculation results of bubble behavior in a rotating cylinder,

involving multicomponent bubbles under simultaneous effect of gravitational and centrifugal fields and discontinuous melting regime.

THEORETICAL

Under effect of the gravitational field only, the bubble will move upwards. When applying the centrifugal force by space rotation, the pressure inside the bubble abruptly increases and the bubble starts to move to the rotation centre. Some gases diffuse out of the bubble and the both pressure and diffusion effects cause the bubble decreases in size. The bubble partial shrinking slows down its separation to the centre. The pressure due to centrifugal force releases during bubble wandering to the centre or curved glass level, the gas dissolution from the bubble eventually stops and the separation effect of the centrifugal force undergoes a complicated dependence as a function of the radial distance. The separation effects are therefore influenced by both the fact that bubble is compressible and that gases may diffuse between the bubble and melt. At isothermal conditions, the radius change of a bubble in a rotating cylinder is governed by equation:

$$\begin{aligned} \frac{da}{d\tau} = & -\frac{2g^2\rho^2a^3}{27\eta\left(p_{ex} + \rho gh' + \frac{\rho\omega^2(r^2 - r_h^2)}{2} + 4\sigma/3a\right)} + \frac{2\omega^4r^2\rho^2a^3}{27\eta\left(p_{ex} + \rho gh' + \frac{\rho\omega^2(r^2 - r_h^2)}{2} + 4\sigma/3a\right)} + \\ & + \frac{RT}{\left(p_{ex} + \rho gh' + \frac{\rho\omega^2(r^2 - r_h^2)}{2} + 4\sigma/3a\right)} \sum_{i=1}^n \frac{k_i}{M_i} (c_{ib} - c_{ia}) \end{aligned} \quad (1)$$

And for pressure of the i -th gas inside the bubble holds:

$$\frac{dp_i}{d\tau} = \frac{3RT}{M_i a} k_i (c_{ib} - c_{ia}) - \frac{3p_i}{a} \frac{da}{d\tau} \quad (2)$$

The total pressure inside of a bubble is given by:

$$p_t = p_{ex} + \rho gh' + \frac{\rho\omega^2(r^2 - r_h^2)}{2} + \frac{2\sigma}{a} \quad (3)$$

And bubble vertical and radial velocities describe equations:

$$v_h = \frac{dh'}{d\tau} = -\frac{2g\rho a^2}{9\eta}; \quad v_r = \frac{dr}{d\tau} = -\frac{2\omega^2 r \rho a^2}{9\eta}$$

(4a,b)

Where a is the bubble radius, τ is time, ρ and η are the glass density and viscosity, p_{ex} is the external pressure, h' is the depth of the bubble under glass level, σ is the surface tension of glass, ω is the angle velocity of the rotating cylinder, r is the bubble radial distance, k_i is the

mass transfer coefficient of the i -th gas, c_{ib} and c_{ia} are the bulk and bubble surface concentrations of the i -th gas in glass, r_h is the radial coordinate of the curved glass level in the depth h below the cylinder top (the cylinder is only partially filled by glass).

The following expression was applied for the mass transfer coefficient:

$$k_i = \frac{D_i}{2a} \left[1 + \left(1 + \frac{4\rho a^3}{9\eta D_i} (g^2 + \omega^4 r^2)^{1/2} \right)^{1/3} \right] \quad (5)$$

When deriving equation (1), the derivative $\frac{dr_h}{d\tau}$ was neglected against $\frac{dr}{d\tau}$.

The question of the optimum cylinder radius arises when starting calculations of bubble behavior in a concrete case. The value may be estimated from the course of the bubble radial velocity between the bubble starting position and cylinder centre (or glass curved level). If the bubble does not react with glass and its initial radius is expressed from the equation of the ideal gas, the bubble radial velocity at radial distance r is:

$$v_r = \frac{8.55E - 2\rho(nRT)^{2/3}}{\eta} \left[\frac{\omega^2 r}{(p_{ex} + \rho\omega^2(r^2 - r_h^2)/2)^{2/3}} \right] \quad (6)$$

Where n is the number of mols of gases in the bubble. In equation (6), the hydrostatic pressure and the member $2\sigma/a$ are neglected in the total pressure term. Equation (6) shows that the bubble radial velocity steadily grows with the angle velocity ω but the dependence on the radial distance may exhibits maximum at the value of r :

$$r(v_{r\max}) = \left[\frac{6(p_{ex} - \rho\omega^2 r_h^2 / 2)}{\rho\omega^2} \right]^{1/2} \quad (7)$$

As the bubble rises during its separation, the value of r_h slightly changes with the bubble position, therefore equations (6-7) are applicable for constant r_h only when $|v_h| \ll |v_r|$ or $\omega \gg 0$.

For the cylinder completely filled by glass then $r(v_{r\max}) = \left(\frac{6p_{ex}}{\rho\omega^2} \right)^{1/2}$, i.e. the maximum of the

bubble radial velocity always exists and its position, independent from the cylinder radius and the initial bubble radius, shifts to the cylinder centre if the external pressure decreases or the angle velocity increases. Figure 1 presents the dependence between the bubble radial velocity and the bubble radial position for different cylinder angle velocities and Figure 2 the dependence between the position of the maximum bubble radial velocity and the cylinder angle velocity for the bubble having the initial radius $3E-4m$ and located in the glass for production of TV bulbs. Obviously is the position of the maximum between about 0.1-0.3m

for the cylinder angle velocities 50-200s⁻¹, intended for calculations. Consequently, the cylinder having radius $R_0 = 0.25m$ was chosen for calculations.

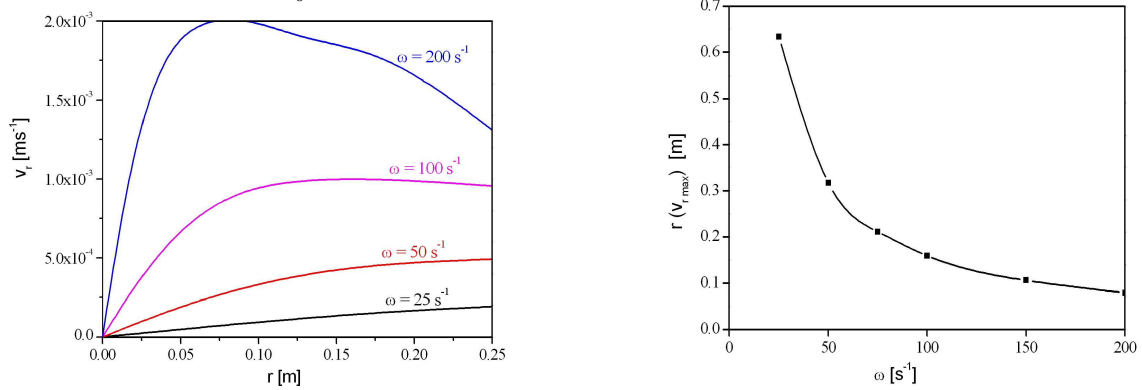


Figure 1 (left): The dependence between the bubble radial velocity and bubble radial position for different ω . The cylinder is completely filled by glass. The bubble radius is 3E-4m, the glass for production of TV bulbs at 1300°C.

Figure 2 (right): The dependence between the radial coordinate of the maximum bubble radial velocity and the cylinder angle velocity.

If the cylinder is only partially filled by glass, the values of both v_r and $r(v_{r_{max}})$ are defined only when $r > r_h$. The maximum value of v_r is formally defined for $p_{ex} > \rho\omega^2 r_h^2 / 2$ but has physical meaning only when $r(v_{r_{max}}) > r_h$ (see Fig. 3 where the maximum exists for $r(v_{r_{max}}) > R_0$). If the inequality is not valid, the radial velocity attains its maximum at the curved glass level (see Fig. 4). The bubble radial velocities in partially filled cylinders are higher than in the filled ones and the difference grows as ω grows too. This is obvious from Figures 3 and 4. Generally, the bubble radial velocities are higher in partially filled cylinders because the denominator in equation (6) gains lower value ($r_h > 0$), i.e. pressure in the partially filled cylinder is lower than in the completely filled one. As ω grows, the ratio between numerator and denominator grows too and the bubble radial velocity attains higher value. The partially filled cylinders appears therefore more convenient, particularly at high ω , despite the volume of refined glass is lower. The question of proper radius of partially filled cylinder may be assessed from bubble radial velocities on the curved glass level ($r = r_h$). Applying equation (6) for two cylinders with different radii and under otherwise identical conditions at $r = r_h$, the ratio between both radial velocities is given by $v_{r1} / v_{r2} = r_{h1} / r_{h2}$, i.e. the bubble radial velocity at r_h is linearly dependent on this radial distance. The partially filled cylinders with greater radius appear thus more efficient. This holds despite the fact that the bubble radial velocity in the cylinder with greater radius exhibits a steeper decrease towards the cylinder mantel,

compared to the smaller cylinder. These facts are depicted in Figure 5 for cylinders having radii 0.25 and 0.5m.

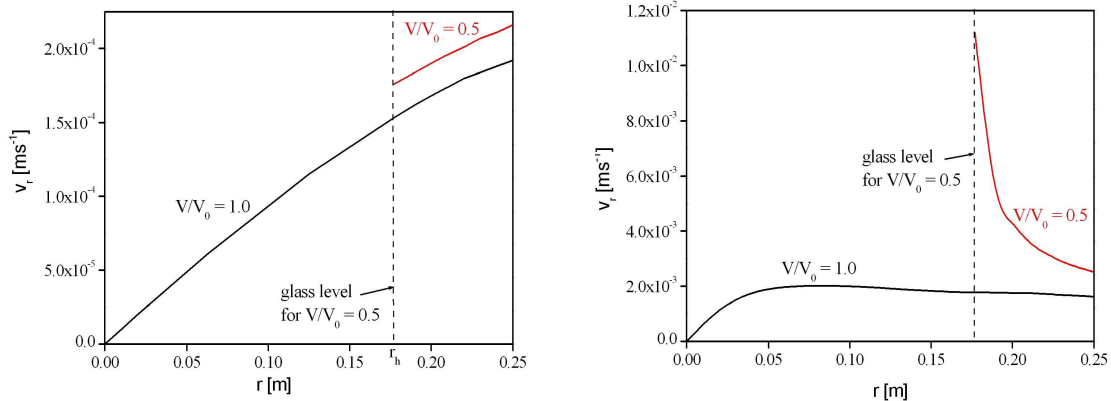


Figure 3 (left): The course of the bubble radial velocity as a function of radial distance for the cylinder completely filled by glass ($V/V_0 = 1$) and half filled by glass ($V/V_0 = 0.5$) at $\omega = 25s^{-1}$. Figure 4 (right): The course of the bubble radial velocity as a function of radial distance for the cylinder completely filled by glass ($V/V_0 = 1$) and half filled by glass ($V/V_0 = 0.5$) at $\omega = 200s^{-1}$. The same glass, temperature and bubble size as in Figs. 1-2.

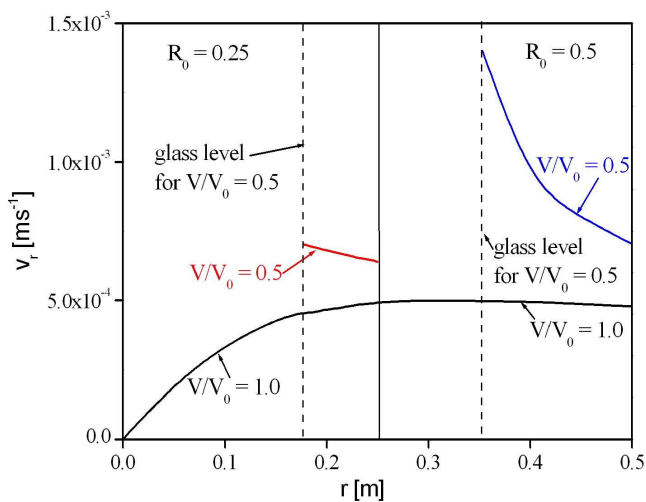


Figure 5: The courses bubble radial velocities as a function of radial distance for cylinders having radius 0.25 and 0.5m. The dependence is common for the completely filled cylinders. The bubble radius is 3E-4m, model glass for production of TV bulbs, $\omega=50s^{-1}$, $V/V_0=0.5$.

The bubble gas content changes however with time because some gases may dissolve in the melt or diffuse into bubbles. The bubble dissolution resulting in low bubble radial velocities is supported by high cylinder rotation velocities, by the presence of gas easily soluble in melt and by long bubble residence times in glass. That is why lower rotation velocities appear more convenient for high temperatures and glasses containing refining agents (the centrifugal force is weak but bubble do not contract or even grow) and higher rotation velocities are suitable for lower temperatures (the centrifugal force is strong and bubble contraction is low due to low content of refining gas in bubbles). If the bubble

dissolution sets at given temperature, the separation of small bubbles is logically difficult due to their additional contraction by gas diffusion.

CALCULATION CONDITIONS

The glass for TV bulbs was applied as a model glass. The glass and gas properties needed to model the bubble behavior are summarized in [6]. The following parameters were examined:

a_0 ($a_0 \in \langle 1E-4; 6E-4 \rangle m; a_0 = 5E-5m$), r_0 ($r_0 = 0.20; 0.225$ and $0.25m$), ω ($\omega = 10, 25, 50, 100, 200s^{-1}$), t ($t = 1300, 1400, 1500^\circ C$), V/V_0 ($V/V_0 = 1; 0.75; 0.5$), R_0 ($R_0 = 0.25, 0.375, 0.5m$), h_0 ($h_0 = 0.5m$).

Where a_0 is the initial bubble radius, r_0 is the initial radial position of the bubble, ω is the cylinder angle velocity, t is temperature, V_0 and V are the cylinder volume and the volume of glass melt in the cylinder, R_0 is the cylinder radius and h_0 is the height of the rotating cylinder. As the standard calculation, the following conditions were chosen: $\omega=50s^{-1}$, $V/V_0=0.5$, $R_0=r_0=0.25m$, $t=1300, 1400, 1500^\circ C$, $a_0 \in \langle 5E-5m; 6E-4m \rangle$. The standard gas was oxygen, carbon dioxide and bubbles containing oxygen, CO_2 , water vapour, N_2 and small amount of argon.

RESULTS AND THEIR DISCUSSION

In the first run of experiments, the behavior of one-component bubbles was followed, namely oxygen bubbles and carbon dioxide bubbles, the former gas represented easily soluble and the latter one the hardly soluble gas in the melt. The typical courses of the oxygen bubble wandering in the form of radial distance versus time are shown in Fig. 6a,b. Only bubbles of considered initial radii $1E-4m$ and $5E-4m$ are plotted in the figure. The two grey horizontal bands in the figure 6a correspond to the radial interval of potential glass levels at $V/V_0=0.5$ and $V/V_0=0.75$. When applying the partial filling the cylinder by glass, the bubble is separated from the melt when reaching its proper position in the grey band, dependent on its initial depth under parabolic glass level. The asterisks in the figure denote the bubble dissolution. The slowing down of the bubble movement towards the cylinder centre is obvious during later stages. This is brought about by decreasing effect of the centrifugal force. Therefore the partial filling of the cylinder by the melt appears to be a good precondition for an effective bubble separation. The almost linear dissolution of small oxygen bubbles is obvious from the right figure 6b whereas bigger bubbles grow due to a pressure decrease inside them. The CO_2 bubbles exhibited a partially different behavior. The CO_2 gas has only a limited solubility

in the melt and the rate of its diffusion is simultaneously restricted by low values of its diffusion coefficient in the melt.

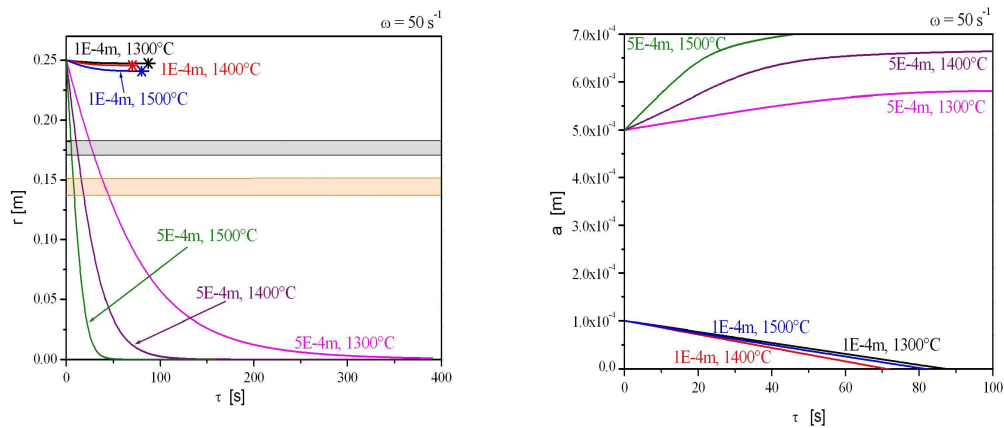


Figure 6a,b: The typical courses of bubble radial distance and bubble radius as a function of time. The standard case, oxygen bubbles.

Among different parameters of the centrifugal refining examined in case of one component bubbles, the cylinder rotation velocity, the initial bubble composition represented by gas solubility in the melt and the initial bubble radius appeared the most important /6/.

Whereas small oxygen bubbles were completely dissolved in the melt especially at higher rotational velocities, the bubbles containing gas almost insoluble in the melt exhibited only the separation mechanism. The mechanism was fast, only slightly dependent on temperature, and it was significantly accelerated by the increasing cylinder rotation velocity. However, the problem of the separation of very small bubbles containing hardly soluble gas arose for very small bubbles as the bubble separation time tends to infinity for the zero bubble size. The obtained results indicated that the problem of the bubble separation may occur for bubbles having the radius less than about 0.1mm /6/.

If bubbles are multicomponent, the question of the initial bubble composition and initial bubble radius becomes significant as in the case of one component bubbles. In the second run of experiments, bubbles of initial radii between 5E-5m and 6E-6m were examined in the same rotating cylinder and under otherwise standard conditions. The stationary bubble composition has been calculated at 1300-1500°C and bubbles of the stationary composition were put into the cylinder. Bubbles thus contained water vapour, oxygen, carbon dioxide, nitrogen and small amount of argon.

Figures 7 and 8 present the final results in form of the dependence between the bubble removal time versus the cylinder angle velocity at 1300 and 1400°C. The results were obtained for bubbles starting from the periphery at the cylinder bottom. Obviously are the removal times for bubble radii less than about 0.2mm too high for effective fining process.

The reason is the fact that almost all bubbles are removed by separation to the melt level and the rate of the separation process is slowed down by the effect of both increasing pressure and diffusion of soluble gases from bubbles into melt. Prior to search for the appropriate way how to exclude small bubbles from the process, the behavior of small bubbles in the rotating cylinder has to be clarified in more details.

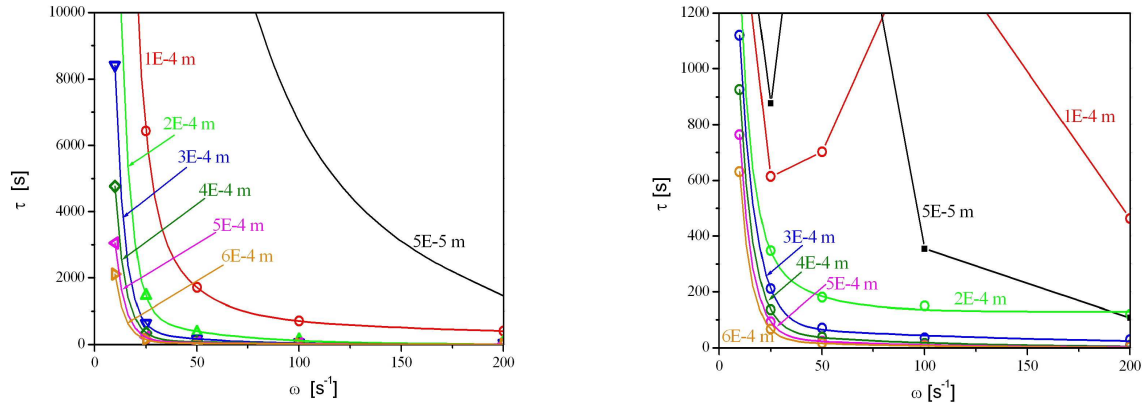


Figure 7 and 8: The bubble removal times as a function of the cylinder angle velocity at 1300 (left Figure) and 1400°C (right Figure).

All bubbles at 1300°C were removed by separation and the bubble removal times for bubbles $a_0=5E-5m$ and $1E-4m$ were between $1E5s$ for $a_0=5E-5m$ and $\omega=10s^{-1}$ and $403s$ for $a_0=1E-4m$ and $\omega=200s^{-1}$. The rapid bubble removal asks therefore for bubbles with initial radius greater than about $1E-4m$ and angle velocity higher than about $25s^{-1}$ (the bubble removal time for $a_0=2E-4m$ and $\omega=50s^{-1}$ is $366s$). The bubble removal times of bubbles at 1400°C exhibit two maxima for the bubble having the initial radius $a_0=5E-5m$ at $\omega= 50s^{-1}$ and for $a_0=1E-4m$ at $\omega=100s^{-1}$. It will be shown later that the high bubble separation times in both cases are caused by the considerable decrease in the original bubble size down to a very low value due to absorption of gas from a small bubble into melt. The bubbles of mentioned sizes dissolve then at angle velocities higher than was the value characterizing the maximum. The overall view on the bubble removal times at 1400°C also shows that the cylinder angle velocity around $25s^{-1}$ appears the optimum value as the bubble removal times move between $876s$ for $a_0=5E-5m$ and $66s$ for $a_0=6E-4m$.

The important reason for slow separation of small bubbles is their already in the theoretical part mentioned reaction with the melt, leading to bubble partial dissolution at higher rotation velocities. The decrease in bubble radius due to gas diffusion is dependent on the bubble inner pressure, the solubility of present gases in the melt and especially on the time the bubble spent at high pressures, i.e. close to cylinder periphery. As small bubbles are slowly separated, their residence times close to the cylinder periphery are high and the decrease in

bubble radii due to gas diffusion is considerable. Consequently, the bubble separation rate additionally decreases by bubble partial (or complete) dissolution. This fact is obvious from Fig. 9 and 10 for bubbles having initial radii 1E-4, 3E-4 and 6E-4m. The relative decrease in bubble gas contents owing to gas diffusion is there obvious at temperatures 1300 and 1400°C. Generally, the bubbles at 1300°C exhibit less significant decrease in their gas content (and consequently the smaller decrease in bubble radius), bubbles at 1400°C grow substantially at lower rotation velocities due to oxygen diffusing into bubbles and the same gas is mostly responsible for their considerable dissolution at high values of ω . The decrease in the bubble gas content is particularly significant for initially small bubbles and high rotation velocities, thus leading for example to the complete dissolution of the bubble with the initial bubble radius 1E-4m at $\omega=200s^{-1}$ and to its high separation time at $\omega=100s^{-1}$ (the bubble radius decreases to only about 2E-5m at 800s).

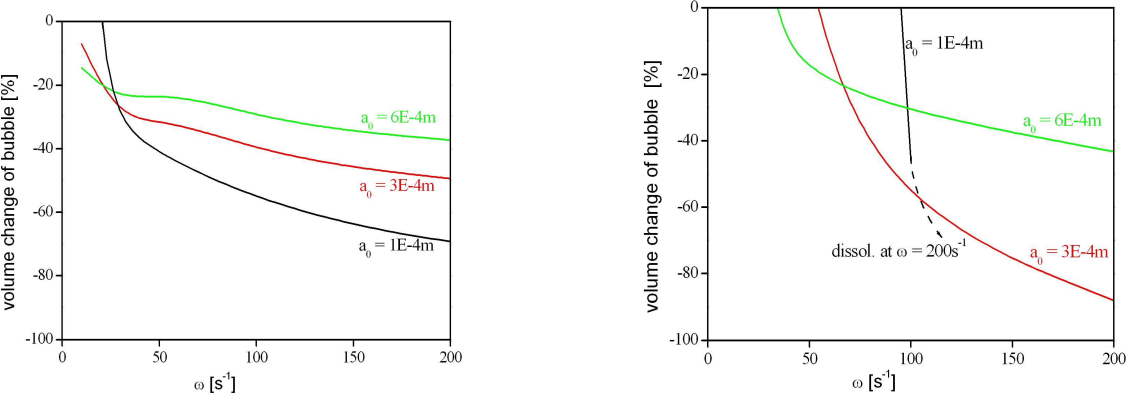


Figure 9 and 10: The relative changes of bubble gas content due to gas diffusion as a function of the cylinder angle velocity at 1300°C (left Figure) and 1400°C (right Figure).

CONCLUSION

The hitherto presented results show the bubble removal under effect of the centrifugal force as a complicated process affected by several factors. Additional calculations are needed provided the unambiguously beneficial conditions could be defined for the industrial application. The potentially positive steps for the application may be summarized as:

- the choice of the optimum cylinder size taking into account its intended rotation velocity
- the restriction of the content of gases in bubbles which are easily soluble in the melt during rotation
- pretreating the melt with bubbles to enable small bubbles to grow (application of reduced pressure or the refining agent, e.g.).

ACKNOWLEDGEMENT

This work was a part of the project No 2A-1TP1/063, "New glass and ceramic materials and advanced concepts of their preparation and manufacturing", realized under financial support of the Ministry of industry and trade.

REFERENCES

1. Beerkens R.: Proc. 7th Int. Conf. on Advances in Fusion and Processing of Glass III, Rochester NY, July 27-31, 2003.
2. Ross C.P.: Am.Ceram.Soc.Bull. 83, 1, 8 (2004).
3. Kunkle G.E., Welton W.M., Schweninger R. L : US Pat. 4,738,938 (1988).
4. Kloužek J., Němec L., Ullrich J.: Glastechn.Ber.Glass Sci.Technol. 73, 329 (2000).
5. US Pat. 4,316,734.
6. Němec L., Tonarová V.: Ceramics-Silikáty 50 (4), 216 (2006).

THE SEARCH FOR GLASS QUALITY

YiFang Cai and Aaron Huber
Johns Manville, Littleton, Colorado, USA

Abstract

Through the long and varied history of glass production, there has always been the challenge to improve. Efforts in the past 50 years have utilized physical models (glycerin tanks etc.), trials and years of experience to gain understanding before moving to computer modeling (CFD). Computer models combined with experience have become the tool of choice to understand and improve glass quality and production during the past two decades. Computer models provide a tremendous amount of information to analyze and draw conclusions. However, there is not one specific parameter that can be used to define glass quality from a glass furnace.

This paper will discuss glass quality indicators from CFD model predictions and show some general examples. Indicators range from temperature contours and streamlines, to post processing particle traces, residence time, melt index, fining index, and silica dissolution. A major challenge is to relate the predicted glass quality to actual glass quality. This challenge will also be discussed.

INTRODUCTION

For a typical continuous fiberglass furnace, a tablespoon of crystals can shut down an entire operation, plugging the thousands of small bushing tips. Similarly, for flat glass and container furnaces, bubbles (seeds) are a major source of defects. The high level of quality demanded for many glass products and the need to maximize throughputs and minimize costs requires a balance impacting both design and operation. Tools to help understand that balance and the associated trade-offs are thus critical to the financial viability of a glass manufacturer.

Efforts in the past 50 years have utilized physical models (glycerin tanks etc., see figure 1), trials and years of experience to gain understanding and achieve improvements before moving to computer modeling (CFD). Computer models combined with experience have become the tool of choice to understand and improve glass quality and production during the past two decades. Computer models provide a tremendous amount of information to analyze and draw conclusions. However, there is not one specific parameter that can be used to define glass quality from a glass furnace. Instead several aspects of the model predictions need to be examined to more accurately predict the actual furnace performance and associated glass quality. Those aspects include: temperatures and flows, particle traces, residence time distributions, melt index distributions, fining index distributions, silica dissolution and bubble tracing.



Figure 1 – Physical modeling (glycerin tank to simulate glass flows) [photo from GTI, D. Rue]

Temperature and Flow Fields

With converged CFD model predictions it is possible to examine the temperature and flow fields throughout the glass furnace. For the flow fields this is especially important as it is difficult or impossible to measure for an operating furnace. Figure 2 shows an example of the predicted glass temperatures down the length of a glass furnace. Examination of the results can identify critical temperature and stagnate or low velocity areas that will negatively impact glass quality. Another important modeling result is the predicted Joulean heat generation for electric heating. Figure 3 shows an example of the Joulean heat generation from an electric boost system. The solution of the Maxwell equations can identify issues with heat generation in refractory and uniformity in the glass.

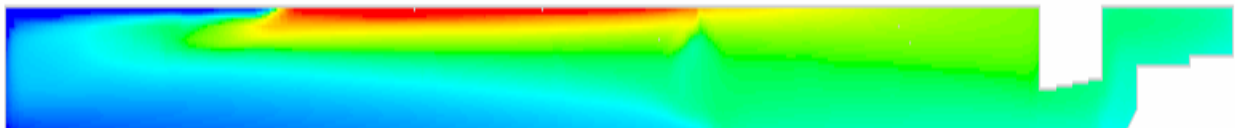


Figure 2 – Predicted glass temperatures along the length of a glass melter

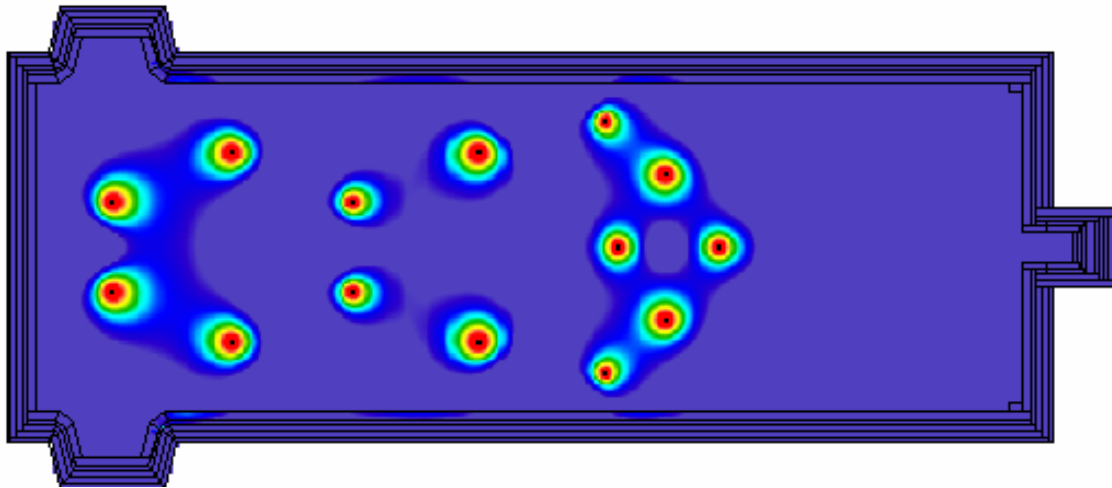


Figure 3 – Predicted Joulean heat generation from an electric boost system

Particle Traces

Once the CFD model has converged with established temperature and flow fields, post processing provides key information from the predictions. One of the first post processing actions is particle tracing. Particle tracing is when particles are released into the converged velocity and temperature fields and traced as they flow to the exit or target plane. Figure 4 shows an example of particle tracing with the first particles to exit the furnace plotted. Particle tracing helps identify short circuits in the flow patterns and potential quality issues.

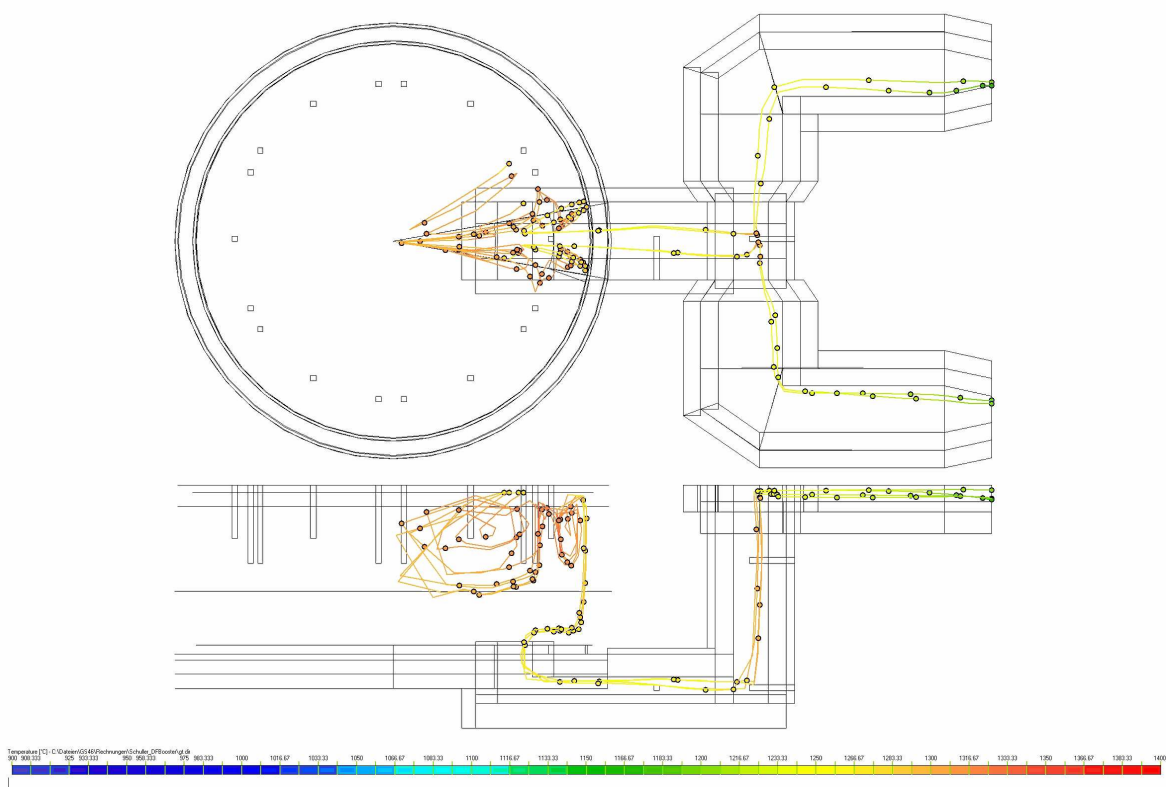


Figure 4 – Particle tracing example from CFD modeling (from Nikolaus Sorg GmbH)

Residence Time Distributions

After releasing several thousand particles with particle tracing, residence time distributions can be generated. The residence time distributions provide valuable information for glass quality. Along with the shortest residence time, the distribution provides information about the bulk glass. Another valuable aspect of predicted residence time distributions is the ability to validate the predicted flow patterns with an experimental tracer study and increase the confidence level of the CFD model results. Figure 5 shows the predicted and experimental results from a tracer study reported by SORG and figure 6 illustrates how CFD modeling can be used to explore different designs or operations to improve the residence time distributions.

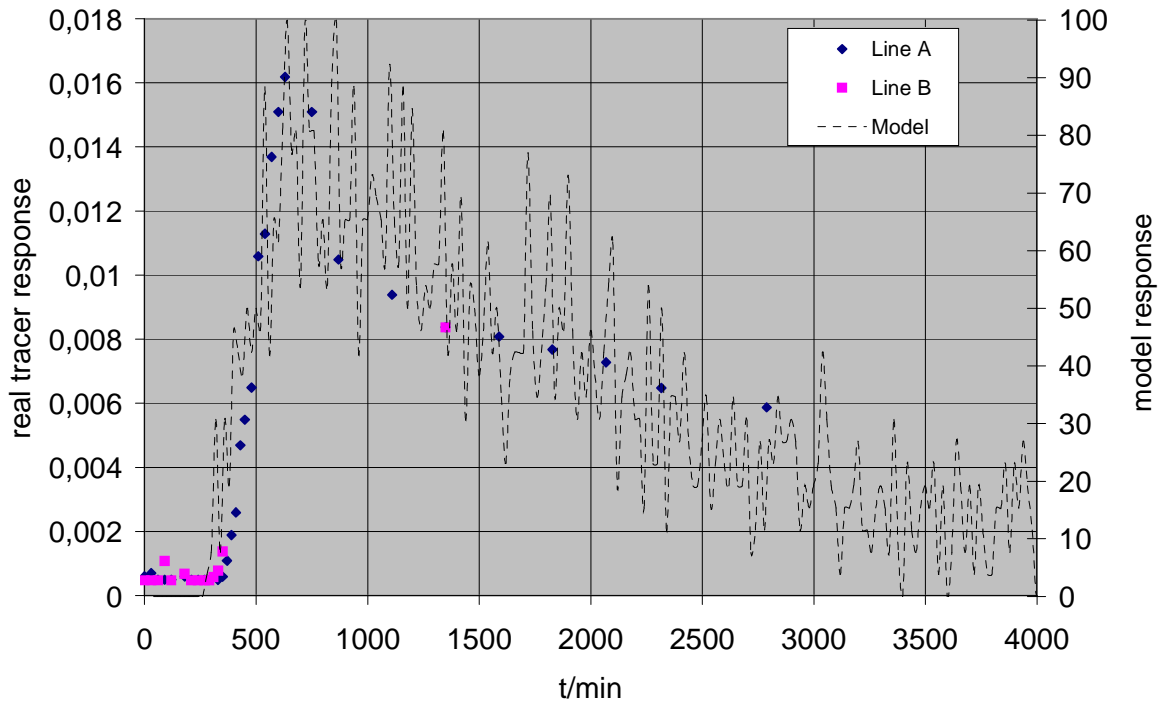


Figure 5 – Tracer results compared to residence time prediction from CFD modeling (from Nikolaus Sorg GmbH)

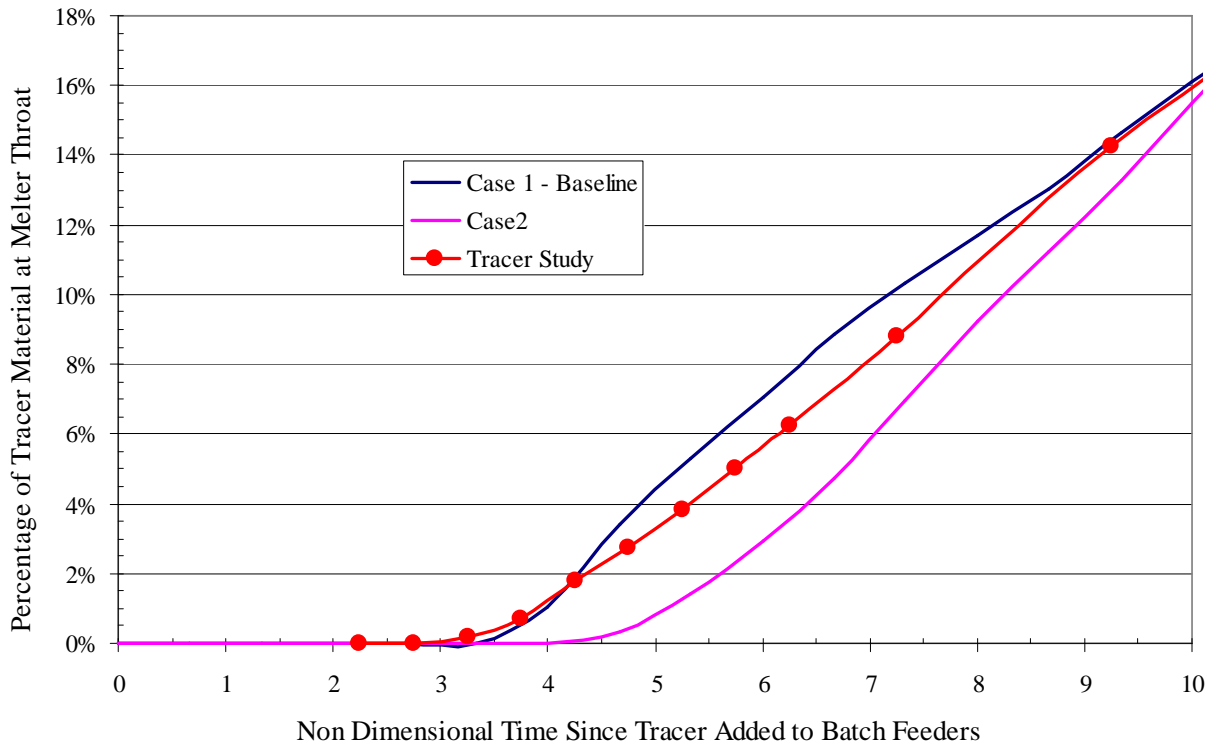


Figure 6. Comparison of measured and predicted melter residence times

Melt Index Distributions

The melt index is used to predict trends in glass quality and is a measure of both time and temperature (viscosity). A higher melt index value predicts improved glass quality. It is defined as following:

$$MI = \int_{\text{trajectory}} \frac{T}{\mu} d\tau$$

Where T denotes local temperature on the trajectory, μ is the local dynamic viscosity of glass and τ is time. A higher melt index value means the glass has experienced either higher temperatures (lower viscosity) at the same residence time, longer residence times at the same temperature (viscosity) or some combination of both.

Melt index trends calculated from predicted flows and temperatures have been accepted and used as an important indicator of glass quality for glass furnace design and operation. Figure 7 is an example that compares the predicted melt index distributions for two cases. This example illustrates the importance of using the distribution and not just a single value to understand differences between the cases. Based on the results shown in figure 7, case 7 has the best minimum melt index, but case 8 has the best mean melt index.

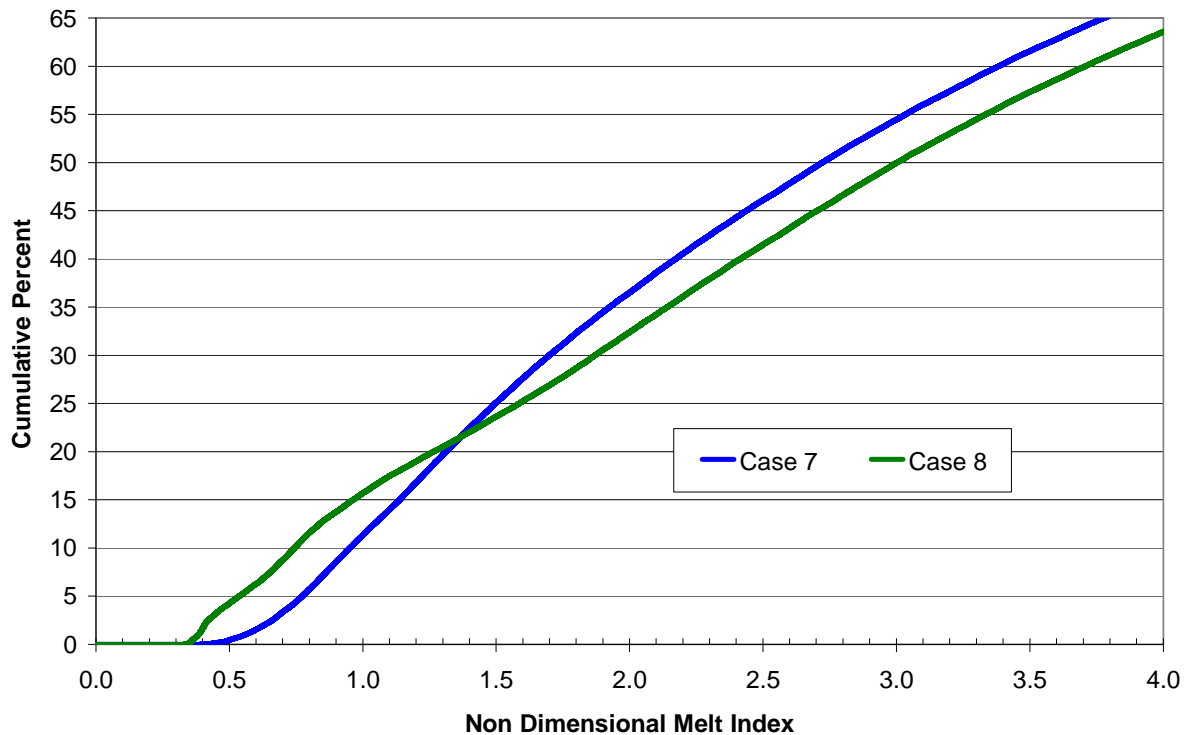


Figure 7. Example of predicted melt index distributions (non-dimensionalized) for two cases
Correlations between actual furnace production and the predicted melt index have shown that

the change in melt index is not a linear relationship. As would be expected, the impact of the melt index on furnace efficiency is dependent on the region of furnace operation. This again illustrates the need to look at more than just the melt index to understand the impact of furnace design and operation on glass quality.

Fining Index Distribution

The fining index is a generalized form of the melting index and indicates the fining potential of a design or operation. A higher fining index indicates improved fining. It is defined as:

$$FI = \int_{trajectory} \frac{(T - A)^b}{\mu^c} d\tau$$

Where T denotes local temperature on the trajectory, μ is the local dynamic viscosity of glass and τ is time with A, b and c user-defined constants. Typically 1400°C is used as a value for A. As with the melt index, the fining index can be used to compare the capability of different designs or operations for the fining operation.

Silica Dissolution and Bubble Tracing

Two other post processing indicators of glass quality are silica dissolution and bubble tracing. For silica dissolution sand grains are input into the predicted temperature and flow fields. Then, using equations based on laboratory derived values the location of final melt out is predicted for each sand grain. Bubble tracing is similar. After releasing bubbles into the temperature and flow fields, equations using laboratory derived values are used to predict the final location of the bubbles, i.e., do they rise to the surface or exit the furnace with the glass.

CONCLUSIONS

In conclusion, there are several predictors of glass quality that can be obtained from CFD modeling. By using these indicators and not just selecting one, a more accurate prediction of the actual operation can be made and the balance between the high level of quality demanded for many glass products and the need to maximize throughputs and minimize costs can be accomplished.

REDUCTION OF COLOR CHANGE TIME ON FLOAT FURNACES BY THE HELP OF 3D NUMERICAL SIMULATIONS

Fabrice Fasilow
Glaverbel CRD

Abstract

The paper describes how simulations can help to improve the color change time on float furnaces. Two types of color changes are considered here: limited by color tone and chemical homogeneity. The first step to consider is the validation of the simulation results with the real situation. This is to have an accurate reference case which is not always straight forward. When this step is performed than parametrical studies can be done to simulate different actions during the change over and to finally select the ones leading to a faster response towards the colorants target. For color changes limited by chemical reams, it is not enough: the color tone can be reached while the glass homogeneity is still not good enough to produce for instance automotive glazing. This is the reason why some chemical homogeneity index must be used to be able to predict the furnace behaviour. In some cases, the homogeneity can be predicted with accuracy but it is not a general rule. The conclusions are that according the furnace design and operating conditions it is difficult to have a "best practice" and it is more a case by case approach when the furnaces already exist.

INTRODUCTION

Glaverbel is one of the major float glass producer and transformer from western to eastern Europe. Among the present float lines, several of the them are dedicated to the production of colored glasses for automotive applications and building glasses. In 2003, the total number of days lost for color changes were equivalent of about 6 months of production of one float line. In today's context of strong market competition it is of course necessary to reduce as much as possible these transition days. Of course optimization of color changes sequences on one furnace and/or determination of adequate production schedules of different lines are trivial to save time and money but there are some limits fixed by the market and the local constraints. It is why reducing the crushing time between the initial and the final glass compositions by pure technical methods were deeply investigated for several years in Glaverbel.

The GTM model from TNO has always been used in Glaverbel for standard steady states studies for many years now. The same model has been used to study color changes and to find best-practices to reduce the crushing times.

Two types of color changes limiting factor will be studied: color changes limited by tint (or light transmission) and color changes limited by chemical reams.

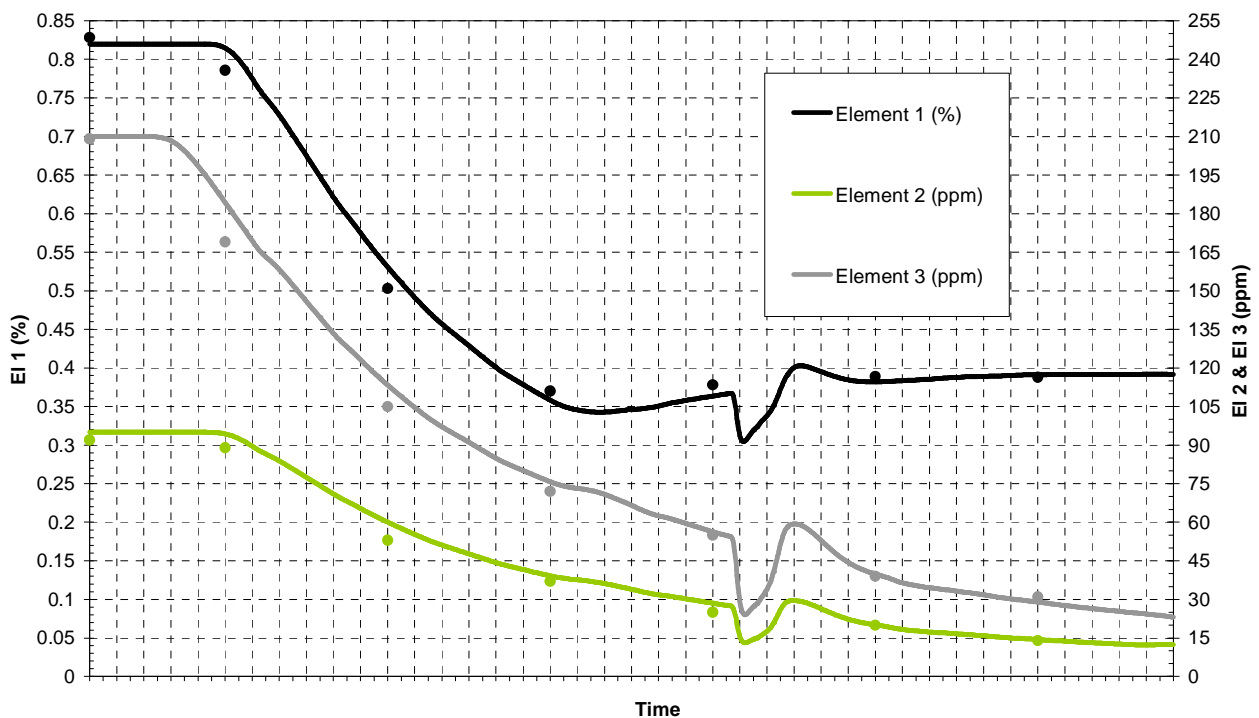
These are the main limiting factors and they are affected by the type of color change, the furnace type (or design) and operational conditions during the color changes.

Some modifications in the model were nevertheless necessary to consider specific phenomena occurring during the color changes. These were provided by the TNO after the first attempts to simulate color changes.

TINT LIMITED COLOR CHANGES

The first step for trying to validate the color change simulations are to compare the colorants evolution in the real product with the model. For this purpose in float glass production, it is possible to analyse the glass samples on the edges of the ribbon and in the center and make analyses on air an tin face.

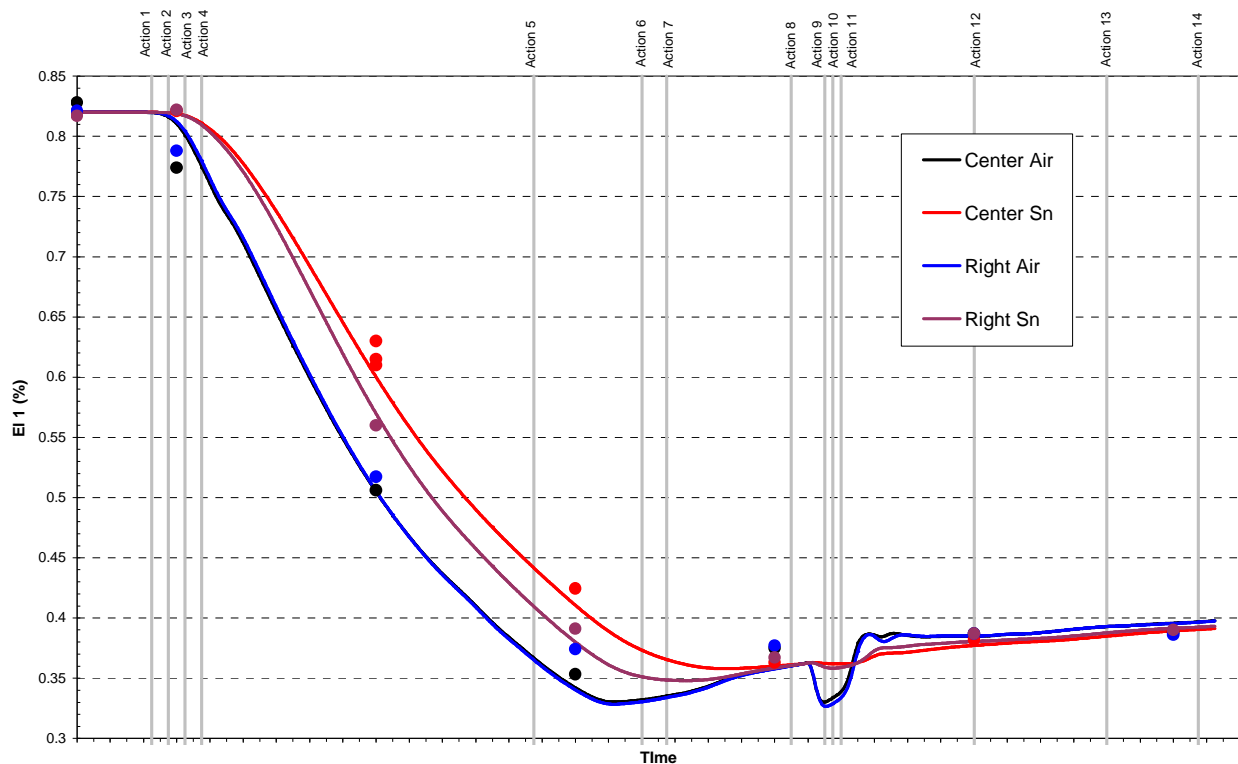
Picture 1 shows the comparison of colorants evolution between the model computation (plain lines) and real XRF measurements (dots) in the center and air face of the glass during change over time. This color change is from a higher iron content glass to a lower iron content glass. There are 3 different coloring agents considered in these products. All the 3 elements were considered in the model. This is simply because the levels of under-doping are not the same for each and they contribute all to the tint limitation. Time = 0h corresponds at the beginning of the under-dope arriving in the furnace for one of these 3 elements.



Picture 1 (plain lines = model / dots= measurements)

It can be seen on picture 1 that the validation between the model and reality is quite good for the 3 colorants. Excepted the bumps predicted by the model during few hours. These bumps are in fact created by removal and insertions of special equipments in the waist.

If the behaviour of iron is considered more in details by comparing air and tin faces for the center and edges of the ribbon, we get the picture 2.



Picture 2 (plain lines = model / dots= measurements)

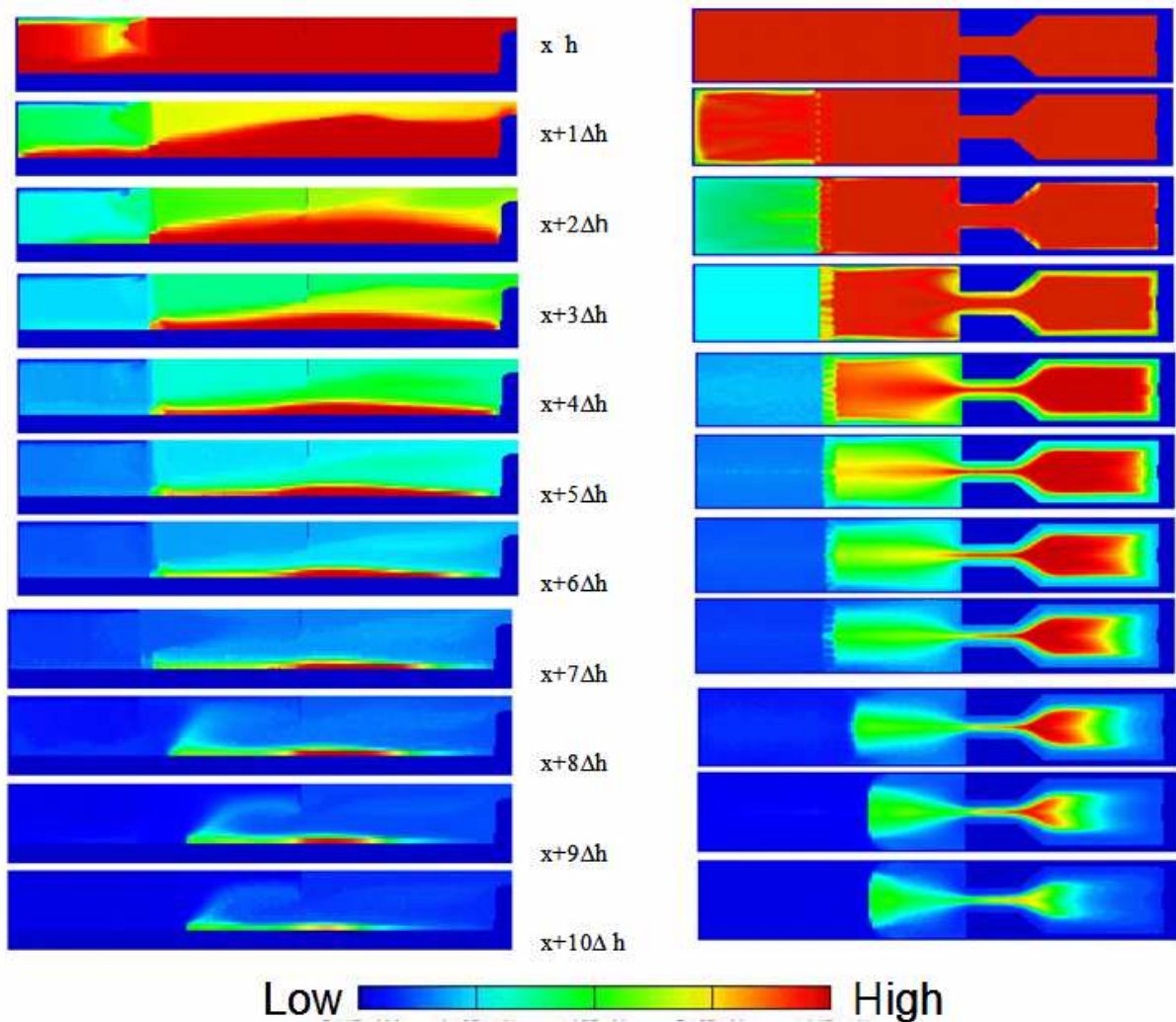
Now it is clearly seen that in the real color change, the behaviour of the surface is different from the tin face. The model is really able to fit the reality.

This result could only be achieved by including in the simulations important factors as :

- Of course correct under/over-doping of colorants during the right time.
- All real actions during the color change (pull changes, bubblers settings, waist coolers actions, insulation actions, fire distribution changes,...) must be considered. Some of these actions are symbolised by vertical lines on picture 2.
- Local density and thermal conductivity depend on the local concentration of colorants.

The good validation is also naturally coming by predicting the right evolution of bottom & surface temperatures during the color change as they are the engine of natural convection in the tank. Usually, a right prediction of colorants evolution goes together with a right prediction of bottom temperatures and vice versa.

Once all these parameters are checked and validated, behaviour of colorants in the furnace can be interpreted (picture 3).



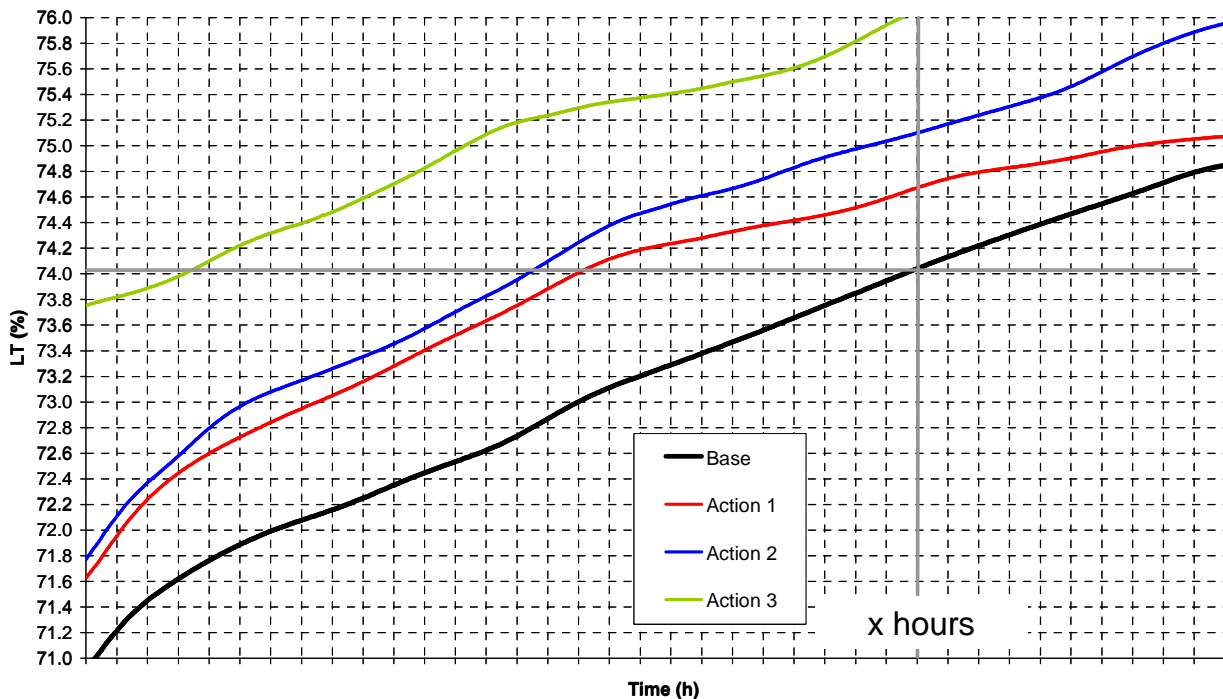
Picture 3: Colorant evolution during the color change

Picture 3 shows the evolution of one colorant in the symmetry plane of the furnace and just above the bottom paving. The combination of both views helps to evaluate the surface wrapping the volume of older glass in the tank. It can be seen that the melting zone is quickly filled by the new glass and efforts should be focused downstream of the tank from the bubblers line to the center of the working-end if the target is to flush away quicker that part of the furnace.

As the mass balance must always be respected and if one of the starting assumption is to consider that 100% of the furnace volume should be filled by the new glass, we have to transform a reactor from a „perfect mixer“ type towards a „piston flow“ like reactor. This is the trend we have to work on if we consider also that the pulls are kept constant from one case to the other.

For this typical color change, all 3 colorants affect the light transmission. It is why to better compare cases between each other we used the criteria of the light transmission formula determined by crucible tests in lab with these 3 colorants.

Picture 4 shows a zoom at the end of the color change of the computed light transmissions evolutions for the base case (the validated one) and 3 other computed actions aiming to shorten the change over. The goal is to reach quicker the target light transmission computed.



Picture 4: Computed light transmissions

It can be seen that for the base case, if we decide that the target transmission is 74%, the target glass is obtained after X h. Action 3 can bring a saving of 24 hours before „X time“ for this color change. Relatively speaking, it is a saving from 15 to 20% in color change time for this typical case.

This clearly shows the capabilities of the models to help to classify in priorities the actions that can be made for improving the situation once we have different possibilities to test.

We are well speaking of 3 different actions here but a big part of the job still needs to be done to find the right timing of these actions : when to start and when to stop ?

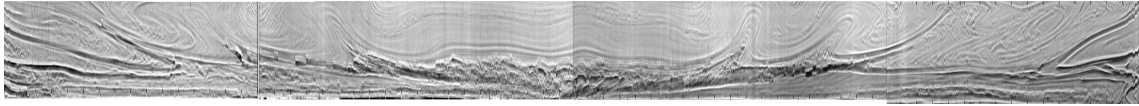
Of course models can help but it is always by working with production people, making real industrial tests and validating the model trends that the best results will come by making the fine tunings.

Also, we must be careful because models usually predict good trends but the absolute values must be considered carefully. It is clear that action 3 is better than action 1 but the theoretical 24 hours savings can be 10 hours in the real life for many reasons.

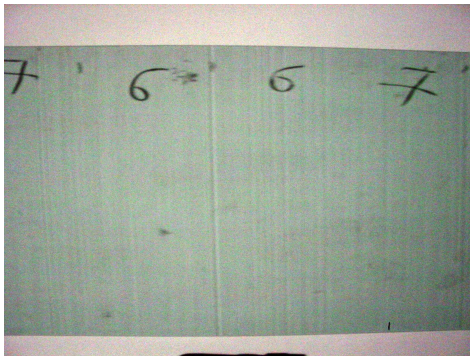
An other aspect in the limitation of this procedure is to avoid the over heating of bottom blocks to speed up the color change. If this happens, the color tone can be reached 10 hours quickly but the glass can be full of bubbles during 2-3 days from devitrified glass re-melting which was accumulated during years along the bottom of the tank. So, the final decision must be made by considering that the yield must not modified after the color change.

COLOR CHANGES LIMITED BY CHEMICAL REAMS

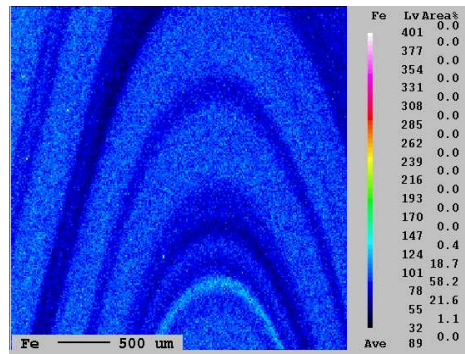
Chemical reams are glass inhomogeneities created by a lack of mixing of glasses of different compositions at the end part of the color change. Picture 5 shows a typical striogram of a ribbon with a strong pattern of chemical reams and picture 6 shows the optical quality of this glass that makes the product rejected for automotive applications.



Picture 5 : striogram of heavy „reamed“ glass



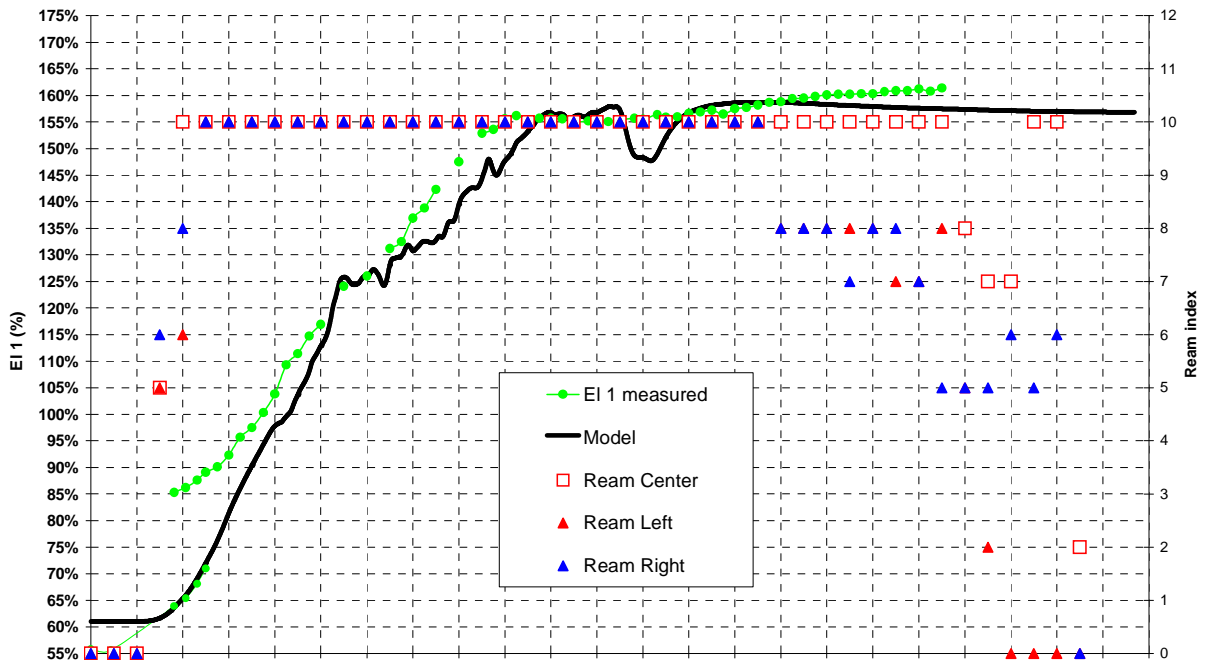
Picture 6: Optical quality of a reamed glass



Picture 7: Fe content scan by microprobe

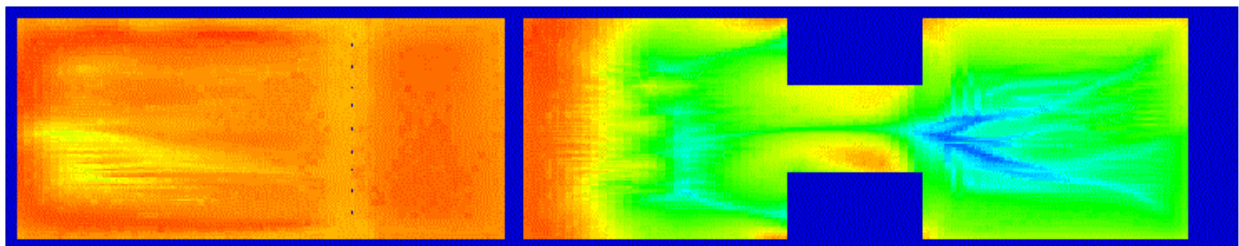
Picture 7 demonstrates by microprobe analyse the high reams are due to gradients of glass compositions and in this case Fe content.

Several 3D simulations were made to catch the formation of these chemical reams in the tanks and picture 8 displays one example of color change where iron contents measured and predicted by the model are in good agreement (left scale). Nevertheless the challenge here is to be able to predict the ream counts (Left, center & right on the right scale) during the color change because these are the limiting factors for the loading and not tint. Note that once the tint is needed we are only at the half of the color change in the sample shown. It is also interesting to observe the quick rising of ream counts at the beginning of the color change and the slow decrease of reams at the end and the different behaviour from left to right.



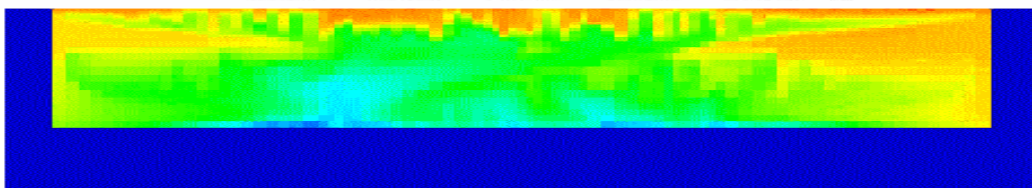
Picture 8: Iron content and ream counts

If the iron predicted by the model inside the tank is observed about the half way of the color change (picture 9&10), it can be seen that the concentration field is not progressing in smooth waves but that there are strong local inhomogeneities in the fining zone and in the working end.



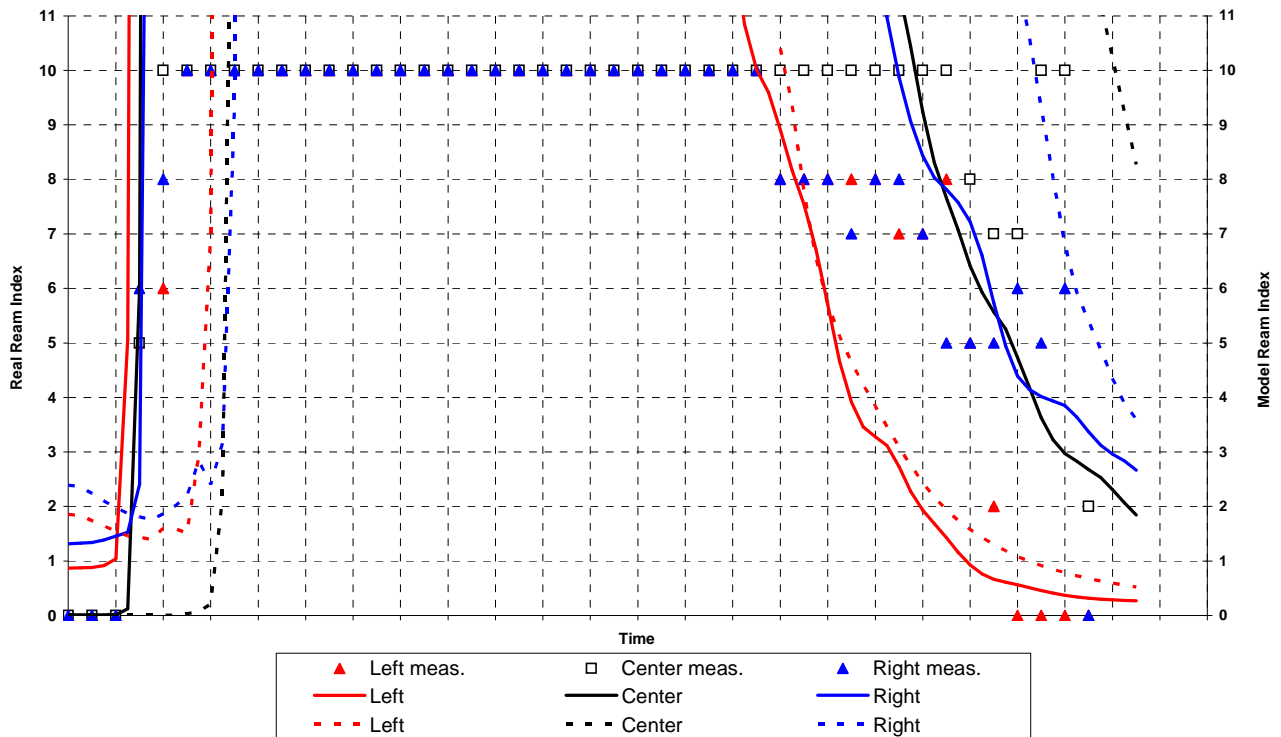
Picture 9: Top view in the middle of the tank

Low  High



Picture 10: Cross view in the middle of working end

A mathematical criteria has been based on these unhomogeneities to try to fit the reality. The result is displayed on picture 11. The criteria can be computed in any part of the furnace. The plain and dotted lines are the results at different positions of the computation inside the tank. The index is also computed in the left, center and right of the tank.



It can be seen that there is quite a good matching in trend if we compare the reality and the model even if it can be perfectible. Nevertheless, the beginning, final, left, center and right trends are respected. The model would have given of course a symmetrical result if the simulations had symmetrical boundary conditions/settings but it was not the case.

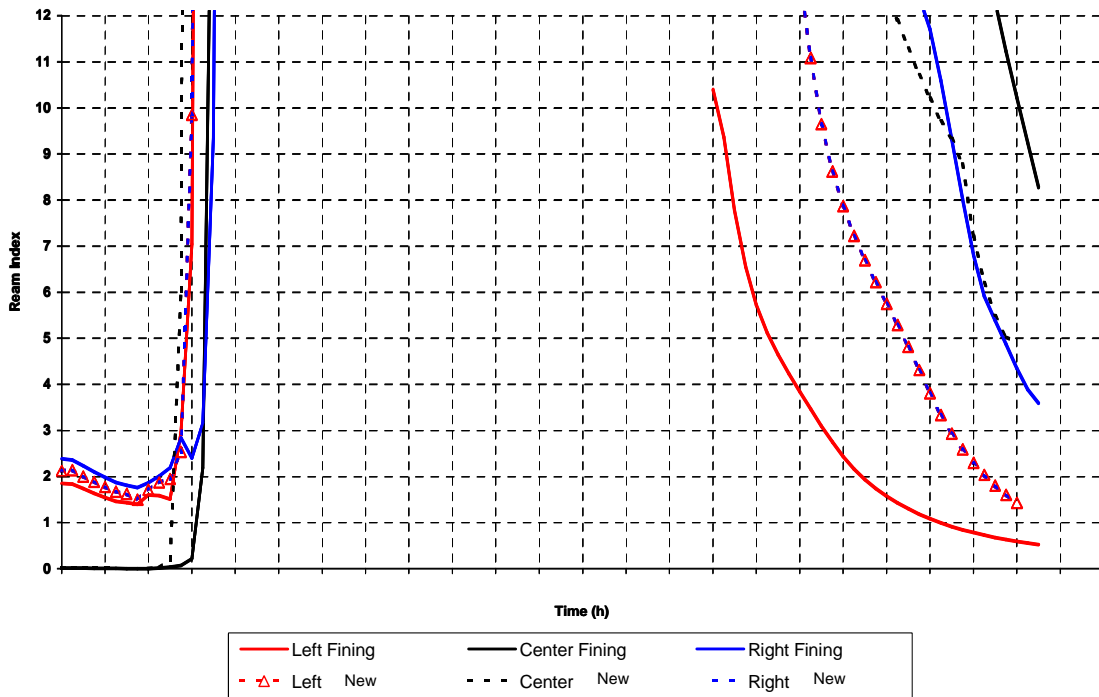
Based on this reference case, several parametrical studies were performed to reduce as quick as possible the „model“ ream counts at the end of the color change.

Picture 12 displays the relative behaviour of the base case ream counts and the parametrical study where the non-symmetrical boundary conditions/settings were input in an other way.

What was on left becomes a little bit worse, right and center are improved.

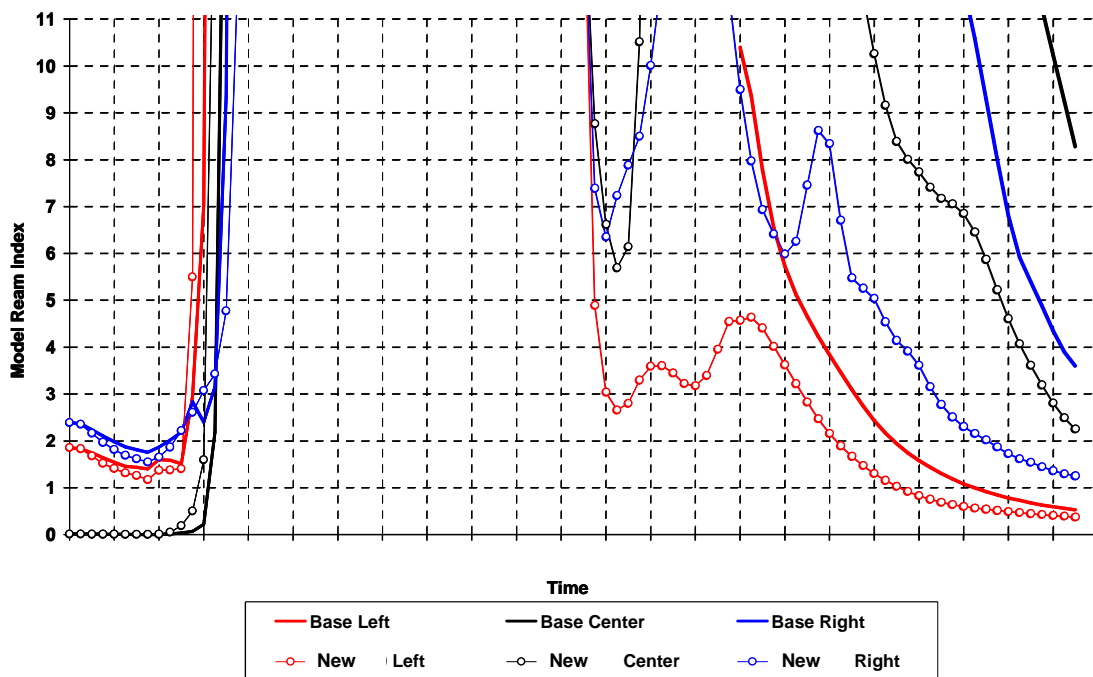
Note that now, the situation becomes symmetrical.

It is clearly seen now that these boundary conditions/settings have an effect on the distribution of the new glass in the furnace. This is then a very good tool to improve the actual situation during the color change to control reams.



Picture 12: Reams predicted by modifying the initial non-symmetrical boundary condition

Picture 13 shows an other example where a stronger over-dope in used.



Picture 13 : Reams predicted by increasing the over-dope

A strongest over-dope for this color change implies an improved homogenisation of concentrations by using the fact that a heavier glass is charged over a lighter glass. The density contrasts accelerate the mixing cells giving at the end of the color change a more uniform concentration field.

This procedure has nevertheless its limits. The limit is the mixing ability of the furnace by the natural convection currents. If the currents created by the surface hot spot and the pull are too weak, we can imagine that the over-doped glass is sinking on the bottom. Once the target glass is fed in the batch, this lighter glass will float on top of the over-doped glass concentrations still staying on the bottom. This will release slowly glass with high reams at the end of the color change.

In extreme cases, this stocking effect of the over-doped glass can be seen because it is expected that with a stronger over-dope, the new glass composition will come quicker. In some cases, by measuring the iron content of the glass leaving the furnace, it can be observed that it is coming very slowly in fact even if the over-dope is increased meaning that some glass is kept inside the tank somewhere. If nothing is anticipated, it can lead to strong overshoots in glass composition compared to the target later at the end of the color change.

This means once again that for this type of color change it is a case by case approach depending on furnace design, insulation, equipments, settings,...

The ream index approach is attractive but it should be said that the validation on other color changes and on other furnace types was less fitting the reality. This means that this index is not yet an „universal“ index and additional tools should be used in parallel to predict the chemical reams behaviour (mass balances during the color change simulations, histograms of iron concentrations in specific areas in the tank,...). These will not be described here.

This modelling approach helped to save about 385 hours of production per year in reality. This is the total saving for all color changes limited by tint and chemical reams if they were done in the same production program in one year.

CONCLUSIONS

This paper described briefly the approach followed in Glaverbel to simulate and reduce color change time.

Color changes limited by tint/light transmission and chemical reams were exposed and a mathematical ream index has been developed. The validation of colorants leaving the furnace and the reality is in a good agreement and it could be achieved by few developments of the existing model and a detailed simulation of all the actions performed on the real furnace. By simulations, it is possible to find operational conditions to reduce the crushing time.

Nevertheless, by experience, the ream index approach should be coupled with other post-simulations analysing tools not described here.

This approach in combination with industrial tests on different types of furnaces helped to reduce color change times of about 385h if all savings are added (and if the same color change program is maintained each years).

Of course with the experience of the production people and the continuous improvement programs, color change times became always shorter continuously and progressively. The simulation approach helped to make strong step in this progressive and continuous improvement.

The optimum settings for color changes really depend on the furnace type, design, insulation, and many other parameters. Initially, the target was to find general best-practices but it is more a case by case approach that can be done with the help of simulations if the furnace is already existing and if we are only dealing with operational conditions.

For new furnaces, models can help also to optimize the design of the furnaces but this is an other story.

EXPERIENCES WITH FLOAT FURNACE MODELING

Petr Schill*, Jiří Brada, Miroslav Trochta
Glass Service, Inc., Rokytnice 60, 755 01 Vsetín, Czech Republic

Abstract

An accurately developed CFD code, the Glass Service Glass Furnace Model, was used for calculation of a case study showing design modification influence on glass flow and temperature distribution inside a float furnace. A three dimensional coupled calculation of the complete furnace was used involving heat transfer between glass space and combustion space. Mainly the bottom turning point position and backward glass flow was studied with respect to the bottom insulation near the waist and to the waist cooler immersion. The glass quality was quantified by quality criteria as melting-, refining, and mixing-index, residence time, critical trajectory parameters, mean temperature in particular furnace part, etc. The relation of furnace design with glass quality was discussed at the end of the paper.

INTRODUCTION

The modeling procedures play important role in investigation of glass melting technology and furnace design. The impact of furnace design and of operation condition setup on glass quality is one of the main goals of modern modeling studies. The latest version of the Glass Service Glass Furnace Model (GS-GFM) is of high calculation sensitivity which is able to handle such details as little changes of bottom insulation or little changes (of mm order) of waist cooler immersion during simulation of a big float furnace. Two such examples are presented here.

Float Furnace case study

Using the GS-GFM code, a huge case study was carried out of 580 MTPD float furnace heated by oil/air 6 port system with under-port burners (3950 kg per hour of oil) and electro boosting under the batch by 490 kW. It was calculated totally 14 cases of modified bottom step design, glass depth, waist cooler design and immersion, and bottom insulation with respect to bottom turning point position and glass circulation pattern which in consequence are the main factors influencing the resulting glass quality.

We are focused here just on two items: (a) on waist cooler immersion and (b) on partial bottom insulation in the waist. During this partial case study all other operation parameters remained same including total fuel flow rate. In the first item, one half of bottom insulation layer was removed in the middle section before waist and under waist and following cases were calculated:

Case 1: No cooling,

Case 2: Weak cooling,

Case 3: High cooling.

In the second item, the waist cooler position was changed and following cases were calculated:

Case 4: Cooler pushed up by 30% (+145mm),

Case 5: Cooler pushed down by 26% (-124mm).

Results of Float Furnace case study

Figure 1. displays comparison of base case and three cases (#1,#2,#3) of removed bottom insulation in waist area using graphical form. Figure 2. shows comparison of base case and two cases (#4, #5) of different immersion of waist cooler. In both the figures, the shift of bottom turning point is well visible.

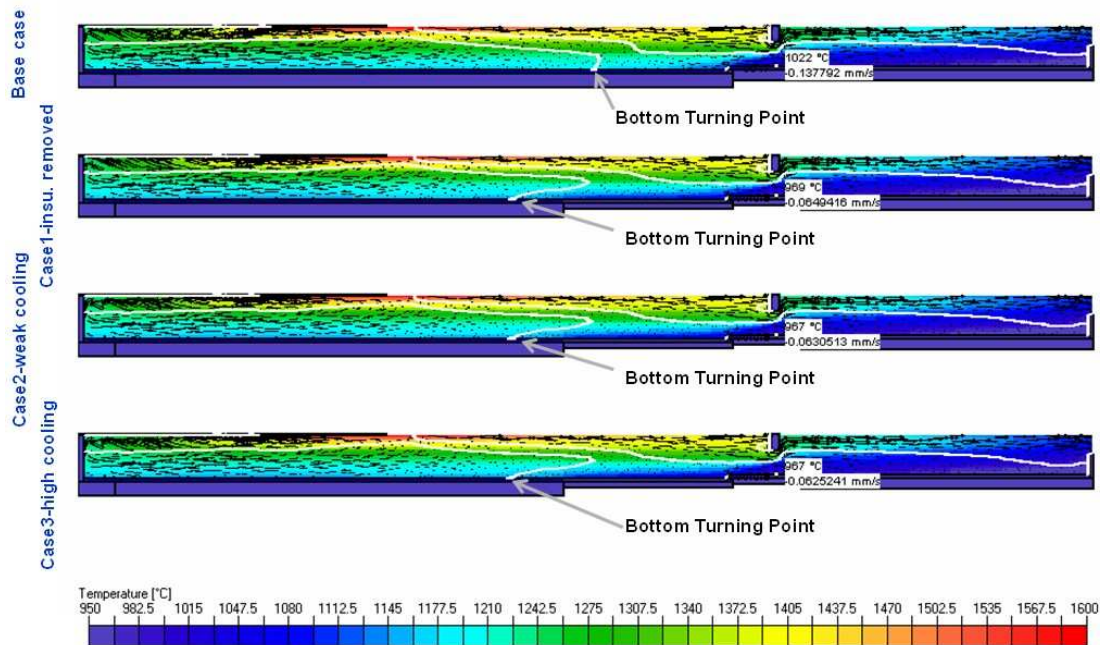


Fig. 1. Float furnace – Base case and Cases #1, #2, #3 of partial remove of bottom insulation and of different additional bottom cooling showing glass flow and positions of the bottom turning point and of the surface hot spring. The pictures are stretched in vertical direction by factor 2 for better visibility. The white line indicates the location of zero longitudinal velocity.

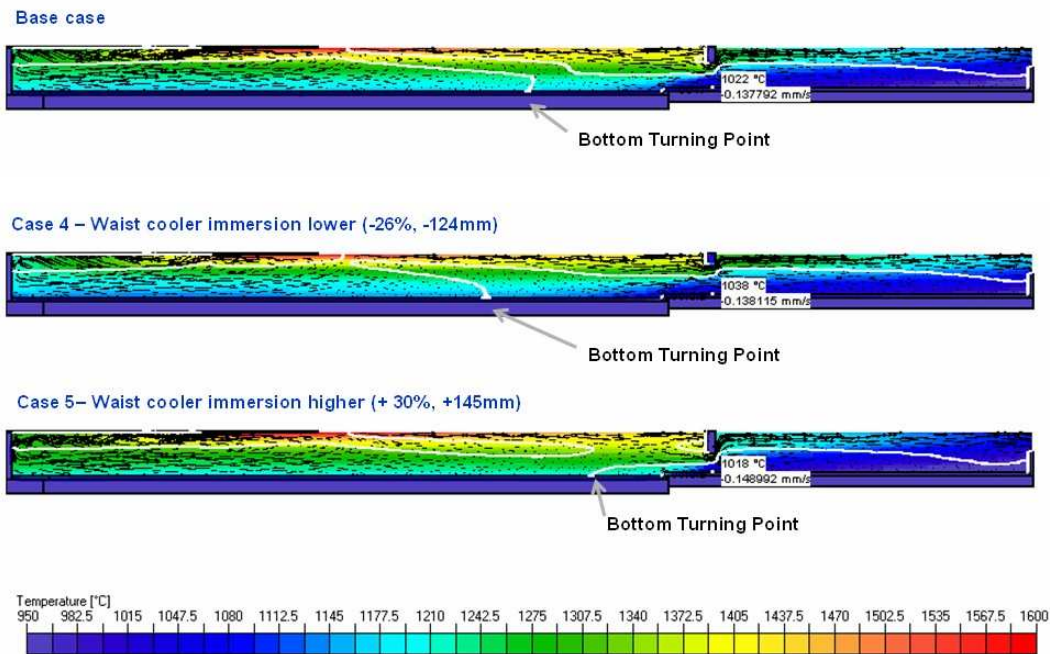


Fig. 2. Float furnace – Base case and Cases #4, #5 of different position of waist cooler showing glass flow and positions of the bottom turning point and of the surface hot spring. The pictures are stretched in vertical direction by factor 2 for better visibility. The white line indicates the location of zero longitudinal velocity.

The results can be summarized as follows:

1. Removing part of bottom insulation under the waist results in following:

- Shift of the bottom turning point far from the waist (by 4.4m)
- Longer bottom back-flow -> positive for removing small bubbles
- Lower bottom glass temperature below the cooler (by 53 °C)
- Lower glass temperature at exit (by 21 °C)
- Lower average glass temperature (by 16 °C)

Additional cooling the weak insulated bottom is of minor effect. In order to keep same exit temperature it is needed to increase the fuel consumption (in case of not changed pull).

2. Moving the waist cooler up results in following:

- Shift of the bottom turning point far from the waist (by 2.2m)
- Longer bottom back-flow -> positive for removing small bubbles
- Higher bottom glass temperature below the cooler (by 16 °C)
- Higher glass temperature at exit (by 41 °C)

- Lower average glass temperature in melter and refiner (by 28 °C)
- Higher average glass temperature in working end (by 32 °C)

In order to keep same exit temperature it is needed to decrease the fuel consumption (in case of not changed pull).

3. Moving the waist cooler down results in following:

- Shift of the bottom turning point closer to waist (by 3.42m)
- Shorter bottom back-flow -> negative for removing small bubbles
- Lower bottom glass temperature below the cooler (by 4 °C)
- Lower glass temperature at exit (by 33 °C)
- Higher average glass temperature in melter and refiner (by 27 °C)
- Lower average glass temperature in working end (by 24 °C)

In order to keep same exit temperature it is needed to increase the fuel consumption (in case of not changed pull)

The quantitative parameters of all cases are summarized in table 1.

	Base case	Case 1	Case 2	Case 3	Case4	case5
Bottom turning point (BTP) position [m]	27.695	23.333	23.285	23.248	25.531	31.119
Surface Hot Spring (HS) position [m]	18.142	18.098	18.072	18.069	17.936	18.207
BTP – shift [m]	0	-4.362	-4.41	-4.447	-2.164	+3.424
HS – shift [m]	0	-0.044	-0.070	-0.073	-0.206	+0.065
Glass Temperature [°C] 56 mm above bottom under the waist cooler	1022	969	967	967	1038	1018
BTP Temperature [°C]	1172.3	1151.4	1149.8	1149.3	1140.0	1206.9
Average Glass Tem. at exit [°C]	1116.8	1096.3	1094.3	1094.1	1157.9	1083.8
Average Glass Tem. in Melter and Refiner [°C]	1289.8	1275.9	1274.4	1274.1	1262.1	1316.9
Average Glass Tem. in Working End [°C]	1091.4	1073.7	1072.4	1072.2	1123.1	1067.0

Tab. 1. List of important parameters of the case study.

CONCLUSION OF THE FLOAT FURNACE CASE STUDY

1. The CFD modeling is able to calculate minor design modification as shifting the waist cooler or changing of bottom insulation.

2. Using Glass Service Glass Furnace Model we are able to quantify following design changes in float glass furnace:

- Removing of part of bottom insulation in waist area supports and prolongs the back flow which is normally positive for glass quality, but needs higher fuel consumption
- Addition cooling of area of weak insulation is of minor effect
- Moving up the waist cooler prolongs the back flow which is positive for glass quality, and needs decrease fuel consumption (exit tem. increased by 41°C)
- Moving down the waist cooler shortens the back flow which is normally negative for glass quality , and needs increase fuel consumption (exit tem. decreased by 33°C)

FAST APPROACH TO REGENERATOR MODELLING – A VALIDATION STUDY

¹Menno Eisenga*, ¹Erik Muijsenberg, ¹Marketa Muijsenberg

²Miroslav Trochta, ²Josef Chmelař

¹Glass Service B.V., Watermolen 22, 6229 PM Maastricht, The Netherlands

²Glass Service Inc., Rokytnice 60, 75501 Vsetin, Czech Republic

Abstract

A new and fast approach has been introduced to include the regenerators in mathematical models of regenerative glass furnaces [1]. In this approach the alternating storage and release of heat in the checkers during the reversal cycles is used to calculate the preheated combustion air temperature in the furnace. The previous paper [2] has presented an example of a coupled CFD calculation for an end-fired container glass furnace including the combustion space, the glass melter and both regenerator chambers. In the present validation study the model results are validated against real furnace data. Temperature and streamline analyses of the flue gases and combustion air flows through various sections of the regenerator chambers are used to investigate and improve the efficiency of the regenerator design, related to uniformity of the gas distribution in the regenerator. Non-uniform gas flows will reduce the overall-efficiency of the heat exchanger, especially when the air intensive passages are not intensively exposed to flue gas flows. Advanced particle tracing techniques are employed to calculate the transport of dust and carry over from the batch in the furnace and to predict potential risk for clogging of checker openings.

- [1] Trochta, M. Mathematical Modelling of Combustion Chambers of Glass Furnaces using GS GFM Package, Proceedings of XXth International Congress on Glass 2004, Kyoto Japan.
- [2] Eisenga, A.H.M. & Trochta, M. 'Fast' Approach to Regenerator Modelling - 8th ESG/ICG and SGT Annual Meeting 2006, Sunderland UK.

ADVANCED PARTICLE TRACING IN GLASS BATH AND COMBUSTION SPACE

Authors: D. Hegen*, C. Müller and colleagues**, A.M. Lankhorst*

* TNO Glass Group, Eindhoven, The Netherlands

** Schott AG, Mainz, Germany

Abstract

From a flow field computed with CFD for glass bath and combustion space it is often difficult to answer questions like

- *Is there a short-cut flow leading straight from the inlet to the outlet?*
- *What is the mixing quality of this flow?*
- *Will small bubbles escape to the glass surface or will they end up in the product?*
- *What is the minimum residence time?*
- *What fraction of the mass flow from inlet 1 will exit through outlet 2?*

Such questions can be answered by means of particle tracing, i.e. releasing a large set of particles and tracing these for a sufficiently long time.

In order to perform particle tracing the velocities determined by CFD are not sufficient as these are only known at certain discrete positions in the grid representation of glass bath and combustion space. Hence, a continuous velocity representation has to be reconstructed from the discrete velocities. Such a reconstruction is not straightforward and if not done properly inaccurate particle tracing results are obtained such as

- *particles getting trapped in closed loops*
- *large deviations between numerical and analytical mean residence time*
- *a strong dependency of results on grid resolution and time step used*
- *particles ending up at unphysical positions such as walls*

This especially may be observed when grid cells are not orthogonal or when large gradients in velocities occur, e.g. caused by the application of bubbling.

In the paper the application of an advanced particle tracing algorithm available in TNO Glass Group's CFD-model GTM-X will be considered and compared to other approaches. The mathematical method in the algorithm is appropriate for flow calculated on multi-level block-structured collocated non-orthogonal boundary fitted grids and allows for the tracing of particles per grid cell by means of an analytical formula. Hence, particle tracing results are independent of time step size. Furthermore, for converged flow fields without dead-water zones it is shown that there is always a perfect match between numerical and analytical residence time. Last but not least, a very fast method is obtained: For an industrial glass tank consisting of 600.000 grid cells particle tracing of 30.000 particles takes only 10 minutes on a 3GHz processor.

Results of a comparison study on a furnace with two bubblers, in which tracing options of several CFD models have been applied, demonstrate that the tracing algorithm of GTM-X is superior. Furthermore, results for two other industrial cases are being discussed from which it is concluded that the presented tracing option of GTM-X is a stable and fast method to evaluate glass quality and to provide answers to the relevant questions for glass bath and combustion flow.

Perspectives on CFD applications in materials processing

Manoj Choudhary, Owens Corning

Jaydeep Kulkarni, Ansys Inc.

9th International Seminar: Mathematical Modeling of Furnace Design and Operation



DELIVERING SOLUTIONS | TRANSFORMING MARKETS | ENHANCING LIVES



Outline



- **Glass industry**
 - Vision 2020 statement
 - Modeling opportunities
 - Example of glass tank modeling
- **Metal industry**
 - Vision 2020 statement
 - Challenges
 - Modeling opportunities
 - Example of furnace design



Glass Industry Goals: Vision 2020



- Operate with production costs 20% below 1995 levels
- Recycle 100% of all glass products in manufacturing
- Reduce current process energy use by 50%
- Reduce air/water emissions by 20%
- Recover 100% of available post consumer glass
- Achieve six sigma quality improvements through automation, process control, optimized glass composition/strength, and computer simulation
- Create innovative products that broaden the market, e.g., flat panel TV



R&D focus areas to achieve these goals



- **Processing:**
 - Advances in melting/refining processes, and fabrication/forming processes
- **Technology:**
 - Development of new glass making techniques, process controls and computer simulations to model new processes
- **Systems:**
 - Improvement in emissions controls, recycling methods and solid waste management
- **Products:**
 - Development of innovative new uses for glass



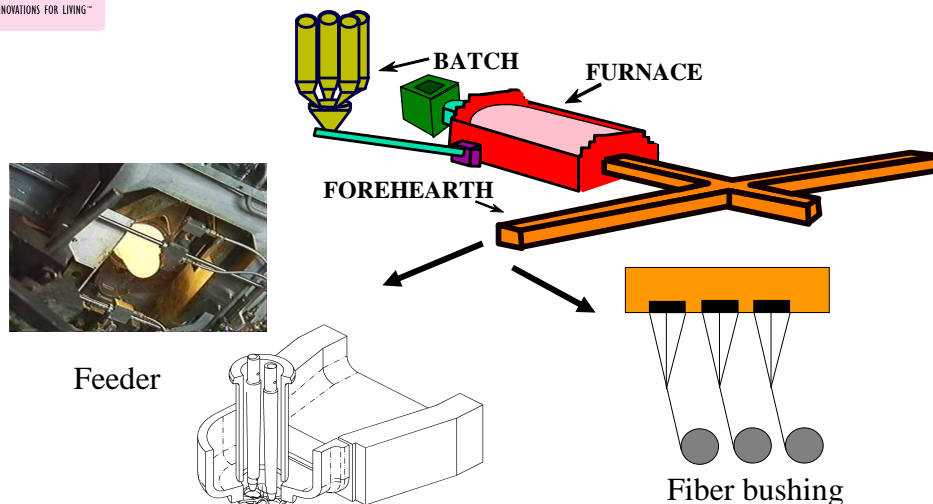
Simulations in Glass Industry



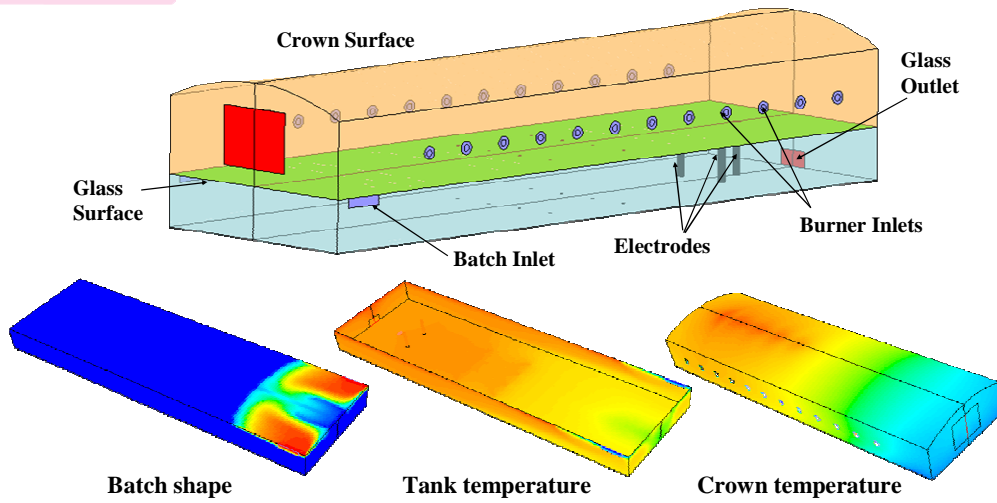
- **Improve energy efficiency:**
 - Glass industry is a highly energy-intensive industry
 - Theoretically, glass making requires 2.2 million BTU of energy to melt 1 ton of glass, but twice that amount is actually used because of inefficiencies and losses
 - Modeling to optimize combustion and heat input to glass in glass tanks
- **Reduce capital costs:**
 - Typical furnace life is 8 - 10 years
 - Furnace rebuild cost \$20 - 50 million + product loss
 - New furnace cost \$120 - 150 million
 - Modeling to prolong furnace life
- **Become environmentally friendly:**
 - Modeling to reduce pollutant production (NO_x and SO_x)
- **Improve product quality**
 - Modeling to reduce defects during glass forming



Glass Melting



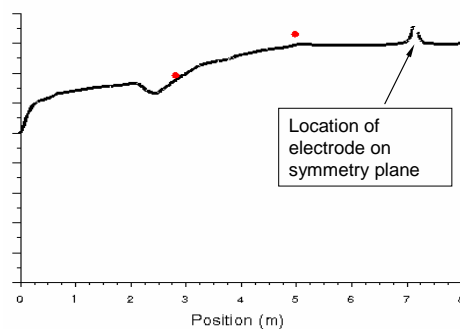
Glass Furnace Modeling



Courtesy of Owens Corning

Validation

Glass Tank Temperature



- The corresponding crown temperatures were within 1.5% of measured values

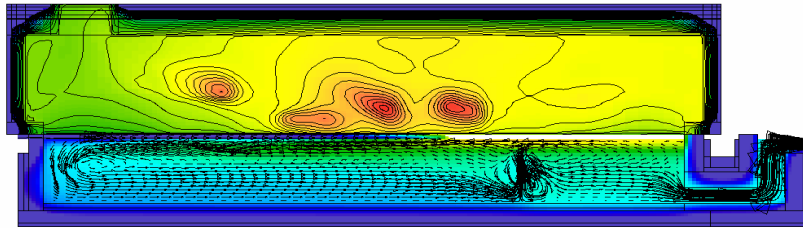


Oxy-Gas Glass Furnace: Integration of batch, combustion, and melt sub-models



INNOVATIONS FC

Integrated Model of The Glass Furnace
Side View (XZ)



Temperature scale: 1300 – 1800 K
Velocity scale: 0 – 0.04 m/s

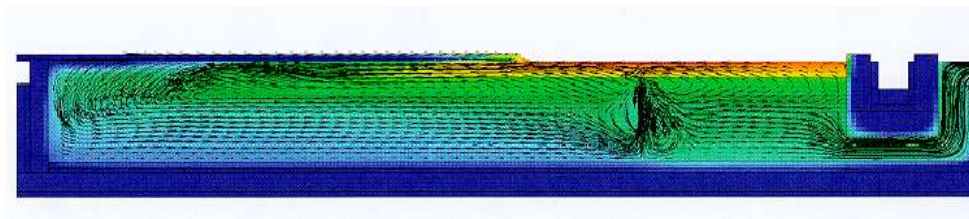


Illustration: Glass quality improvement

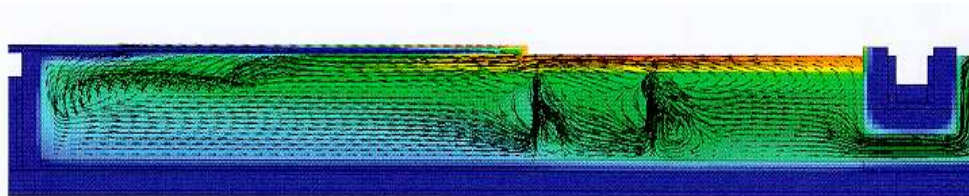


INNOVATIONS FOR LIVING™

Case 1: ONE ROW OF 5 BUBBLERS



Case 2: TWO ROWS OF 5 BUBBLERS



(Δ MI ~ + 19% ; Δ SDI ~ + 12.5%)



Illustration: Glass Quality Improvement

Case	Position from the front wall		Bubb. rate	No. of stones	Δ Rear UG temp.	Δ Mid UG temp.	Δ Front UG temp.
	1 st Row	2 nd Row	[Nm ³ /hr]		[K]	[K]	[K]
1	0.4	0.2	1.49	570	0	0	0
2	0.4	0.26	1.49	439	-12	-8	-6
3	No bubbling			NA	-37	-32	-47
4	0.4	0.2	1.16	305	-15	-10	-11
5	0.4	0.2	2.98	776	+8	+11	+17
6	0.4	No bubb.	1.06	396	-13	-10	-16



Illustration: Reduction in Particulate Emissions

Item	Furnace A	Furnace B
NaBO ₂	1	1.36
NaOH	0.011	0.01
HBO ₂	0.25	0.34



Illustration: Furnace design for high efficiency

Source: Bauer et al, "Advanced Furnace Design Using New Oxy-Fuel Burners", 60th Conference on Glass Problems, Am. Cer. Soc., pp 1-8 (1999)

	Traditional designs			LoNOx Melter		
	end port	side port	side port	side port	side port	end-fired
Burners	oil	gas	gas	gas	gas	gas
Fuel	air	air	oxygen	air	oxygen	oxygen
Oxidant	regenerator	recuperator		recuperator		
Heat exchange	95	97	100	100	100	100
Fuel	5	3	0	0	0	0
Electric Boost	48	32	0	24	0	0
Preheated air	12	26	23	15	19	19
Struct. Heat loss	72	71	27	64	22	22
Exhaust gas	0	0	0	9	11	11
Preheated batch	63	34	48	43	57	60
Glass melt	63	34	48	52	68	71
Glass melt batch preheat						



Aluminum Industry: Vision 2020

- **Accelerate rate of aluminum use in existing and emerging markets**
- **Recycle 100% of aluminum**
 - Only 40% is recovered for secondary refining (USEPA, 1995)
 - Recycling requires 5% of the energy to produce secondary metal as compared to primary metal and generates only 5% of the greenhouse gas emissions (Source: 1999 Life Cycle Inventory Report for International Aluminum Institute, May 2000).
- **Improve net impact on the environment over life cycle of products**
- **Produce zero non-beneficial emissions (CO₂, VOCs, CFCs, SO_x, NO_x, Hg, HCl, landfill)**
- **Define next generation energy efficient processes**
- **Reduce cost of metal production and products by 25%**
- **Reduce energy use in melting by 25%**

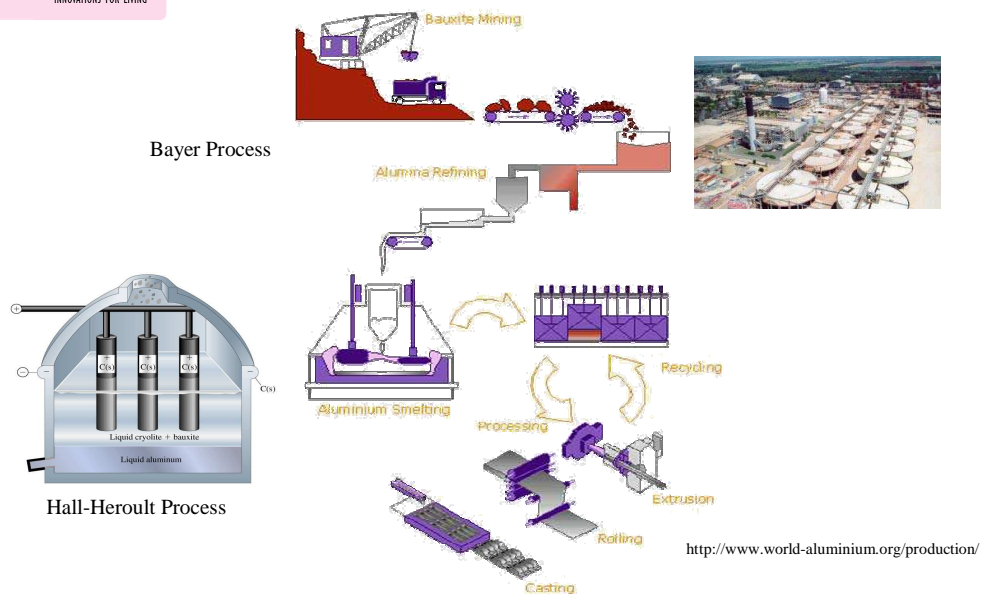


Simulations in Aluminum Industry

- **Reduce cost of production**
 - Smelting process requires 11-15 kWh for each kg of molten aluminum (annual production is about 20 million tons)
 - Use modeling to optimize energy use
- **Reduce emissions**
 - Number of sources
 - Grinding, Calcination, handling materials producing particulates
 - CO₂, VOCs, CFCs, SO_x, NO_x, Hg, HCl, landfill
- **Improve quality**
 - Control microstructure development for better mechanical properties
 - Use modeling for heat treating furnaces to ensure uniform and controlled heating / cooling



Aluminum Processing



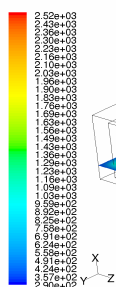


Example: Optimizing Aluminum Furnace

- **How to do it?**
 - Re-design it? (expensive)
 - Change burner locations (can be costly)
 - Assess the efficiency of the current operation of the furnace
 - Examine the flow field and energy usage to find ways of improving efficiency
 - Past modeling work has shown that adjusting fuel/air ratio, burner loading and injection angles can reap huge benefits
 - Try new ideas with modeling



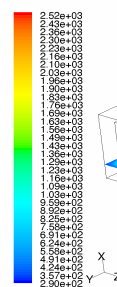
Temperature Comparison (same amount of fuel in each case)



Contours of Static Temperature (k) Oct 25, 2005
FLUENT 6.2 (3d, dp, segregated, pdf20, ske)

air case

$$T_{\max} = 1920 \text{ K}$$



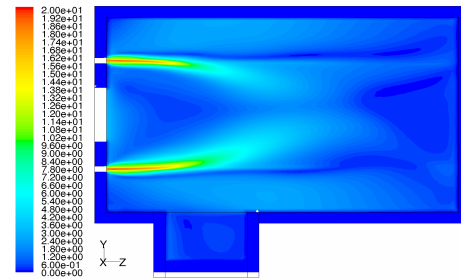
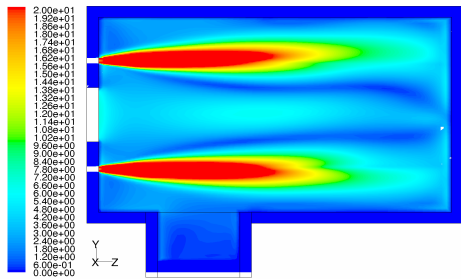
Contours of Static Temperature (k) Oct 25, 2005
FLUENT 6.2 (3d, dp, segregated, pdf15, ske)

Pure oxygen case

$$T_{\max} = 2520 \text{ K}$$



Velocity Comparison

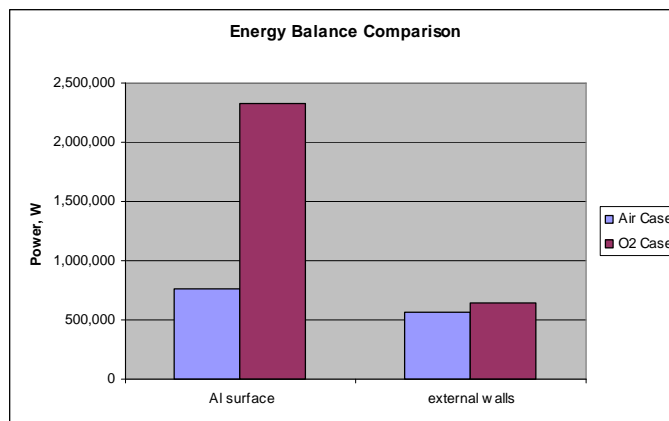


Energy Balance Comparison

Efficiency

$$\eta_{\text{air}} = 24\%$$

$$\eta_{\text{O}_2} = 37\%$$





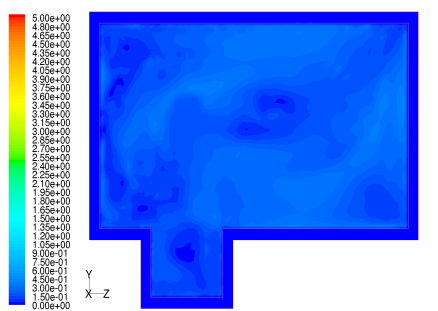
Improving Energy Transfer Further

- **Lowering aluminum temperature at the top surface will lead to more heat transfer to the melt**
 - Molten aluminum will be hotter on the top and colder on the bottom
 - One way to lower the melt temperature is to mix the melt.
 - Can be mixed by impeller(s) or by pumping



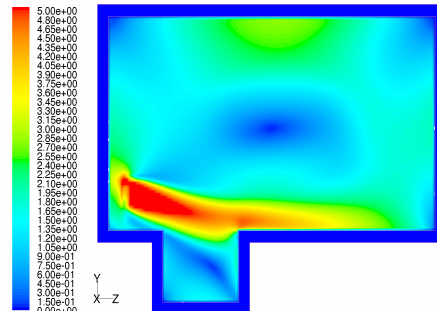
Melt Velocity Distribution

No mixing



Contours of Velocity Magnitude (m/s) Oct 25, 2005
FLUENT 6.2 (3d, dp, segregated, ske)

Pumping

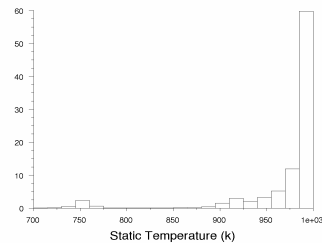


Contours of Velocity Magnitude (m/s) Oct 25, 2005
FLUENT 6.2 (3d, dp, segregated, ske)

- **Only pumps along the wall were considered with a fixed pumping power**
- **Pumps have the advantage of allowing control over direction**

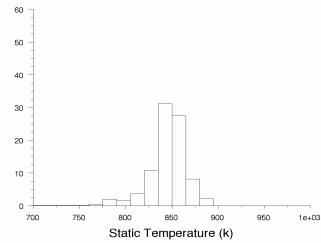


Temperature Variation Inside the Melt from Top to Bottom



Histogram of Static Temperature
Oct 25, 2005
FLUENT 6.2 (3d, dp, segregated, ske)

no agitation



Histogram of Static Temperature
Oct 25, 2005
FLUENT 6.2 (3d, dp, segregated, ske)

pump-1

- **Modeling shows that mixing homogenizes (and lowers) the temperature**
- **This may help offset the effect of the higher heat flux**



Concluding Remarks



- **Process industries have set ambitious goals for improving production and energy efficiencies and reducing emissions.**
- **CFD based modeling will play an important role in achieving these goals.**
- **Examples from the glass and metals processing industries were discussed to illustrate the role of modeling.**

THE FOSSIL FUEL FIRED GLASS FURNACE – A THERMOCHEMICAL REACTOR ATTACHED TO AN IMPERFECT HEAT EXCHANGER

Reinhard Conradt
Department of Mineral Engineering and Chair of Glass and Ceramic Composites
RWTH Aachen, Germany
Tel. +49-241-809-4966, Fax +49-241-8092-129, E-mail conradt@ghi.rwth-aachen.de

INTRODUCTION

For the past years, energy prices seem to have increased considerably, with no upper threshold visible yet. As glass industry sensitively depends on energy prices as one of its major economic factors, the glass community pays even more attention than usual to any yet unexploited possibilities of energy saving [1]. However, implementing energy saving measures in an effective way requires a realistic self-assessment of the acquired state of energy utilization – and this is not an easy task, especially not for small and medium size enterprises. Benchmarking [2] has been used as a tool to support the self-assessment procedure. However, assessing one's relative position of energy utilization among a lot of competitors does not yet offer the slightest clue on how to improve an individual operation. Therefore a realistically attainable self-assessment should be based on a long-term observation of the own performance, evaluating the set of production parameters which are documented anyway during daily production routine. The present paper sketches the development of self-assessment formulae designed to just serve the purpose outlined above. Based on earlier investigations [3-4], it makes use of a zero-dimensional approach to fossil fuel fired glass furnaces. The combustion space and the attached heat recovery system constitute, so to speak, a power station transferring process heat to the tank constituting, so to speak, a chemical reactor.

HEAT BALANCE

Any self-assessment must be based on correct and self-consistent data. Therefore, the following treatment is based on a first law heat balance (see fig. 1). The heat balance is valid for a specific production situation (the ratios of individual quantities may change with time, pull rate, etc.). It may be expressed, either in terms of heat quantities H referred to 1 t of produced glass [kWh/t], or to powers Q' [kW], or to heat fluxes q [kW/m²] referred to the melting area A . As shown in figure 1, the above quantities are linked by the production rate m' [t/h], and by the pull rate r [t/(m²·h)], respectively. The heat balance may be referred to the complete installation:

$$H_{in} = H_{ex} + H_{wu} + H_{wo} + H_{stack} + H_{ux};$$

the furnace:

$$H_{sf} = H_{in} + H_{re} = H_{ex} + H_{wu} + H_{wo} + H_{off};$$

$$H_{in} = H_{ex} + H_{wu} + H_{wo} + H_{off}(1 - \eta_{re}); \quad \text{with } \eta_{re} = H_{re}/H_{off};$$

the heat exchanger:

$$H_{off} = H_{re} + H_{stack} + H_{wx};$$

the combustion space:

$$H_{sf} = H_{in} + H_{re} = H_{ht} + H_{wo} + H_{off};$$

$$H_{in} = H_{ht} + H_{wo} + H_{off}(1 - \eta_{re});$$

the tank:

$$H_{ht} = H_{ex} + H_{wu}.$$

With the exception of the wall losses H_{wu} and H_{wo} , all individual quantities are quantified easily by evaluating: the amount of glass produced, the amount of fuel and air (or oxygen) used, the temperature levels of the offgas at the entrance and exit of the heat recovery system (T_{off} and T_{stack} , respectively), of the pre-heated air (T_{re}), as well as of the melt (T_{ex}) pulled from the furnace. Performing a long-term evaluation of the above sub-balances already yields most valuable information on the efficiencies (and potential weaknesses) of the individual components of the installation. The amounts of heat related to the combustion space are derived by combustion calculations, the ones related to the pull of glass are derived from the heat content ΔH_T of the glass melt at T_{ex} , and the standard heat ΔH_{chem}^0 of the batch-to-melt conversion. The latter two quantities constitute the intrinsic heat demand (or exploited heat) H_{ex} of the process:

$$H_{ex} = (1 - y_C) \cdot \Delta H_{chem}^0 + \Delta H_{T=T_{ex}}$$

where y_C is the fraction of cullet per t of glass. H_{ex} can be calculated from the batch and glass composition at high accuracy [5-6] (calorimetric verification: [7]). The wall loss figure H_{wx} and the sum $H_{wo} + H_{wu}$ are determined by the difference to the rest.

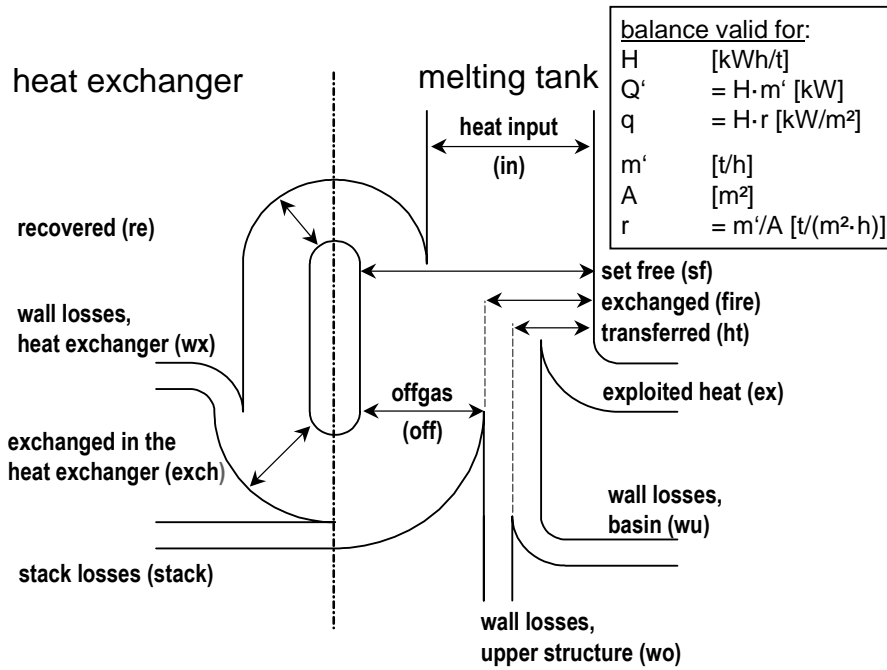


Fig. 1. Heat balance of a glass melting tank furnace with heat recovery system

CONVENTIONAL HEAT TRANSFER

Within the heat balance in figure 1, the heat H_{ht} transferred to the tank is a crucial quantity. It is by H_{ht} only that the “power station” and the “chemical reactor” can be balanced separately. Note that in contrast to 3-D furnace models, H_{ht} is a quantity integrated over the entire exchange interface A . It does not reflect any local details, hence, is not referred to any locally distributed temperatures. Like all other quantities summarized in figure 1, it is a balance-sheet item, nevertheless accurately reflecting the overall performance of a glass furnace. The details of the conventional approach of heat exchange are sketched in figure 2. The relevant temperature levels are: the adiabatic flame temperature T_{ad} (also comprising the heat contained in the pre-heated air), the temperature T_0 of the environment, and the temperatures T_{off} and T_{ex} mentioned before. The heat capacity fluxes $\dot{m}'_L \cdot c_L$ and $\dot{m}'_H \cdot c_H$ of the cold and hot stream, respectively, as well as the heat transfer function (number of transfer units) NTU_{ht} are determined by quantities derived from the heat balance, plus a yet unknown overall heat transfer coefficient α [W/(m²·K)]:

$$\dot{m}'_L \cdot c_L = r \cdot A \cdot \frac{H_{ex}}{T_{ex} - T_0}; \quad \dot{m}'_H \cdot c_H = r \cdot A \cdot \frac{H_{in}}{T_{ad} - T_0}; \quad NTU_{ht} = \frac{\alpha \cdot (T_{ad} - T_0)}{r \cdot H_{in}} .$$

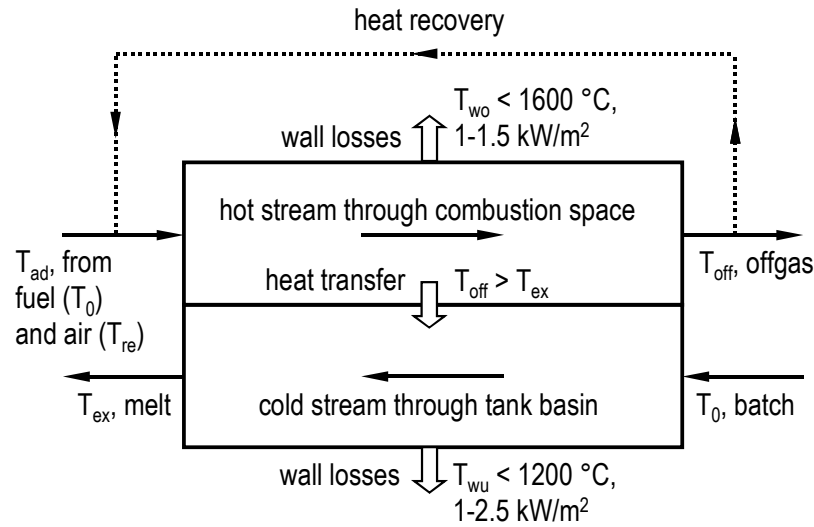


Fig. 2. The glass furnace presented as a counter-flow heat exchanger operating between temperature levels T_{ad} (adiabatic flame temperature) and T_{off} (offgas temperature) on the hot stream side, and T_0 (ambient temperature) and T_{ex} (pull temperature) on the cold stream side

Using the abbreviations Δ_{ex} and z_{HL} ,

$$\Delta_{ex} = \frac{T_{ex} - T_0}{T_{ad} - T_0}; \quad z_{HL} = \frac{\dot{m}_H \cdot c_H}{\dot{m}_L \cdot c_L};$$

the solutions for H_{ht} , T_{off} and T_{ex} read:

$$H_{ht} = \frac{H_{ex}}{\Delta_{ex}} \cdot \left[1 - \frac{1 - z_{HL}}{1 - z_{HL} \cdot \exp(-NTU_{ht} \cdot (1 - z_{HL}))} \right];$$

$$T_{off} = T_{ad} - (1/z_{HL}) \cdot (T_{ad} - T_0) \cdot \left[1 - \frac{1 - z_{HL}}{1 - z_{HL} \cdot \exp(-NTU_{ht} \cdot (1 - z_{HL}))} \right];$$

$$T_{ex} = T_{ad} - (T_{ad} - T_0) \cdot \frac{1 - z_{HL}}{1 - z_{HL} \cdot \exp(-NTU_{ht} \cdot (1 - z_{HL}))}.$$

For reasons of simplicity, the formulae above do not comprise the wall losses yet, but this is easily added.

One specific feature of glass production manifests itself in an approx. constant value of T_{ex} .

Thus, the unknown quantity α is readily obtained as:

$$\alpha = \frac{r \cdot H_{in}}{(1 - z_{HL}) \cdot (T_{ad} - T_0)} \cdot \ln \left(\frac{1 - \Delta_{ex}}{1 - \Delta_{ex} / z_{HL}} \right) .$$

Like NTU_{ht} , α depends of the pull rate r . The above equations, if extended for the effects of wall losses, form a basis to assess the ratio $\eta_{ex} = H_{ex}/H_{in}$, i.e., the overall process efficiency, as a function of the pull rate r , the pull temperature T_{ex} , and the adiabatic flame temperature T_{ad} .

RADIATIVE HEAT EXCHANGE

An alternative integral approach to H_{ht} based on radiation exchange between combustion space and glass melt has been presented before [8] (see fig. 3). The individual heat fluxes transported

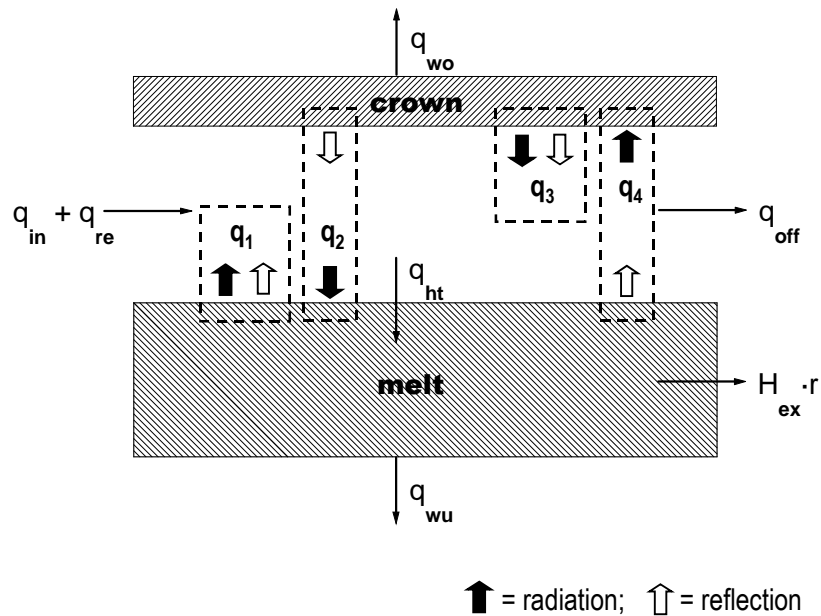


Fig. 3. Simplified radiation exchange model for the combustion space of a glass furnace [8]; q = heat fluxes in kW per m^2 of melt surface; index 1: leaving the melt; 2: directed towards the melt; 3: leaving the crown; 4: directed towards the crown; other indices: see figure 1

by emission and reflection of heat radiation constitute the following equation system:

$$\begin{aligned} q_1 &= C_s \cdot \varepsilon_m \cdot T_m^4 + (1 - \varepsilon_m) \cdot q_2; & q_2 &= C_s \cdot \varepsilon_{gas} \cdot T_{gas}^4 + (1 - \varepsilon_{gas}) \cdot q_3; \\ q_3 &= C_s \cdot \varepsilon_{wo} \cdot T_{wo}^4 + (1 - \varepsilon_{wo}) \cdot q_4; & q_4 &= C_s \cdot \varepsilon_{gas} \cdot T_{gas}^4 + (1 - \varepsilon_{gas}) \cdot q_1; \end{aligned}$$

which, in turn, yields solutions for q_1 to q_4 as well as for $H_{ht} = (q_2 - q_1)/r$ and $H_{wo} = (q_4 - q_3)/r$. It is true, information on the emissivities ε of the glass bath surface (m), the furnace atmosphere (gas), and the crown refractories (wo) is quite uncertain. But when combining the above results to those obtained by the conventional heat transfer approach, and with measured values of T_{off} and T_{ex} , then a self-consistent data set of ε_m , ε_{gas} , ε_{wo} can be generated for an individual furnace, which is of great value in a self-assessment attempt. The combined approaches help to quantify the calorific and thermal aspects of glass production showing how much energy has to be employed to make available a workable glass melt at a temperature level T_{ex} and at a certain pull rate r .

THE TANK AS CHEMICAL REACTOR

Nothing has been said so far on the limits of the pull rate stemming from the required quality of the produced glass. No doubt, a high glass quality corresponds to long dwell times τ_m of the melt in the tank and vice versa. For example: A high quality float glass reaches values of $\tau_m \approx 70$ h while a beer bottle may require less than 24 h. The principle is illustrated in figure

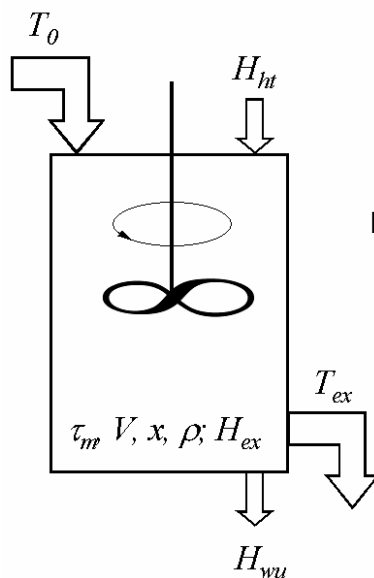


Fig. 4. Black box model of the tank presented as chemical reactor with volume V , dead volume fraction x , density ρ and mean dwell time τ_m of the melt; H_{ex} is the intrinsic heat turnover, H_{ht} is the amount of heat transferred to the reactor, H_{wu} is the amount of heat lost through the reactor walls; input and output temperature levels of the reactants and the product are T_0 and T_{ex} , respectively

4:

Let τ_{Qu} denote the dwell time required to reach a specifically high glass quality, and τ_{ex} the time to reach an average quality. Then the corresponding pull rates r_{Qu} and r_{ex} , respectively, are given by [9]

$$r_{Qu} = \frac{\rho \cdot V \cdot (1-x)}{\tau_{Qu} \cdot A}; \quad r_{ex} = \frac{\rho \cdot V \cdot (1-x)}{\tau_{ex} \cdot A} .$$

The ratio r_{ex}/r_{Qu} is equal to $\tau_{Qu}/\tau_{ex} \equiv K_{Qu}$, where $K_{Qu} > 1$ denotes a quality factor valid for a high quality glass relative to an average quality glass. The enhanced dwell time τ_{Qu} changes the amount of heat H_{ht} to be transferred to the reactor like

$$H_{ht} = H_{ex} + H_{wu} = H_{ex} + \frac{q_{wu}}{r_{ex}} \cdot K_{Qu} \quad ,$$

where q_{wu} denotes the more or less pull independent heat flux through the lining of the reactor. Finally, let us express the amount of heat transferred to the reactor by using the temperature level T_{off} as determined experimentally, or alternatively, as calculated from figure 2. Then, the following ratio of heat transferred to heat employed, H_{ht}/H_{in} , is obtained as

$$\frac{H_{ht}}{H_{in}} = \frac{\Delta T_{ad} - \Delta T_{off}}{\Delta T_{ad} - \eta_{re} \cdot \Delta T_{off}} \quad ;$$

here, ΔT_j denotes the temperature difference $T_j - T_0$, $j = ad, off$, and $\eta_{re} = H_{re}/H_{off}$ denotes the efficiency of the heat recovery system. Thus, the quality dependent amount of employed heat H_{in} is given by

$$H_{in} = H_{ex} \cdot \frac{\Delta T_{ad} - \eta_{re} \cdot \Delta T_{off}}{\Delta T_{ad} - \Delta T_{off}} \cdot \left(1 + \frac{q_{wu}}{H_{ex} \cdot r_{ex}} \cdot K_{Qu} \right) \quad .$$

SECOND LAW APPROACH FOR FINITE TIME OPERATIONS

An alternative approach to the relation between the amount of heat H_{ex} intrinsically required and the amount H_{ht} to be transferred to the reactor is sketched in figure 5: A quasi endoreversible cyclic process generating a useful power output q_{ex} is operated between two

$$q_{ex} \leq q_{ht} \cdot \left(1 - \frac{T_0}{T_{ht}} \right) \quad ,$$

heat reservoirs at T_{ad} and T_0 , respectively [10-12]. A parallel heat leak is taken into account, too. The upper threshold of q_{ex} is given by a Carnot type relation

yet the intermediate temperature level T_{ht} is strongly dependent on the rate of operation: At infinitely slow operation, T_{ht} approaches T_{ad} , thereby maximizing the term $(1 - T_0/T_{ht})$, but minimizing q_{ht} , yielding a very small q_{ex} . At very high operation rates, q_{ht} is large, but $(1 -$

T_0/T_{ht}) becomes very small, again yielding a very small q_{ex} . In-between these extremals, q_{ex} assumes a maximum.

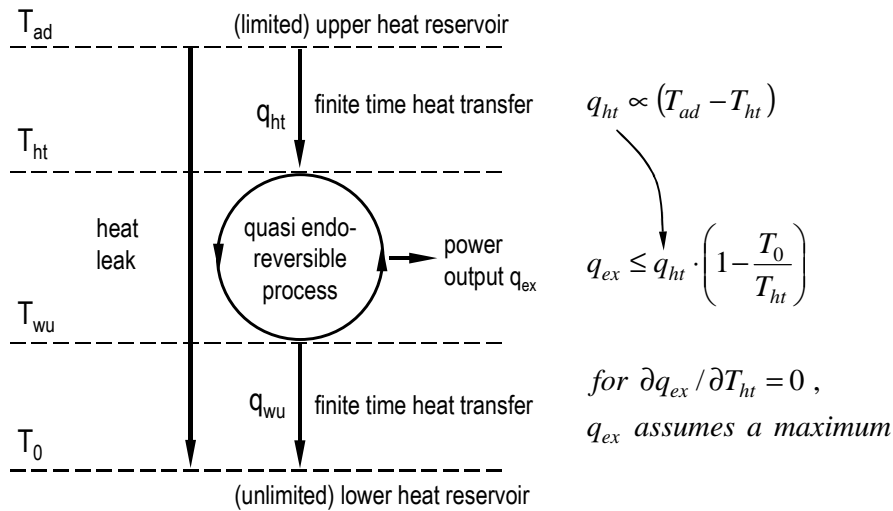


Fig. 5. So-called Curzon-Ahlborn cycle [10] operating at a finite rate between two heat reservoirs T_{ad} and T_0 ; depending on the operation rate, the internal temperature levels T_{ht} and T_{wu} deviate from the levels of the heat reservoirs

The evaluation of this cycle yields a lower threshold for the amount of overall heat H_{in} required to make available an amount H_{ex} , reading

$$H_{in} \geq \frac{H_{ex}}{1 - \sqrt{T_0/T_{ad}}} .$$

It is true, the application of this principle to glass melting may be questioned on the ground that $q_{ex} = r_{ex} \cdot H_{ex}$ does not represent an amount of heat converted to work. On the other hand, the rate dependent amount of power q_{ex} pulled from the furnace may be considered as an equivalent of work even if it is not used for this purpose. The consequences of the treatment are illustrated in figure 6: The ratio of an arbitrarily chosen pull rate r to the maximum pull rate r_{max} achievable by a given furnace is plotted as a function of the overall efficiency $\eta_{ex} = H_{ex}/H_{in}$. This is done for the unrealistic case of the absence of any heat leak as well as for a low and a high heat leak. It is interesting to note that the treatment yields the same type of efficiency vs. pull rate relations as the conventional heat transfer treatment, however, with some additional information: It reveals the difference between a furnace operation at optimal efficiency of heat exploitation versus an operation aiming at maximum glass output. These two points of operation are, in fact, the external in-between which a producer may optimize

his production process. On the other hand, this type of plot may also be used to determine the extent at which the pull rate may be lowered for quality reasons without impairing too much the efficiency of heat exploitation.

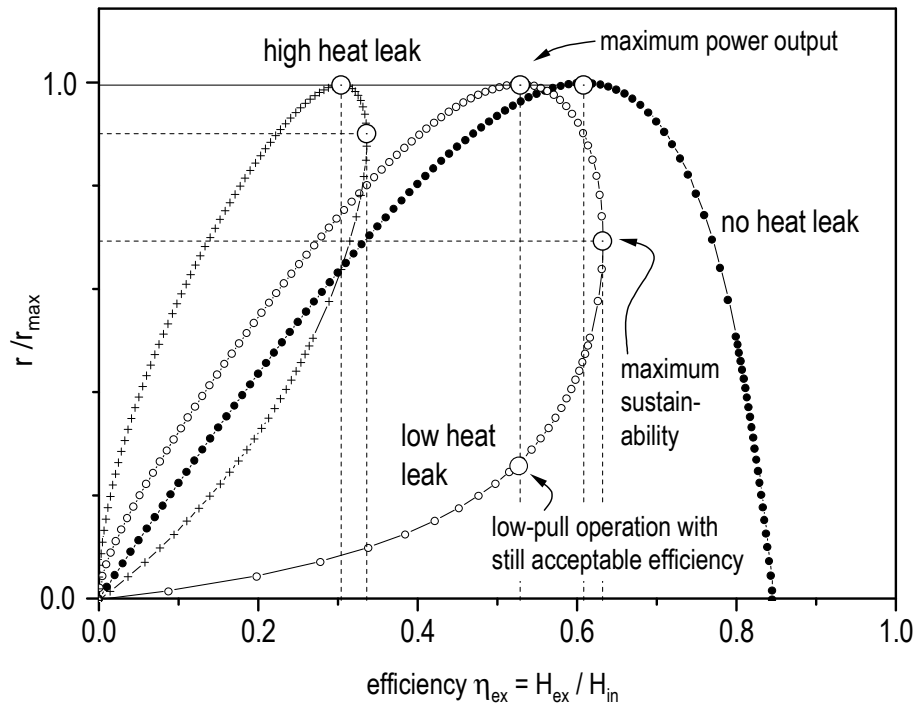


Fig. 6. Ratio of an arbitrarily chosen pull rate to a maximum pull rate, plotted as a function of the overall thermal efficiency of a Curzon-Ahlborn process [10]; three different degrees of heat leak are evaluated

CONCLUSIONS

A simplified treatment of fossil fuel fired glass melting tank furnaces was unfolded, conceiving the furnace as a heat exchanger attached to a chemical reactor. In order to reach full quantification of the result, the approach was based on a conventional heat balance. The heat transfer from the combustion space to the tank was modeled by two complementary approaches, i.e., by a conventional heat transfer model applied to a heat exchanger operated in counter-flow mode, and by a simplified radiation model [8]. The important issue of glass quality was implemented by using a reactor-chemical approach [9]. This approach allows one to compare the increase of heat demand due to quality-based extended dwell times in the tank to operations aiming at intermediate glass qualities only. Finally, an unconventional approach successfully used in the optimization of energy conversion [10-12] was applied to glass melting. This approach allows one to discern between operations aiming at a maximum output of produced glass versus operations aiming at minimizing the amount of energy

consumed per unit of produced glass. All individual approaches presented can be combined. They constitute a simple yet powerful tool to perform a self-assessment of production efficiency based on data recorded in every factory during day-to-day production routine.

REFERENCES

- [1] C.P. Ross, G.L. Tincher: Glass melting technology: A technical and economic assessment. Project Report No. DE-FC36-021D14314. M. Rasmussen, ed. The U.S. Department of Energy 2004.
- [2] R. G. C. Beerkens, J. van Limpt: Energy efficiency benchmarking of glass furnaces. 62nd Conference on Glass Problems, Illinois 2001
- [3] A. R. Cooper: An overall view of continuous glass making. *Glass Technol.* 21 (1980), 87-94.
- [4] R. Conradt: The Glass Melting Process-treated as a cyclic process of an imperfect heat exchanger. *Advances in Fusion and Processing of Glass. Ceramic Transactions* 141, (2004), 35-44.
- [5] R. Conradt, P. Pimkhaokham: An easy-to-apply method to estimate the heat demand for melting technical silicate glasses. *Glastechn. Ber.* 63K (1990), 134-143.
- [6] R. Conradt: Chemical structure, medium range order, and crystalline reference state of multicomponent oxide liquids and glasses. *J. Non-Cryst. Solids* 345 & 346 (2004), 16-23.
- [7] C. Madivate, F. Müller, W. Wilsmann: Thermochemistry of the glass melting process – Energy requirement in melting soda-lime-silica glasses from cullet-containing batches. *Glastechn. Ber. Glass Sci. Technol.* 69 (1996) No. 6, 167-178.
- [8] M. Lindig: The challenge of conventional furnace design. *Glass Technol.* 46 (2005), 109-112.
- [9] L. Nemeč: Energy consumption in the glass melting process. Pt. 1. Theoretical relations. Pt. 2. Results of calculations. *Glastechn. Ber. Glass Sci. Technol.* 68 (1995), 1-20, 39-50.
- [10] F. L. Curzon, B. Ahlborn: Efficiency of a Carnot engine at maximum power output. *Am. J. Phys.* 43 (1975), 22-24.
- [11] B. Andresen, R. S. Berry, M. J. Ondrechen, P. Salamon: Thermodynamics for processes in finite time. *Acc. Chem. Res.* 17, 1984, 266-271.
- [12] P. Salamon, K. H. Hoffman, S. Schubert, R. S. Berry, B. Andresen: What conditions make minimum entropy production equivalent to maximum power production? *J. Non-Equilibrium Thermodynamics* 26 (2001), 73-83.

GLASS HOMOGENEITY AND PHYSICAL MODELLING

Jan Kučera
Laboratory of physical modelling – GTM
Hradec Králové, Špitálské 182
mail - kucera_gtm@mbox.vol.cz

Tomáš Krobot
Glass Service, Inc.

Abstract

Mechanical homogenization is capable of achieving the required levels of glass homogeneity. At present, physical modelling is the only exact method for designing and analyzing new homogenization systems. The improvement of physical modelling methods and the use of models those are close to actual systems lead to the discovery of phenomena which can radically influence the final glass homogeneity. This article describes the possibilities of creating non-homogeneous particles around stirrers and the impact of stirrers on cords.

1 GLASS HOMOGENEITY

Glass homogeneity is perhaps the most frequently mentioned glass property since the discovery of melting of this “beautiful but cunning mass”, as frequently referred to by the famous Czech glass scientist Dr. Volf. To-date, there have been two turning points in the process of obtaining homogenous glass. The first one occurred in 1798 when P. L. Guinand stirred molten glass with a cylinder of fireclay. The second turning point dates back to the 1960's when the propeller, blade and helix stirrers were introduced specifically for homogenisation of optical glasses. Since then the improvement of glass homogenisation has depended only on the modification of known stirrers and fine-tuning of stirrer systems.

The beginning of physical modelling of glass processes is intertwined with homogenization of optical glass. The development of a testing method for glass homogeneity, detailed requirements on glass quality and development of physical modelling prompt us to think about glass homogeneity. Is it at all possible to melt glass and process it in such way as to reach homogenous substance in a given product? Which factors lead to glass homogeneity and which factors cause the creation of non-homogeneity?

The process begins with a heterogeneous batch and ends with a substance with areas of aligned structure which smoothly gradates into an unaligned structure.

The term glass homogeneity is not defined explicitly. Glass is considered to be homogenous when it is free of areas with different refraction index or inner stress. Generally, some accept homogenous glass with bulk areas with the same refraction index and the same expansion coefficient but different composition. It is not acceptable to rate such glass as homogenous. Consider, for example, the glass for optoelectronic, where the thickness of the semi product

is less than 0.6 mm, and the required thickness tolerance is 0,001 mm, the acceptable level of non-homogeneity must be at least one, or better yet two orders less. To properly process such semi products, the standard methods for glass homogenization with paddle or helix stirrers are no longer adequate. New stirrers and homogenization processes must be developed step by step.

In this article, we are not going to deal with the application of physical modelling to solve glass homogenization. Instead, we will point out several phenomena we monitored while modeling various homogenization systems, which can, to some degree, be generalized. These monitored phenomena can fundamentally influence glass “homogeneity”.

The process of glass homogenization is a deeply laminar process ($Re < 1$). As a result, any inhomogeneity can be only stretched and spread by stirrers. No inhomogeneity can be chopped as the process of homogenization is sometimes interpreted to be capable of.

The physical modeling of homogenization is based on monitoring of tracers inserted into defined localities. Two types of tracers are used – continual tracers simulating sources of inhomogeneity, and unit tracers with a defined volume simulating random inhomogeneity. The trajectory and visibility of the tracer is evaluated during and after the process of the tracer going through the homogenization system.

In many cases there are only two tracer characteristics that are evaluated behind the homogenization system – tracer visibility and the lack thereof. The actual behavior of the tracer behind the stirrers is usually not monitored or studied. We found that the behavior of tracers behind the stirrer can actually uncover the origination of glass defects.

2 SINGLE STIRRER

2.1 *Virtual chopping of stray streaks / cords*

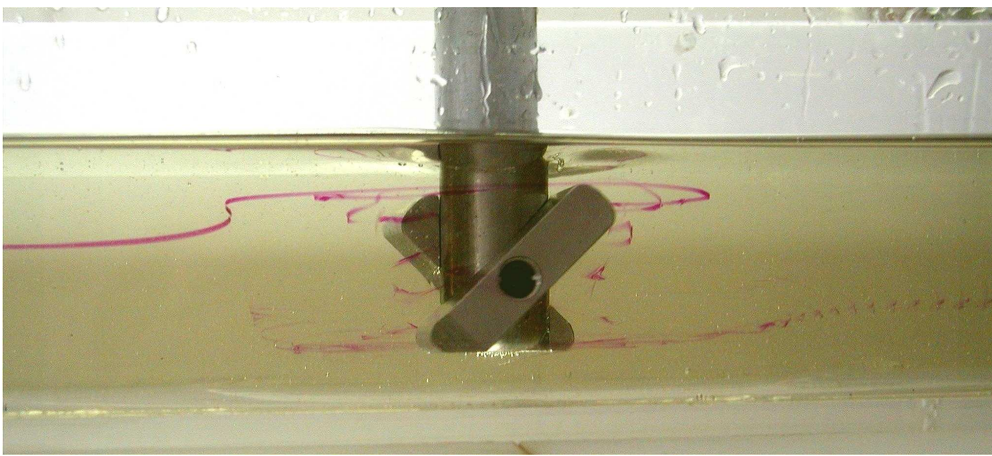


Fig. 1 shows a typical tracer progress through a stirrer

Upon initial inspection of the picture above, one might conclude that the stirrer has chopped up the continual tracer into separate inhomogeneities. However, a detailed analysis must take into consideration the fact that we are not monitoring a streamline but instead a stream tube which consists of an endless number of streamlines each following a unique trajectory. The streamlines can mingle, form nodes and create images of a separate inhomogeneity behind the stirrer. The actual stirrer blade can also create the nodes. Once the tracer is directly affected by the blade, it accepts the actual velocity of the blade for the period of time it needs to pass through the blade; after passing through the blade, the tracer begins to lose the obtained velocity. The result is the squeezing and compressing of the streamlines on the blade face and an apparent disintegration of the continual tracer.

Figure 2 below shows another mechanism of creating tracer nodes. Each mass element of the tracer is affected not only by the stirrer's radial force, which turns the liquid but also by the sum of the axial pumping and the centrifugal forces. The result of the above mentioned forces is a spiral trajectory of the tracer. The actual resultant force toward the mass element of the tracer is dependent on the actual relative positions of the blade and the mass element. It is clear that the combination of the periodic changes in the forces on the mass element of the tracer and the radial velocity gradient result in some kind of an overlapping of the tracer with visibly sharper areas of the tracer. (See Fig. 2).



Fig.2 shows an overlapping of the tracer

We can therefore conclude that the blade stirrer converts a smooth stream tube into a periodically highlighted structure.

A different example of a node point behavior is dependent upon the inter-phase tension between the inhomogeneity and its surrounding environment (bulk glass). If the actual inter-phase tension has the tendency to spread the inhomogeneity instead of concentrating it around knots, we can expect fewer problems with homogeneity.

In the example described above, the tracer stream tube is divided into independent streamlines primarily as a result of the impact of the axial pumping force and the periodic changes in tracer's velocity. In cases where this axial pumping force is weak relative to the dominant centrifugal force component, the inhomogeneity is stretched where the radial force can reach it; once it moves away from this zone however, it continues its flow in an unchanged form.

2.2 *Stirrer's strings*

We can observe recurring strings behind the stirrer even without inserting a tracer or other inhomogeneity to the model liquid. These strings are visible at a suitable illumination of the model. To be able to record such strings we used a simple laser system whose sensor can expose even very faint strings.

Each inhomogeneity deflects or diffuses the laser beam and the laser sensor then records any signal change. We used this methodology to test a stirrer that was placed in a canal with a homogenous model liquid running through it – see Fig.3.

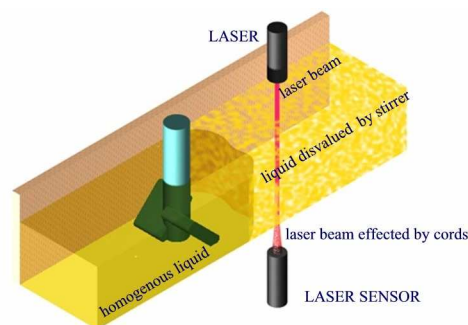


Fig.3 laser sensor

Figure 4 below shows the response of the laser sensor relative to the stirrer's revolutions per minute (RPM). Based on the measurements recorded, the intensity and frequency of the cords correspond with the stirrer's RPM.

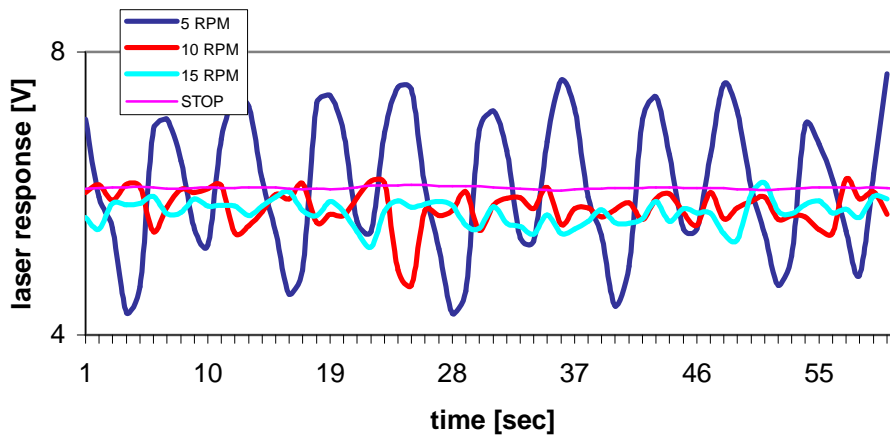


Fig. 4 shows the response of laser sensor

The results evoke the question of where and why the cords are created and is it possible to apply such observation to glass? From glass homogenization perspective, the model conditions used for this experiment can be considered ideal. (Isothermal conditions and relatively low viscosity $\sim 20\text{Pas}$).

If we accept the hypothesis that the model liquid in front of the stirrer is homogenous, then there are two possible explanations for the optical inhomogeneity behind the stirrer:

(1) The blending of the liquid surface into model liquid or (2) the creation of the optical cords as a result of shear stresses on the blade edges. Either option is merely a speculative explanation of the monitored events based on our long term study of various mixing systems. The blending of the surface layers of the liquid seems to be a logical explanation. The surface tension creates some sort of a membrane on the liquid surface which is disturbed near the stirrer and mixed into the model liquid. If the same behavior also applied to glass, the results would be much more pronounced since surface properties in glass have a greater influence than in the model liquid.

We can monitor changes in the refraction index near the blade edges especially if these edges are sharp. The influence of shear stresses on index refraction of the model liquid is one possible explanation we should consider. If the glass structure is taken into account, we can expect similar results in glass.

The performance of the simple laser sensor presented above confirms the visual monitoring of inhomogeneity created by a stirrer action in a homogenous liquid.

The scientific explanation of the monitored effects will require the development of new, more precise measurement methods for both physical modeling and measuring glass homogeneity.

The above mentioned problems are high-order. We find markedly worse cords behind the stirrers at real processes.

3 STIRRER SET

3.1 *Non correct design of the stirrers*

The aim of this article is to point out that the poorly designed stirrers and above all the design of spout can destroy acceptable glass quality.

The next picture shows typical case of ineffective homogenization. The stirrers pump up bottom usually cordy glass to main stream without significant homogenisation.

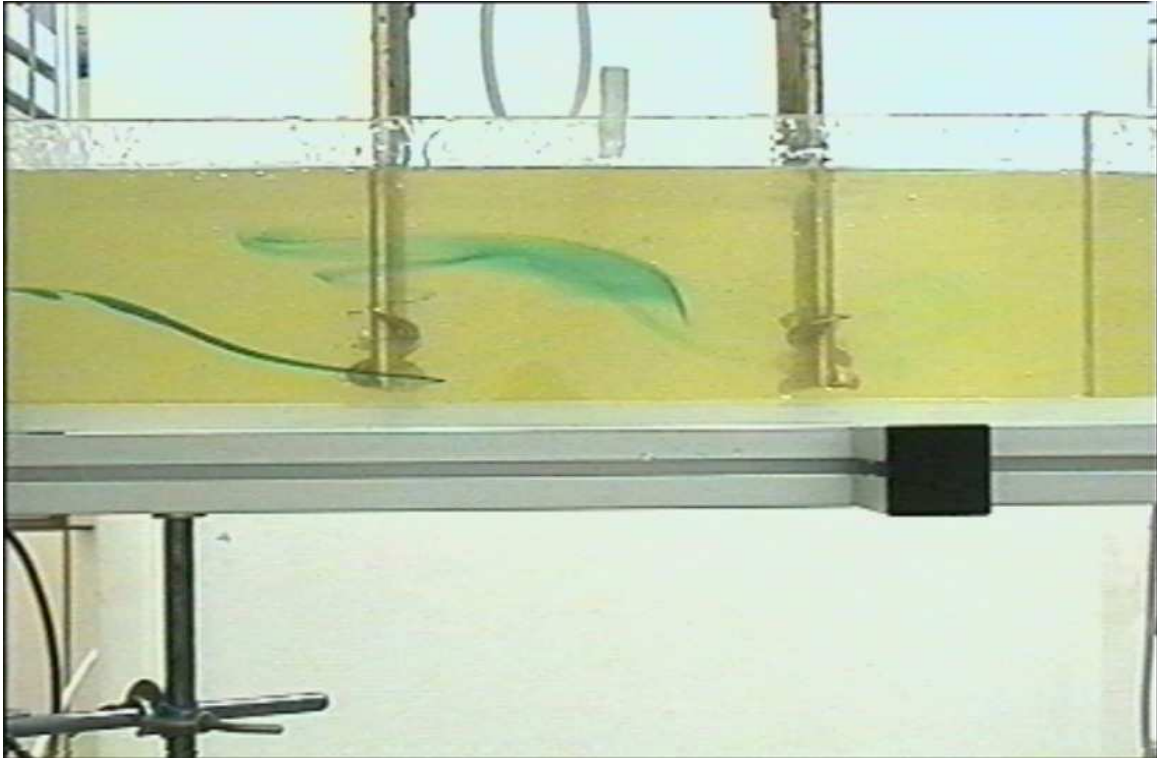


Fig. 5 cord slipping in between stirrers

Whirls in front of stirrers and behind the stirrers are additional example of inhomogeneity origin. There is stagnant glass in the calm center of every vortex and the whirl tails transport such glass to the bottom. If the whirl tail is not stirred up perfectly the cords are in a final product.

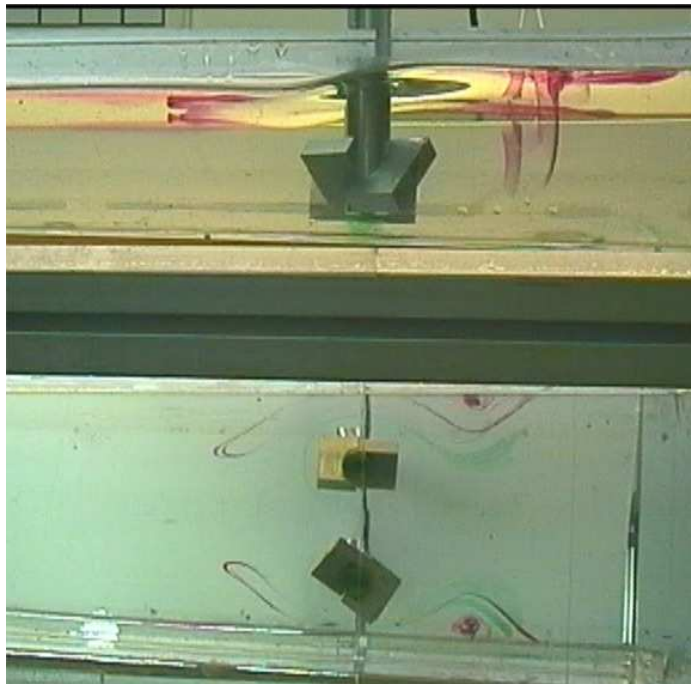


Fig. 6 vortex in front of stirrer

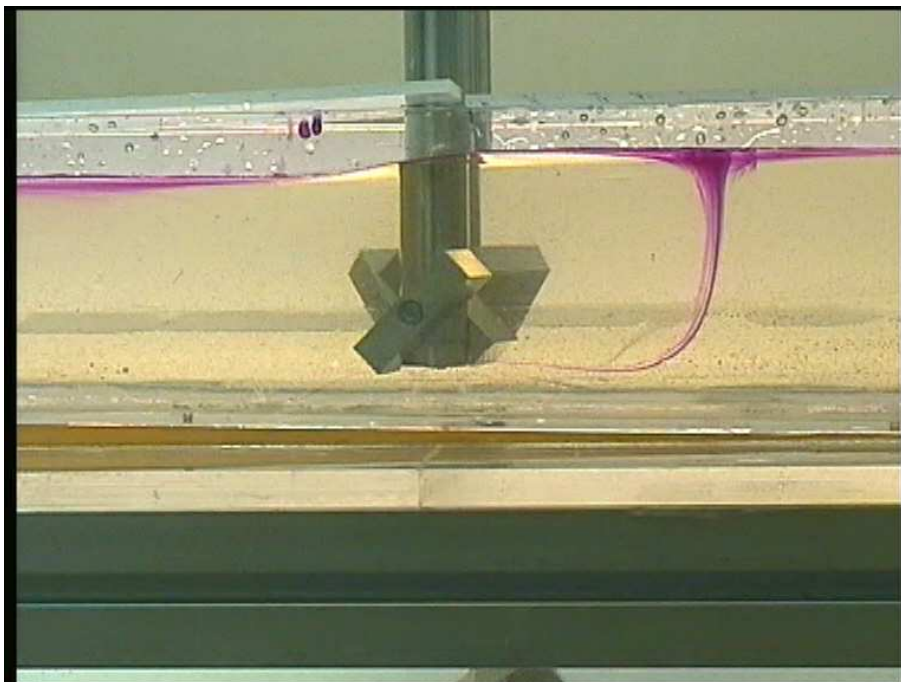


Fig.7 vortex and vortex tail

4 SPOUT AND HOMOGENIZATION

The glass homogenization is usually focused on stirrers and the spout design is leavened out. The design of the spout remains for long time without any turning point. There are two basic types of the spouts:

Hartford type – sleeve, sometimes with turbex and plunger

Gobber type – deep spout with Pt or ceramic gobber

Both types run with dead areas on the surface and such dead areas are endless sources of cordy glass

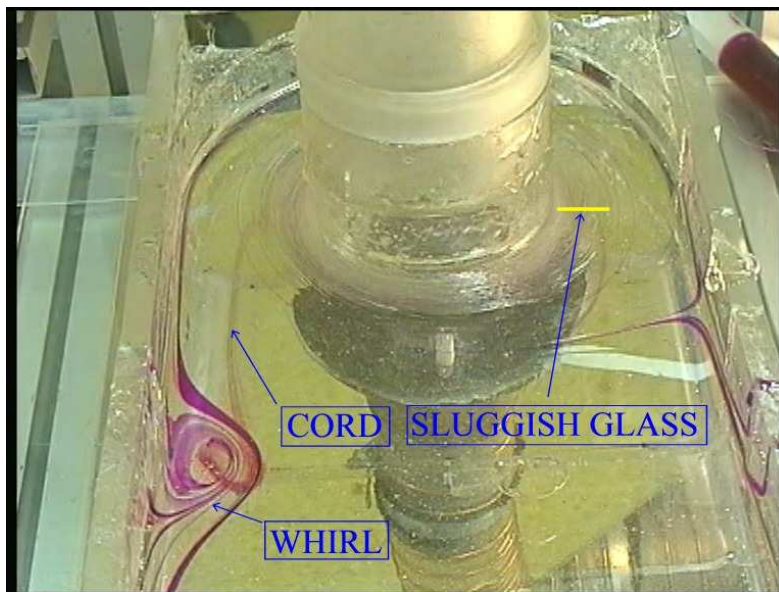


Fig. 8 Spout as rubbish heap of the all feeder

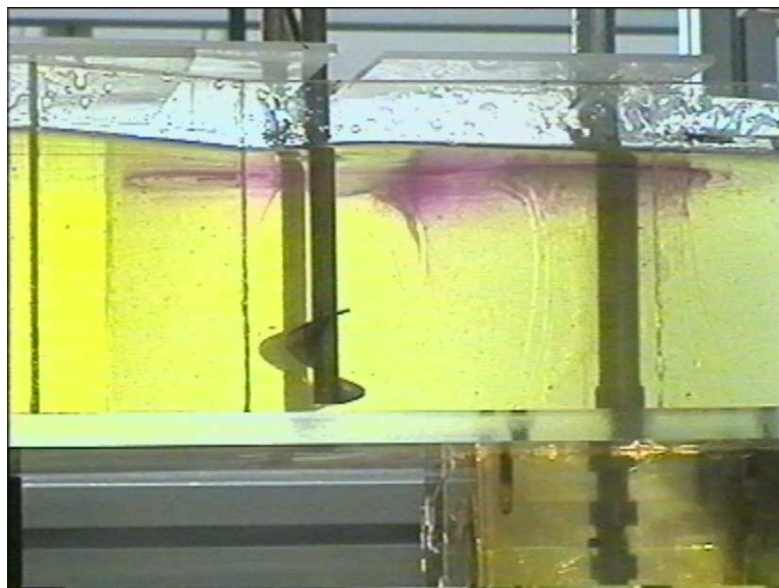


Fig. 9 Dead areas on the surface of a gobber spout

5 CONCLUSION

The aim of this article was to point out selected phenomena which accompany glass homogenization and which can significantly influence final glass homogeneity.

The results of physical modeling help to design such homogenization systems that reduce unfavorable effects of stirrers and spout design. At present, only physical modeling can disclose and determine weak points of existent homogenization systems.

New approaches to glass homogenization based on deep knowledge of the homogenization process will have to be used in order to satisfy customer requirements on glass homogeneity. The physical modeling ought to go before starting a real process to avoid operation problems and degradation of investment in homogenization system.

It could be too expensive adventure to design and put in operation a new homogenization system without a prior physical modelling study.

LASER EVALUATION METHOD OF PHYSICAL MODEL HOMOGENIZATION

Jan Kučera, Laboratory of physical modelling – GTM
Tomáš Krobot - GS
Miroslav Skřivan – Consultant GTM
Róbert Bódi - GS

Abstract

The physical modeling of mixing technology in the glass process has so far been based on stream visualization utilizing color tracers inserted into the model. However, rapidly increasing requirements for glass quality necessitate improved homogenization systems. Since the visual evaluation of these model designs appears to be inadequate, a method for objective evaluation of mixer effectiveness has been developed. This method is based on the oscillation of a laser beam caused by the residual tracers that remain after they pass through the homogenization system (these residual elements have different optical properties). If any inhomogeneity breaks through the bundle of the laser rays, it will change the intensity of the beam. A CCD sensor then detects and evaluates the resultant intensity range/array of the laser beam that passed through the model. The result is an objective evaluation of the homogenization effectiveness that is independent of the evaluator

Motto

The general principles of mixing and homogenizing viscous liquid by a combination of attenuation and diffusion seem to be reasonably well understood, but knowledge is not so complete that accurate theoretical predictions can be made for any particular system.

Cooper's 1966 still holds true today. To move the forecast closer to the accurate theoretical predictions for any particular system the new laser method for evaluation of homogenization systems was developed.

INTRODUCTION

Physical modeling provides invaluable information about stirring systems in glass technology. The visualization of color tracers inserted into a transparent liquid is a simple technique that provides important information about a given system and its ability to homogenize. Since the color tracers are injected into the transparent liquid across the entire cross section of the feeder, we have the ability to analyze the homogenization efficiency of any given stirring configuration. Every tracer passing through the stirrers is recorded on video and compared with others tracers. The color intensity of each tracer that made it through the stirrers then determines the degree to which inhomogeneity has been eliminated through mixing. This traditional method can identify weak points of the system and enable us to either optimize it or design a new system built to given specifications. This method, which has been used for 50 years, is essentially based on visual monitoring of a process which makes it dependent upon a "human factor". Our extensive experience with modeling different homogenization

systems led us to develop an objective method for the evaluation of efficiency of each individual system. Without an objective evaluation method we could not explain or characterize certain experiment phenomena such as the cords created by stirrers in homogenous liquid.

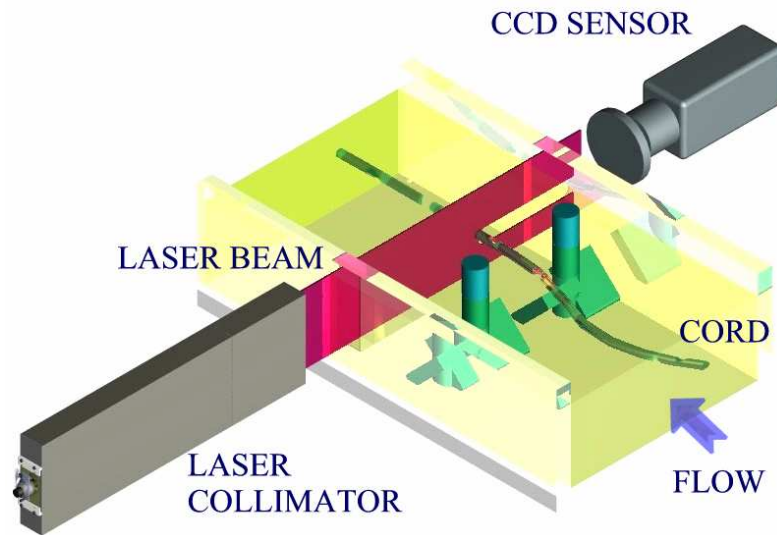
Several possible methods of inhomogeneity detection have been tested. They include the luminescence method, the resistance method based on measuring local conductivity, and finally the laser method. The best results were achieved with the laser method which is based on the oscillation of a laser beam as a result of residual inhomogeneity.

The laser method has uncovered new data for physical modeling which have previously been unavailable. This method uses a laser beam as a source of homogenous light which is then diffused by the tracers and therefore its intensity is changed in the entry point. Unlike in the traditional physical modeling, it is not necessary to use color tracers in laser modeling since the laser beam diffusion is caused by a different tracer index of refraction. As a result, this type of modeling is even closer to reality where inhomogeneity is defined as the one location with different optical properties. The quality of modeling is further enhanced by our improved ability to detect inhomogeneity. In addition to an improved ability to capture even the slightest change in the pseudo-homogeneous environment, we can obtain data about the tracer size, intensity, and, equally importantly, its residence time in the stirring system.

The Laser Method

Using this method, a laser beam is collimated so that it cuts through the entire cross section of the feeder model - from the liquid surface to the bottom of the model. The laser is positioned behind the stirrer set so that its beam is perpendicular to the direction of the liquid flow. The distance between the laser and the stirrer set has to be sufficient enough for the evaluated liquid stream in the detection area to represent the homogeneity of the liquid in the entire system. The laser beam, which cuts through the entire model, is recorded by a CCD camera. Figure 1 below depicts the model equipment.

Fig. 1. Equipment for a laser Method



Tracers are injected to several places in front of the stirrer set by volume, $0,5\text{cm}^3$ for each. The positions of injection must characterize the entire cross section of the feeder. The tracer liquid is transparent and of a higher refraction index than the host model liquid. This method is very sensitive and provides data about the tracer mix exiting the stirring area of the feeder. By recording the laser beam we obtain a set of sequenced laser images which are then converted into a matrix of values characterizing the laser intensity. The result of a mathematical data analysis of the intensity data is a graph depicting the tracer passing through the laser beam. Figure 2a shows an intensity curve of the laser beam when there is no tracer passing through the laser beam (background – green color). The corresponding laser intensity values range between 0 and 255. The measured data represented by the green curve is overlaid by the polynomial curve (red). Figure 2b compares the same curves in Figure 2a with the curve representing the laser beam intensity when the tracer passes through the laser beam (blue).

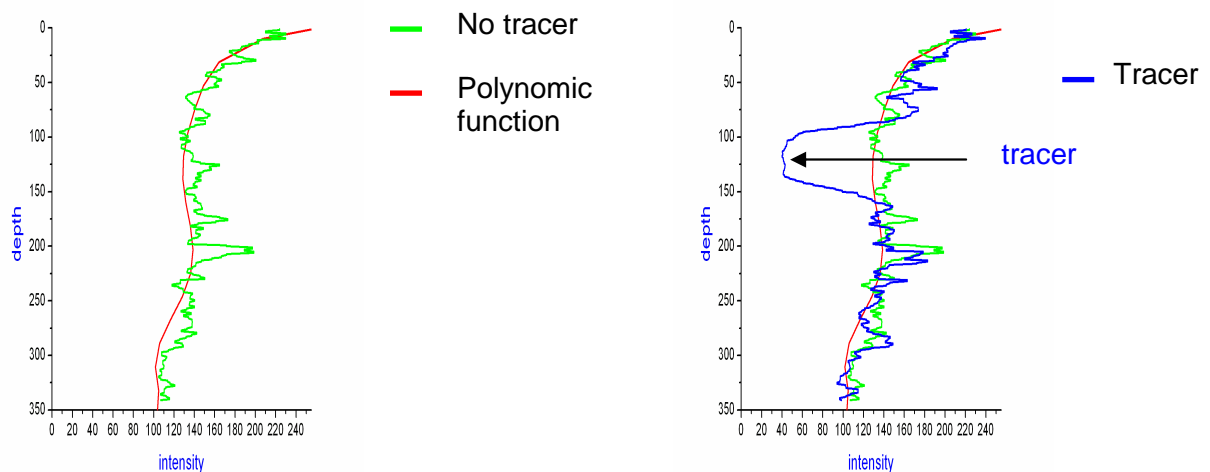


Fig. 2. Intensity distribution of laser beam

Figure 3 provides information about the tracer residence time in the mixing area. This plot diagram shows single frames of laser intensity structure sequentially one after the other.

Fig. 3. Intensity distribution of laser beam in time

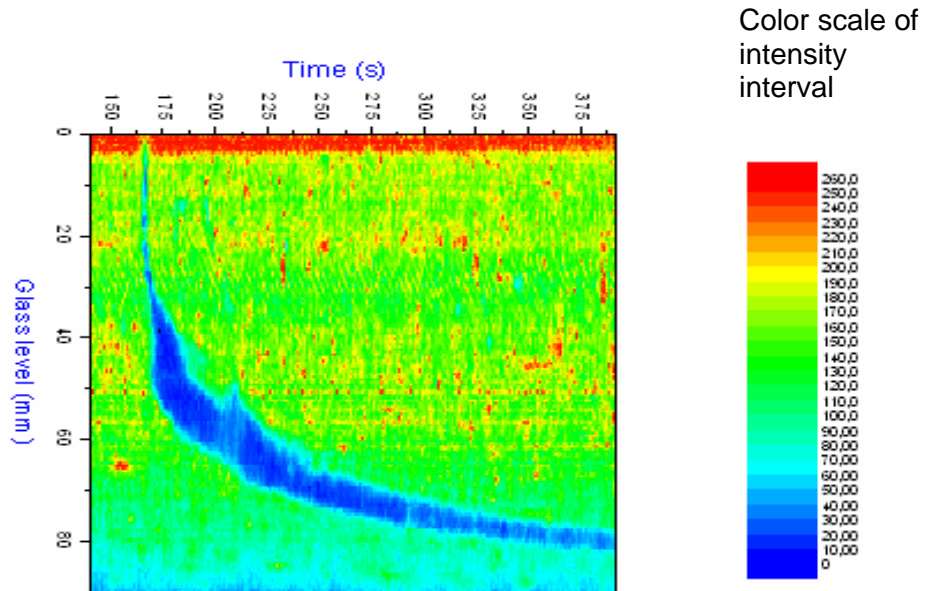
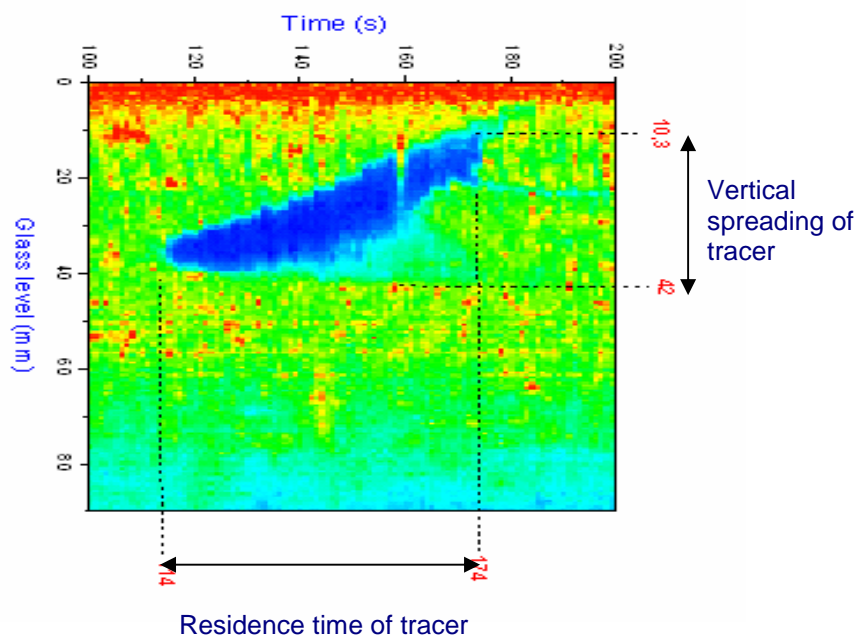


Figure 3 indicates that this particular tracer recording was stopped prematurely since the tracer is still being detected in the mixing area. The recording was stopped based on a visual monitoring which implies that the laser method is more sensitive than visual observation. Figure 4 shows the entire residence time of the tracer in the system in addition to its vertical spread and the pass-through section (top third of the liquid depth).

Fig. 4. Intensity distribution of laser beam in time



Stirrer's cords

The laser method has confirmed a new phenomena: the stirrers create inhomogeneity which is very difficult to detect by any other method. The degree to which these cords are created depends on the RPM of the stirrers, the shapes of the stirrers' blades, and the overall design of the stirrers. Figure 5 compares the trend in cord creation as a result of different RPM of the tested stirrer sets.

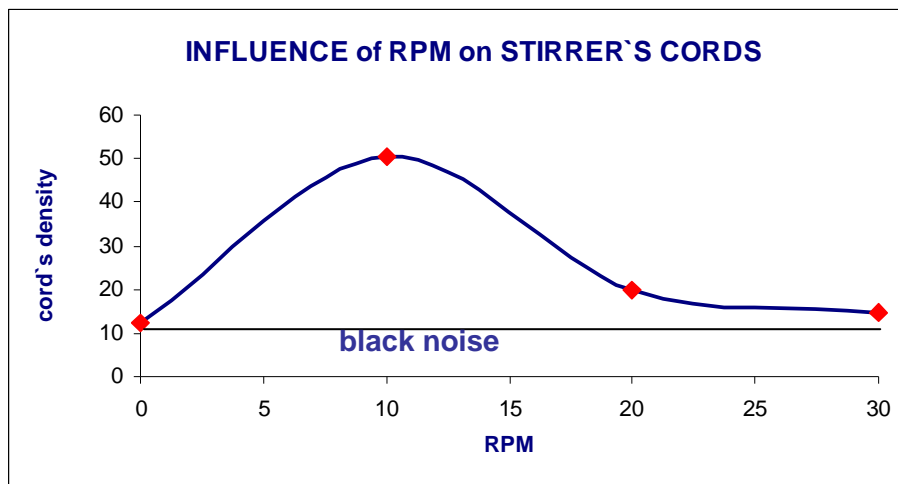


Fig. 5

CONCLUSION

The laser method opens new possibilities for physical modeling. It is a sensitive instrument for tracer detection behind the stirrer set in a homogenization system. This generates data about the real efficiency of the whole homogenization system. The model liquid in the initial testing was pseudo homogenous which well simulated real, every-day conditions. Adding another laser to the system could prove to be another step forward in advancing this method. This equipment diversification would enable us to obtain three-dimensional (3D) images and data related to the tracer. The resulting statistical evaluation of the data would then provide information about system efficiency and significantly improve our ability to compare it with other systems. In general, the laser method offers a new view on the homogenization process and corrects some generally accepted "myths" about stirrer homogenization. The testing results and data offer a new perspective on homogenization in viscous liquid.

EXPERT SYSTEM III ON GLAVERBEL FLOAT LINES FROM THEORY TO PRACTICE

Laurent Bakalarz - Olivier Mal
Michael Demeyere - Antonella Contino
Glaverbel - AGC Flat Glass Europe

Abstract

The theoretical potential benefits of the use of expert systems in the glass industries are well documented. Although expert systems were already in use since a couple of years within the US branch of the AGC group, these were not used within Glaverbel until recently. This paper describes the first installation of ESIII within Glaverbel.

After a brief reminder of the expected theoretical benefits of the use of expert systems on float lines, this paper focuses on the practical aspects of the installation of ESIII on the float line of Boussois 2, producing ca. 700 MTPD of clear glass in thicknesses ranging from 2 to 12 mm. At first, the different steps of the installation are briefly described, with a focus on its implication on the day-to-day production. Then, we concentrate on the observed performances of the system and its acceptance by the production team. Finally, we conclude with potential future steps, not only in Boussois but more generally within the AGC group.

INTRODUCTION

Generally speaking, expert systems are defined as (1) multi-input multi-output (2) model based predictive control systems. When applied to the control of float furnaces, their multi-input multi-output property enables them to control (classically) all bottom and/or crown temperatures by acting on all burners settings simultaneously. Their model based predictive control property is reflected in the fact that the stability of the control is obtained by means of certain “knowledge” of the dynamics underlying the process. This knowledge can be obtained either by an identification or by means of a (faster than real time) simulation of the process to be controlled.

Expected benefits of experts systems are induced by the stabilization of the controlled output parameters. Indeed, fluctuations on crown and bottom temperatures are naturally encountered on float lines. In order to avoid operating the furnace at too low temperatures, high set-points are therefore classically selected such that the lowest value of the fluctuating temperatures always is above a certain limit. When properly designed, expert systems tend to reduce the natural fluctuations observed on crown and bottom temperatures. As a result, they enable selecting lower set-points and thereby reducing energy consumption, as illustrated in Figure1. In addition, it might be reasonably expected that this stabilization should have a positive impact on overall glass quality, although this might be particularly difficult to evidence in reality.

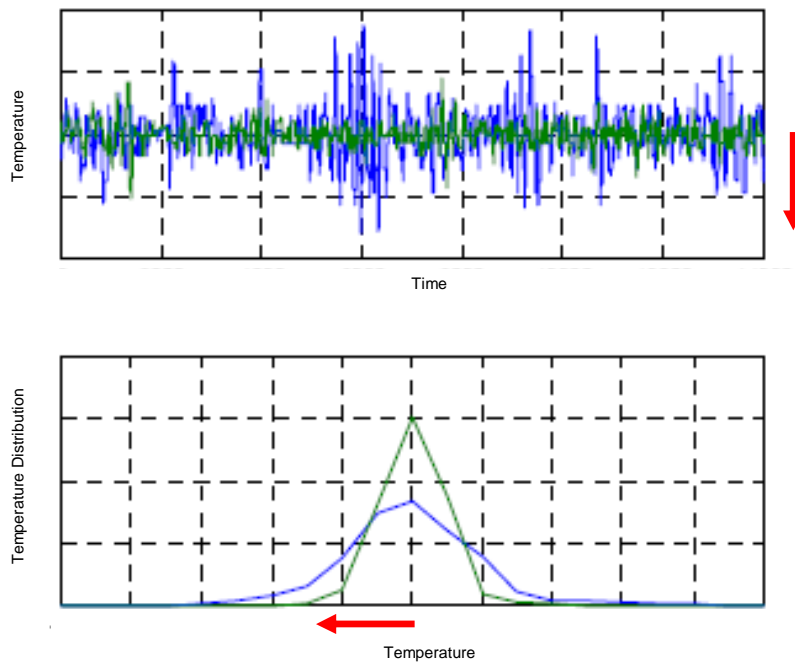


Figure1. Expected benefits of expert systems on energy consumption.

Traditional control in blue; ESIII control in green; potential action to gain energy in red.

In 2005, Glaverbel decided to install for the first time an expert system on one of its float located in Boussois. As explained here above, the main driver of the installation was precisely to test the potential of expert systems to reduce the quantity of energy needed to produce each ton of glass produced on the Boussois float line. The choice of Boussois as test furnace was made purposely because it has a stable production and it was already very good in energy consumption.

Although this installation was the first one to be carried out within the Glaverbel group, it was not by far the first installation within the Asahi Glass Company. Indeed, the expert system developed by Glass Service (ESIII in its latest version) was already installed on several float lines of AFG (sister company of Glaverbel in the USA), where it proved to be very effective in a.o. enabling the control of float lines subjected to fluctuating calorific power of natural gas. Even though the situation of the float line in Boussois is not exactly comparable to the one encountered on the float lines operated by AFG, the existence of past experience with ESIII within the AGC group was decisive for the decision to install this latter system in Boussois.

ESIII INSTALLATION

As shown in Figure2, several steps were followed in order to implement ESIII in Boussois. These steps are needed in order to provide the system with the necessary knowledge of the dynamics of the process in place on the float line. Controlled variables were the crown and canal temperatures. Manipulated variables were the fuel flow rates on each burner port and the dilution air flow rate in the working-end.

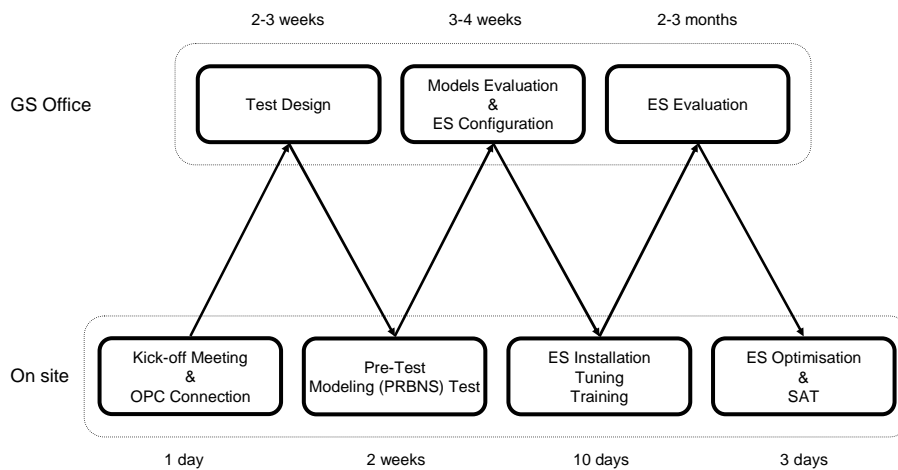


Figure2. Steps in the installation of ESIII.

Potentially the most critical step for the continuity of the float operation was the so-called Pseudo Random Binary Noise Sequence (PRBNS) test where all burner ports are activated simultaneously in order to capture the fully coupled nature of the dynamics. However, this went on very smoothly as the sometimes drastic constraints put by Glaverbel on admissible ups and downs in crown temperatures movements were fully taken into account by Glass Service without impacting the quality of the identification.

The results of the modeling steps are shown on the table given in Figure3. This table can be read in two ways. On the one hand, one can clearly identify for each incremental increase of fuel the dead time and dynamics of increase that it induces on each crown temperature. On the other hand, one can identify for each crown temperature that one wants to control which burner ports might be activated.

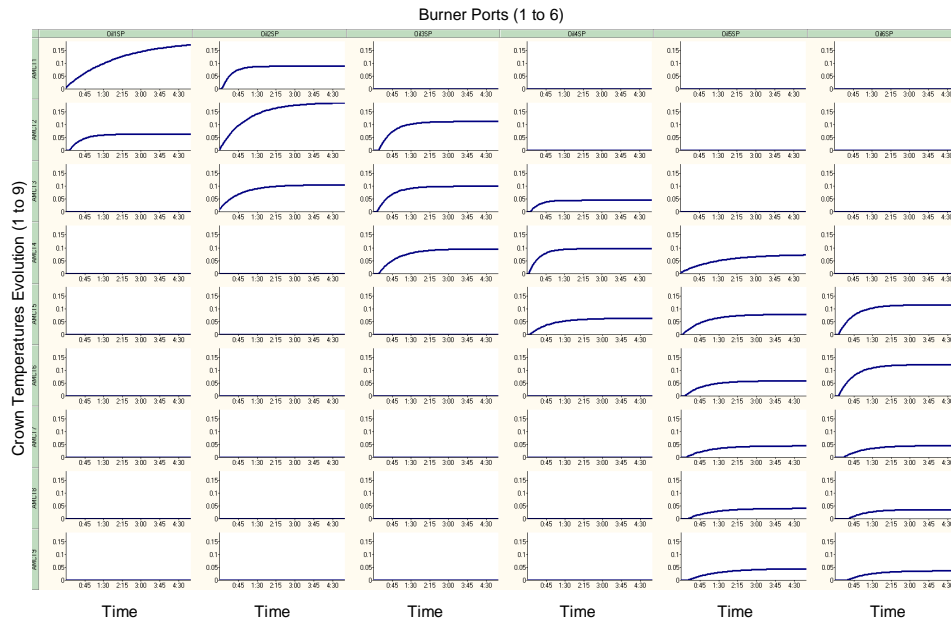


Figure3. Obtained melter models from modeling test.

Due to the excellent collaboration between the Glaverbel and Glass Service teams, the installation of ESIII went very smoothly, the most critical step having been finally the OPC connection. A snapshot of the screen installed in the control room of the furnace is given in Figure4.

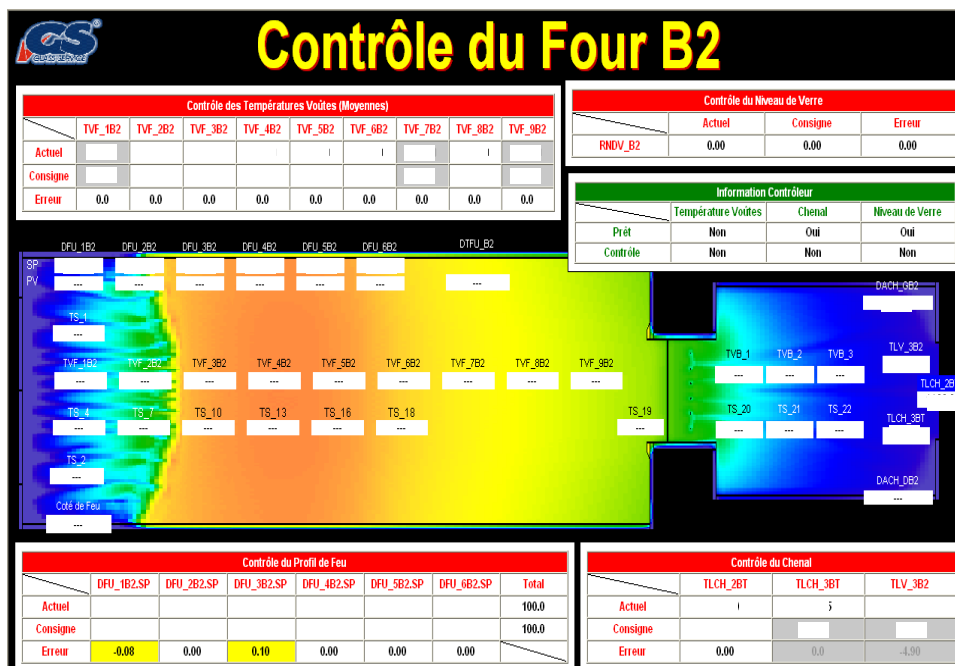


Figure4. Snapshot of the ESIII screen in Boussois.

ESIII PERFORMANCE

One of the first objectives of the installation was the stabilization of the crown and canal temperatures. As some of these temperatures were known to have more impact on the overall glass quality, priorities were put accordingly. An example of the stabilization observed on canal and (one of the) crown temperatures is given in Figure5. As can be seen, the better stability of ESIII is obtained by means of a much more important reactivity of the flow rates on the different burner ports than could ever be reached by manual actions. In practice, the set points on the fuel flow rates are actualized every 240 seconds.

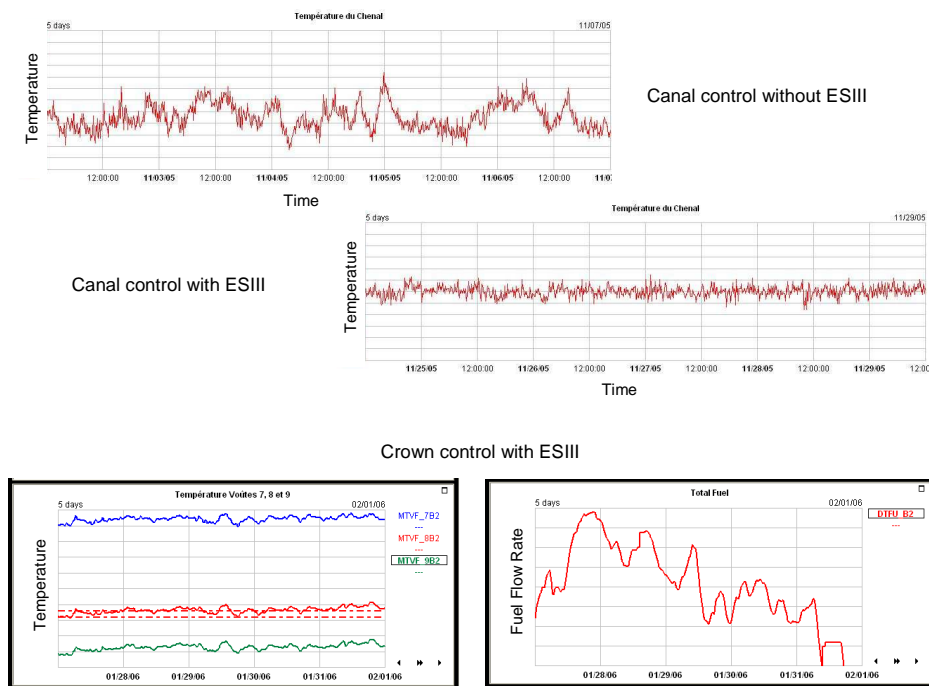


Figure5. Example of control of canal and crown temperatures.

(Top) Evolution of canal temperatures with and without ESIII.

(Bottom) Evolution of crown temperatures and fuel flow rates with ESIII.

Even more than crown and canal temperatures stabilization, the main objective was energy gain. Putting into evidence the effect of the use of ESIII on the specific consumption is far from being obvious. The approach used by Glaverbel to this end was (1) to collect past specific consumption records on the furnace; (2) to build a model of specific consumption taking into account effects like age of the furnace, pull, cullet, etc.; (3) to compare the observed specific consumption with the use of ESIII against the ones that would be expected without the use of ESIII (and are given by the extension of the model of specific consumption built on past records). The result is illustrated in Figure6.

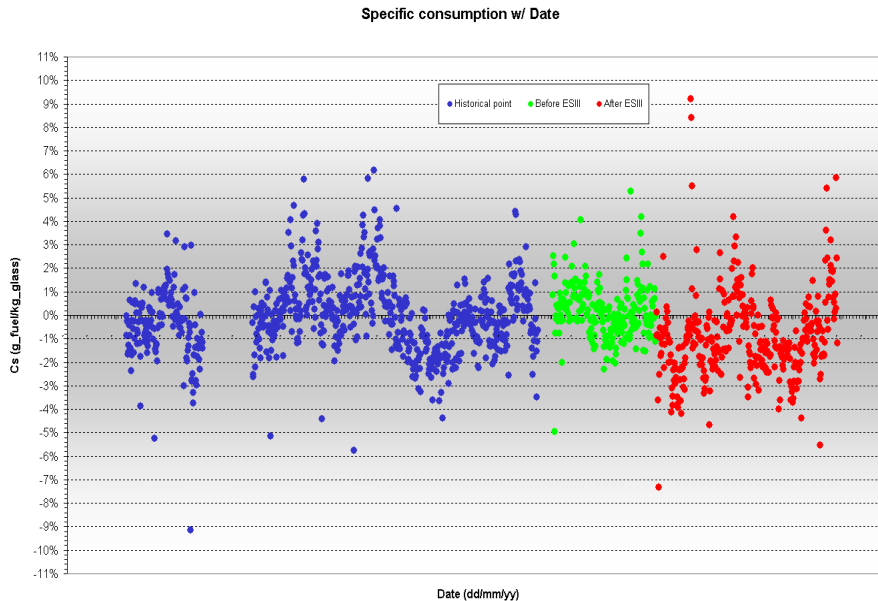


Figure6. Comparison of specific consumption before and after ESIII.

This method is far from being perfect. First of all, the model is not able to explain all fluctuations of specific consumptions observed in the past, and cannot therefore be expected to predict perfectly what would have been observed without the use of ESIII. In addition, the effects of all actions done since the installation of ESIII are combined into one single figure. Finally, this method does not take glass quality into account. Nonetheless, this critical (but to our view only available) approach seems to indicate that the furnace might be using less fuel than in the past. However, the numbers are not conclusive and one might state that this part of the objective is still under progress.

Three other observed advantages of ESIII are worth to be mentioned.

- At first, the stabilization of the crown and canal temperatures enables more easily than in the past to evidence influences of specific temperatures on the overall glass quality. And consequently to control much more precisely than in the past these latter temperatures.
- The same is true for the effect on energy consumption of specific actions made on the furnace, as these latter will immediately be reflected in movements of the manipulated variables by the expert system.
- Finally, the acceptance of the system by the line operators was excellent. All of them found that the system facilitates their work and allows them to concentrate on other topics than in the past.

CONCLUSIONS

Based on the above mentioned results, Glaverbel decided to install definitively the system in Bousois. As already mentioned, there is still further work to be done in collaboration with Glass Service.

- Although the analysis shown here above seems to indicate a potential energy saving, Glaverbel still believe that the system in place has an even greater potential. Further work will be devoted to adapting the crown temperatures set-points and fine-tuning the strategy used for control, now that the confidence in the system is established.
- A second issue that needs to be addressed is the batch visualization. Indeed, in some cases, the batch line might move forward due to the reduction of energy without being evidenced in the crown temperatures. At these moments, it is necessary for the operators to take the lead over ESIII as this latter is blind against this phenomenon (and would therefore not react properly). A very positive development would be that the position of the batch line be fed into the system by means of the information coming from well-positioned cameras looking at the batch.

The coming months will be devoted to go further into these developments. As can be seen, taking full advantage of the system is a relatively long process, but Glaverbel is confident that, with the help of the AGC group and of Glass Service, both objectives will be met in the near future.

ACKNOWLEDGEMENT

The authors would like to thank Josef “Pepe” Müller, Frantisek “Franta” Matustik and their colleagues from Glass Service for the excellent and fruitful collaboration in this project. We would also like to thank John Page from AFG and Jiri Bilek from Glaverbel Czech for their kind and much appreciated help.

10 YEARS' EXPERIENCES WITH ADVANCED FURNACE CONTROL (EXPERT SYSTEMS *ES II*TM AND *ES III*TM)

Josef Müller, Josef Chmelař, Róbert Bódi, František Matuščík
Glass Service Inc., Rokytnice 60, 755 01 Vsetín, Czech Republic

Abstract

*Glass Service was established by a group of former furnace engineers and glass scientists in 1990. The major company activities at that time were related to glass melting, conditioning and forming. But there was not any tool for advanced process control. Too slow computers to handle large optimization problems on-line, simple control loops considered as well working and quite conservative glassmakers - it was not a good starting position for advanced process control. Thus the first **Expert System ES II**TM was not implemented earlier than in 1996.*

*Since that time a lot of work has been done in this field. Now, 10 years later, there is updated version of **Expert System (ES III)**TM, there are more than fifty Expert Systems installed around the world on various glass furnaces and belonging parts. Besides this there are gathered extensive experience and know-how. Unfortunately, there are also some issues related to process control that have not been solved yet.*

*The given paper summarizes major **ES III**TM features and real glass producers' benefits. The future potential opportunities are discussed at the end of this paper as well.*

EXPERT SYSTEM OVERVIEW

Expert System, either version *ES II*TM as *ES III*TM, covers a supervisory multi-variable model based predictive control in time and space. This definition is not too understandable to people not familiar with process control, thus let's try to explain it more in details.

Word *supervisory* means that **Expert System** implementation preserves primary control level – all devices (PLCs, internal switches) as well as up to date control mechanisms (PID loops, availability to change inputs manually). It enables to stop *ES III*TM because of furnace devices service or maintenance while primary control can still be in use (if requested). *ES III*TM even can use some primary control level elements as a part of advanced process control.

Next word, *multi-variable*, means that more inputs can be handled at the same time to affect more outputs. This property belongs between basic characteristics of all glass processes. For example, look at float furnace. Apparently, total gas is only one of inputs that affect crown temperatures. The next one is batch feed rate. And batch composition (the next one) is maybe even more important. An ambient temperature also correlates with crown temperatures. So it can be concluded that crown temperatures are affected not only by one variable (total gas), but by many more. On the other hand – there is not only one crown temperature. There are more ones with different importance for process control. And we have not discussed yet the effects of glass level, canal temperatures, oxy-boosting use, etc.

All of them affect (or are affected by) process control too. Overall, the process control is complex problem where more inputs and more outputs play less or more important roles in.

Next important portion of **Expert System** definition is the word *model* (model based control). It strongly corresponds with major used control techniques. This control uses information about process variables history and mathematical approximation of process behavior – model. Its knowledge is important for process control and its expected behavior in future. At each moment there are available next planned control actions in future as well as estimated future behavior of temperatures and other controlled variables.

The remaining words from definition seem to be understandable. In spite of it, there are properties not mentioned in definition and describing **ES III™** too.

- **Safety.** Every system you are going to use for continuous glass production has to be safe. At first, it is necessary to be ready to stop advanced control system in case that communication between systems (**ES III™** and DCS) fails. Next, **ES III™** contains fault detection logic. It refuses to react on variable values that they are out of specified interval or their process value changed more than allowed with the physical process properties (typical for thermocouple failure).

An off-line simulator could be included into safe tools too. Would you like to know how the process will react with different process control settings? Or even would you like to try it but don't you want to violate your valuable glass production? The off-line simulator offers to you to experiment with these settings off-line, in simulation mode. Thus you can look for best-fitting solution that fully matches your ideas about precise process control while you are producing high-quality glass. The final solution can be applied as settings on real process control then. You also can store these settings through Process Settings Manager. This manager contains recipes for various glass production types so these settings are always ready to be applied on the process – it eliminates the potential mistakes caused by hand made inputs.

- **Flexibility** coming especially from the entire package of algorithms devoted to process control. It happens that some variables affecting process behavior are not predictable – you can estimate future behavior with small reliability then. At this moment the model based predictive controller (MPC) cannot consider these variables as its known inputs. Thus it is necessary to find out the alternative ways how to get such variables back to the game. Except for MPC controller there is fuzzy controller and classic rules based

systems available for use. These tools are very powerful and can work either separately or together. It gives to process control designer a big chance to choose the strategy that fits optimally.

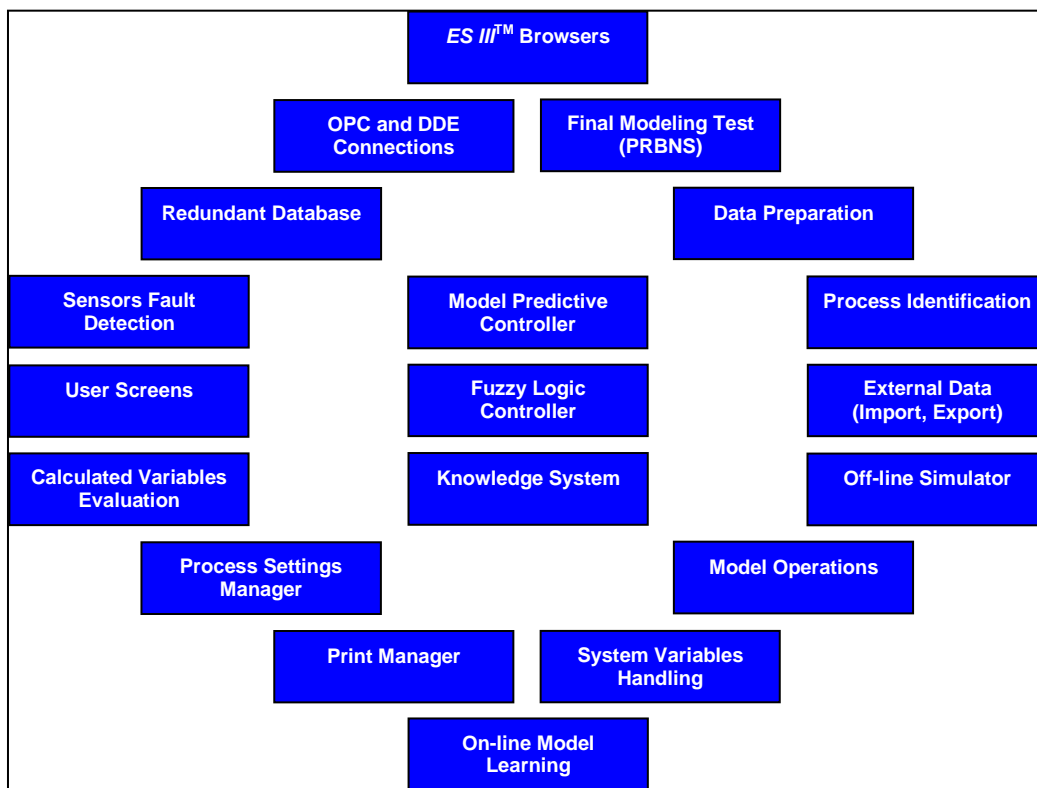


Figure 1: Summary of *ES III™* system features

- **Control System Enhancements.** Beside all properties mentioned above there are further tools that belong almost to the plant information system and not to the process control system only. Among those tools can be included internal database (gathers and stores data in requested form and timing), user screens (serves for visualization of all available data including data from database), reports (either printed out at specified time of the day or stored as PDF document), etc.

At the end of this paragraph just remember that actually there are 2 different *ES III™* system versions – runtime and developer. Runtime version serves as a standalone application running on computer on-line and using (optionally) all features offered by *ES III™*. A typical representative of runtime version is turn-key delivery application done by Glass Service application engineers. You don't need to know how to configure controllers, how to get model from process data, how to design user screens, etc. You will just start runtime version and everything is already prepared for you. The software that allows you to make own solutions that is used for those works is called also *ES III™* system - developer version. This software

contains package for work with models and data, for design of specific final modeling tests, browsers, etc. It is up to you what is better for you – to buy **ES III™** as turn-key delivery application or to do it on your own. Simply said – having **ES III™** system in developer version the end user can build-up the entire advanced process control project. Such project is loaded by runtime version that will work on-line in accordance with the project specification.

BENEFITS RELATED TO EXPERT SYSTEM USE

It is nice to have the system for advanced process control full of features that exceed similar application but nobody will ask for these features if the benefits related to process control are missing. So let's go through the most important benefits and try to look at real process results.

Before doing it let allow to make a comment for graphs and references given further. There are used some examples from our experiences in the field using **ES III™**. At second, the axes at graphs are dimensionless. On the other hand - the graphs that show the property before **ES III™** implementation and after it are of the same scale (time, values). Thus these graphs are comparable enough.

- **Temperature stability** is one of the most important parameters in glass process production and almost all other benefits are somehow linked to this parameter. Temperature stability in the melter has a positive impact on the amount of defects, the temperature stability close to forming area (canal for float, forehearths for fiber, TV glass, container, etc.) makes the forming easier – the glass is more homogeneous and together with well set up temperature setpoints thus fits better the request for final production.

Figure 2 shows the comparison of two data samples of the same length (one month) from float furnace. The subject of the charts is refiner temperature. This temperature is very important for the production. Apparently, after **ES III™** implementation (bottom chart) the temperature is more stable comparing to situation before **ES III™** implementation (top chart). Also the straight line indicates that now the temperature is following a setpoint.

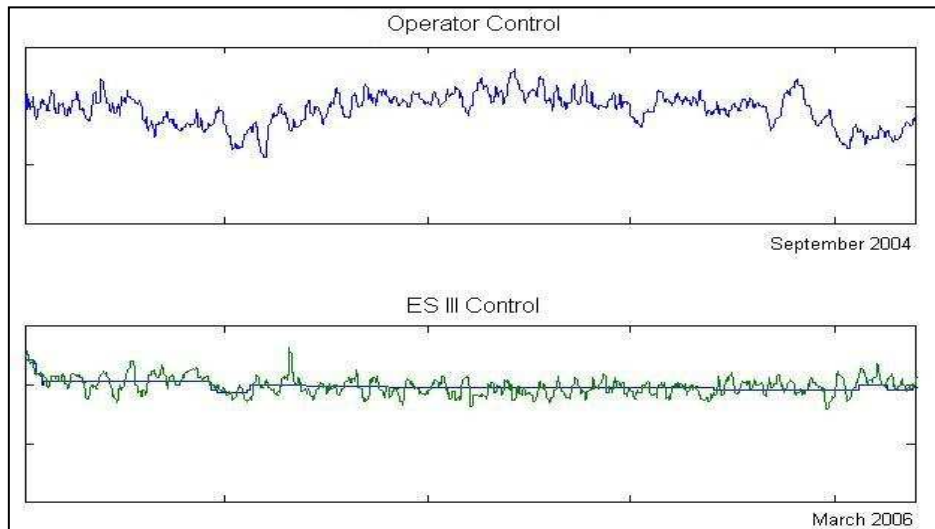


Figure 2: Temperature stability (float furnace, refiner temperature)

Similar situation can be seen in Figure 3 where throat temperature in fiber furnace is displayed. While throat temperature within one month observation oscillates before **ES III**TM implementation in range $\pm 15^{\circ}\text{C}$, after the **ES III**TM implementation this oscillation was reduced to $\pm 5^{\circ}\text{C}$ (the observation period was of the same length – one month).

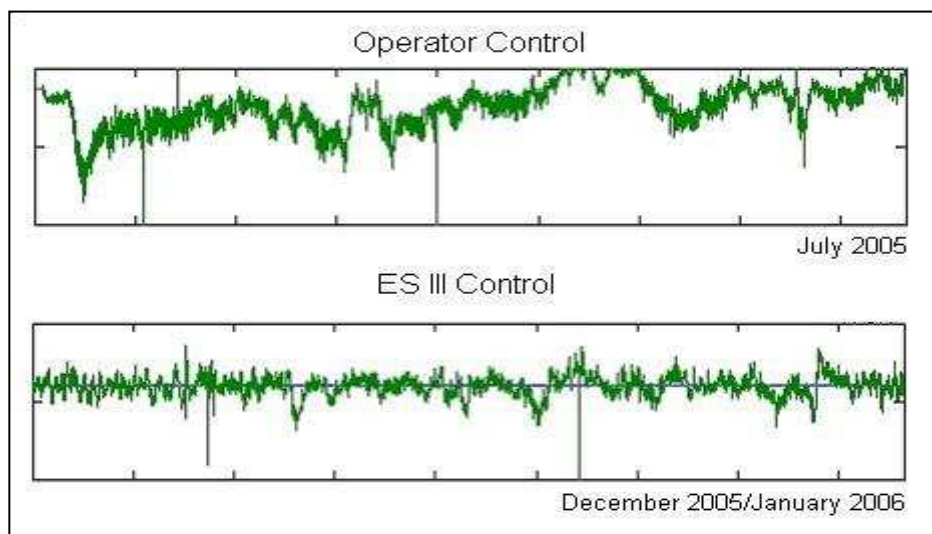


Figure 3: Temperature stability (fiber furnace, throat temperature)

Finally the third example (Figures 4 and 5) is devoted to forehearth temperature stability. Very often the glass temperatures are not controlled at all or are not controlled with sufficient precision. The influence on forming is clear then – unstable glass temperatures leads into often changes on producing devices (for example actions on spinner (fiber-insulation) or bushings (fiber – composite)). Together with temperature stability

demonstration you can also discover how advanced control balances the error to reach all those setpoints even if there is only one heating that affects them together.

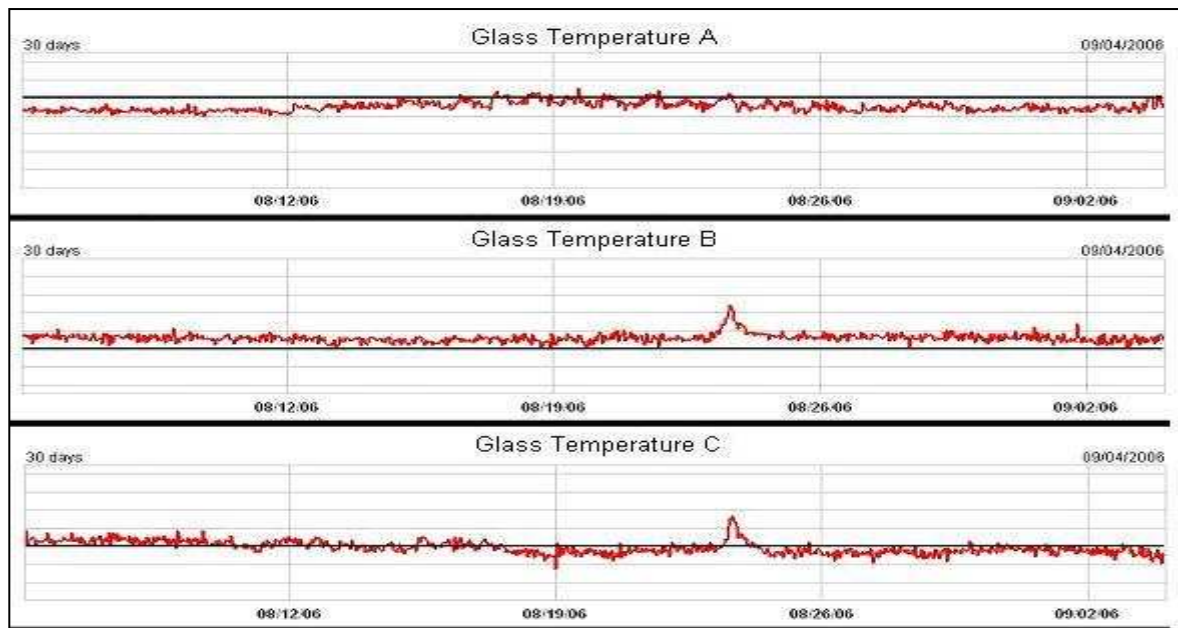


Figure 4: Temperature stability (fiber furnace, forehearths, glass temperatures, no *ES III*TM)

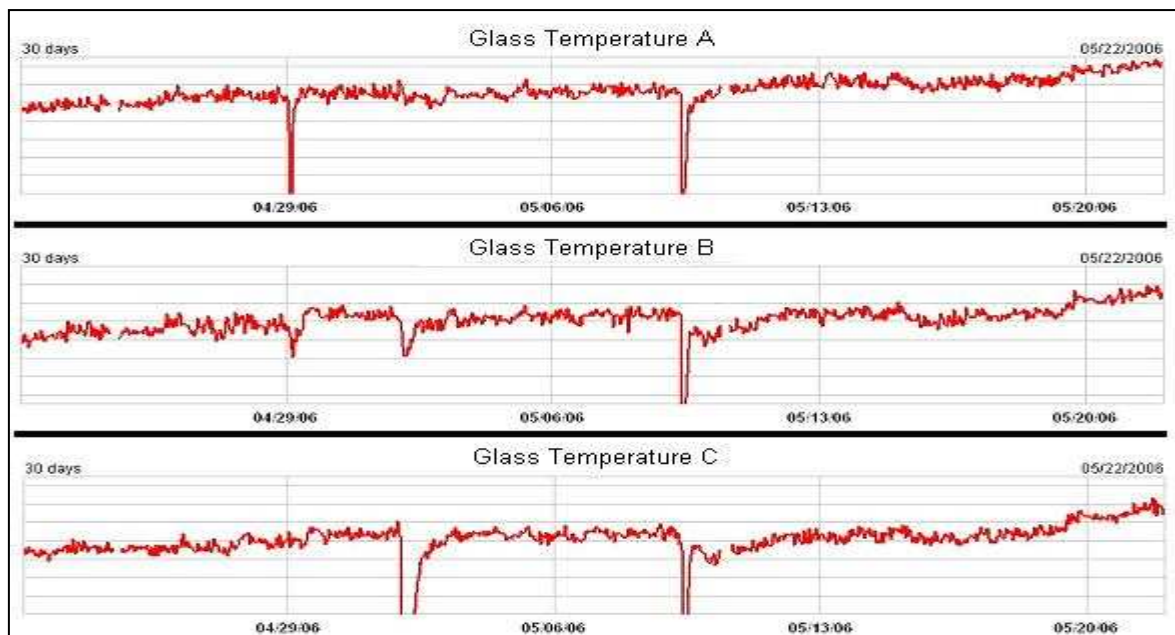


Figure 5: Temperature stability (fiber furnace, forehearths, glass temperatures, *ES III*TM)

- **Energy savings** is linked to temperature stability indirectly. Why? It is well known that hotter glass is in principle better than colder glass. Thus if temperature oscillates and is not settled on the setpoint it is better to setup this setpoint higher than really requested

temperature. This is a protection against the production troubles caused by cold glass. When temperature is stabilized there is space for temperature setpoint decreasing. Going with temperature setpoint lower means that it is unnecessary to heat up so much in comparison with higher setpoint definition. And this is exactly what you need to do for energy savings. Besides temperature fluctuation generates more defects coming from refractory interaction, so when the temperatures are more stable, less defects will be generated and we can allow lower temperatures in the melter (that would be required to reduce defects) This principle is given schematically on notoriously known Figure 6.

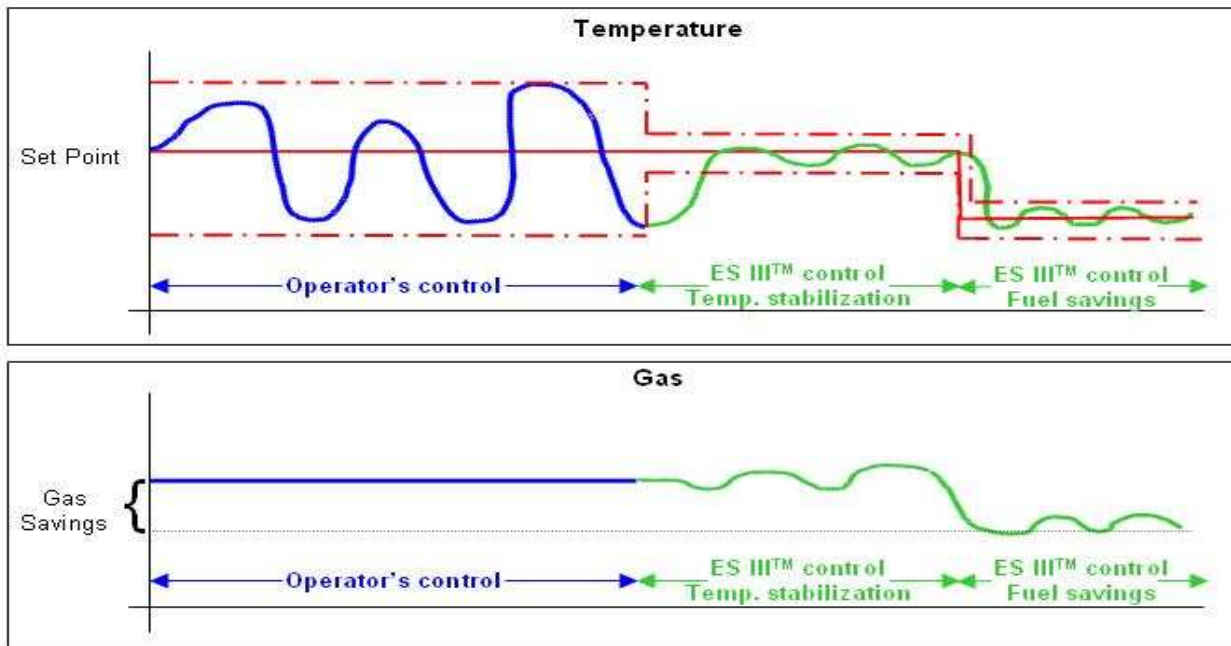


Figure 6: Fuel reduction due to temperature stabilization

Now we can compare this philosophy with reality. Look at Figures 2 and 3 again. In both cases the temperature stability has been improved. While the setpoint stayed at the original level in the first case there is very small energy cost reduction. Contrary to this the second case indicates the setpoint was lowered and energy consumption decreased as well.

Anyway, it is very difficult to evaluate energy savings exactly. There are other parameters effecting energy use. The first one is the timing for comparison periods. When you compare data of the same length before and after **ES III™** implementation, it also depends on factors like outside temperature or batch composition (cullet percentage, etc.). Obviously, the winter's consumption is higher in comparison with summer period. Next, the furnace is ageing with time and usually energy usage would increase. The analogy can be seen for lower cullet percentage in glass versus higher cullet percentage.

Increase of the pull rate is another typical parameter that affects energy savings evaluation. It cannot be said that **ES III™** system installation leads into pull rate increasing automatically. But it can correspond with some logic. When temperatures oscillate a lot and glass quality is not too bad but also not excellent – there is no space for pull rate increasing. After **ES III™** implementation suddenly temperatures are more stable. This stability can affect glass quality in a positive way (see further). So there are good conditions to increase pull rate and use the furnace potential at maximum.

To eliminate the effect of the pull rate increase there can be used for evaluation of energy savings the ratio between energy consumption and production tonnage. To add some example, compare the following Figure 7 and Figure 8. Both of them are from the same process and from the same evaluation. The first figure indicates that the total consumption doesn't depend on **ES III™** implementation. Or even there can be seen very small energy increasing while **ES III™** is used. When you evaluate the same consumption and consider different pull rates it gives completely different results. Apparently, the pull rate has been increased after **ES III™** installation while total energy stayed at the same level like before doing it.

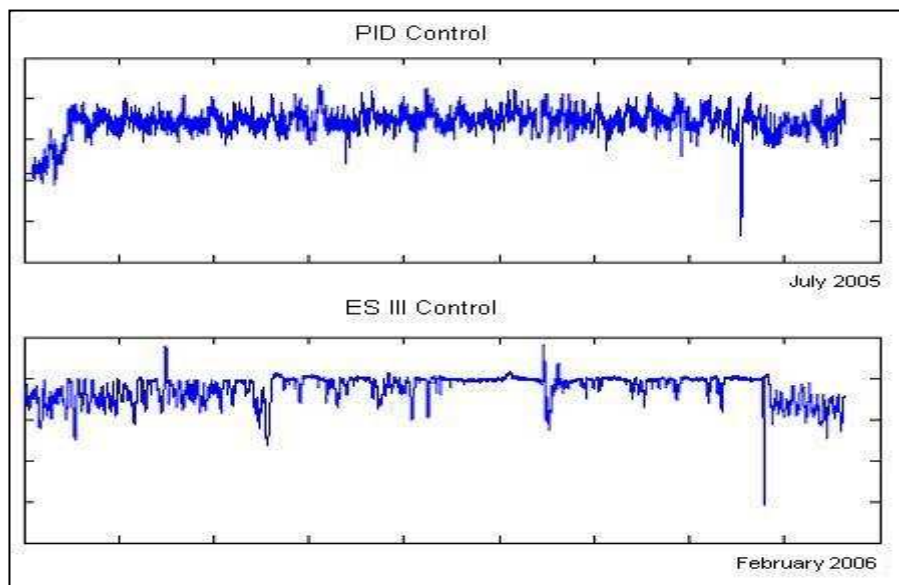


Figure 7: Total energy consumption

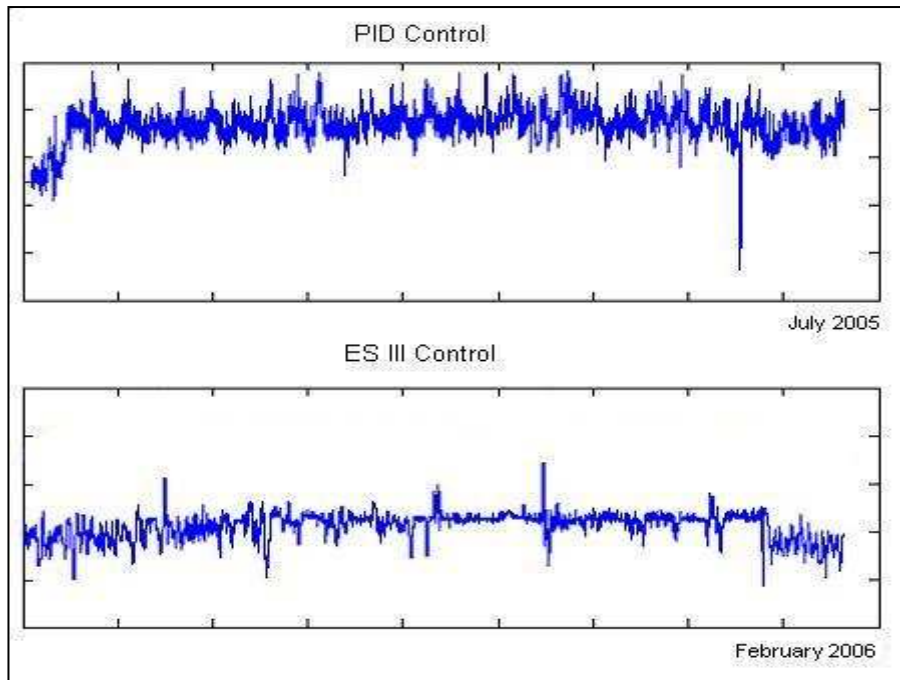


Figure 8: Consumption per ton of produced glass

- Glass quality improvement.** Doing the clear conclusion that *ES III*TM causes glass quality improvement is impossible. But there are some indicators that stable dynamics in the process can affect the resulting glass quality. For example, there were evaluated two data samples of the same length (9 months each). While the production before *ES III*TM implementation contained 4.34% of glass with defects related to raw pull rate, after *ES III*TM implementation this number decreased at 3.36%. (see Figure 9)

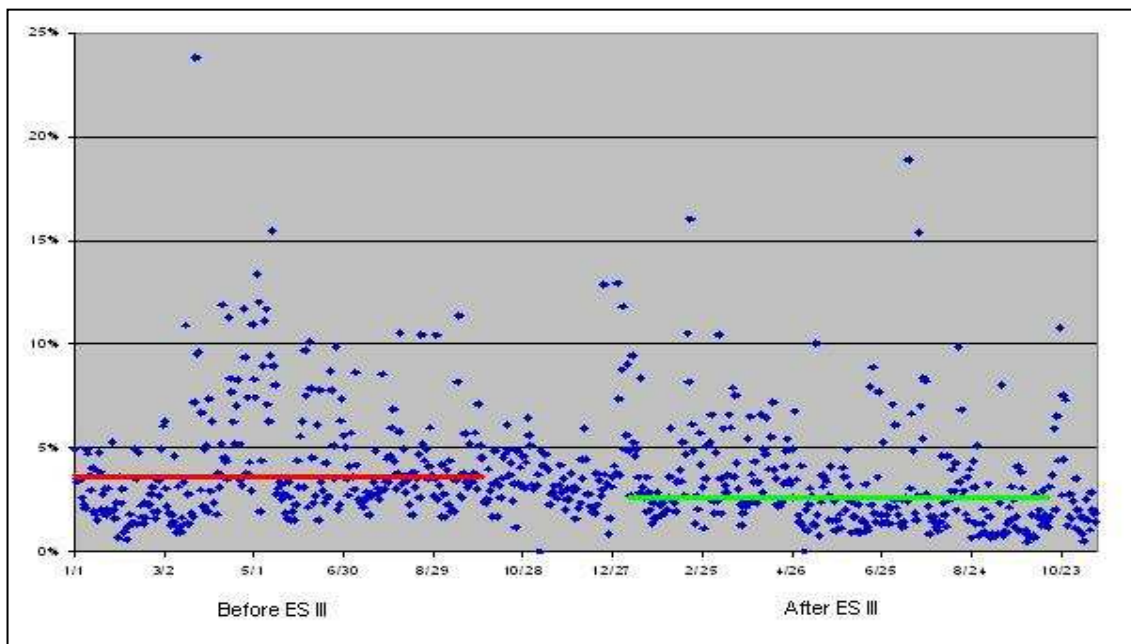


Figure 9: Glass defects evaluation (red and green colors are averages)

- **Net yield increasing.** Glass quality improvement is one factor affecting the net yield. The stabilization of temperatures in refiner and in canal (float furnaces) has positive impact on next forming too. A steady ribbon width would bring less edge losses. Together with higher thickness stability it results into higher productivity then. For fiber production the temperature stability in forehearths brings breakage reduction about tens of percents, etc.
- **Recovery time shortening.** As a last item within the section about **ES III™** system benefits let's mention the time you need for big production changes or for recovery after some services. An example can follow: a big pull rate change in a float furnace. These changes are in tens of tons of daily production. The automatic job change shrinks the time at necessary technological minimum.

For fiber glass producers there is analogy with bushing change. This operation is quite common, let say 1-2 changes of each bushing within 1 year. Talking about timing, bushing change took before **ES III™** implementation 10-16 hours of time. After **ES III™** system implementation this time shrinks at about 25%. Look at Figures 10 and 11 for details. Also pay attention to the glass temperature stability for all displayed glass temperatures. If remaining glass temperatures are stable it indicates that the production on neighboring bushings is not disturbed.

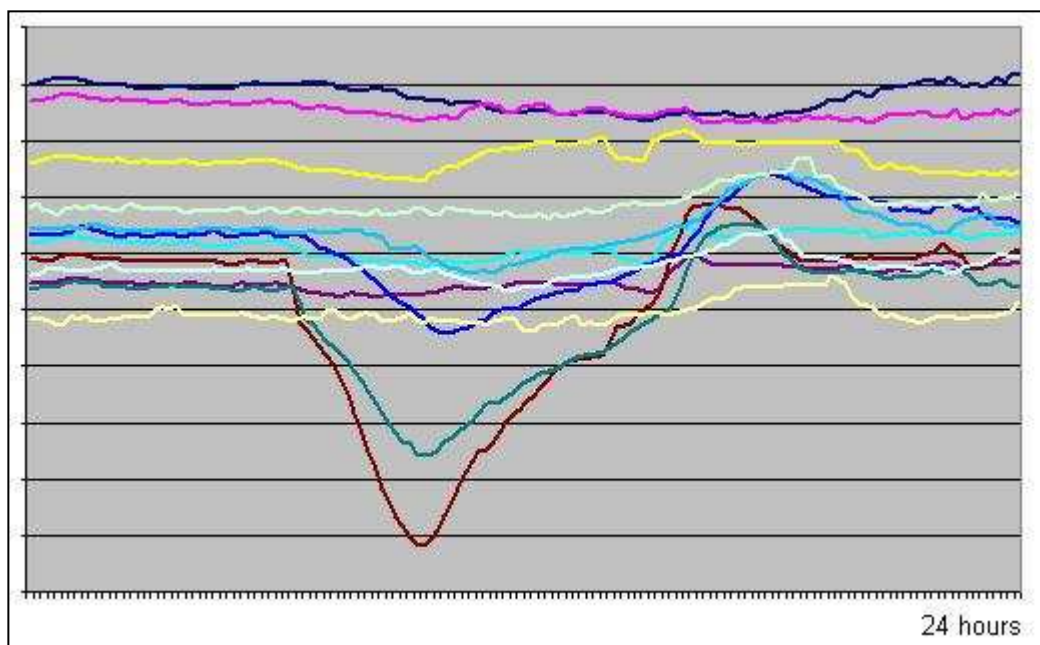


Figure 10: Glass temperature during bushing change (before **ES III™**)

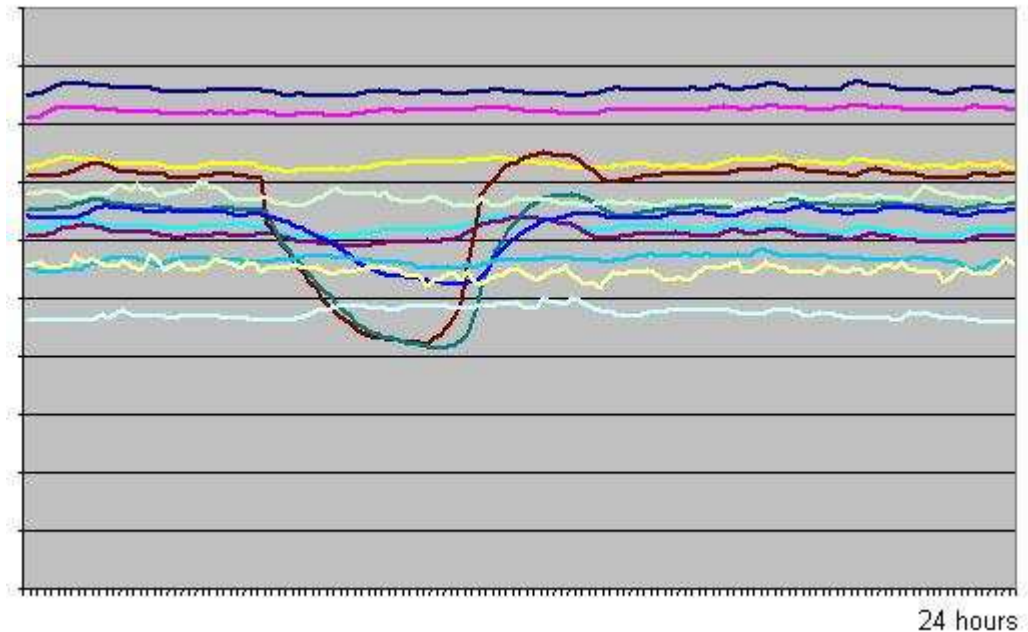


Figure 11: Glass temperature during bushing change (with **ES III™**)

EXPERT SYSTEM FUTURE

The future of **Expert System** is not only to implement **ES III™** system on the process. Still there are some issues that should be solved. The goal of those issues is the same – to allow even higher quality production to our customers.

- **On-line batch camera analyzer.** Motivation for this tool lies in fact that especially on float furnaces the batch line position belongs to the most observed parameters. If batch line position is not in optimal location the operators reduce or add some gas/oil to stabilize it. In automatic control the information about batch line position is very often missing. And it can cause big troubles in final glass production. For example, if non-melted batch will get behind a bubbling. This example demonstrates that it is necessary to know about actual batch line position. There are several ways how to say to advanced process control – batch coverage is too short or too long. As a batch line detector can be used manual input from operators (not recommended) or temperature changes on thermocouple in crown close to ideal batch line position (sometimes not reliable), etc.

On-line batch camera analyzer works on different basis. The images of glass level surface from camera are analyzed on-line so as a result there is the amount of batch in sectors of selected region. Thus the information about batch coverage (or batch line

position – depends on selected criteria) is quantified and such information can be used for process control in advance.

To demonstrate it let's look at Figure 12. On the right side there are pictures from furnace (top) and modification of this picture (bottom). Bottom part also contains the evaluated region (grid). Each sector representing one field of grid is evaluated independently. On the left side of the screen there is table with percentage evaluation of surface covered by non-melted batch in appropriate sector.

The same figure also shows one of the common problems with similar batch camera analyzers – camera cleanness. The camera cleanness is very important assumption in order to batch camera analyzer works well and reliable. In case of more carbon particles on camera this 'dark patch' can be considered as island of the non-melted batch. Thus the analyzer has to automatically detect the carbon particles and eliminates a sector affected by this from further consideration. The operator is warned about dirt on the camera then.

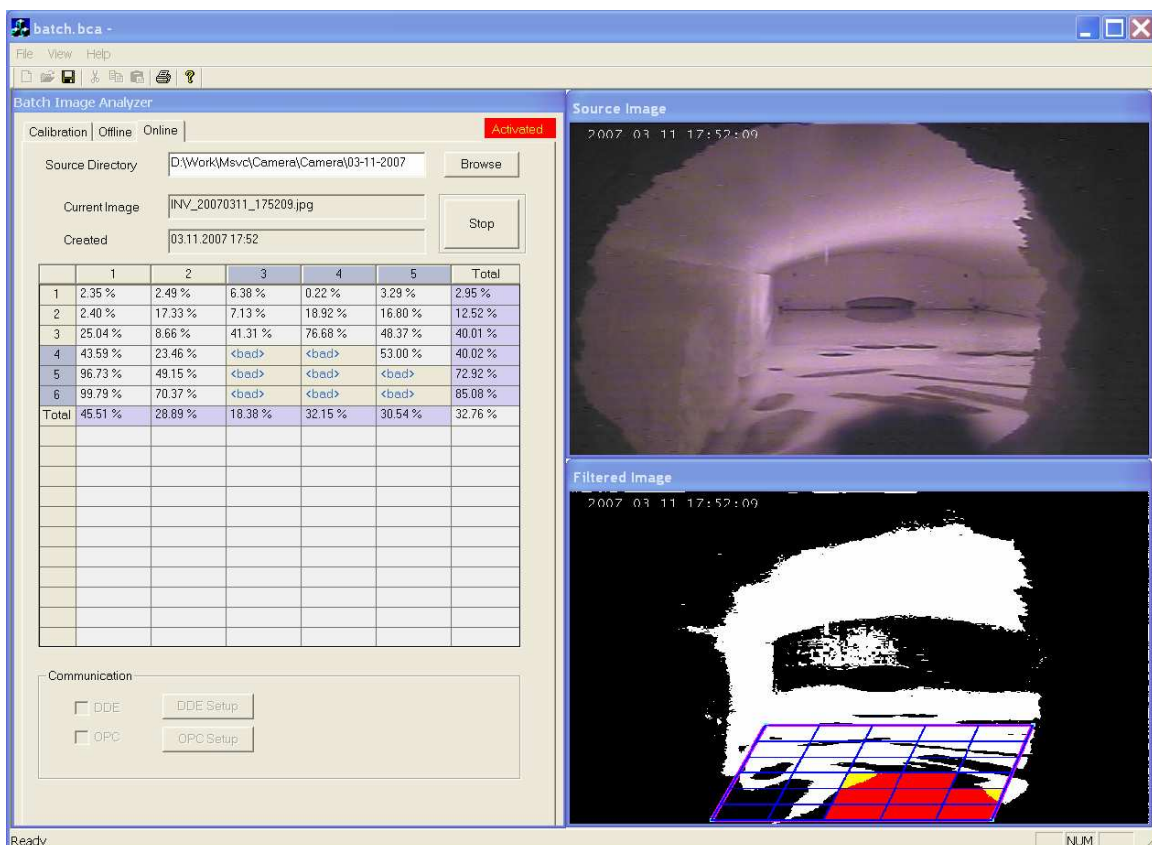


Figure 12: ES III™ On-line batch camera analyzer

- **Direct quality control** is the next issue for better process control. As was mentioned in paragraphs above there are some positive results indicating that glass quality increases after **Expert System** implementation. But direct quality control is not the objective of process control yet. Thus it is important to do the insight analysis of real process and quality data. Based on those data comparison the pattern recognition of scanned defects can be done. It means that there is built up the knowledge base containing the information about defects and the reasons of their occurrence. It is a good starting point for getting an answer on question 'what parameters really influence resulting glass quality?'

The **ES III™** and GS GFM (Glass Furnace Model) coupling can be used for verification of obtained results as well as for melting conditions optimization.

REFERENCES

- [1] Josef Müller, Robert Bódi, Josef Chmelař: How to Make Glass Furnace Control Easier: Advanced Optimal Control by Expert System **ES III™**, Proceedings of the VIII. International seminar on mathematical simulation in glass melting, Velké Karlovice 2005, p. 200
- [2] Josef Müller, Josef Chmelař, Robert Bódi, Erik Muysenberg: Aspects of Glass Production Optimal Control, Proceedings of the VII. International seminar on mathematical simulation in glass melting, Velké Karlovice 2003, p. 157
- [3] Josef Müller, Robert Bódi, František Matušík: Expert System ES III - A System for Optimal Glass Furnace Control, Glass - Monthly Journal (Vol. 81, No. 9, October 2004)
- [4] Josef Chmelař, Erik Muysenberg, Robert Bódi: Optimizing Glass Production with Expert System ES-II, Proceedings of the VI. International seminar on mathematical simulation in glass melting, Velké Karlovice 2001, p. 101
- [5] Erik Muysenberg, Josef Chmelař, Robert Bódi: Supervisory Advanced Control of Glass Melters by GS Expert System ES-II, Proceedings of the V. International seminar on mathematical simulation in glass melting, Horní Bečva 1999, p. 162
- [6] Peter Mikulecký, Robert Bódi, Josef Chmelař: Towards Total Glass Quality Management, Proceedings of the IV. International seminar on mathematical simulation in glass melting, Horní Bečva 1997, p. 172

ADVANCED MODELLING OF FOAM AND VOLATILIZATION FOR EVALUATION OF DIFFERENT COMBUSTION SYSTEMS

L. Thielen, A.F.J.A. Habraken, A.M. Lankhorst, P.J.P.M. Simons, O.S. Verheijen
TNO Glass Group, Eindhoven, The Netherlands

Abstract

In the paper we describe two sub-models of our glass-dedicated CFD-model GTM-X: the dynamic foam model and the volatilization model. In the dynamic foam model the balance between foam formation and foam destruction determines the local foam layer thickness. In the volatilization model, the dependency of the volatilization flux on the glass surface temperature and flow in the combustion space is modelled by means of empirical relations.

Both models are used to study the influence of combustion space refractory height and burner location on the energy efficiency and the volatilization flux of HBO. The furnace is an oxyfuel fired fiber glass furnace producing 100 tons/day of borosilicate fiber glass, heated by 6 burners.. With respect to a base case, three parameter variation simulations have been carried out: 1) Burners lifted 10 cm, 2) Burners lowered 10 cm, and 3) Crown lifted 10 cm with respect to glass surface.

The parameter variation study shows that the volatilization rate of boron species is very sensitive to the crown height: a 25% reduction in HBO emission can be obtained by increasing the crown by only 10 cm. This reduction can result in a savings of 100 ton/year of colemanite (boron batch compound).

INTRODUCTION

TNO Glass Group is an international knowledge provider towards the glass industry and helps their global customers to innovate their processes. As a part of its portfolio, TNO Glass Group has developed the glass-dedicated boundary-fitted CFD-model GTM-X, describing all relevant phenomena in the complete glass melting process such as: flow, temperature, melting, multi-phase flow, electrical fields, chemical reactions, radiation and combustion.

GTM-X is a complete model for glass melting furnaces, combining both the combustion space and the glass bath in one efficient solver. Changes in process conditions or furnace design influence the melting performance, energy consumption, pollutant emissions and glass quality. By aid of sub-models, including batch melting, electrical boosting, forced bubbling, volatilization, refractory corrosion, redox and glass quality indices, these effects can be determined. The model is extensively tested and validated on industrial furnaces.

For a correct prediction of the heat transfer from combustion space to glass in coupled simulations, a good estimate of the foam layer thickness is essential. Therefore, a dynamic foam formation model has been developed. In this model, the local foam production rate is determined from the amount of fining gases (O_2 and SO_2) produced. The fining gas production is determined by a thermodynamic equilibrium or redox model. The foam destruction rate is determined from the stability of the lamellae of the produced foam

bubbles, which depends on temperature, gas and glass composition. The balance between foam production and destruction determines the local foam layer thickness.

At the glass surface chemical species evaporate into the combustion space. This volatilization flux from the glass to the combustion space depends on local values of the glass surface temperature, H_2O , CO_2 and CO concentrations and velocities and turbulence intensities above the glass surface. Empirical relations, describing the dependency of above-mentioned parameters, have been obtained from extensive lab experiments and from measurements in industrial furnaces. These relations are implemented in GTM-X, leading to a strong combination of empirical and detailed flow and temperature data, enabling accurate prediction of emission levels of volatile components.

In the first part of this paper, the background of the dynamic foam model and the volatilization model is explained to show how these complex phenomena are modelled within GTM-X.

In the second part, an example application of GTM-X is shown. This application deals with the effects of changes in refractory height and burner location with respect to the glass surface on the volatilization flux of HBO in a fiber glass producing furnace. With respect to a base case, three parameter variations have been carried out. The results will be discussed and conclusions on the best (i.e. lowest volatilization flux) set-up will be drawn.

DYNAMIC FOAM MODEL

In the dynamic foam model, the thickness of the foam layer depends on the gas production beneath the glass surface. From the redox model (not discussed here) the gas production due to chemical reactions in the glass melt is obtained. This gas production is used to calculate the growth of the foam layer at the glass surface. The destruction of the foam bubbles is calculated from the stability of the lamellae. The balance between growth and destruction determines the number of bubbles and thus the thickness of the foam layer, acting as an insulation layer between glass and the combustion space.

The redox calculation estimates the local gas production in the glass melt. The produced gas is removed from the melt and escapes the glass melt at the surface. When the amount of gas is large, a foam layer can develop on the glass surface. To calculate the gas production at the glass surface, the integral of the local gas production over the height of the furnace is calculated. A new layer of bubbles in the foam is created when the amount of gas produced in the glass below the bubble is equal to the volume of one bubble.

After a bubble is created, the thickness of the lamellae of a single bubble decreases in time. When the thickness of this bubble is smaller than a critical thickness, the bubble erupts. The thickness of the bubble lamellae can be calculated using the mass and momentum balance of the glass in the lamellae [1,2].

In the foam layer, a number of bubbles lie on top of each other. The glass flows from the top layer of bubbles into the lamellae of the underlying bubbles. Therefore, the thicknesses of the underlying bubbles depend on the top bubbles. When the thickness of the top layer is smaller than the critical thickness the bubbles in the top layer erupt and the underlying layer becomes the top layer. In steady state, a balance between layer creation (due to gas production) and layer eruption (due to the stability of the lamellae) is obtained.

VOLATILIZATION MODEL

The volatilization model describes the volatilization of chemical species from the glass surface into the combustion space. The evaporated mass of a certain specie depends on the temperature of the glass, the partial pressures of H_2O , CO and CO_2 in the combustion space and the turbulent mass transfer coefficient. This coefficient depends of the the average magnitude of the gas velocity above the glass surface and the turbulence intensity of the flow in the combustion space. All these parameters are used in an empirical relation. The empirical relation is derived, based on experiments on the volatilization of components by TNO [3,4].

The evaporated mass, calculated by the model, is imposed as a boundary condition for the convection-diffusion equation for the chemical species.

INDUSTRIAL EXAMPLE

GTM-X is used to simulate the effect of changes in refractory height and burner location with respect to the glass surface on the volatilization flux of HBO_2 . This volatilization flux leads to a depletion of boron from the glass. As a result an overdose of boron (an expensive raw material) needs to be added to the batch. Furthermore, the pollutant HBO_2 (meta-boric acid) needs to be removed from the combustion gases by expensive flue gas scrubbers.

Therefore, simulating the volatilization flux is of practical important since it can result in significant cost savings for industrial furnaces. This because a reduction of the HBO_2 flux due to parameter variations leads to lower raw material and pollutant removal costs.

For a borosilicate fiber glass furnace, the major volatile component is an evaporation product of boron (B_2O_3). The boron in the glass melt reacts with the water vapor in the combustion space and forms into meta-boric acid. The reaction mechanism is given by:



The models described before are applied in the simulation of an E-glass furnace. The capacity of the furnace is approximately 100 tons/day of borosilicate fiber glass. In the glass bath two rows of bubblers are situated. Also electrical boosting is applied, with a power input of 500 kW. The total melting surface area is around 90 m^2 . The furnace is fired by six oxy-fuel burners. The burners are in staggered positions. The total firing rate of these burners is around 7.5 MW.

GEOMETRY AND COMPUTATIONAL SET-UP

The geometry of the furnace can be seen in figure 1. At the sides of the furnace, the batch chargers and the small burner inlets can be seen. In red the stack for the combustion flue gases is shown.

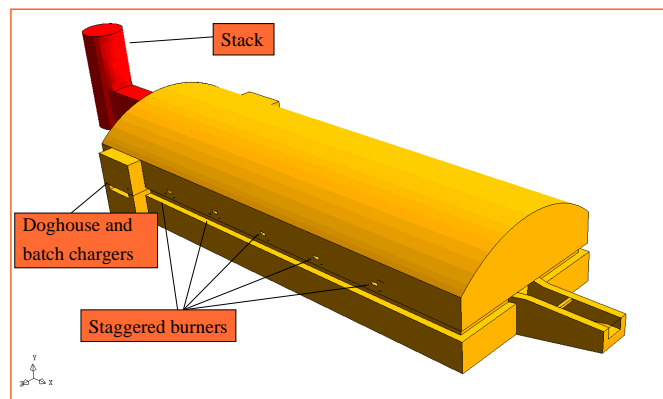


Figure 1: External geometry of the furnace, showing the batch chargers, the staggered burners and the stack for the combustion gases.

In figure 2 a view inside the glass bath is given. In this view the two bubbler rows are indicated, as well as the location of the eight boosting electrodes. Furthermore the thick walls surrounding the glass bath can be seen, in combination with the outlet channel for the molten glass.

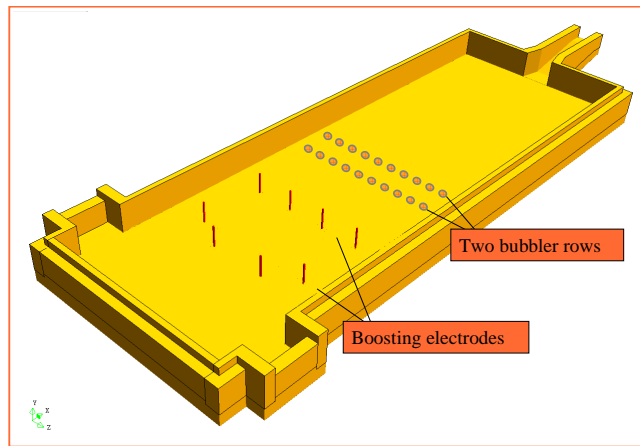


Figure 2: Internal geometry of the furnace, showing the bubbler rows and boosting electrodes.

Figure 3 presents a general view of the grid division. The grid for the simulation consisted of 440 blocks and the total number of volumes was around 700.000. The simulation of one parameter variation took about one day on a two processor Windows PC. To accurately model the large velocity gradients around the burner inlets, the grid is locally refined around the burners.

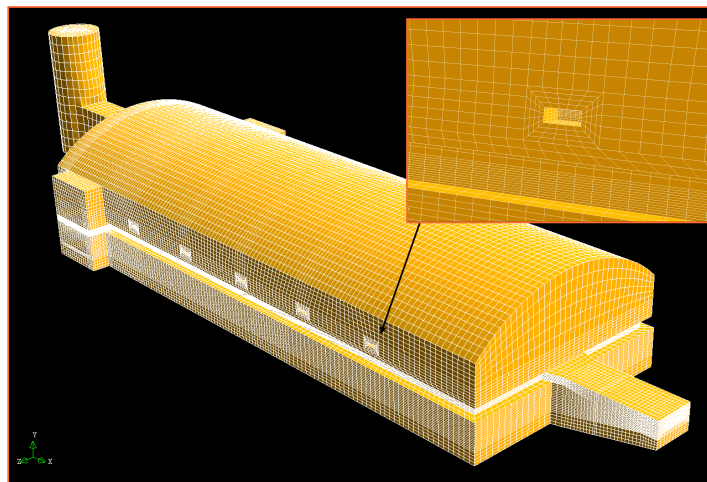


Figure 3: Grid division of the entire furnace. In the zoom the refined grid around the burner inlets can be seen.

The parameters refractory height and burner location were varied in this industrial example. In total, four different situations were modelled: The base case (case 1), the burners lifted 10 cm (case 2), the burners lowered 10 cm (case 3) and the crown lifted 10 cm (case 4). These situations are sketched in figure 4.

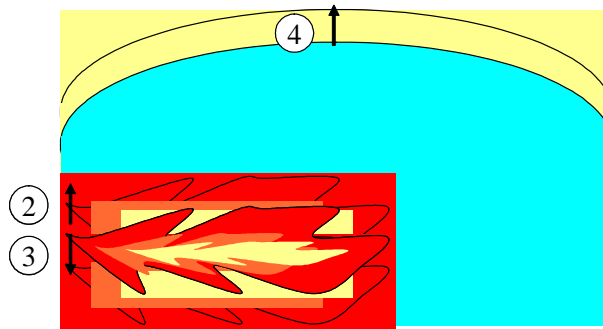


Figure 4: Sketch of the 4 different situations. The variations are shifts in the burner position and a shift in the crown position.

GENERAL RESULTS OF A SIMULATION

First some results of the base case will be shown to give a general view of the results. In figure 5 the temperature distribution on the glass surface can be seen. The region with the highest temperature (hot spot) is located under the burners at the downstream end of the furnace. At this hot spot, the bubbler rows force the flow upwards. As a result the cooler glass at the bottom of the glass bath is transported upwards to the glass surface. The thermal imprint of this cooler glass can be seen from the small areas with lower temperatures in the regions just beside and between the two bubbler rows.

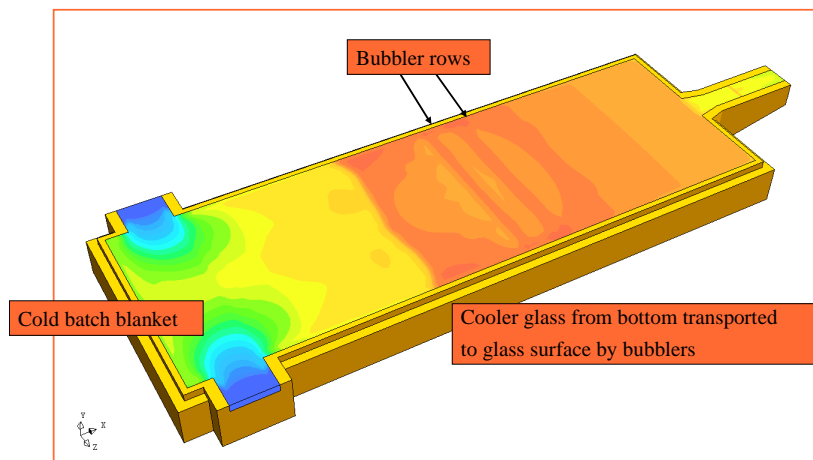


Figure 5: Temperature distribution on the glass surface.

The flow in the combustion chamber is determined by the location of the burners and the shape of the flames. In figure 6 this shape can be seen from the isosurfaces of the absolute velocity. Due to the staggered positions of the burners, the flames do not “hit” each other directly. However, still some deflection of the flame tips can be seen.

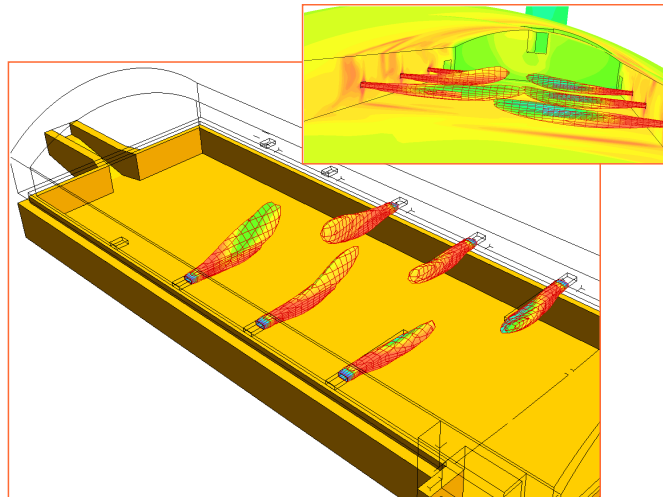


Figure 6: Flame shapes of the staggered flames in the combustion space. Shown are isosurfaces of the absolute velocity, superimposed is the temperature distribution.

In figures 7 and 8 the gas release and foam distribution can be seen. Figure 7 shows the gas release from the redox model. The fining gases O_2 and SO_2 are released in the regions with the highest glass melt temperatures. The dynamic foam formation model (combined with the redox model) predicts secondary foam between batch tip and bubblers and beyond the second bubbler row (see figure 8). The predicted foam layer thickness is found to be between 2 and 8 mm, corresponding well with industrial observation.

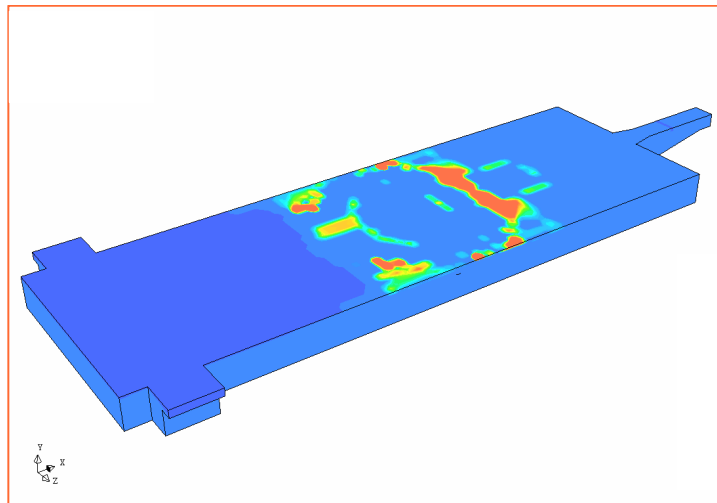


Figure 7: O_2 and SO_2 gas release at the glass surface.

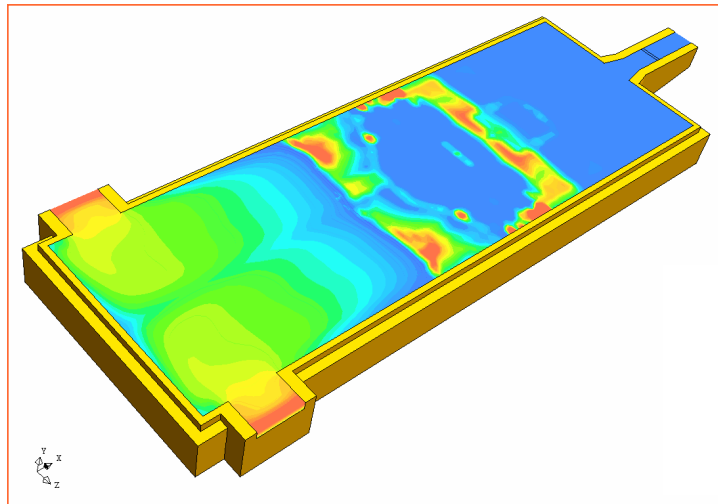


Figure 8: Overlay of batch concentration and foam layer thickness at the glass surface.

In figure 9 the result of the volatilization model is shown. It shows the calculated HBO_2 (metaboric acid) concentrations in the combustion space. In the hot region near the front wall, most HBO_2 evaporates from the glass surface, resulting in peak values in this region. As the HBO_2 is transported towards the stack the concentration decreases, due to dilution with the flue gases from each burner.

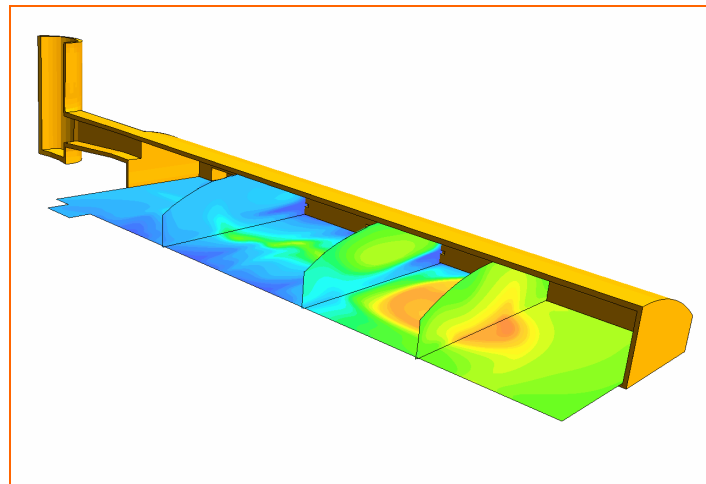
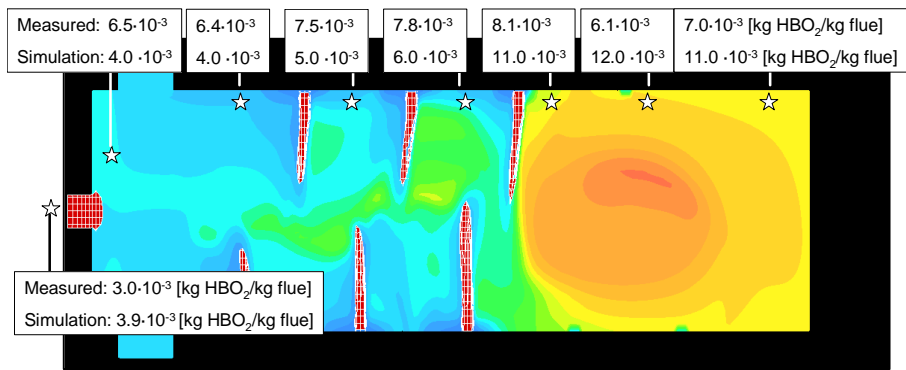


Figure 9: HBO_2 concentrations in the combustion space.

RESULTS OF THE PARAMETER VARIATIONS

To evaluate the volatilization flux, both the volatilization rates at the glass surface as well as the HBO_2 concentration in a plane through the burners are calculated.

The simulated HBO_2 concentrations in a plane through the burners are shown in figures 10 (case 1) and 11 (cases 2, 3 and 4). In figure 10 also measured values of the HBO_2 concentration at selected locations are given. These measurements were performed in a similar type of furnace with a different burner system. The agreement between simulated and measured values is good. Especially the overall evaporation flux agrees very well with the experiment, as can be seen from the values in the stack.



Case 1

Figure 10: Simulated and measured HBO₂ concentrations in a plane through the burners for case 1.

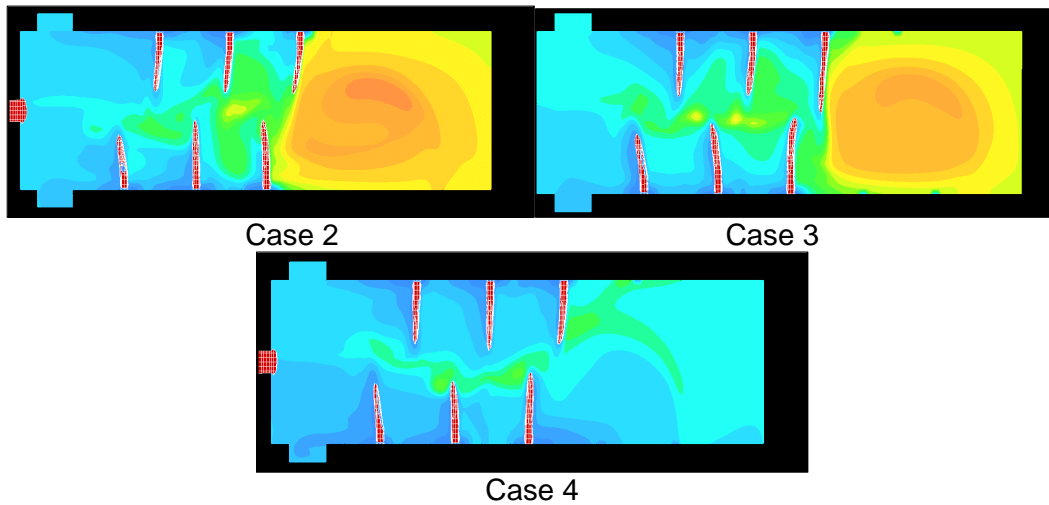
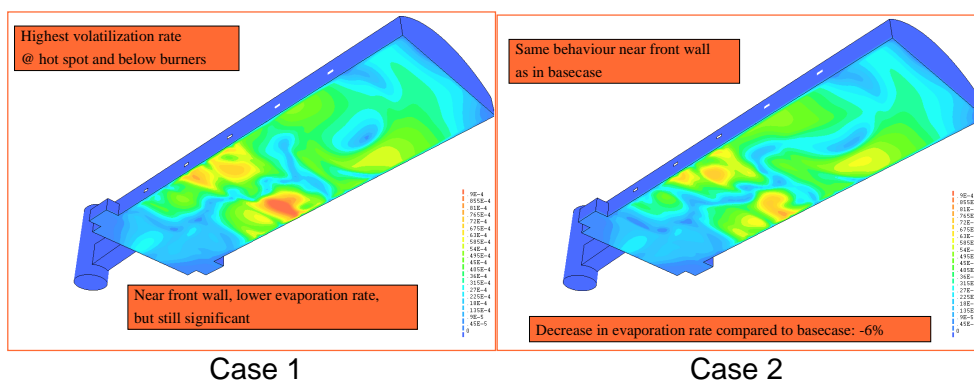


Figure 11: Simulated HBO₂ concentrations in a plane through the burners for cases 2, 3 and 4.

In figure 12 the volatilization rates at the glass surface for all four cases are shown. High volatilization rates occur at the hot spot and below the burners.



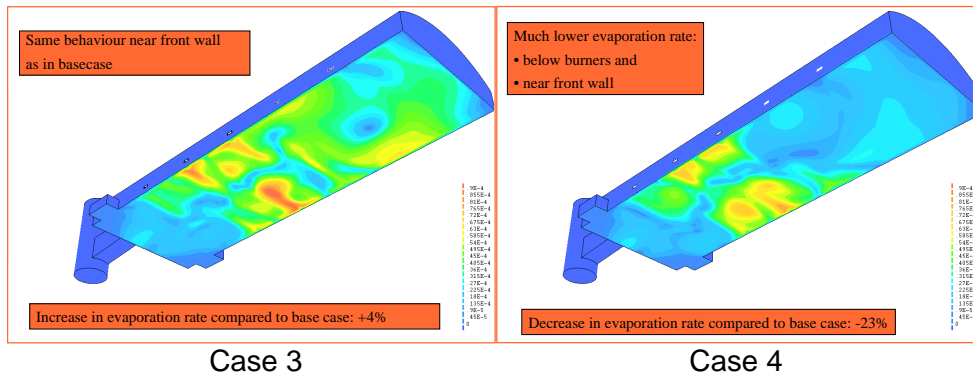


Figure 12: Simulated volatilization rates of HBO₂ at the glass surface for all 4 cases.

The results of the four simulations are summarized in the table below. In this table the total volatilization flux at the glass surface is shown. Also the simulated and measured HBO₂ concentration in the stack are given. In the last column the change in volatilization flux with respect to the base case (case 1) can be seen.

	Volatilisation HBO ₂ flux kg/s	HBO ₂ in exhaust gr/hr	measured similar furn gr/hr	Change in Vola flux %
1) basecase	3.11E-03	11211	10646	0.0%
2) burners 10 cm lifted	2.93E-03	10553	10646	-5.9%
3) burners 10 cm lowered	3.27E-03	11759	10646	4.9%
4) crown 10 cm lifted	2.39E-03	8612	10646	-23.2%

When comparing the HBO₂ concentrations for cases 2 and 3 with case 1 (figures 9 and 10), no big difference is seen. However, case 4 shows significantly lower HBO₂ concentrations. The same applies to the volatilization rates (figure 10): case 4 shows a significantly lower overall evaporation rate (-23.2%) compared to cases 1, 2 and 3. It is concluded that a large decrease in the volatilization flux can be achieved by lifting the crown (case 4). By comparison, changing the burner position has a smaller effect on the volatilization flux.

CONCLUSIONS

In this paper the capability of GTM-X to model the multi-physical phenomena in glass melting furnaces was demonstrated.

In the first part two models, present in GTM-X, are described: the dynamic foam model and the volatilization model. The first model describes the balance between growth and destruction of bubbles in the foam layer, resulting in a calculated foam thickness distribution on the glass surface. The second model gives an empiric expression for the volatilization flux of species from the glass surface, based on the temperature of the glass surface and parameters in the combustion space.

In the second part a typical industrial application is given. GTM-X is used to simulate a fiber glass producing furnace. The results showed that foam thickness predicted by the model corresponds well to industrial observations. The calculated results for the HBO₂ concentrations in the furnace were in good agreement with measurements in a similar furnace.

Furthermore, a parameter study was done with the aim to reduce the volatilization flux of HBO₂ at the glass surface in this furnace. Reducing the volatilization flux results in lower operating costs. Simulations done with GTM-X showed that changing the burner location does not have a large effect on the volatilization flux. The crown height variation had a much larger impact on the volatilization flux. The simulation showed a 25% lower volatilization rate for the case with a larger crown height. This can result in a savings of 100 ton/year of colemanite (boron batch compound).

REFERENCES

- [1]. SCHAAF VAN DER, J. and BEERKENS, R.G.C., A model for foam formation, stability, and breakdown in glass-melting furnaces, *Journal of Colloid and Interface Sciences*, Vol 295, pp. 218-229, 2006
- [2] BEERKENS, R.G.C. and SCHAAF VAN DER, J., Gas release and foam formation during melting and fining of glass, *Journal of the American Ceramic Society*, Vol. 89, No. 1, pp. 24-35, 2006
- [3]. LIMPT VAN, J.A.C. and BEERKENS, R.G.C., Reduction of superstructure corrosion and emissions by modern furnace design and optimized operation, In *Proceedings of XX ATIV Conf. Modern Technologies and Techniques for Glass Manufacturing*, Italy, 2005
- [4]. LIMPT VAN, J.A.C. et al., Mass transfer relations for transpiration evaporation experiments, *Int. Journal of Heat and Mass Transfer*, Vol 48, pp. 426-428, 2005

SIGNIFICANCE OF RAYLEIGH NUMBER FOR ALL-ELECTRIC MELTING

Josef Smrček
ELECTROHEAT s.v.p.d. Praha
(near to English)

Abstract

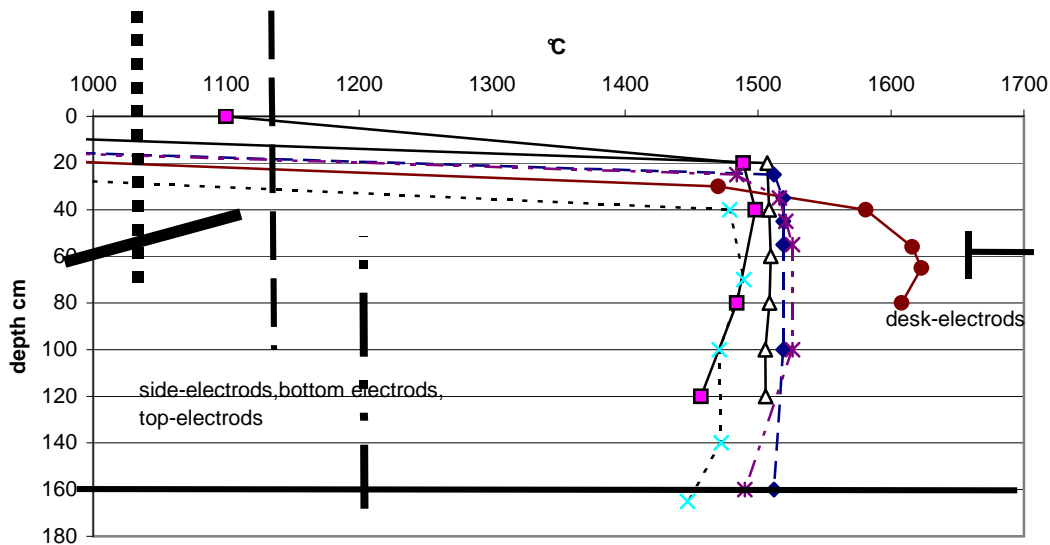
The vertical temperature gradient in the tanks with aspect ratio greater as 2 (up to 5) was measured and case of the Rayleigh-Bénard thermal convection in volumetric heated horizontal layer adiabatic walls, only with the upper wall isothermal (cooled), describe this temperature distribution in all-electric melting tanks. Thus, the critical value of Rayleigh number is the point of beginning of thermal convection in the tank. Because the glass melt have all properties temperature-dependent, is necessary this- and another factors to discuss.

INTRODUCTION

The glass-melting in the all-electric tanks is vertical, thus the pull-flow has opposite direction as bubbles ascending. The pull-rate is almost about 5 cm/hour and after Stokes' law have the same ascending velocity bubbles with diameter about 0,05-0,1 mm. Also, when there was no convection, comes to throat only this gisp even without fining agents. But the tracer-measurements indicate, that actual vertical descending maximal velocity is at least 10-times greater (0,5-1 m/hour). Thus, the thermal convection is the important factor for the melting output and glass quality.

In the last 20-years was measured the temperature gradient in the different all electric tanks with the methode „cartouche“ [1] and with Pt-sonde. The values were sampled in [2] and an overview is on the fig.1

Fig.1 Measured temperatures in all-electric furnaces with variable electrode-arrangement



Left is schematically described placement of rod electrodes, with the same line-type is rights described the temperature measurement. Unfortunately only to 20 cm under bath was measured – because the boundary between bath and glass melt was very unsure. The geometric height of tanks was 120-160 cm, the actual height of glass melt was 5-20 cm lower (the bath- height). Every tank was measured at almost 3-times, but another day. The cartouche method has mistake about 10-20 K thanks the glass melt mixing in the surrounding of thermocouple (about 5 cm).

Absolutely right on fig.1 is the typical temperature measurement (from some hundreds) on the tank with flat electrodes – this tank is only 80 cm deep, the live height of glass melt is about 60 cm.

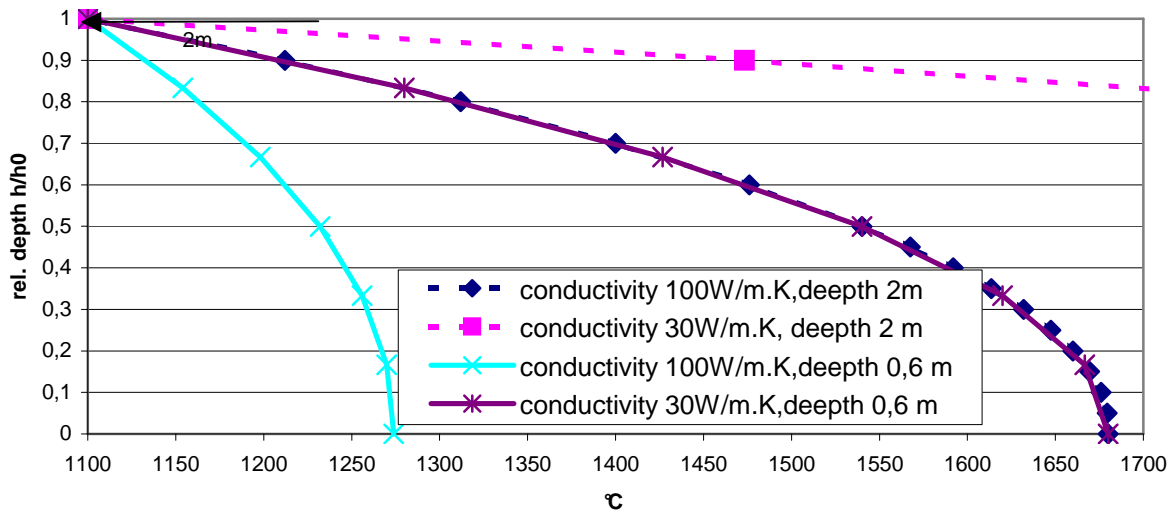
The measured tanks were the great – the aspect ratio (ratio of smaller horizontal dimension to height) $\Gamma = 2-5$. The glass was every white with Fe_2O_3 content 0, 02 – 0, 06%.

It is obvious that the course of all measurements is the same – almost isothermal from the bottom to the height of 0, 05 - 0,2 m under boundary bath-glass melt. This absolutely does not agree with the theoretical courses of temperature after the known simple equation

$$T_x - T_0 = \frac{Q}{2\lambda} x^2 \quad (1)$$

where T_0 is temperature of boundary bath – glass melt (900°C soda-calc. glass, 1100°C boro-silicate glass) – fig 2.

Fig 2. Computed vertical curve of temperature in the tank 0,6 and 2 m deep, with the same melt rate 100 kg/m².h. Heat conductivity of glass melt = 30 and 100 W/m.K. Deep tank needs high conductivity=high convection.



There is computed the theoretical course of temperature from boundary bath- glass melt against dimensionless height with volumetric rate of energy generation (constant in the whole tank) – Q and some thermal conductivity - λ. It is obvious, that the choosed value of conductivity λ= 30 W/m.K give the macabre temperatures in the height 2 m, on another side the conductivity 100 W/m.K gives unreal pleasant low gradient in the height 0,6 m. Only great conductivity in deep tank and small conductivity in shallow tank have nearly the same course (height and conductivity are nearly in the same ratio) and the values near to measurement. It is obvious, that in the deep tank must be the computational, virtually, conductivity over 100 W/m².K, in the shallow tank under 30 W/m².K. Naturally, the vertical distribution of energy generation, here constant, in the really tank depending on the electrodes-placement, influenced the temperature – gradient. (But on the fig.1 is not to see this influence.)

This agree with fig 1, there is temperature gradient on the deep tank maximal 50 K/m in the bottom part, melting heat flow 60 kW/m², thus

$$\lambda_{\text{virtually}} = 60000/2 \cdot \text{W/m}^2 / 50\text{K/m} = \text{min. } 300 \text{ W/m.K} \quad (2)$$

Only on shallow tank (0,6 m) is gradient higher –400 K/m, thus there is convection slowly - $\lambda_{\text{virtually}} = 75 \text{ W/m}$.

Equation (1) shows too, that maximal temperature in the tank rises with tank depth. Thanks parabolic dependence on height, with

$$Q = q/H \quad (3)$$

risers the maximal temperature in the tank even by decrease of volume heat generation Q

$$T_H = \frac{q}{2\lambda} H - T_0 \quad (4)$$

with the tank depth in spite of constant q- surface heat generation = melting output.

Thus, the convection must take place. The measured temperature-course are very analogous to well known courses in Rayleigh-Bénard convection. The glass tank is near the case with volumetric heat generation, what begun theoretical to study Roberts [3] and experimental namely Kulacki and his school [4]. The Ra-number is is very sophisticated

$$Ra_E = g.(\beta / \alpha.\eta). \Delta T.H^3 \quad \text{Rayleigh 1916}$$

external Ra_E for endless layer between two rigid boudaries with temperature difference ΔT ,

$$Ra_I = g.(\beta. /2.\lambda. \alpha.\eta) . Q.H^5 \quad \text{Roberts 1967}$$

internal Ra_I for adiabatic volume with isothermal upper surface and homogen internal heat source Q.

It is obvious, that the depth H is for Ra the most important. If is the conductivity unknown, is possible after Hrma [5] to describe

$$Ra_{\Delta T} = g.(\beta.\rho.c_p. / \eta. r) . \Delta T^2 H^2 / G \quad \text{Hrma 1980}$$

where

() – glass properties – all properties are f(T)

β – volume expansivity K^{-1}

ρ - density kg/m^3

η – kinematic viscosity m^2/s

c_p – specific heat $J/kg.K$

λ – heat conductivity $W/m.K$

α - heat diffusivity = $\lambda/c_p.\rho$ m^2/s

r - melting heat (= heat capacity+ reaction heat) J/kg

Output characteristics

ΔT – temperature difference K

Q - volume heat current to *upper surface* = melting enthalpy W/m^3

(not volume all heat releasion= incoming power)

G - bath input per upper surface $kg/m^2.sec$

q – upper surface heat current W/m^2

Geometric characteristics

H – depth m

Γ – aspect ratio, smaller horizontal dimension/depth

The ratio of the all heat flux to conductivity flux is Nusselt Number

$$Nu = q / (2 \cdot \lambda \cdot \Delta T / H) = \lambda_{\text{virtual}} / \lambda_{\text{cond}}$$

This agree with eq.(2). From Kulacki and Emara [3] is Nusselt-Number in this volume-heat release cavity

$$Nu = 0,389 \cdot Ra^{0,228}$$

and Nu is about 3 in shallow tank and 10 in deep tank. Influence of some other factors:

- thermal conductivity (radiation conductivity, effective conductivity)

Measured values of the radiation transmissivity (Roseland-approximation) or the effective values from measuring of temperature gradient on steady state in the standing layer [6] gives high values -80 – 100 W/m.K and over, the values from unsteady heat flow measurements gives values to 30 W/m.K. It is therefore reasonable to use not Roselands-, but Plancks – average absorptions- coefficient in the measured spectrum 1 – 3 μm , or the geometrical average of both [7,8] to express the radiation conductivity. The value 30 W/m.K as effective conductivity seems to reasonable estimation. Ungans equation [9]

$$\lambda_{\text{ef}} = 5,386 - 0,02168 \cdot T + 0,00002058 \cdot T^2$$

is therefore the best. Choudhary [17] gained very close values of residence time distribution to the tracer measurements with the value 1,73 W/m.K.

- viscosity

Another problem is with strong temperature dependence of viscosity. Often is used the “mean viscosity” in the half height of tank, another authors express also the slope of viscosity

$$\eta(\Theta) = \exp(-b(\Theta)), \text{ with } \Theta = T/T_0, \text{ some dimensionless temperature}$$

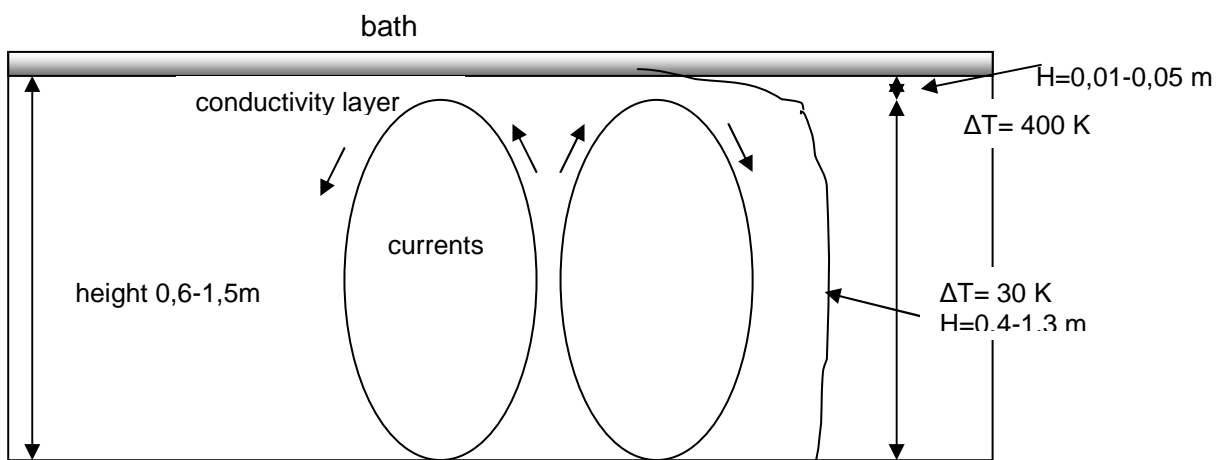
Influence of slope \underline{b} is up today not clear [10, 11, 12]. From observation the bath layer of different glass melts is obvious, that greater \underline{b} implicate height of conductivity layer under crust and crust height too. On the soda-calc glass melt was the former up to 1 cm, on

borosilicate up to 5 cm, the latter 1 mm and 5 mm. This layer is described also on lithosphere [15].

The rough idea of the convection is on fig.3. The convection come up to (or near to) bottom and are created from rolls or three-dimensional cells.

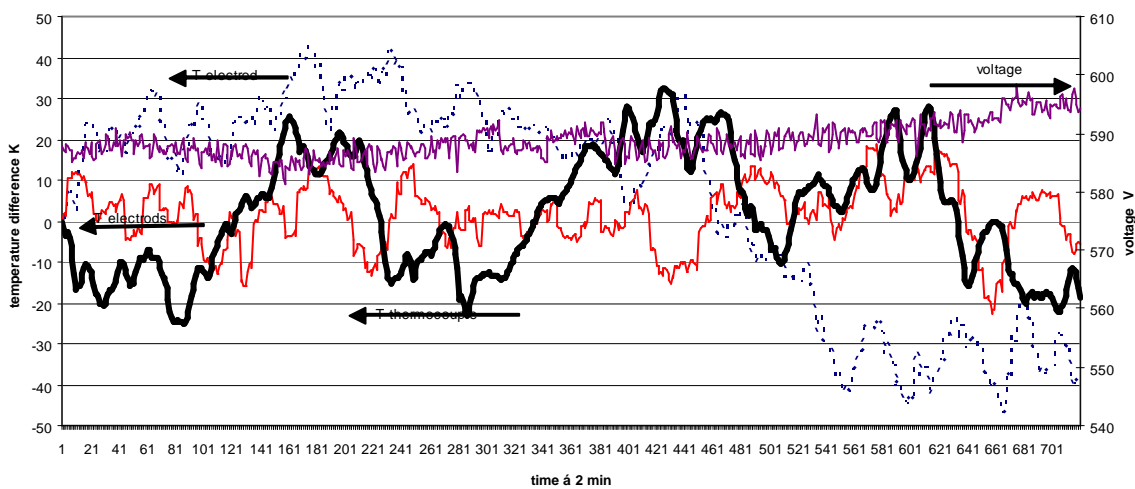
The rolls are stable up to about Ra_E 8000. Increasing Ra induced cross-roll and zig-zag instabilities and from $Ra_l = 23000$ begin the bimodal oscillating instabilities (after Busse and Whitehead [13]). Beginning this oscillation depend on square of Prandtl number Pr^2 . The period of this oscillation depend on $Ra^{-2/3}$ [13]

Fig3. Convection in all-electric tank



The actual behavior of all-electric tank we are observing within last 12 years on operational tanks. On fig 4 is an example

Fig 4 Full operation, temperature about 1500-1550°C .Comparison of computed temperatures on electrodes from locally resistance (U/I_e) - always difference against first value, and measured temperature and oscilation of voltage



There is the recording of glass melt temperature 40 cm under bath, and also computed temperatures from voltage and currents respective electrodes

$$\Delta T = (I/U - I_0/U_0)/(I_0/U_0)/c$$

I, U – actual current and voltage respective electrodes

I₀, U₀ – comprised values (first in time row)

c – slope of electrical conductivity of glass melt (0,0015 - 0,0025 K⁻¹)

ΔT – difference between actual and compared state K

It is to see, that both electrodes and thermocouple have the same amplitude and mostly also period, thus both temperatures are representative for its place and exist some period typical for the all tank. The comparison with the progress of voltage shows, that voltage influence the temperature in the very long time part (200 min), or very speed oscillation, 2-4 min (control), not in periods 35-66 min as the temperature.

Thus, we compare on figs 5,6 two state on the same tank, the same glass melt, but different pull and temperature.

It is obvious, that the tank with 1/3 pull has no thermal convection – whether temperature nor its Fourier analysis has some peaks. In full operation is to see the two frequencies (periods) 36 and 60 min. The main frequency t₁ = 36-45 min (the fluctuation is given by unsteady height of live layer, due to unsteady bath layer – difference up to 10 cm represent the H² value fluctuation 1:1,44) is for this type of tanks and glass typical [14]. As the mean time constant after conductivity t₀ = H²/α = 10 hours, what is lower as theoretical geometric mean delay time in the live volume t_g = 16 hours computed from pull, and the dimensionless main period τ = t₁/t₀ = 0,060-0,075.

It roughly correspond to Busse and Whitehead [13] - value 0,03-0,04 for greater Ra. Kirchartz and Oertel [18] found in air the main period τ = 0,1 with Ra = 39000. Dubois and Bergé [19] in oil with Pr = 130 found for Ra = 400 000 τ = 0,01.

Kwang-Ok Lim et al. [16] uses mean time t₀ = H²/η, (after viscosity) for horizontal flow and the period was τ = 1,9, also in real time hundreds second

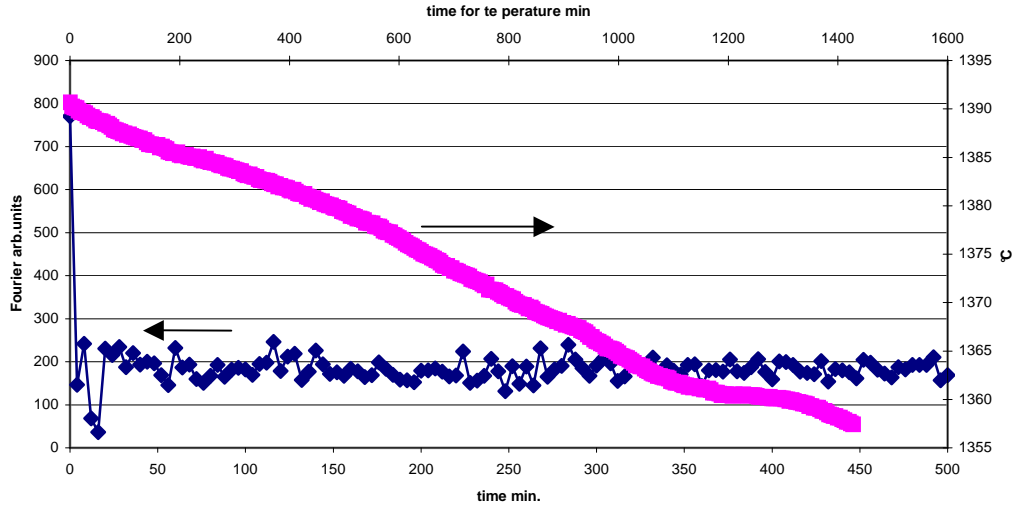
We can attempt for rough estimation of critical Ra_i from the three observations :

state	height	mean temperature	Ra _i – estimation	glass
1/3 pull	0,6 m	1380°C	7.000	borosilicate
½ pull	0,6	1450	10.000	borosilicate
full pull	0,6	1550-1600	40-55.000	borosilicate

The viscosity and conductivity was used after mean temperature. The critical Ra_i is therefore between 10.000-40.000, near to lower value.

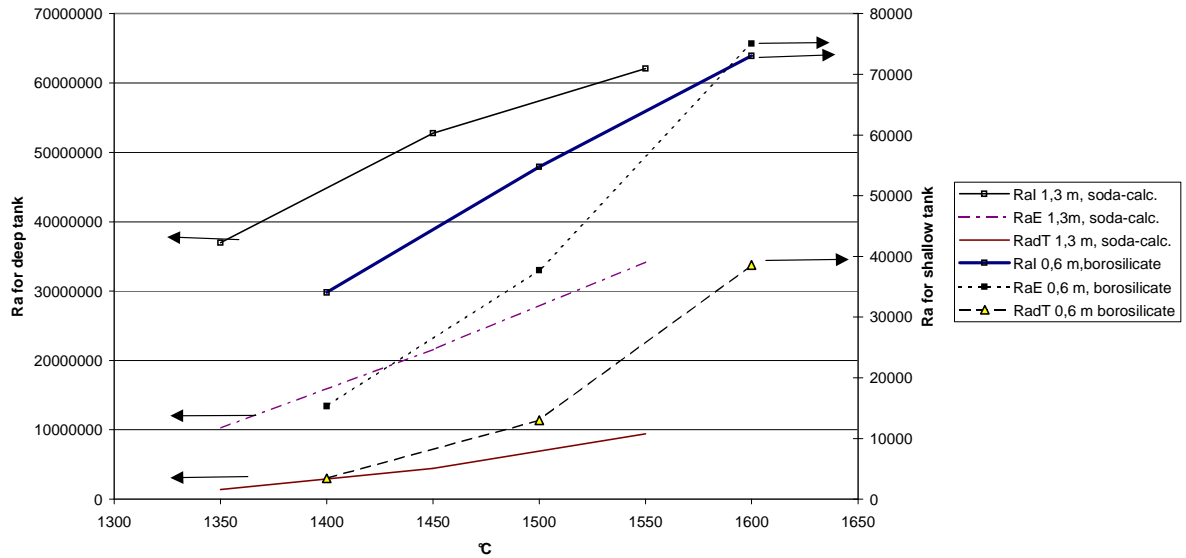
This not agree with Kulacki value 1344 [3]. On the deep tank is Ra 10⁷ -10⁸, critical value is hard in operational conditions to attain.

Fig 4 Temperature in glass melt within 1/3 of nominally pull, lowest temperature. Rights temperature, lefts its Fourier analysis



On fig 7 is comparison of computed Ra_l , Ra_E and $Ra_{\Delta T}$ for thermal conductivity after Ungan, viscosity for max. temperature and estimated ΔT . Thanks different height and viscosity is difference between both tanks three order

Fig 7. Computed Ra after Rayleigh, Roberts and Hrma for shallow tank with borosilicate glass and deep tank with soda-calc.glass



CONCLUSIONS

- 1/ In the all-electric glass melting tank is Rayleigh-Bénard convection with velocity at least 10-times more as the pull velocity (0,5-1 m/hour).
- 2/ The effective thermal conductivity of glass melt not exceeds value 30 W/m.K
- 3/ The critical internal Rayleigh number Ra_i in actual all-electric tanks (no adiabatic, wall losses 5 kW/m²) is estimated near value 10-15.000
- 4/ The convection in tank with specific output 2000 kg/m².day and more is cellular, bimodal
- 5/ The dimensionless main oscillating period is $\tau = 0,06-0,075$

LITERATURE

- [1] M. Knap: Measurement of temperature gradients in glass melt in all-electric furnaces. Orig czech. Proceeding of 2nd conference on electric melting of glass. Ústí nad Labem 1969 p. 86-98
- [2] Smrček, J. Temperature field in all electric furnace. Orig Czech. Proceedings of 11th conference on glass. Czech glass society ČSS Luhačovice 2005
- [3] Kulacki, F.A., Emara, A.A.: Steady and transient thermal convection in a fluid layer with uniform volumetric energy sources. J.Fluid Mechanics vol 83,part 2(1977),s.375-39
- [4] Roberts,P.H.: Convection in horizontal layers with heat generation.Theory. J.of fluid mechanics. Vol. 30 (1967) s 33-41
- [5] Hrma, P.: Similarity in modelling of electrical melting of glass. Orig czech. Proceeding of 5th conference on electric glass melting. Ústí nad Labem 1980, s.71,-75
- [6] Blažek,A.,.Endrýs,J.Kada,J.: Strahlungswärmeleitfähigkeit von Glas. Glast.Ber. 49 (1976),s.75-81
- [7] Smrček,J.,Endrýs,J.: Spectral transmissivity of glass melt in high temperature. (How many heat come through melted glass with radiation?).Orig czech. Sklář a Ker. 546 (2006),No 1,2,s.1-6
- [8] Matsushima H.,Viskanta R.: Effects of internal radiative transfer on natural convection and heat transfer in a vertical crystal growth configuration. Int.J.Heat mass transfer 33(1990) No-.9,s.1957-1968
- [9] Urgan A.,Viskanta R.: Three-dimensional numerical modeling of heat transfer in a glass melting tank.. Part 2. Glastechn.Ber. 60 (1987), No 4,p. 115-124

- [10] White, D.B. : The planforms and onset of convection with temperature-dependent viscosity. *Journal of Fluid Mechanics*, vol 191 (1988) s. 247-286
- [11] Stengel, K. C., Oliver, D.S., Booker, J.R.: Onset of convection in a variable-viscosity fluid. *Journal of Fluid Mechanics*, vol.120 (1982), s. 411-431
- [12] Giannandrea, E., Christensen, U.: Variable viscosity convection experiments with a stress-free upper boundary and implications for the heat transport in the Earth's mantle. *Physics of the Earth*
- [13] Busse, F.H., Whitehead, J.A.: Oscillatory and collective instabilities in large Prandtl number convection. *J. Fluid Mech.* vol. 66 (1974) part 1, p. 67-79
- [14] Smrček, J. : Konvektionswärmestrom in Glasschmelzwannen. *Glastechn. Ber.* 57 (1984) No. 121, s. 307-312
- [15] C. Dumoulin, et al. : Onset of small-scale instabilities at the base of lithosphere: scaling laws and role of pre-existing lithospheric structures. *Geophys. J. Int.* (2005), 160, p. 344-356
- [16] Kwang-Ok Lim et al. Primary and secondary instabilities in a glass-melting furnace. *Numerical Heat transfer, part A*, 36 (1999) p. 309-325
- [17] Choudhary M. K.: A modeling study of flow and heat transfer in an electric melter. *Journ. of Non-Crystalline Solids* 101 (1988) p. 41-5
- [18] Kirchartz K.R., Oertel Jr H. Three-dimensional thermal cellular convection in rectangular boxes. *J. Fluid Mech.* vol 192 (1988), p. 249-286
- [19] Dubois M, Bergé P.: Experimental evidence for the oscillators in a convective biperiodic regime. *Physics Letter* 76A (1980) p. 53-56

ACKNOWLEDGMENTS

This work was supported by Ing Marie Smrčková, patent and trade mark attorney, No. grant 720624.

GLASS TANK REINFORCEMENTS

Wolfgang Simader
PLANSEE Metall GmbH
A-6600 Reutte/Tyrol
Austria

Abstract

The lifetime of different glass tanks can vary greatly between a few months and several years. It depends on many factors such as the glass composition and temperature, but also daily production quantities.

The duration of a tank campaign is determined by the rate of wear within the tank and the subsequent failure of important functions. The following areas of the glass tank are critical:

- *dog house*
- *throat channel*
- *bubble maker*
- *wall*

Cladding with molybdenum sheet protects these critical areas of the glass tank against wear, maintaining their form and reliability for longer periods. This of course helps to optimize the manufacturing process and glass quality and significantly improves the service life of the glass tank.

A very important topic is the effect of the glass tank reinforcements on operation parameters of an electrical heated glass tank. To demonstrate that there is no relevant influence a mathematical simulation was done by our partner Glass Service.

INTRODUCTION

The production of glass began hundreds of years ago. Despite this long history the manufacturing processes for glass are still being constantly evaluated and optimised. Various topics dominate current discussions. Key words such as higher strength, low weight, less impurities and greater cost effectiveness are frequently heard at glass conferences and in discussions between glass producers. Competition from alternative materials such as plastics for bottles is increasing rapidly.

Every glass producer is forced to improve product quality, but at the same time to reduce the costs for consumers. Possible ways to increase cost effectiveness, for example, are to reduce the production of reject parts and prolong the campaign length of a glass tank.

Great effort has already been made to increase the lifetime of a glass tank. The quality and corrosion resistance of the refractory bricks has been improved year by year. Sintered refractory bricks have been replaced by cast refractories to protect the most heavily worn sections of a furnace in particular. But even the cast quality exhibits corrosion rates that cannot be ignored. The only way to drastically improve the corrosion resistance of glass tank parts that are exposed to heavy wear is to protect them with metal. Only a few metals can withstand the high temperatures required for the production of glass. Figure 1 shows a

comparison of the corrosion resistance of different metals and AZS material to the most commonly used glass melts. This diagram shows how limited the possibilities are.

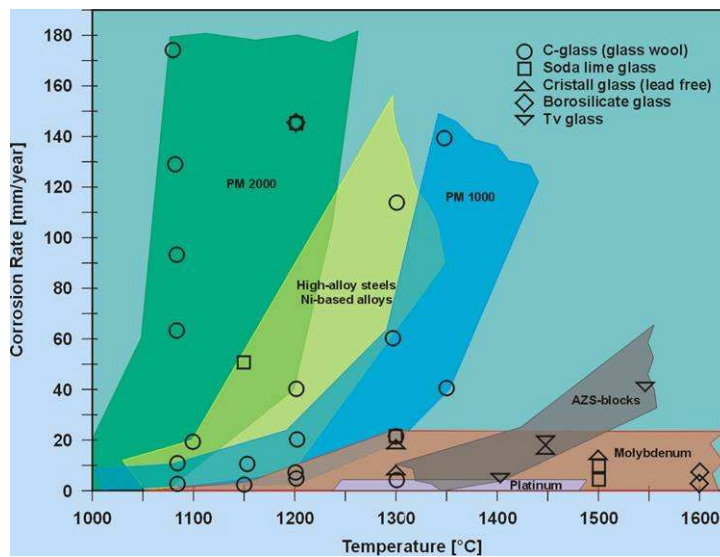


Figure 1: Corrosion resistance of different metals and AZS material

Iron & iron-based alloys and nickel & nickel-based alloys are not able to fulfil the high requirements of glass production. The melting point of these metals or alloys is much too low and even when used below this temperature, they show high corrosion rates and pollute the glass heavily when immersed in the melt. Two metals have already been proven to exhibit good corrosion resistance without pollution of the glass melt - platinum and molybdenum. The corrosion resistance of platinum is unrivalled, but closely followed by molybdenum. Two main differences exist between these metals:

- the oxidation resistance
- and the price

Platinum is the only metal currently used which can withstand corrosion and oxidation. The oxidation resistance (figure 2) of molybdenum is poor and therefore it requires special protection from oxidizing atmospheres until it is immersed completely in the glass melt. Nowadays this can be achieved with a coating, called SIBOR[®], which will be described in the following paragraph. The big difference between molybdenum and platinum is the price. Platinum is a precious metal and must be priced at a market rate, which is determined day-to-day by the stock market. 10 to 15 grams of platinum cost approximately the same as 1 kg of molybdenum sheet already coated with SIBOR[®]. The quantity of platinum required is much too high for most uses and it is therefore limited to very special applications such as platinum feeders for special glasses with very high purity levels.

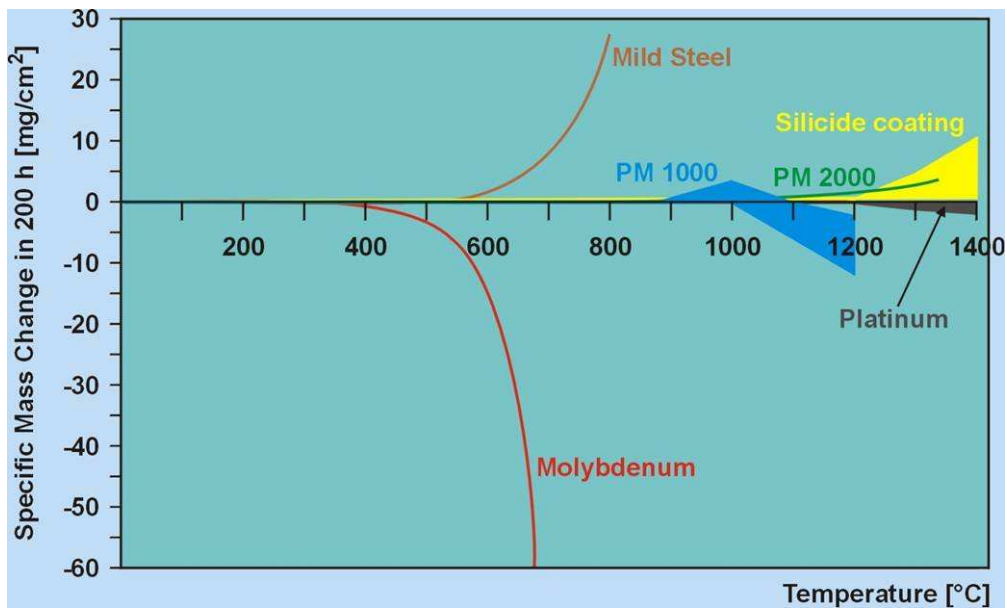


Figure 2: Oxidation resistance of several materials

SIBOR® COATING

As mentioned above and shown in figure 2, molybdenum has a poor oxidation resistance at temperatures above 600 °C (1112 °F). In principle, various solutions exist to protect refractory metals like molybdenum against oxidation: alloying, packing with ceramic powders, glassification, cooling, application of protective gases (e.g. hydrogen, argon, ...), cladding with platinum or - last but not least – coating with an impervious layer.

The only coating which can guarantee an “oxidation free” period is the so-called SIBOR® coating. This patented coating consists of silicon and 10 % boron by weight and it is applied to sand blasted molybdenum surfaces using a plasma spray process. The coated molybdenum parts are then annealed to ensure outstanding oxidation resistance. Figure 3 shows three cross sections of a molybdenum sample with SIBOR® coating after each production step [3a.. SIBOR® coating as sprayed, 3b ... SIBOR® coating after annealing, 3c ... SIBOR® coating after 400 hours in use in air at a temperature of 1450 °C (2642 °F)].

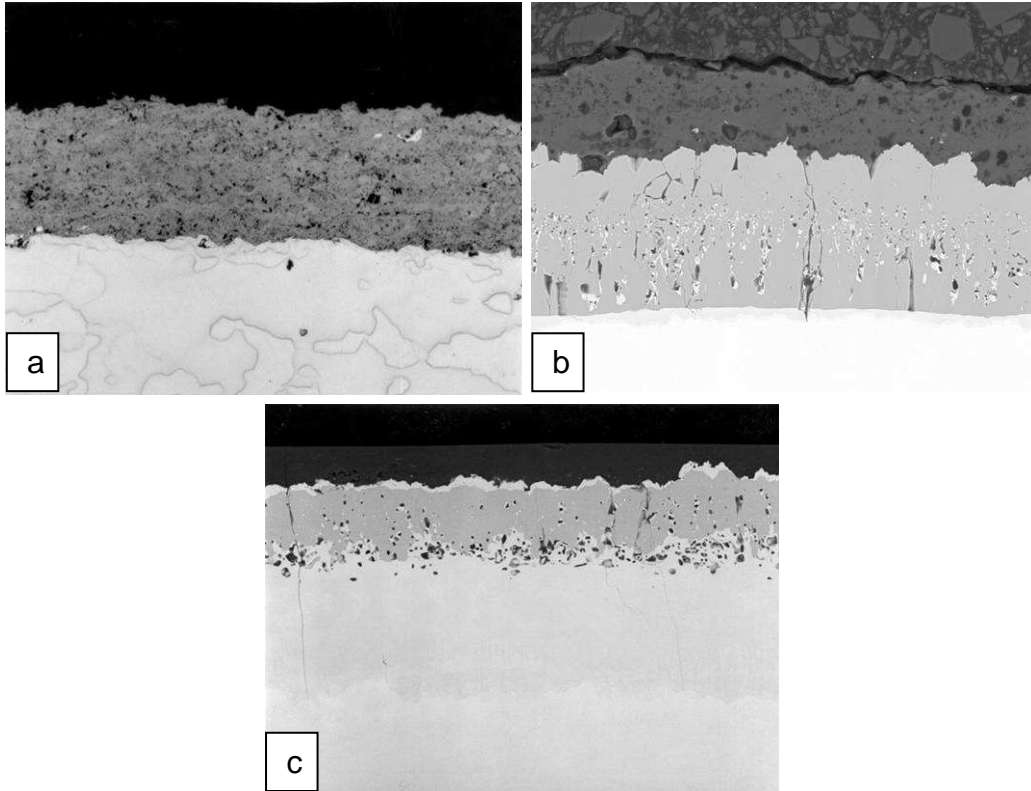


Figure 3: Cross sections of molybdenum with SIBOR[®] coating

The SIBOR[®] coated molybdenum parts (glass melting electrodes or glass tank reinforcements) can be installed in a cold glass tank before the up-tempering process starts. The parts will remain in tact without any oxidation throughout heat-up, even with a slow up-tempering rate of 5 to 10 °C per hour. It is guaranteed to last as follows: 5000 hours at 1200 °C (2192 °F), 500 hours at 1450 °C (2641 °F) and 50 hours at 1600 °C (2912 °F). This time/temperature performance enables glass producers to install the molybdenum parts easily and safely in a cold tank. Further advantages of the SIBOR[®] coating are the properties of the layer. The SIBOR[®] coating is not as brittle as ceramic coatings like the SiCrFe coating and silicide coatings (e.g. MoSi) and can withstand normal handling during the installation process without chipping. The SIBOR[®] coating will be dissolved by the glass within a few days. At the beginning bubbling can occur, but it will decrease rapidly after 24 hours. Due to the composition of this coating (Si, B) it will not cause any discoloration or contamination of the glass melt.

GLASS TANK REINFORCEMENTS

The lifetime of different glass tanks can vary greatly between a few months and several years. It depends on many factors such as the glass composition and temperature, but also daily production quantities. Opal glass, for example, is a very aggressive glass and a tank campaign lasts only a few months. Glass tanks for container glass (soda-lime glasses) have a service life of up to 10 years (6-8 years on average). The duration of a tank campaign is determined by the rate of wear within the tank and the subsequent failure of important functions.

The performance of the SIBOR[®] coating mentioned above now makes it possible to use the good corrosion resistance of molybdenum to protect the areas of a glass tank that are exposed to heavy wear in most glass melts (Figure 1). Some of these areas are critical for the lifetime of the glass tank, others are critical for the performance of the tank and the glass quality.

The critical sections are marked in Figure 4, which shows a schematic diagram of a typical glass tank:

- 1 dog house
- 2 bubble maker and wall
- 3 throat channel

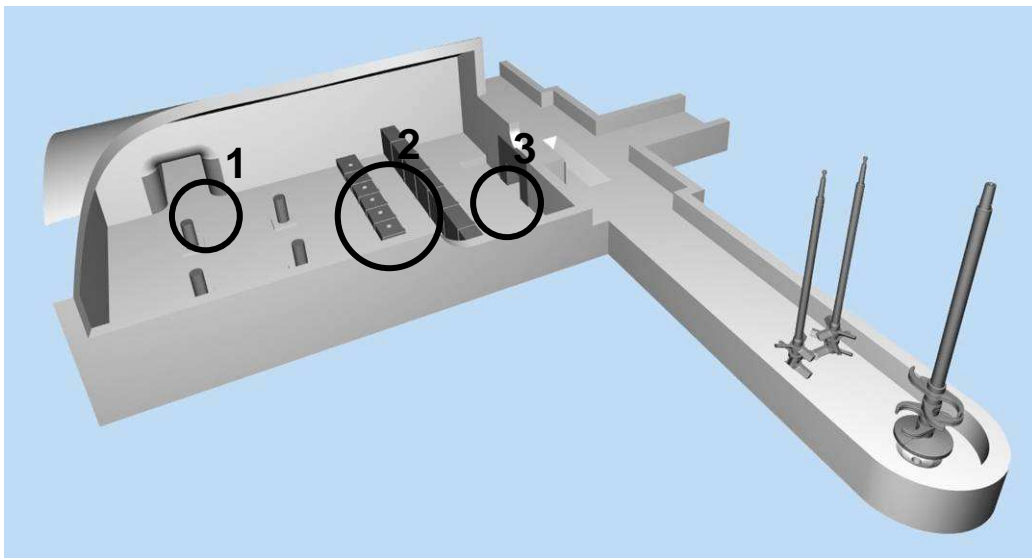


Figure 4: Schematic diagram of a glass tank showing critical areas

- The “doghouse” – where the raw materials for glass production are introduced into the glass melt – heavily stressed due to the oxygen content of the batch and the formation of foam

- The “bubble maker” – where large, defined bubbles are added to the molten glass to agglomerate the little bubbles – heavily stressed by corrosion and erosion processes
- The “crosswall” – controls the convection streams in the melting area and the transition time of the glass melt – heavily stressed by corrosion and erosion processes
- The “throat channel” – the transition between the melting area and the working end and the feeders – heavily stressed by corrosion and erosion processes

The appearance of the crosswall and the throat channel at the end of the tank campaign as shown in the Figures 5 and 6 is very familiar to all glass producers.

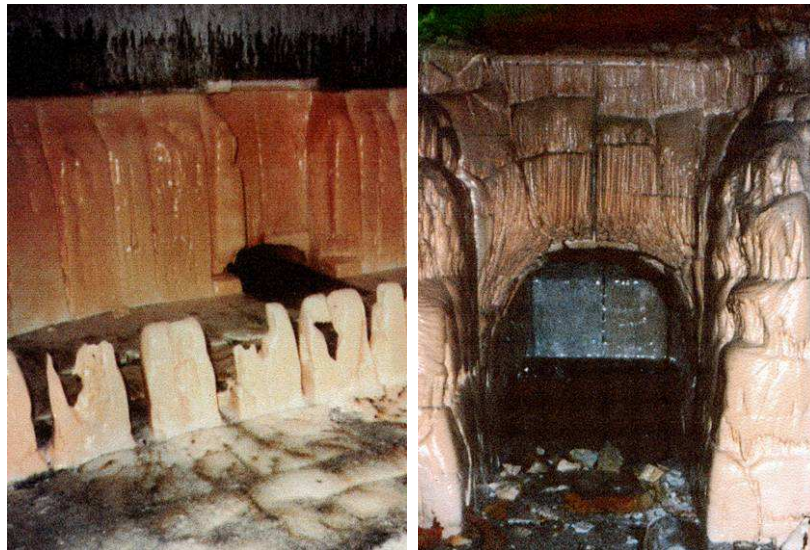


Figure 5 and 6: Corroded crosswall and throat channel at the end of a tank campaign

Cladding with molybdenum sheet protects these critical areas of the glass tank against wear, maintaining their form and reliability for longer periods. This of course helps to optimize the manufacturing process and glass quality and significantly improves the service life of the glass tank.

EXAMPLES OF GLASS TANK REINFORCEMENTS:

Generally speaking, glass tank reinforcements are molybdenum sheets (thickness 6-10 mm, 0.25-0.4”), which are made into various shapes and forms using bending and machining processes. 100 % of the surface is then coated with SIBOR® to achieve complete oxidation resistance of the whole assembly.

Tank components made of molybdenum can easily be fixed to the tank using different methods:

- 1) Clamping between the refractory bricks
- 2) Fixing with bolts that are inserted through the sheet into the refractory brick
- 3) Simple covering of the parts requiring protection such as the wall or the bubble maker

Figure 7 shows a doghouse reinforcement. Simply formed molybdenum sheets are fixed with pins onto the corner bricks of the doghouse. This helps to prevent corrosion to the bricks as the batch enters and often produces foam in this area.

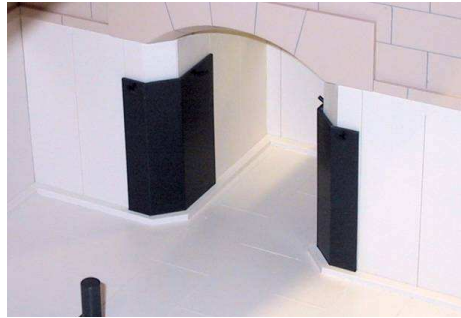


Figure 7: Doghouse reinforcement

Figure 8: Bubble maker / wall protection

Figure 8 shows a simple bubble maker cover. The same principal can also be used to protect walls. The “U – channel” is simply placed over the refractory bricks and clamped between the bottom bricks. It ensures that the form and function of the bubble maker (or wall) are maintained for a long period.

The most critical area in a glass tank is of course the throat channel. This section is located between the glass tank itself and the working end and controls transition time and glass flow. The throat channel construction consists of several refractory bricks (two side bricks, one top brick and several bricks for the channel). To guarantee good corrosion protection it is also necessary to cover the joints in the brick. This is only possible if the reinforcement plates used have a greater width and height than the individual bricks and they have to be fixed to the outside of the bricks (cladding). Figure 9 shows how a throat channel can be effectively protected.

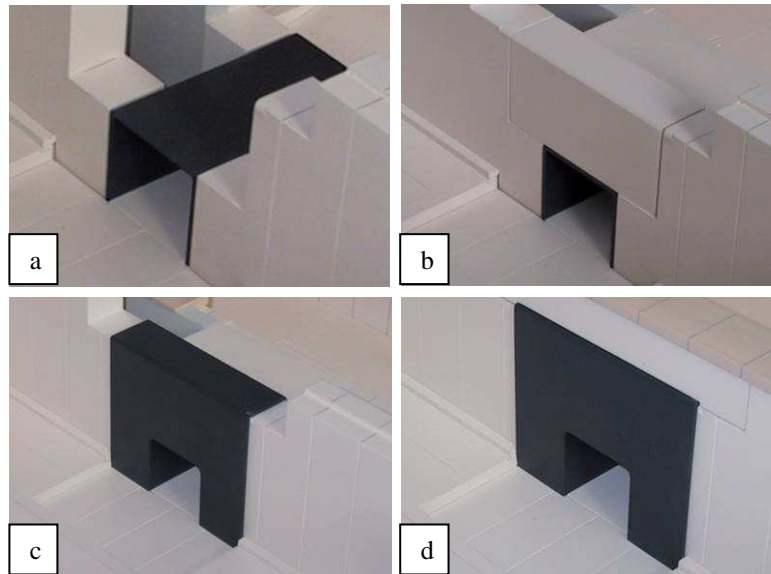


Figure 9: Schematic diagram of a throat channel reinforcement

The throat channel protection assembly consists of two parts: the front plate and a “U”-channel (Figure 10). This is necessary for ease of handling and installation. The connection between the two parts is specially designed and produced to prevent any penetration of the glass.

Similarly other components such as flow pipes inserted in a cross wall (used to generate additional convection currents) and delivery pipes can be produced in molybdenum and protected against oxidation. In such cases SIBOR[®] coating is required on all surfaces.

The design of each glass tank reinforcement is adapted to suit individual customer requirements after discussion between the glass producer and/or the furnace constructor and PLANSEE.

Such parts can be installed easily by either the glass producer, the furnace constructor or by PLANSEE.

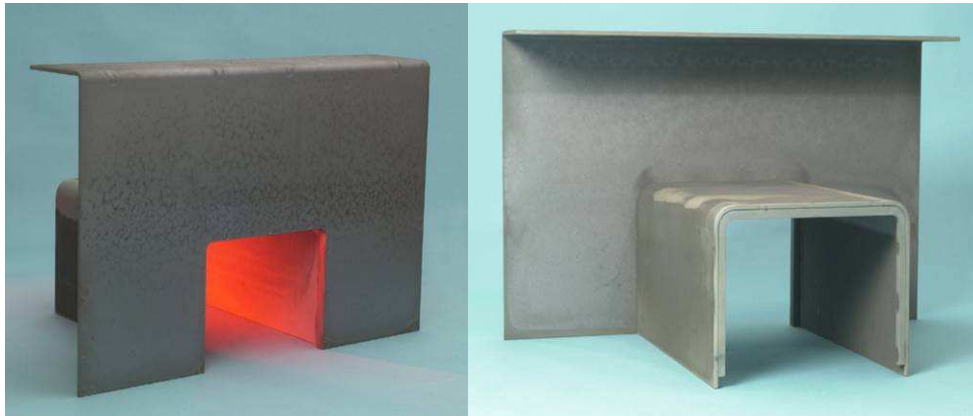


Figure 10: Throat channel protection - front and back views

MATHEMATICAL SIMULATION OF AN ELECTRICAL HEATED GLASS TANK EQUIPPED WITH GLASS TANK REINFORCEMENTS:

An often asked question is the electrical behaviour of glass tank reinforcements in an electrically heated glass tank. Especially the influence on the glass flow and the temperature distribution is interesting, but also the question if a glass tank reinforcement is influencing the electrical potential and resistance between the electrodes.

A model was built up for an electrical boosted container glass tank (Figure 11) and later on in a case study the glass tank reinforcements were installed (Figure 12). Furthermore the simulation was done with changing electrode positions and finally also a change from bottom boosting to horizontal electrodes (Figure 13).

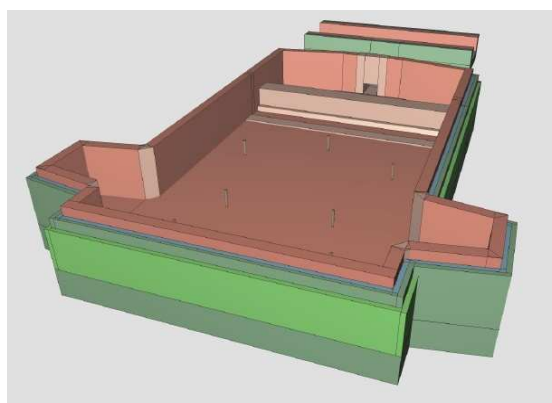


Figure 11: Electrical heated container glass tank (base case) with bottom boosting

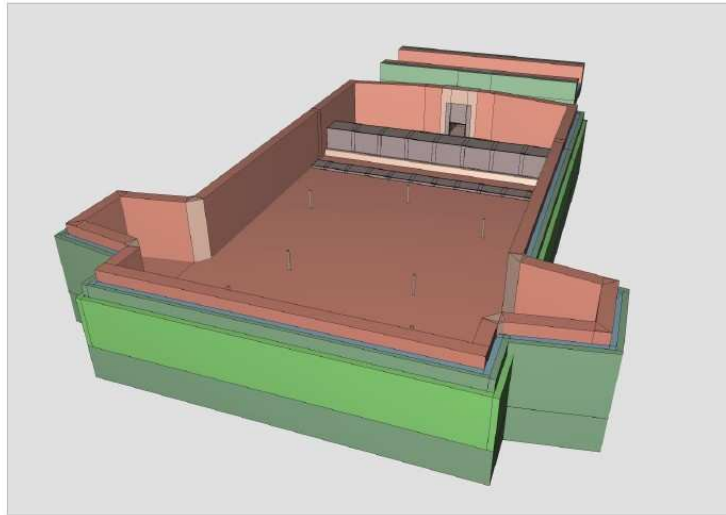


Figure 12: Electrical heated container glass tank with bottom boosting and installed bubble maker, wall and throat channel protection.

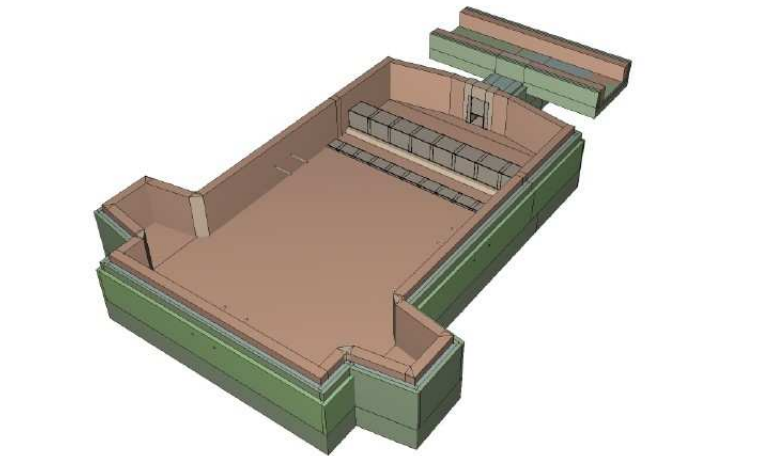


Figure 13: Electrical heated container glass tank with horizontal electrodes and installed bubble maker, wall and throat channel protection (horizontal electrodes instead of the bottom boosting)

The results with the highest interests are the influence of the glass tank reinforcements on the flow of the glass melt including the velocity profile and the temperature distribution inside the melting tank. Figure 14 demonstrates the velocity profile and flow of the glass melt. On the upper side of the figure the unprotected reference glass tank and on the lower side the

glass tank which includes the molybdenum glass tank reinforcements for bubble maker, cross wall and throat channel.

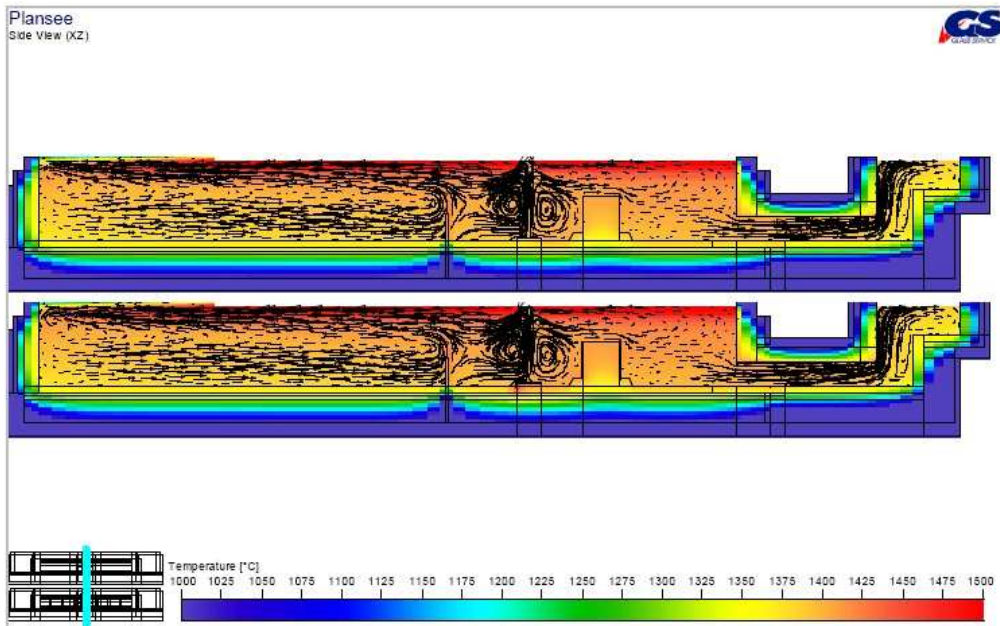


Figure 14: Velocity profile and flow of an electrical boosted container glass tank. Upper picture is the base case and lower picture the glass tank including the glass tank reinforcements for bubble maker, cross wall and throat channel

As can be seen the glass tank reinforcements don't have any impact on the flow of the glass melt.

Furthermore the temperature distribution is interesting for the design of a glass tank and is shown in detail in Figure 15.

The upper figure demonstrates again the base case of the glass tank not including any molybdenum reinforcements. The figure in the middle is the same glass tank but equipped with the molybdenum reinforcements and the lower figure demonstrates the result when the electrode with the shortest distance to the first reinforcement is located 500 mm more away from the reinforcement.

In both cases of a glass tank with reinforcements the temperature at the bubble maker reinforcement increases by about 25 °C compared to the unprotected glass tank. This temperature difference becomes even lower with the change of the electrode position. Nevertheless is the influence on the temperature distribution in both cases neglectable.

The same is valid for a glass tank with horizontal electrodes (Figure 16). A slight temperature influence is visible on the bubble maker corners but also here the values are neglectable. It is here also more obvious that the increase of distance between electrodes and reinforcements decreases the temperature influence.

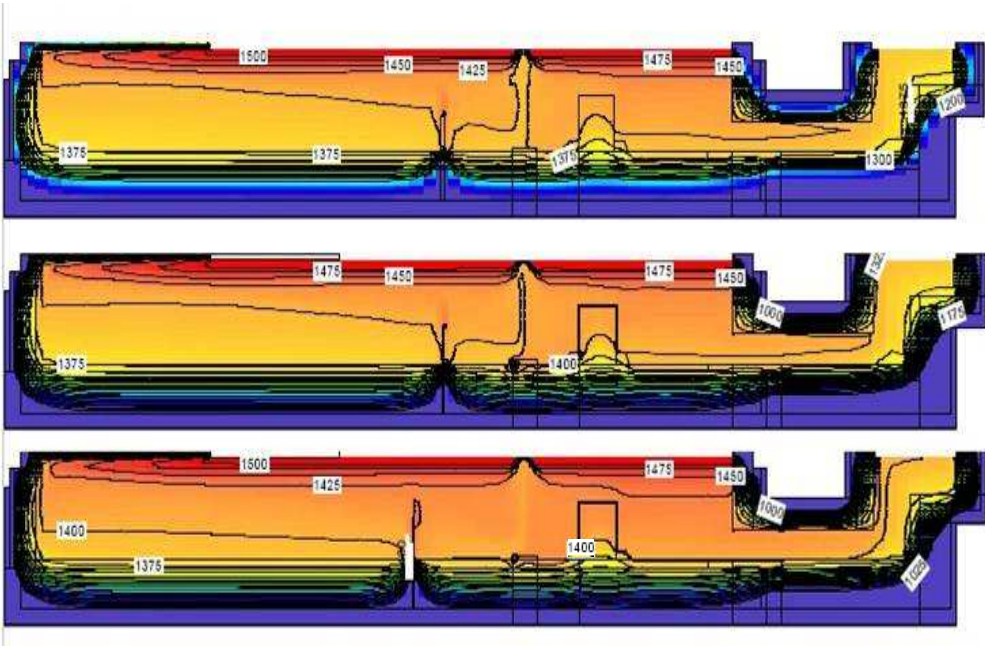


Figure 15: Temperature distribution in an electrical boosted container glass tank with and without reinforcements and with changed electrode position.

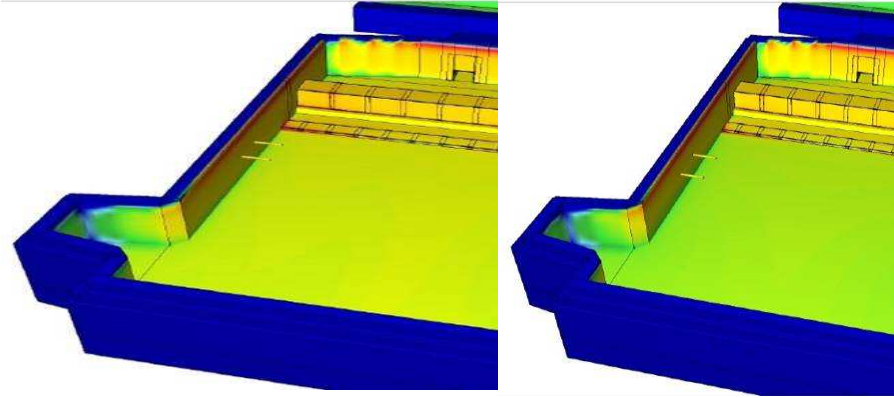


Figure 16: Glass tank with horizontal electrodes and glass tank reinforcements and changing electrode positions.

As a conclusion it can be said that glass tank reinforcements can increase the lifetime of a glass tank and especially of the most critical areas due to the excellent corrosion resistance of molybdenum in most glass melts. Furthermore it was possible by a mathematical

simulation to answer the question if there exist influences of the glass tank reinforcements on the flow and velocity profile and the temperature distribution inside the glass tank. All analyses show clearly that there are no or neglectable influences on the production parameters of a glass tank.

At this position I would like to thank our Partner Glass Service, BV from the Netherlands who carried out the mathematical simulation of the glass tanks in a narrow cooperation with PLANSEE Metall GmbH.

LECTURES

1st Glass Forming Simulation Workshop

June 27, 2007

Hotel Lanterna
Velké Karlovice, Czech Republic

APPROACH TO THE MODELLING AND OPTIMIZATION OF GLASS FORMING CYCLE

Ivo Matoušek
Technical University of Liberec

Abstract

The claims on ensuring high quality of manufactured products and improving efficiency of the glass forming can not be ensured by conventional methods of the forming cycle proposal already. The effective approach to the identification of weak points of glass forming cycle itself and its subsequent optimisation is an application of tools of virtual modelling. Computer model enables monitoring of individual stages of the whole glass forming cycle and its application already in pre-manufacture stage allows reducing physical prototyping, the rate of product rejects and material waste as well as accelerating cost-effective product development. In the paper the approach to the prediction, localisation and identification of potential technological problems is shown. The computational analysis itself is based on fully coupled thermo-mechanical strategy. Constitutive behaviour of glass melt is described through generalised non-Newtonian viscous model. Close attention is paid to reliability of acquired outputs and to the problem of prediction of technological defects already in pre-manufacture stage. Therefore, based on the analysis of defects and technological problems typical for manufacturing pressed assortment, criteria allowing their identification and localization are suggested. In the contribution the process of optimisation of glass forming cycle is also presented. Attention is aimed mainly to the problem of effective modification of temperature fields' distribution in glass forming tools.

INTRODUCTION

The forming process is the source of problems continually; it influences the effectiveness of the whole manufacture process as well as quality of final products on principle. The introduction of new, above all non-standard assortment into the manufacture process is related to a considerable growth of demands for the forming process. The claims on ensuring high quality of manufactured products considerably rise with increasing complexity of product to be formed. In order to achieve high production quality as well as to improve efficiency of the glass forming, the comprehensive optimization of the whole glass forming cycle is necessary even in pre-manufacturing stage.

Conventional methods of the forming cycle proposal based on empirical basis allow neither effective evaluation of individual influences, which affect the course of the forming cycle, and their interactions, and consequently nor effective optimization of the course of the forming cycle. The effective method for monitoring individual stages of glass forming cycle and subsequent optimization is to use of comprehensive tools of virtual simulation.

REAL GLASS FORMING CYCLE

One of the typical glass forming technologies is pressing comprising individual, mutually separated stages that are repeated cyclically (Fig. 1). The forming cycle starts by feeding glass melt into the working cavity of a glass mould. After contact with the mould-working surface, the glass gob is deformed by its own weight. At the same time, an intensive heat exchange occurs on the interface between the glass melt and mould. It finds expression in considerable viscosity increase in surface layers of the glass gob as well as in temperature rise of the mould-working surface. Pressing is the predominant operation of the whole forming cycle during which glass melt is submitted to considerable mechanical load, due to which the shape of glass with relatively low viscosity is

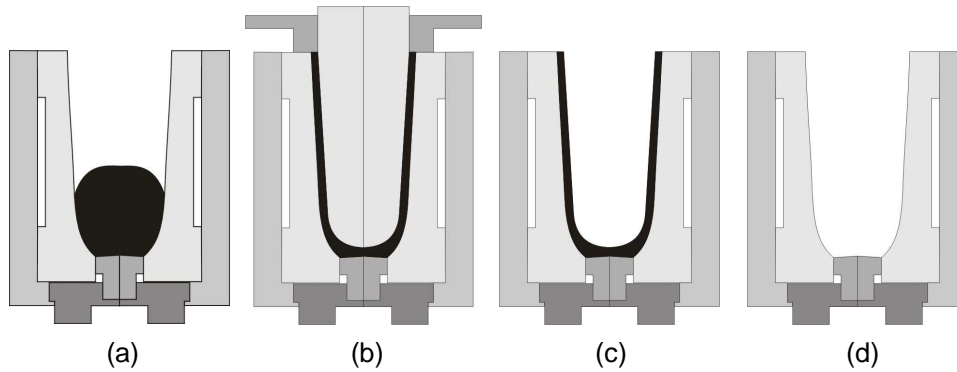


Fig. 1: Individual stages of glass pressing cycle.

(a) Feeding, (b) Pressing, (c) Glass cooling, (d) Mould cooling.

viscosity is

changed within a very short time. Although this stage of the forming cycle is practically negligible from time point of view, it has crucial influence on the production quality. In remaining part of the pressing cycle, the glass pressing is cooled in the glass mould, and the mould is prepared for the next forming cycle.

NUMERICAL MODEL

The glass forming process is a complex thermo-mechanical problem with a strong interaction between glass heat transfer and viscous flow of molten glass. So numerical modelling of glass forming involves a coupled non-linear solution of heat and mass transfer. The equations of mechanical and thermal equilibrium in a set of Lagrangian coordinates are:

$$\rho \frac{dv_i}{d\tau} = X_i + \frac{\partial \sigma_{ij}}{\partial x_j}, \quad (1)$$

$$\rho \cdot c \cdot \frac{\partial T}{\partial \tau} = \text{div}(k \cdot \text{grad}T) - 3K\alpha \Delta T \dot{\epsilon}_{kk} - s \dot{\sigma}'_{ij} \dot{\epsilon}_{ij}, \quad (2)$$

where \mathbf{X} is the body force, \mathbf{v} is velocity, τ is time, $\boldsymbol{\sigma}$ is the Cauchy stress tensor, $\boldsymbol{\sigma}'$ is the time derivative of deviator stress tensor, T is temperature, k is thermal conductivity, c is the specific heat, K is the bulk elastic modulus, α is the coefficient of thermal expansion, $\boldsymbol{\epsilon}$ is the strain rate tensor, s is the fraction of viscous work that is converted into heat.

Glass is actually a viscous-elastic liquid over its whole forming range but, in the forming range, the elastic part of the deformation is almost negligible and so stress deviator tensor can be related to the viscous strain rate tensor through generalised non-Newtonian flow model:

$$\sigma'_{ij} = 2\eta(T, \dot{\epsilon}) \dot{\epsilon}_{ij}, \quad (3)$$

where

$$\sigma'_{ij} = \sigma_{ij} + p\delta_{ij}, \quad (4)$$

in which p is the hydrostatic pressure, η is highly temperature dependent viscosity that in the forming range at sub critical deformation rates can be described by Fulcher equation [1]. Generally, taking into account the influence of strain rate, the viscosity can be expressed as:

$$\eta = \frac{A + \frac{B}{T - T_0}}{1 + \left(A + \frac{B}{T - T_0} \right) \cdot \frac{\dot{\epsilon}_t}{\sigma_{lim}}}, \quad (5)$$

where A , B , T_0 are empirical constants, $\dot{\epsilon}_s$ is shear strain rate and σ_{lim} is cohesive stress [2].

In the forming range the molten glass can be considered to be incompressible ($\dot{\epsilon}_{kk} = 0$). To get acceptable results, the simulation model must address all aspects glass pressing influencing (composition, machinery, technological parameters, material properties of particular components incl. temperature dependences, boundary conditions time runs etc.). Relatively good agreement between the numerical model and real forming cycle can be obtained by means of verified inputs and simulations of sequences of several forming cycles attaining quasi-static temperature balance in virtual forming tools [3, 4].

PREDICTION OF TECHNOLOGICAL PROBLEMS

In the automatic manufacture of pressed glass, many technological problems have occurred influencing both the efficiency of the forming cycle and production quality. But only some of them can be identified directly by means of the virtual model in the pre-manufacture stage (on the bases of analysis of the course of temperature and strain fields in the glass melt being formed and also in forming tools), such as:

- **underpressing** due to an insufficient pressing force of the press,
- **glass melt sticking** caused by the glass mould local overheating; under actual conditions the critical temperature of sticking can be defined by the empirical relation [5]:

$$T_S = \frac{A + B}{0,81 \log p + 1,26 \log \tau + 5,47} + T_0 \quad (7)$$

where p is pressure, τ is time, and A , B , T_0 are empirical constants,

- **pressing deformation** after its taking out of the mould as a consequence of insufficient amount of heat removed from glass melt during the forming cycle; for pressed

assortment mean viscosity $\eta=10^7$ Pas is usually considered to be the critical value. Because of a limited knowledge of rheological properties of the glass melt and owing to the used computational model, any prediction of defects caused by bad glass workability is very problematic. In addition to an excessive creation of chill marks on the surface of formed products, a viscous-elastic response can, under the critical strain-time conditions, give rise to substantial transient stresses which could be the source of some defects known as „checks“.

So, for an identification of areas where technological problems caused by the “bad glass workability” can occur, the methodology was suggested proceeding from the assumption that the surface quality of formed products is influenced by the local interactions of temperature and strain rate. Then the level exceeding critical values of the strain rate expressed in the k_M (8) coefficient serves as a criterion of defect occurrences (above T_g).

$$k_M = \frac{\dot{\varepsilon}}{\dot{\varepsilon}_c}, \quad (8)$$

where $\dot{\varepsilon}$ is an actual strain rate and $\dot{\varepsilon}_c$ is a critical strain rate for onset of shear thinning.

The area, where the k_M coefficient exceeds the limit value markedly, is critical from the technical point of view. The surface quality of products is always acceptable when $k_M \leq 1$ (glass melt formed has properties of non-Newtonian liquid).

PREDICTION OF CRITICAL POINTS OF REAL GLASS FORMING CYCLE

In the automatic manufacture of pressed glass, especially the production of non-standard products is problematic as far as shapes and dimensions. As an example of such assortment, a tall slender pressing (Fig. 2a) made of lead crystal (height – 250mm, weight - 2 kg) pressed using the mould (Fig. 2b) and water cooled plunger at 6-section turntable machine. Glass forming mould is made of steel X12Cr25Ni20 and plunger of ANSI 431. A specific problem of forming of this assortment is simultaneous pressing of 6 modifications differing in pattern shapes. For the numerical modelling, small differences in shapes, given by dissimilarities of particular patterns, were neglected; attention was paid to an evaluation of the time development of basic characteristics of the forming cycle (temperatures, strain, and strain rates) in connection with smooth products, i.e. without “cuts”.

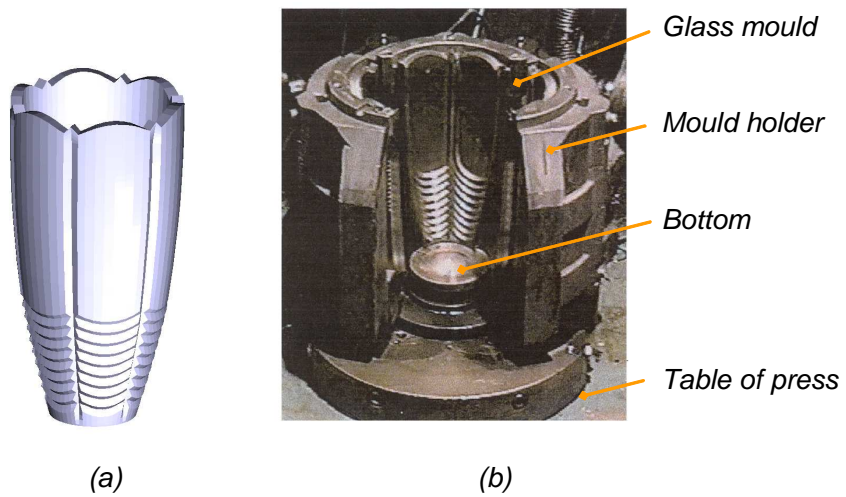


Fig. 2: (a) Geometrical model of the vase, (b) Glass mould.

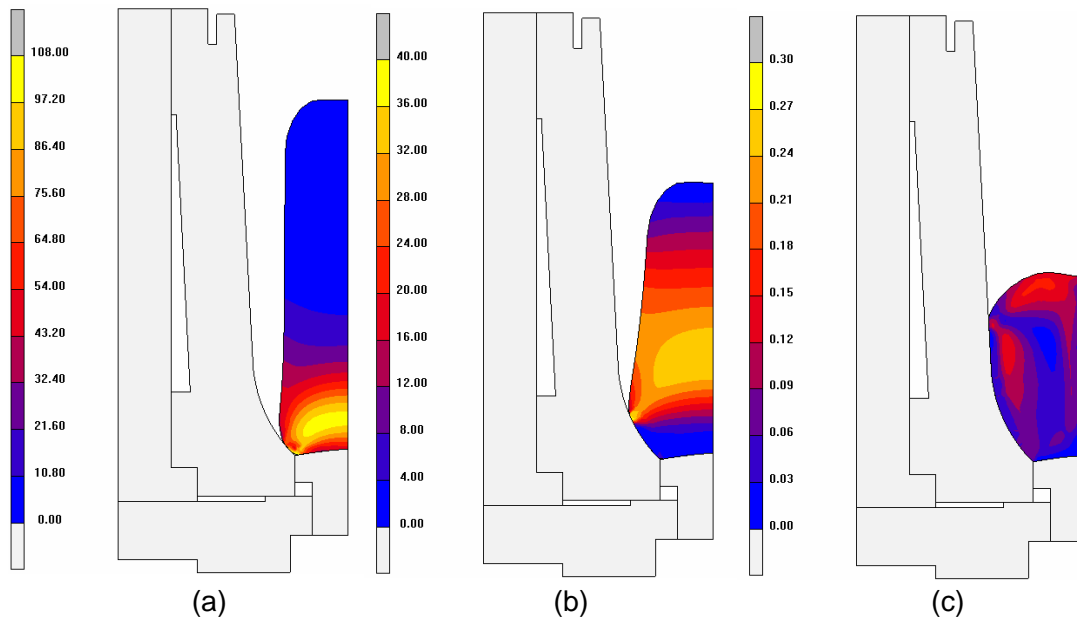


Fig. 3: Distribution of strain rates in glass melt in the selected moments during the first stage of forming process:
 (a) Time 0,45 s. (b) Time 0,47 s. (c) Time 3,3 s.

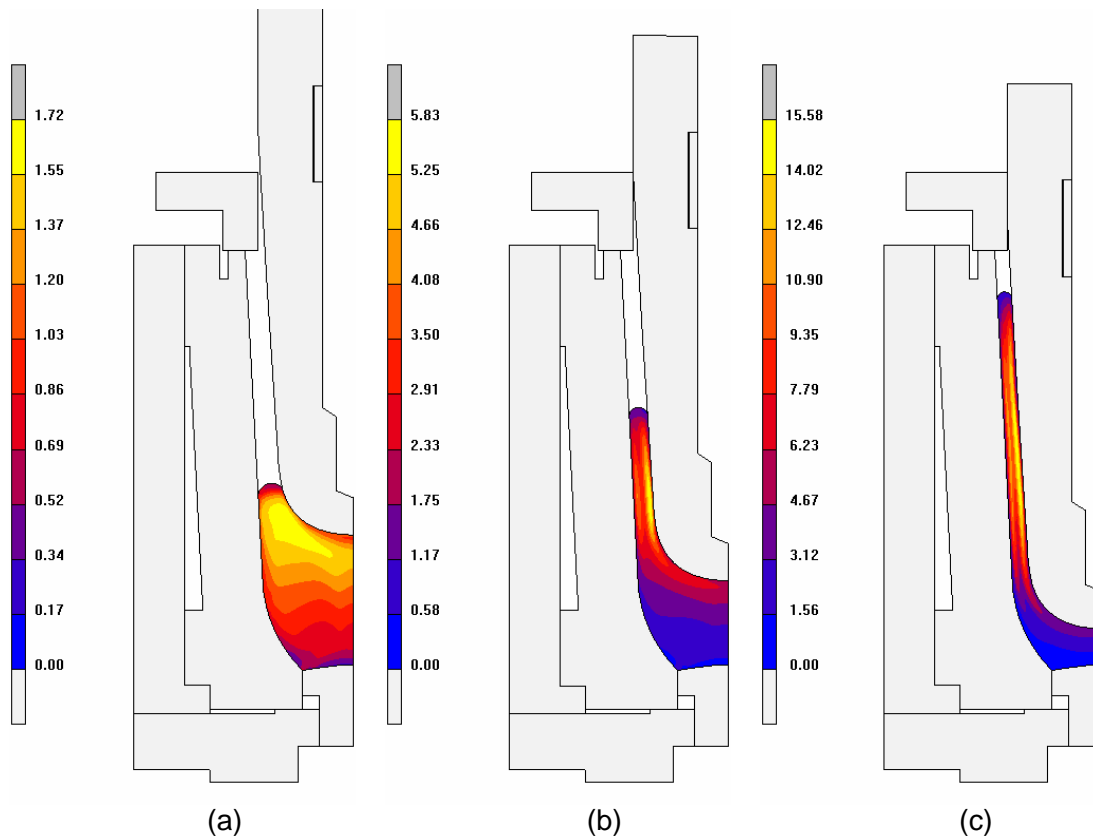


Fig. 4: Distribution of strain rates in glass melt in selected moments during pressing:
(a) Time 3,7 s, (b) Time 4,2 s, (c) Time 4,65 s.

Evaluation of the strains and strain rates during the first forming stage, i.e. between the moment of feeding and start of pressing, is shown in Fig. 3. When glass melt falls to the mould working cavity, considerable changes of the glass gob shape occur being in progress ca 0,5s (time interval between 0,45 and 1s from the moment of the glass melt feeding). In the following stage – up to the contact with the pressing plunger – deformations of the glass gob are minimal already; strain rate peaks reach overstepping value 100 s^{-1} (true strain rate after

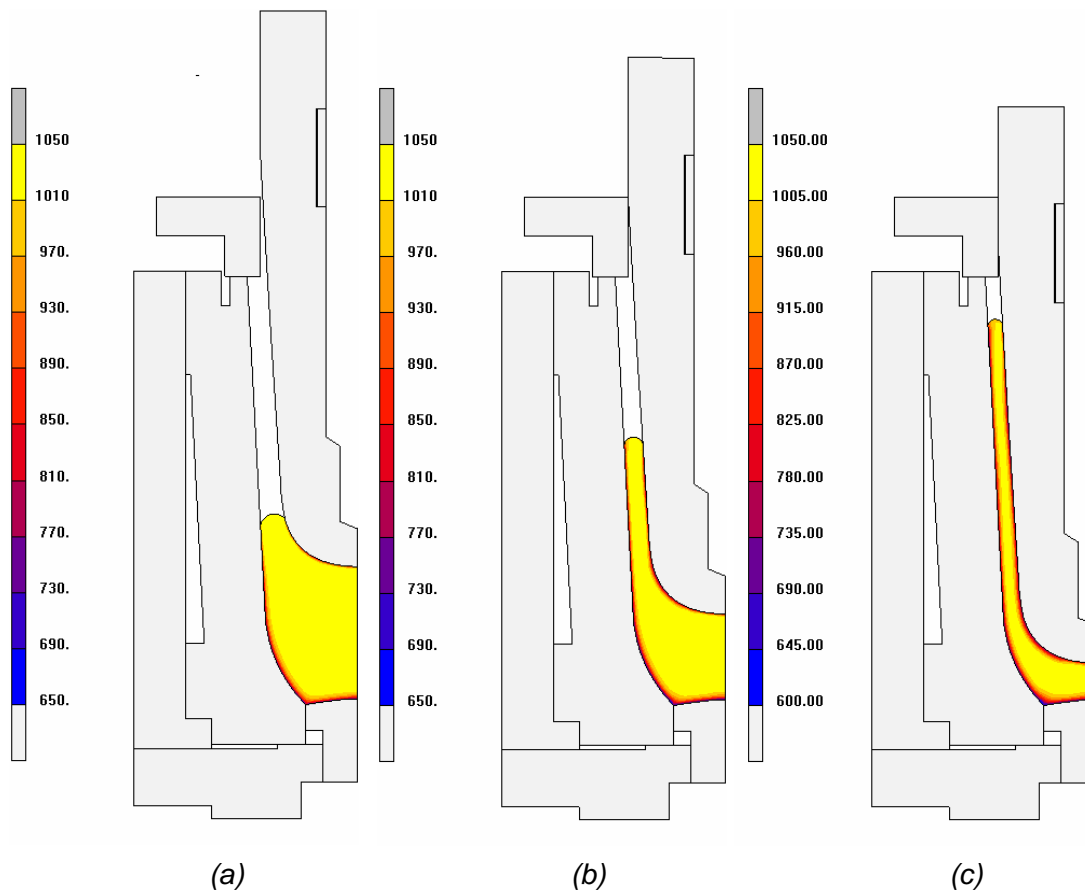


Fig. 5: Temperature distributions in glass melt in selected moments during pressing:
 (a) Time 3,7 s, (b) Time 4,2 s, (c) Time 4,65 s.

dropping) in the course of the whole interval. Maximal drop in temperature of the glass melt

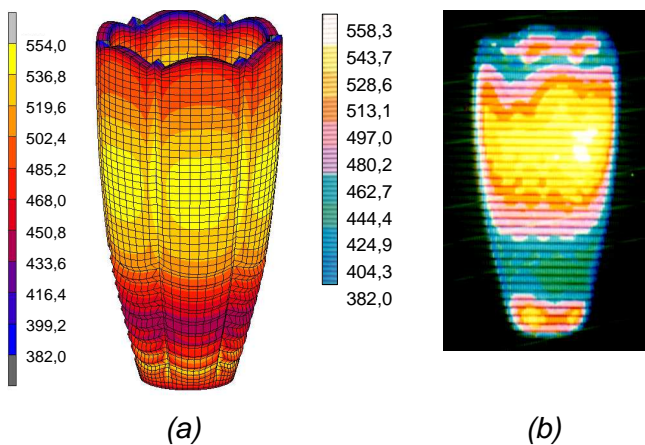


Fig. 6 Verification of virtual model– temperature distribution at the moment of product taking out
 (a) - Numerical model, (b) - Operational measurements (wavelength 5 - 5,5 μm)

in the contact with the mould surface attained ca. 400°C when the pressing was starting. The pressing process itself (the first contact between the plunger and glass melt) starts delaying 3 s from the moment of the glass melt feeding. In the course of forming, the glass melt is forced into the working cavity which is created by the mould, plunger, and pressing ring. In the same time, owing to the enlarged contact area between the glass melt and forming tools, a process of glass surface cooling has been intensified step by step. That is accompanied by the viscosity increase.

During pressing, the area of the strain rate maximum is moved along the plunger nose upwards up its direction; maximal value of the strain rate increases gradually (during pressing) and it reaches value ca 25 s^{-1} (Fig. 4) in the final forming stage. The development of temperature fields at chosen moments of the forming cycle is given in Fig. 5.

The criteria given in the chapter 4 were used for an evaluation of virtual forming cycle. On the

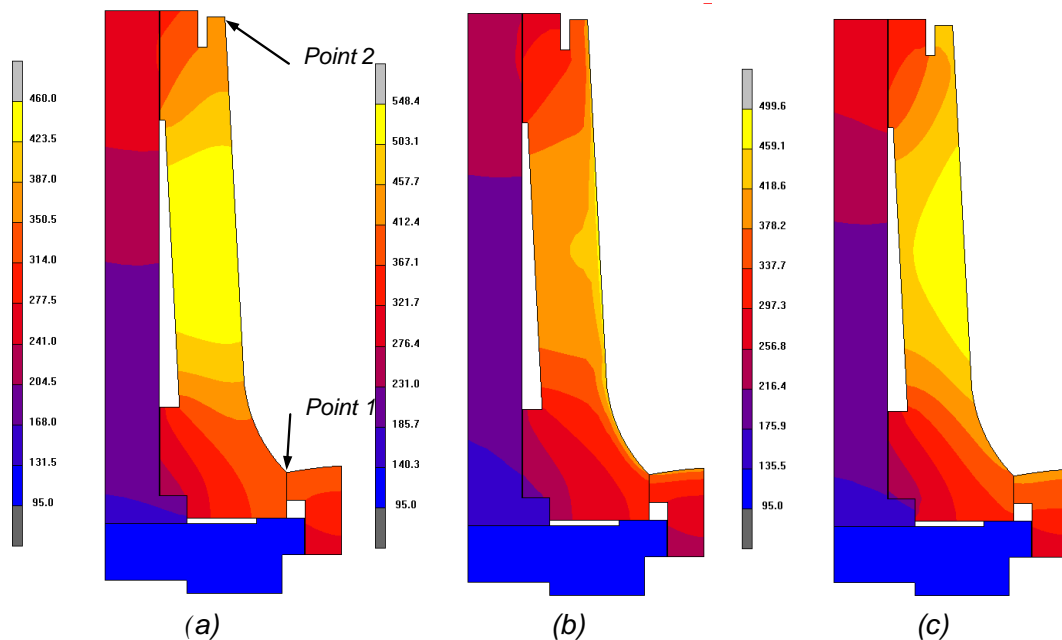


Fig. 7: Distribution of temperature fields in the glass mould:

- (a) Time 0 s - glass feeding. (b) Time 5 s glass pressing (moment of pressing up).
(c) Time 88 s - product taking out.

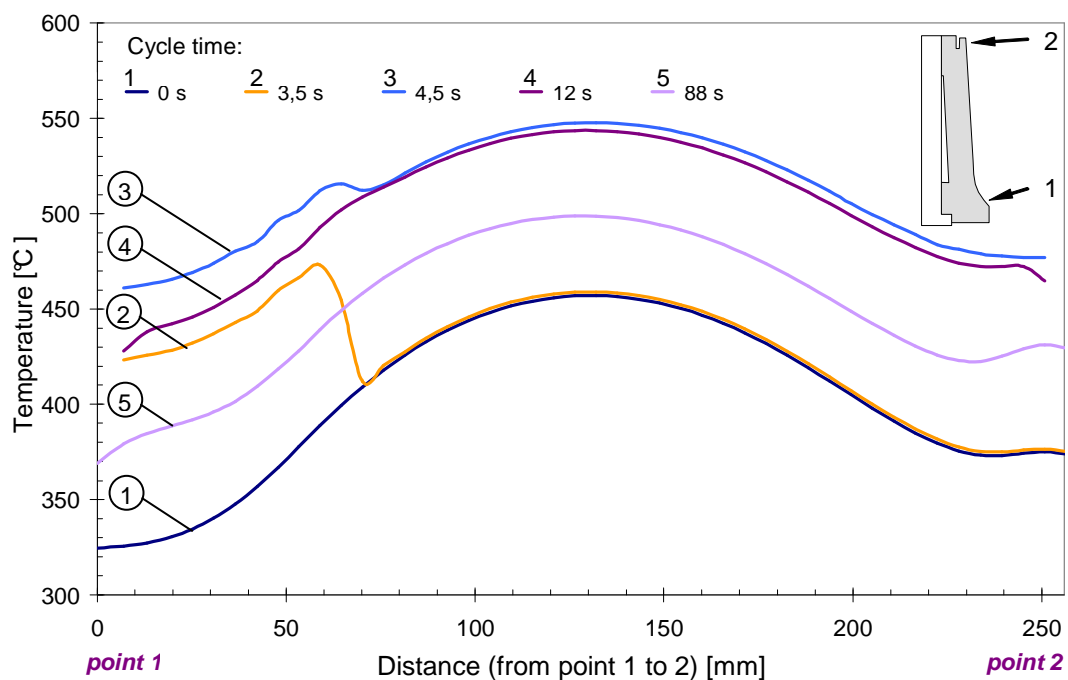


Fig. 8: Distribution of temperature along working surface between point 1 and 2

basis of the analysis of the course of temperatures and strain rates, it can be stated that:

- **pressing force of the press seems to be sufficient,**
- during pressing, **the glass melt sticking will not occur** – identified temperature of the mould working surface lies under sticking temperature (ca 560°C); maximum temperature at the moment of feeding is approx. 460°C (during the pressing process ca 546°C) - see Fig. 7-8 (in Fig. 6 distribution of temperatures in the glass product in the moment of its taking out is shown – this calculation has been used for virtual model identification),

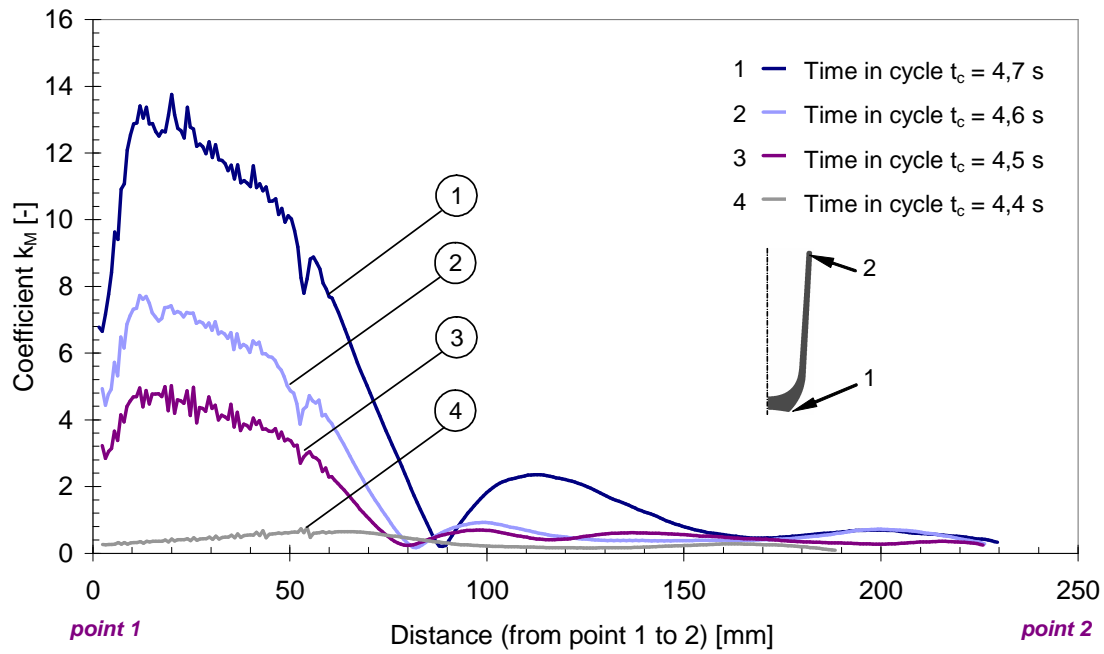


Fig. 9: Distribution of coefficient k_M along outer surface of pressing between point 1 and 2 for chosen times

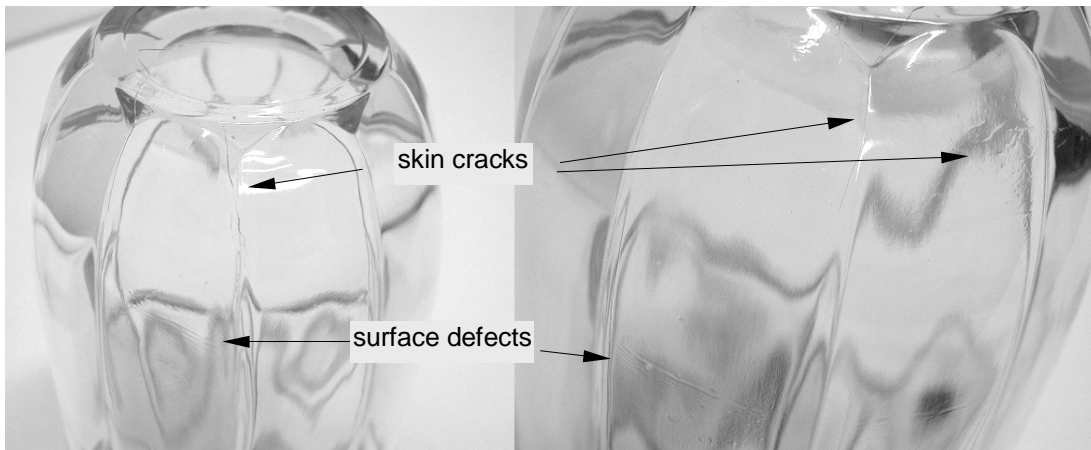


Fig. 10: Areas with defects occurrence on outer surface of final production

- after taking out **spontaneous strains will not happen** – assumed mean pressing temperature is approx. 560°C in the moment of its taking out; this temperature corresponds to the viscosity of ca. 8,5 Pas which is sufficient for the pressing shape stability,

- based on the analysis of strain rates and temperatures evolution in the contact area of the glass melt and forming tools, **surface defects on lower part of the product external surface** can be assumed, because k_M coefficient in the critical area (external surface limited by the pressing bottom and horizontal plane at a distance of about 70mm from the pressing bottom) exceeds the limit value considerably (Fig. 9). Localisation of predicted defects on manufactured production is in relatively good accordance with operational experience (see Fig. 10).

OPTIMISATION OF GLASS FORMING CYCLE

Technological problems in the automatic production of pressed glass are frequently caused by uneven distribution of temperature fields in forming tools. So the optimisation process of the pressing cycle results often in modifications of the design and cooling of forming tools.

Based on a practical experience, the complex methodology was formulated optimising the real forming cycle course. The general computational program using finite-element method (MSC-MARC) is a core of the system being complemented with special subroutines allowing the whole forming cycle to be simulated. The optimization process itself is based on a two-stage strategy. In the first stage the basic technological parameters (boundary conditions) are optimized. In the following one, attention is focused on evaluation and subsequent optimization of forming tools design and cooling.

With respect to the quasi-stationary character of temperature fields in glass forming tools, it is difficult to determine optimization criteria allowing the distribution of temperature fields to be evaluated effectively in the course of the whole cycle. An effective solution is a time discretisation of the forming cycle, which allows focusing on two, from the technological point of view, the most important time intervals: molten glass feeding and pressing.

The important step of the whole optimization process is a determination of the optimization criteria. Because the great numbers of optimization standpoints can exist and some of them can act against each other, it is suitable to characterize the optimal state by means of minimization of weight functional including different factors (forming cycle reduction, heat removal optimization, distribution of temperatures both in glass melt and the mould, distribution and run of strain rates during the pressing process, service life of the glass mould, etc.).

Taking some of these criteria into consideration (amount of removed heat from glass melt during the forming cycle, uniform distribution of temperatures along the working surface of the glass mould, etc.), it is possible to describe the purpose functional (for the example mentioned above) as follows [6]:

$$\hat{J}_s = \mu_1 (T(t_c)_{MAX} - T_{MIN})_{t_c=0} + \mu_2 \sqrt{\frac{1}{L} \int_{\Gamma} (T(t_c) - T_{ref})^2_{t_c=0} d\Gamma} + \mu_{p1} \max(T(t_c) - T_{KRH})^+ + \mu_{p2} (T(t_c) - T_{KRS})^-_{t_c=0}, \quad (9)$$

where: μ are weight coefficients, L is length, T is temperature.

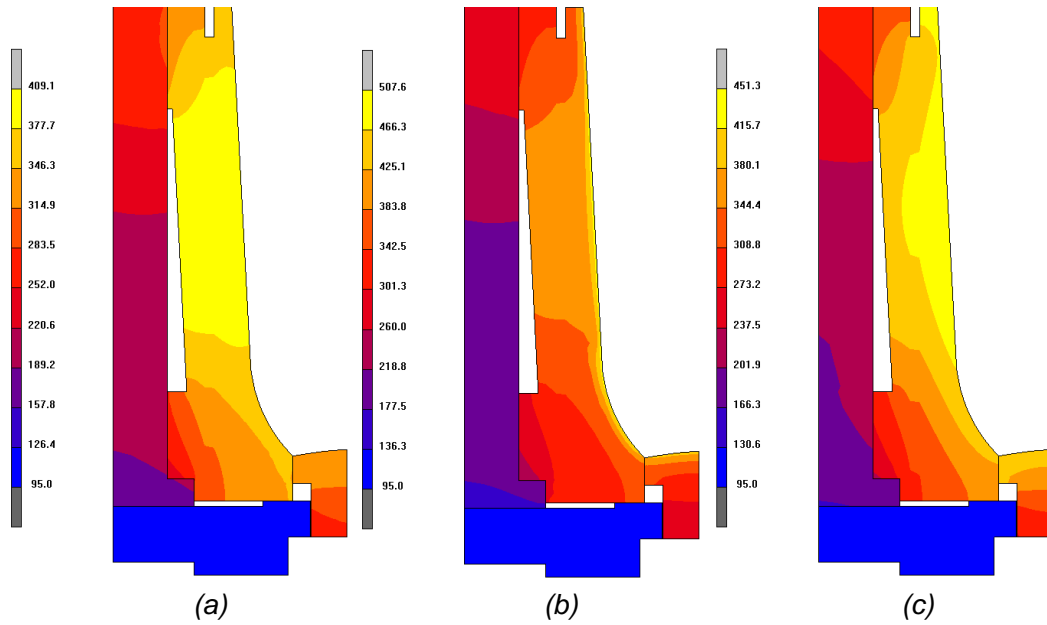


Fig. 11: Distribution of temperature fields in the glass mould – optimised solution:
 (a) Time 0 s - glass feeding. (b) Time 5 s - glass pressing (moment of pressing up).
 (c) Time 88 s – product taking out.

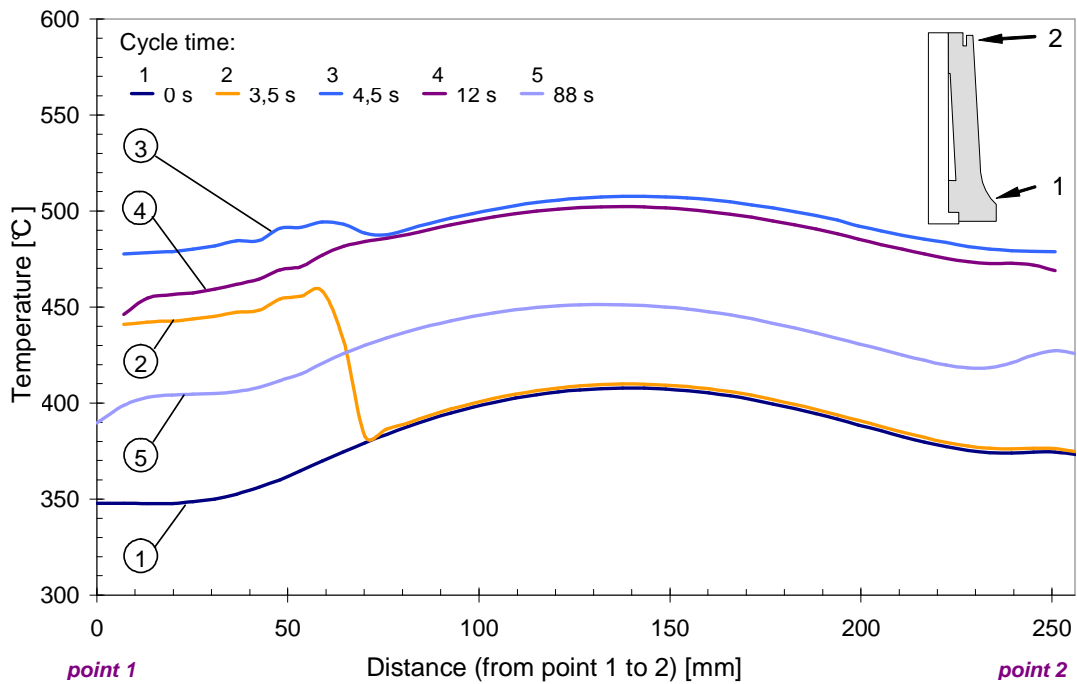


Fig. 12: Distribution of temperatures along working surface between points 1 and 2
 Optimised solution.

Minimization of the purpose functional J_s is achieved by a modification of model parameters. Optimized technological parameters (boundary conditions) and a theoretical proposal of the forming tool design and cooling are the results of the optimization process.

The given optimization process was also used for the design and cooling modifications of above analysed glass moulds. A fundamental problem of the analysed assortment production lies in considerable temperature differences along the mould-working surface when glass melt is fed (lower part of the mould is substantially colder than central part; the differences reach up to ca 130°C, see Fig. 8). These differences influence negatively stability of the whole forming cycle and quality of final production. Based on the initial analysis of the suggested forming cycle course, several alternatives for the modification of the mould design and cooling were prepared. When calculations were carried out, an optimization algorithm was applied (9); the main optimization criterion was to minimize the temperature gradient along the mould working surface when glass melt was fed as well as to minimize the temperature peaks during the forming process.

From the practical point of view, the most important part of the optimization process is a proposal of actual technological or design modifications. The effective way of such modification of the mould design is the approach based on the global modification of temperature fields that allows controlling temperature field's distribution in the whole body of glass forming tools. Such design of forming tools ensures their reliable functioning and high quality of products manufactured in relatively wide range of technological parameters. In this concrete case, the practical realization is based on the simplest method – application of thermo-exchange elements.

The distribution of temperature fields in the optimized glass mould in the moment of feeding and in the course of the pressing process is presented in Fig. 11. It results from the Fig. 12, where the distribution of temperatures along the working surface in the moment of feeding respective pressing is drawn up (in agreement with plot in Fig. 8), that this technical solution allowed substantial reducing maximal temperature differences along the working surface in the moment of glass melt feeding for about 80°C, from ca 130°C at the optimization process beginning up to ca 50°C at the solution realized; maximal temperature was reduced by ca 50°C during the pressing process. As a result of a homogenisation of temperature fields, k_M coefficient value decreased by ca 85% in the critical area. Moderate growth of coefficient k_M can be observed in the central area of formed pressing [8]. Besides significant improving stability of the glass forming cycle and production quality, this optimized solution allows the total cycle time to be reduced significantly (for about 10 %).

CONCLUSION

In the paper possibilities of use of virtual simulation tools for the monitoring of glass forming cycle are shown. Possibilities to detect and localize technological problems are demonstrated using the example from technological practice. The optimisation approach,

based on global modification of temperature fields, allowing the reliable functions of forming tools working in relatively wide range of technological parameters, is presented. Results of the numerical simulation were verified in the praxis. Glass moulds of the initial design were the source of technological problems - pressed products had many defects (especially checks) in the product bottom part. On the contrary, outstanding feature of the glass moulds having optimized designs was relatively high production quality.

ACKNOWLEDGMENTS

This work was created in the frame of research project No. MSM 4674788501, which is financed by the Ministry of Education of the Czech Republic.

REFERENCE

- [1] Fulcher, G. S. J.: Analysis of recent measurements of the viscosity of glasses Amer. Ceram. Soc., 1925 (8), 6, p. 339 - 355
- [2] SIMMONS J. H., OCHOA, R., SIMMONS, K., MILLS, J. J.: Non-Newtonian viscous flow in soda-lime-silica glass, J. Non-Crystall. Sol., 1988 (105), p. 313-322
- [3] MATOUŠEK, I., 2002, Numerical simulation and optimisation of glass forming cycle, Proc. of 2nd Coll. on Modelling of Glass Forming and Tempering, Vallenciennes (FR).
- [4] MATOUŠEK, I., 2000, Approach to the optimisation of glass pressing cycle, Proc. of the first Slovak glass conference, Trenčín (SK)
- [5] Smrček, A.: Machine glass forming, SNTL, Prag 1981
- [6] MATOUŠEK, I., 1999, The improvement of product quality based on numerical simulation of glass forming cycle, Proc. of the 5th ESG Conf. – Glass science and technology for the 21st century, Prag (CZ)
- [7] MATOUŠEK, I.: Optimisation of Glass Pressing Cycle in Pre-manufacture Stage, Glastech. Ber. Sci. Tech. Vol. 77C. p. 290-300. ISSN 0946-7475
- [8] MATOUŠEK, I.: Prediktivní optimalizace v procesu tvarování skloviny, Sklář a keramik, 2006, roč. 56, č. 9, s. 198 – 205. ISSN 0037-637

ADVANCED SIMULATION OF 3D GLASS BOTTLE FORMING

Gerard de Leede, Rik Koch
GS Improve BV

Vincent Bouwman, Gertjan Kloosterman
Abaqus Benelux BV

Abstract

Production of glass bottles requires blowing of the glass after entrance of a gob of molten glass in the blank mould. The final shape of the bottle is highly dependent on the viscosity of the glass, the blow-pressure and the temperature distribution in the glass and the mould and simulation of this complicated process enables optimization of the process conditions. During simulation of blowing of the glass, the mesh has to be adapted due to the extreme deformations of the mesh. Using the existing ALE-technique for this kind of applications requires a lot of user-intervention and trial-and-error to create a mesh that suits both the initial and final topology of the glass. To reduce the user-time and to be able to run this kind of analyses automatically based on an arbitrary base-geometry, a completely automated remeshing/rezoning procedure is set-up. In this procedure the analysis is divided in a number of sub-analyses after each of which a new (3D) geometry of the glass is created based on the deformed mesh. Using a map-routine the solution from the previous analysis is mapped on the new mesh such that continuation of results is ensured. Using the automated remeshing capability, simulations of the glass bottle forming process have successfully been performed, enabling for example optimization of process settings. Due to the generic set-up of the remeshing procedure it can easily be used for other simulations that require adaptive meshing as well.

MODELING OF SOME QUALITY ASPECTS IN TABLEWARE FORMING PROCESSES

P. Vrabel, N. Krečmer¹, V.Cúth¹, L. Zhang², G. de Leede², R. Koch²

Rona, J.S.C., Schreiberova, 02061 Lednické Rovne, Slovak Republic, Vrabel@rona.sk

¹The Alexander Dubček University of Trenčín, Faculty of Industrial Technologies in Púchov, I. Krasku 491/30 020 01 Púchov, Slovak Republic, krecmer@fpt.tnuni.sk

²Glass Service Improve, Watermolen 22, 6229 PM Maastricht, The Netherlands, : L.Zhang@gsimprove.nl

Abstract

Defect source understanding is one of major factors in process quality control. Glass forming modeling was used to quantify influence of different process parameters on investigated balances of mass, heat and momentum. Two processes were taken as examples (i) pressing and (ii) blow-blowing. Two commercial Finite element method codes in 2D and 3D modes were used for models of different complexity with respect to process and material. The emphasis was given to such a physical aspect, which was necessary in order to follow the material properties related to investigated defect. Two types of glass models were adopted (i) elastic model and (ii) visco-elastic model with relaxation. All models were partially validated by experimental measurement of temperature. Computed glass tensile stress and radial wall thickness inhomogeneity were taken as the critical parameters for defects called “cracked bottom” and “optical radial irregularity”, respectively. Also calculated Equivalent von Mises Stresses of mould material indicating exceeding yield point were related to regions of mould damage. The intensity of the mentioned physical properties correlated well with locations of defects. The obtained results were used for process setting analysis leading to defect reduction.

IMPROVING THE BOTTLE PRODUCTION BY MODELLING

Rik Koch
GS Improve BV

Abstract:

The bottle production is already an "ancient" technology. Some experts say that in the last two decades no real improvement on the basics of the technological concepts was seen. Part of this poor development can be related to the market, which was showing decreasing margins for the producers.

With the growth of the computation power and the knowledge of numerical simulation, a relative cheap research and development tool can be acquired where in history millions of euros needed to be invested.

As a demonstration of the computing capability an outline is presented of the current states of the IS machines for a virtual machine. The improvement can be shown on conceptual design of molds, to improve the cooling capacity, for a better production speed, and/or quality issues for a nicer/stronger bottle.

The mold cooling and the effect on the glass temperature, the homogeneity of the glass temperature, the run-in time of the mold can be studied, quickly and in detail. A new glass product design tested on internal pressure and load pressure can be evaluated in a few minutes.

These forming models now start to penetrate into the market and it demonstrates that modern manufacturers are willing to follow the path which is shown by modeling. I believe that we start to move into a new era where manufacturing without the assistance of forming modeling will be inconceivable.

SIMPLIFIED BUNDLE MODEL FOR FIBERS FORMING

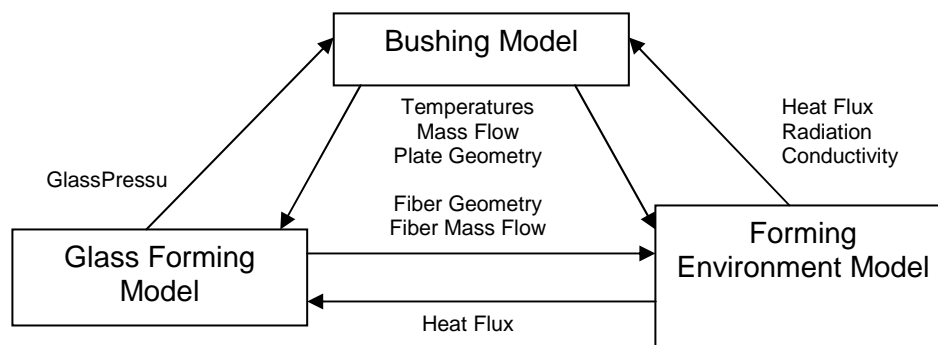
M. Moravský, J. Boroš
2M CONSULTING - SOFTWARE - GLAS

Abstract

Some of the difficulties for modeling of fibers forming:

- Parallel modeling of some thousands individual but strong interfering drawing processes needed
- Big range of geometry scale is needed to be included in one drawing process: from bushing - range 10^{-1} m, to end diameter fibers – range 10^{-5} m
- Description of boundary and boundary conditions of the forming area

To handle these difficulties in effective way following division into three coupled models was invented:



More detailed description of the glass forming model:

1. Able to compute: velocity field, thickness distribution, and temperature field of each fiber
2. Influence of surface tension included
3. Internal stress computations accordingly to visco-plastic and visco-elastic behavior (depending on deformation speed)
4. Two modes of calculation possible:
 - constant drawing speed applied at the lower end of fiber – standard drawing situation
 - gravity driven moving of the glass – situation after breakage of the fiber
5. Fast enough to compute parallel hundreds of fibers on PC platform

Possible areas of use for the glass forming model:

Investigate the stability criteria for drawing process, particularly:

- influence of glass properties, pullrate and its sudden changes, glass temperature and its changes
- coupled with forming environment model the influence of cooling of the forming area as well as influence of already broken fibers to neighbor fibers
- coupled with bushing model influence of glass temperature distribution inside of bushing

FORMING MODELLING OF FLOAT GLASS: TIN BATH, BENDING AND TEMPERING MODELLING

Gerard de Leede
GS Improve BV

Petr Schill
Glass Service, Inc.

Erik Muijsenberg
Glass Service, B.V.

Abstract

The modelling of the tin bath is a complex task, since there are many challenges to solve with such mathematical model. There is free flow of glass onto the tin bath from the lip stone.

The glass shape on the tin bath is also a free surface forming problem, there is forced and convective flow in the tin bath, gas flow above the tin bath, and there is usually a radiative heating structure above part of the tin bath.

The state-of-the-art various sub models and an effort to create an integrated model taking into account the most important interactions are discussed.

Once float glass is produced, the glass is often bended and/or tempered. The modelling of this process is less complex than the tin bath, but here we face another technical challenge: the visco-elastic behaviour of the glass.

Modelling addressed issues related to bending, tempering, development of the temporary and residual stresses and the final shape of the glass.